



Technische Universität München

TUM School of Medicine and Health

Exploring the lifecycle of synaptic mitochondria in the healthy and diseased nervous system

Athanasia Natalia Marahori

Vollständiger Abdruck der von der TUM School of Medicine and Health der Technischen Universität München zur Erlangung eines **Doctor of Philosophy (Ph.D.)** genehmigten Dissertation.

Vorsitz: Prof. Dr. Stefan Lichtenthaler

Betreuer: Prof. Dr. Thomas Misgeld

Prüfende der Dissertation:

1. Prof. Dr. Angelika Harbauer
2. Prof. Dr. Christian Behrends

Die Dissertation wurde am 16.01.2024 bei TUM School of Medicine and Health der Technischen Universität München eingereicht und durch die TUM School of Medicine and Health am 08.03.2024 angenommen.

Summary

Neurons extend their processes far away to form specialized contact sites—synapses—with other cells. Synaptic loss underlies many devastating diseases of the nervous system, beginning with degeneration of the nerve terminals before pathology slowly spreads to the soma in a “dying-back” pattern. Mitochondria are multifaceted organelles that significantly shape synaptic function by providing energy in the form of ATP, buffering Ca^{2+} ions, and metabolizing neurotransmitters, among many other tasks. Maintaining an appropriate number and quality of mitochondria (‘mitostasis’) is considered to be a key process in healthy synapses. Unlike the soma, however, axons and synapses are thought to lack most of the machinery for mitochondrial turnover, specifically for biogenesis and degradation of mitochondria. Instead, axonal transport developed to replace peripheral mitochondria continuously with “new” mitochondria from the soma (anterograde transport) and shuttle “old” mitochondria to the soma for degradation (retrograde transport). This intricate link between mitochondrial dynamics and turnover makes mitostasis a logistical challenge for neurons, especially for extended projection-type neurons such as those affected by Amyotrophic lateral sclerosis (ALS) or Parkinson’s disease (PD). As a solution to this problem, local mechanisms for mitochondrial turnover have been proposed, although the interplay between such local and global forces largely remains unknown *in vivo*. In particular, whether local, compartment-specific mechanisms of mitostasis determine the synapse-specific vulnerability in disease remains unknown. The aim of this thesis is to explore these questions via a novel optical ‘pulse-chase’ assay. Based on transgenic mice that express photoswitchable proteins in neuronal mitochondria, this assay allowed tracking mitochondria on a single-organelle level over an extended period. Due to its relevance in motor neuron disease, as well as its excellent experimental accessibility and large size, the mature neuromuscular junction was used as a model synapse. This approach allowed me to sketch multiple aspects of the ‘lifecycle’ of synaptic mitochondria *in situ*: (1) on the one hand, “new” mitochondria are specifically targeted to synaptic sites via fast anterograde transport from the soma to share their contents with the residual pool of synaptic mitochondria via fusion, which constitutes a unique behavior uncharacteristic of typical stationary axonal mitochondria. (2) On the other hand, the bulk (75%) of mitochondrial degradation occurs directly at the synapse, where a reiterative degradation system of perinodal “checkpoints” was discovered that establishes mitochondrial mass balance. This system captures dysfunctional mitochondria from the retrograde stream of moving mitochondria and redirects them to local “hotspots” of lysosomal degradation, refuting the canonical textbook view that long-range retrograde transport is responsible for most mitochondrial elimination in axons. In murine models of motor neuron disease, this mechanism was largely amplified. Interestingly, this distal mechanism was mediated via optineurin, a motor neuron disease-related mitophagy adaptor, but not by PINK1 and parkin, which are mitophagy

mediators implicated in Parkinson's disease. This leads to the conclusion that *in situ* mitostasis is a highly compartmentalized process with implications for cell type- and compartment-specific vulnerability in neurodegenerative diseases. To summarize, optical 'pulse-chase' imaging allows important insights into how mitostasis is established within neurons and will hopefully present as a useful tool to further investigate mitostasis in future work.

Zusammenfassung

Nervenzellen dehnen ihre Ausläufer sehr weit aus, um spezielle Kontaktstellen – Synapsen – mit anderen Zellen zu bilden. Der Verlust von Synapsen liegt vielen verheerenden Erkrankungen des Nervensystems zugrunde, beginnend mit der Degeneration von Nervenenden, bevor sich die Pathologie in einem „Dying-back“-Muster langsam in Richtung Zellkörper ausbreitet. Mitochondrien sind vielschichtige Organellen, die die Funktion von Synapsen maßgeblich beeinflussen, indem sie neben vielen anderen Aufgaben Energie in Form von ATP bereitstellen, Ca^{2+} -Ionen puffern und Neurotransmitter metabolisieren. Die Aufrechterhaltung einer angemessenen Anzahl und Qualität der Mitochondrien („Mitostase“) gilt als Schlüsselprozess für gesunde Synapsen. Im Gegensatz zum Soma wird jedoch angenommen, dass Axonen und Synapsen die meisten Mechanismen für den mitochondrialen Umsatz, insbesondere für die Biogenese und den Abbau von Mitochondrien, fehlen. Stattdessen entwickelte sich axonaler Transport, um periphere Mitochondrien kontinuierlich durch „neue“ Mitochondrien aus dem Soma zu ersetzen (anterograde Transport) und „alte“ Mitochondrien zum Abbau in Richtung Soma zu transportieren (retrograde Transport). Dieser komplizierte Zusammenhang zwischen mitochondrialer Dynamik und Umsatz macht die Mitostase zu einer logistischen Herausforderung für Neuronen, insbesondere für Neuronen vom Projektionstyp, die beispielsweise von Amyotropher Lateralsklerose (ALS) oder der Parkinson-Krankheit (PD) betroffen sind. Als Lösung für dieses Problem wurden lokale Mechanismen für den mitochondrialen Umsatz vorgeschlagen, wobei das Zusammenspiel zwischen solchen lokalen und globalen Kräften *in vivo* weitgehend unbekannt ist. Insbesondere bleibt unklar, ob lokale, kompartimentspezifische Mechanismen der Mitostase die synapsenspezifische Anfälligkeit für Krankheiten bestimmen. Das Ziel dieser Arbeit ist es, diese Fragen mithilfe eines neuartigen optischen „Pulse-Chase“-Assays zu untersuchen. Basierend auf transgenen Mäusen, die photoschaltbare Proteine in neuronalen Mitochondrien exprimieren, ermöglichte dieser Assay die Verfolgung von Mitochondrien auf der Ebene einzelner Organellen über einen längeren Zeitraum. Aufgrund ihrer Relevanz bei Motoneuronenerkrankungen sowie ihrer guten experimentellen Zugänglichkeit wurde die reife neuromuskuläre Verbindung als Modellsynapse verwendet. Dieser Ansatz ermöglichte es, mehrere Aspekte des „Lebenszyklus“ synaptischer Mitochondrien *in situ* zu skizzieren: (1) Einerseits werden „neue“ Mitochondrien über schnellen anterograden Transport vom Soma gezielt zu synaptischen Standorten geleitet, um ihren Inhalt mit den ansässigen synaptischen Mitochondrien durch Fusionen zu teilen, was ein für stationäre axonale Mitochondrien untypisches Verhalten darstellt. (2) Zum Anderen findet der Großteil (75 %) des mitochondrialen Abbaus direkt an der Synapse statt, wo ein sich wiederholendes Abbausystem perinodaler „Kontrollpunkte“ entdeckt wurde, das ein mitochondriales Massengleichgewicht herstellt. Dieses System fängt dysfunktionale Mitochondrien aus dem retrograden Strom sich bewegender

Mitochondrien ein und leitet sie zu lokalen „Hotspots“ des lysosomalen Abbaus um. Das widerlegt die übliche Lehrbuchansicht, welche besagt, dass retrograder Transport für den Großteil des mitochondrialen Umsatzes in Axonen verantwortlich ist. In Mausmodellen für Motoneuronenerkrankungen wurde dieser Mechanismus in besonderem Ausmaß verstärkt vorgefunden. Interessanterweise wurde dieser distale Kontrollmechanismus über Optineurin vermittelt, einen Mitophagie-Adapter der im Zusammenhang mit Motoneuronenerkrankungen steht, jedoch wurde der Mechanismus nicht über PINK1 und Parkin vermittelt, welche Mitophagie-Mediatoren sind, die an der Parkinson-Krankheit beteiligt sind. Dies führt zu der Schlussfolgerung, dass die Mitostase *in situ* ein stark kompartimentierter Prozess ist, mit möglichen Auswirkungen auf die zelltyp- und kompartimentspezifische Anfälligkeit bei neurodegenerativen Erkrankungen. Zusammenfassend lässt sich sagen, dass die optische „Pulse-Chase“-Bildgebung wichtige Einblicke in die Entstehung der Mitostase innerhalb von Neuronen ermöglicht und sich hoffentlich als nützliches Werkzeug zur weiteren Untersuchung der Mitostase in zukünftigen Arbeiten erweisen wird.

Table of Contents

1. Introduction.....	1
1.1. Neuronal architecture.....	3
1.1.1. Projection-type neurons.....	3
1.1.2. Neuromuscular synapses.....	6
1.2. Mitochondria.....	9
1.2.1. Ultrastructure and function.....	10
1.3. Mitochondrial dynamics.....	13
1.3.1. Fission.....	13
1.3.2. Fusion.....	14
1.3.3. Motility and anchoring.....	16
1.4. Mitochondrial turnover.....	18
1.4.1. Mitochondrial birth.....	19
1.4.2. Mitochondrial degradation.....	20
1.5. Neuronal mitostasis.....	21
1.5.1. Mitochondrial specialization in neurons.....	22
1.5.2. Matching to local demands.....	24
1.5.3. Quality control in neurons.....	26
1.6. Aims of the thesis.....	28
2. Materials and Methods.....	30
2.1. Experimental animal models.....	30
2.1.1. Transgenic reporter lines.....	30
2.1.2. Knock-out and disease models.....	31
2.1.3. Generation of mouse lines.....	32
2.2. Molecular biology.....	32
2.2.1. Genotyping.....	32
2.2.2. Molecular cloning.....	33
2.2.3. Generation of adeno-associated virus (AAV) particles.....	35
2.3. Surgery.....	35
2.3.1. Neonatal injection of AAV into brain ventricles.....	35
2.3.2. Photoconversion of the intercostal nerve <i>in vivo</i>	35
2.3.3. <i>In vivo</i> imaging in sternomastoid muscles.....	36
2.4. Tissue preparation and microscopy.....	36
2.4.1. Acute nerve-muscle explants and widefield live microscopy.....	36

2.4.2.	Photoswitching protocol	37
2.4.3.	Vital dyes and live compounds	38
2.4.4.	Tissue fixation and histology	39
2.4.5.	Confocal and Airy scan microscopy	40
2.4.6.	Electron microscopy.....	40
2.5.	Data analysis.....	41
2.5.1.	Fluorescence intensity and UV-dose-response curves.....	41
2.5.2.	Mitochondrial transport and shape.....	42
2.5.3.	Tracking and organelle motility analysis	43
2.5.4.	Mitochondrial capture experiments	44
2.5.5.	Lysosome distribution in axon terminals	44
2.6.	Image representation	45
2.7.	Statistical analysis.....	45
2.8.	Buffers and solutions.....	46
3.	Results	48
3.1.	Optical pulse-chase imaging assay.....	49
3.2.	Resolving mitochondrial shape	54
3.3.	Anterograde delivery of mitochondria to synapses	59
3.3.1.	Mitochondrial turnover rate in synapses	59
3.3.2.	Destination of anterograde transport	60
3.3.3.	Modes of mitochondrial delivery	62
3.3.4.	Mitochondrial fusions in synapses	66
3.4.	Mitochondrial degradation in synaptic terminals	68
3.4.1.	Synaptic mitochondria are partly removed by retrograde transport	68
3.4.2.	Synaptic mitochondria are captured before exiting the NMJ.....	69
3.4.3.	Mitochondrial capture occurs at distal nodes of Ranvier.....	71
3.4.4.	Damaged mitochondria are preferentially captured	74
3.4.5.	Mitochondrial capture in motor neuron disease	76
3.4.6.	Hotspots of lysosomal activity in axon terminals.....	79
3.4.7.	Mitophagy dynamics in axon terminals	81
3.4.8.	The PINK1/parkin pathway is not essential for mitochondrial capture	83
3.4.9.	Optineurin mediates mitochondrial capture.....	86
4.	Discussion.....	88
4.1.	Methods to study mitochondrial fate <i>in vivo</i>	89

4.2.	Renewal of synaptic mitochondria	92
4.3.	Distribution by anterograde transport	93
4.4.	Linking fusion and anterograde transport.....	94
4.5.	Compartmentalized mitophagy pathways	96
4.6.	Mitochondrial diversity and neuronal compartmentalization	99
4.7.	Future directions	101
5.	Danksagung	103
6.	References	104

1. Introduction

“[...] I believe the brain to be the most potent organ in the body. So long as it is healthy, it is the interpreter of [...] consciousness [...] and comprehension. [...] This is my reason for asserting that the diseases which attack the brain are the most acute, most serious and most fatal [...].”

The Sacred Disease, Hippocrates (ca. 400 BC)

Disorders of the nervous system belong to the leading causes of death and disability in the early 21st century, placing a substantial burden on society (Chin & Vora, 2014; GBD Neurology Collaborators, 2019; World Health Organization, 2020). A healthy nervous system allows one to assimilate information about the environment (perception) and to integrate those perceptions with internal states and memory (intelligence) for responding accordingly (action; Kandel et al., 2021); however, a diseased nervous system severely limits those fundamental aspects of human life. Neurodegenerative diseases such as Alzheimer’s (AD), Parkinson’s (PD), or Amyotrophic lateral sclerosis (ALS) are characterized by a slowly progressive decay of nerve cells (*neurons*) over time (Salvadores et al., 2017). Most neurons are terminally differentiated (non-dividing) cells of beautiful complexity, which makes them lack substantial regenerative capacities, resulting in neuronal cell death being mostly irreversible (Li & Chen, 2016; Mahar & Cavalli, 2018). In most neurodegenerative diseases, a specific neuronal subpopulation is affected first and foremost before the degeneration spreads to other regions of the nervous system (Chen & Herrup, 2008; Fu et al., 2018; Saxena & Caroni, 2011). Degeneration of specific neuronal subpopulations reflects the characteristic driving symptoms of a disease: for example, motor neuron diseases such as Amyotrophic lateral sclerosis (ALS) are primarily characterized by progressive paralysis (Boillee et al., 2006; Bruijn et al., 2004), whereas basal forebrain cholinergic neuron loss experienced in Alzheimer’s results in complex psychiatric symptoms such as memory loss (Schliebs & Arendt, 2011). The cause of this ‘selective vulnerability’ remains puzzling (Saxena & Caroni, 2011), especially considering how many affected molecular pathways are shared among common neurodegenerative diseases (Gan et al., 2018; Henstridge et al., 2016; Wilson et al., 2023). The term ‘selective vulnerability’ could also be used to appreciate another peculiarity: the distal regions of neurons, especially those carrying synapses, are the most vulnerable compartments (Fu et al., 2018) and degenerate early on before cells die as a whole (Adalbert & Coleman, 2013; Salvadores et al., 2017). For example, Alzheimer’s and Parkinson’s disease are typically considered synaptopathies (Imbriani et al., 2018; Kneynsberg et al., 2017; Meftah & Gan, 2023; Wong et al., 2019; Zott et al., 2018). Similarly, motor neurons degenerate in a ‘dying-

back' pattern, where the pathology initiates distally then slowly spreads retrogradely towards the soma (Alhindi et al., 2021; Cappello & Francolini, 2017; Chung et al., 2017; Dadon-Nachum et al., 2011; Fischer et al., 2004; Fischer & Glass, 2007; Orr et al., 2020). Understanding specific mechanisms that maintain the neuronal periphery may be useful in explaining neurodegenerative pathogenesis, and cell-type specific differences in synaptic maintenance pathways might explain disease-specific cellular vulnerability (Dadon-Nachum et al., 2011; Fu et al., 2018; Wong et al., 2019).

Neurons have developed intricate mechanisms to maintain homeostasis in their neurites: intracellular transport, cytoskeletal stability and plasticity, protein and organelle turnover by autophagy and proteasomes, control over RNA localization and localized translation, and support by Glia cells are just a few examples (Cioni et al., 2018; Maday, 2016; Maday et al., 2014; Nave, 2010; Wang et al., 2012). These maintenance mechanisms are key to neuronal health, the cost of their failure being evidenced in neurodegenerative disease (**Figure 1.1**; Gan et al., 2018; Mead et al., 2023; Wilson et al., 2023). In particular, mitochondria are small but important organelles that lie at the heart of axonal maintenance (**Figure 1.1**; Misgeld & Schwarz, 2017).

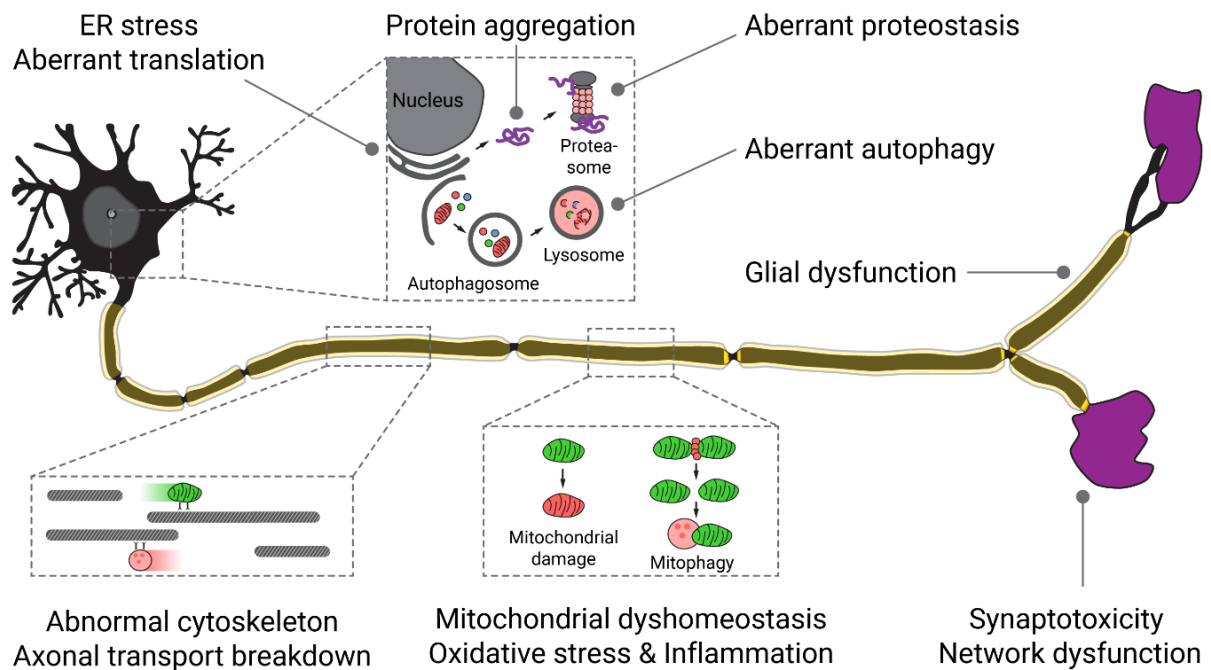


Figure 1.1 | Disrupting the mechanisms that maintain axonal homeostasis is a key factor in neurodegenerative diseases. Modified from Gan et al. (2018); Mead et al. (2023); Wilson et al. (2023).

Mitochondria play an exceptional role in maintaining brain function, as they provide energy in the form of ATP, buffer cytosolic Ca^{2+} ions, and metabolize neurotransmitters while fulfilling many other important tasks (Kann & Kovacs, 2007; Picard & McEwen, 2014). The brain is an “energy-hungry” organ that consumes a disproportionate amount of energy: Humans allocate 20% of their

body's oxygen consumption to the brain, even though it only makes up ~2% of body weight (Harris et al., 2012; Kety, 1957; Mink et al., 1981; Rolfe & Brown, 1997), underscoring the extraordinary importance of neuronal mitochondria for ATP supply (Attwell & Laughlin, 2001; Harris et al., 2012; Howarth et al., 2012). Disrupting mitostasis in any manner has detrimental effects on cellular health. Perhaps not surprisingly, mutations and deletions of mtDNA cause severe developmental syndromes that primarily affect high-energy organ systems such as the brain (Tuppen et al., 2010; Vafai & Mootha, 2012). Moreover, the vast majority of neurodegenerative diseases are associated with mitochondrial defects (De Vos et al., 2008; Hafezparast et al., 2003; Maday et al., 2014; Mariano et al., 2018; Nunnari & Suomalainen, 2012; Rugarli & Langer, 2012), and mitochondrial dysfunction has been identified as a major contributor to aging, which is also an important risk factor to develop a neurodegenerative disease (Balaban et al., 2005; Ghosh-Choudhary et al., 2021; Lopez-Otin et al., 2023). Interestingly, the largest component of ATP is not consumed by the neuronal cell body but by its distal, synapse-bearing arborizations (Harris et al., 2012), suggesting a hypothetical link between regional mitochondrial vulnerability and “dying-back” neurodegeneration.

The functional, molecular, and morphological processes that govern ‘mitochondrial function’ versus ‘mitochondrial dysfunction’ have been studied extensively in various cultured cell systems that aimed at “boosting” mitochondrial function in therapeutic or anti-aging settings (Monzel et al., 2023). While important insights have been gained from reductionist cell cultures, transferring the knowledge to the *in vivo* situation is not trivial, as mitochondria are extremely malleable organelles that adapt to their environment in cell-type-specific manners (Misgeld & Schwarz, 2017). Specifically, the abundant diversity that mitochondria display means that something that is considered a “function” in one cell type may very well manifest as a “dysfunction” in another cell type (Monzel et al., 2023). This argues that to fully understand (and potentially treat) mitochondrial pathology in neurodegenerative disease, it will be key to elucidate the fundamental mechanisms of mitochondrial maintenance in tissues with fully matured neurons. The diversity of mitochondrial function and morphology in different neuronal compartments suggests that neurons maintain mitochondria using compartment-specific mechanisms (Collins et al., 2002; Monzel et al., 2023; Pekkurnaz & Wang, 2022).

1.1. Neuronal architecture

1.1.1. Projection-type neurons

Over 100 years ago, Santiago Ramon y Cajal pioneered modern neuroscience by using innovative histological techniques to propose the *neuron doctrine*, identifying the individual

neuron as the basic structural and functional unit of the nervous system (Yuste, 2015). Neurons are an extreme case of cellular polarization, forming functionally distinct, elaborate *subcompartments* (Craig & Banker, 1994; Takano et al., 2015). Specifically, multiple thin processes (*neurites*) protrude from the cell body (*soma* or *perikaryon*) to connect to other cells via *synapses* (Kandel et al., 2021), which allows neurons to form specialized circuits to fulfill specific computations. Neurites are subdivided to allow information flow in a directional manner: multiple short *dendrites* receive synaptic input from other cells and send it towards the soma, whereas a single long process called *axon* transmits these signals from the soma to other cells (Takano et al., 2015). Interestingly, the cytoplasmic volume of most neurites largely surpasses the volume of the soma, which enables neurons to form thousands of synapses and establish a huge variety of potential circuit wiring patterns (Luo, 2021; Misgeld & Schwarz, 2017). The diversity of neuronal circuits results in an impressive variability of neuronal morphology *in vivo* (Luo, 2021; Miterko et al., 2018; Richards & Van Hooser, 2018).

Projection-type neurons are some of the most “extreme” examples when comparing neuronal architectures, as these neurons develop axons that can span many meters in length (Misgeld & Schwarz, 2017). For example, reconstructions in the rat brain showed that dopaminergic neurons of the substantia nigra pars compacta (SNc) directly project a small-caliber, mostly unmyelinated axon from a tiny soma—~ 100 μm in diameter—across the brain only to branch profusely once it reaches the striatum (Matsuda et al., 2009). This massive distal axonal arborization reaches a total length of ~50 cm with hundreds of thousands of synapses (Bolam & Pissadaki, 2012; Matsuda et al., 2009), exceeding the number of synapses formed by other basal ganglia neurons by two orders of magnitude (Bolam & Pissadaki, 2012; Matsuda et al., 2009). Extrapolation of these findings to human SNc dopaminergic neurons estimates millions of synapses and many meters of total axon length (Bolam & Pissadaki, 2012). Other projection-type neurons, such as cholinergic neurons or neurons of the corticospinal tract, have very similar characteristics—initially projecting a very long and unbranched axon up to many meters (termed proximal or ‘stem axon’) to innervate its targets via a highly branched distal arborization that bears the synapses (see next section on cholinergic neurons, also **Figure 1.2**). (Misgeld & Schwarz, 2017)

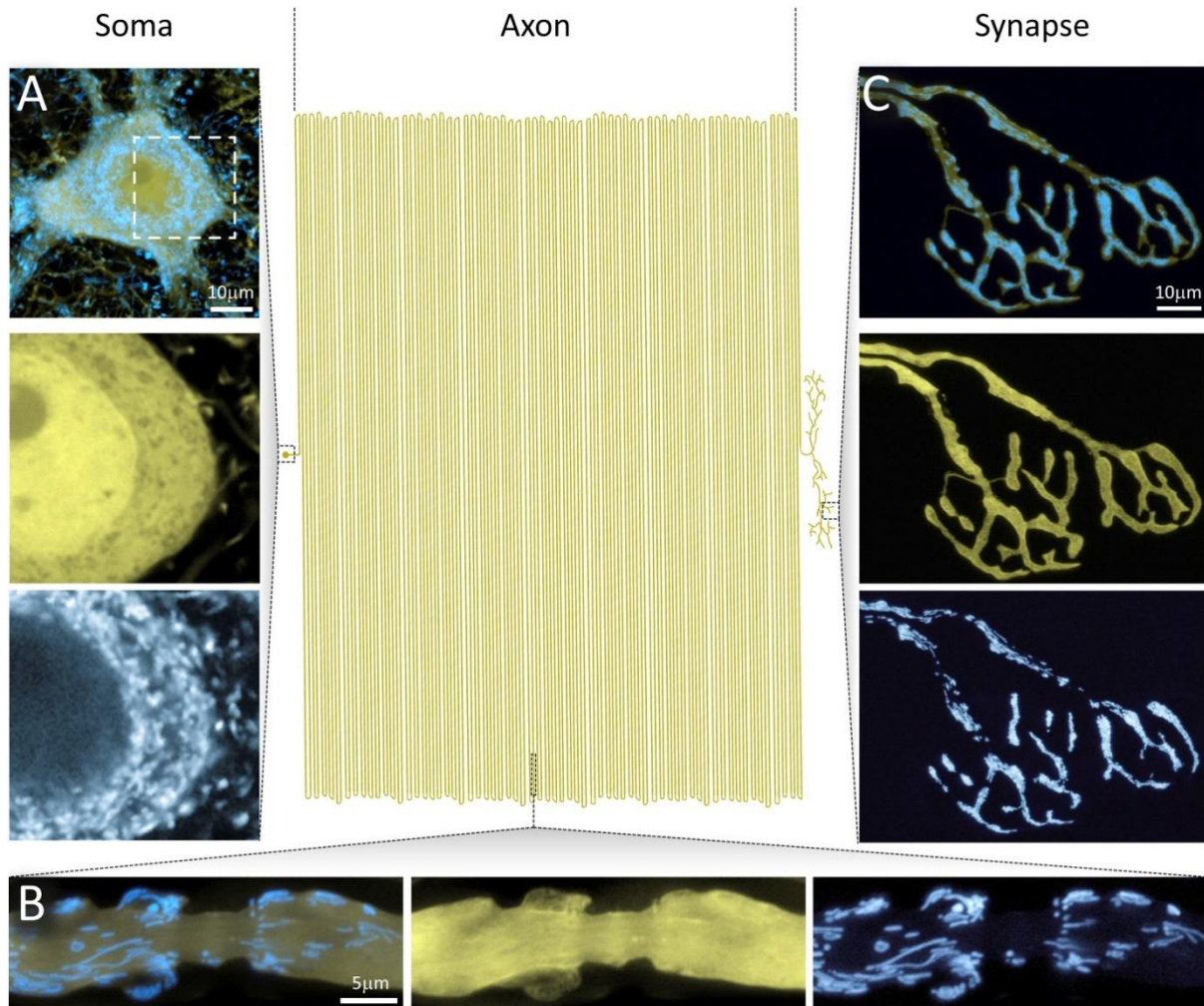


Figure 1.2 | Architecture of a mature mouse α -motor neuron (yellow, cytoplasm) with labeled mitochondria (blue). **a** soma, **b** axons, **c** neuromuscular junctions in the transgenic mouse line *Thy1-YFP-16* (yellow, neuronal cytoplasm) \times *Thy1-mito-CFP* (blue, mitochondria). This work has been re-printed from Misgeld and Schwarz (2017) with permission from Elsevier under Rightslink License-No. 5704741048469.

Neurons face unique challenges in maintaining their morphology—how neuronal *compartmentalization* is established and maintained over a lifetime remains a fundamental question in neuronal cell biology (Craig & Banker, 1994; Guedes-Dias & Holzbaur, 2019). Maintaining large axonal arbors is more stressful than maintaining smaller arbors (Pacelli et al., 2015), and projection-type neurons with large axonal arbors are known to be more vulnerable to neurodegeneration (Braak & Del Tredici, 2009). The extreme geometry of these neuron types has been suggested to contribute to their selective vulnerability in neurodegenerative diseases (Bolam & Pissadaki, 2012; Surmeier et al., 2017). Large axonal trees consume extraordinary amounts of energy and are more vulnerable to reduced oxygen and glucose levels (Bolam & Pissadaki, 2012; Fu et al., 2018; Hunn et al., 2015), which is primarily metabolized by mitochondrial oxidative phosphorylation (Kety, 1957; Sokoloff, 1960). To supply the demand for nutrition at these axons' distal sites, neurons developed an intricate axonal transport machinery to shuttle components such as mitochondria between the soma and the periphery (MacAskill &

Kittler, 2010; Maday et al., 2014; Misgeld & Schwarz, 2017; Nicholls & Ferguson, 2013; Sheng, 2014). In projection-type neurons, axonal health is thought to depend excessively on cellular trafficking, as defects of this machinery preferentially result in the degeneration of these neurons (Hunn et al., 2015). Looking at the dimensions of a projection-type neuron (**Figure 1.2**), it seems astounding how the small soma can assume and coordinate the entire turnover of an axonal tree that surpasses its dimensions by a multitude. As a matter of fact, some reports suggest that there might be a “limit” (i.e., axon length, branch complexity) at which an arbor becomes too metabolically demanding to receive an adequate supply, resulting in a switch of axon homeostasis toward local mechanisms (Hagemann et al., 2022). In a disease-related model (“stressor threshold” model), neurons that have intrinsic homeostasis “weaknesses” are those that experience selective (i.e., early) vulnerability to neurodegeneration when compared to “resistant” neurons (Saxena & Caroni, 2011). Axon branch size and complexity might be such a “weakness” (Misgeld & Schwarz, 2017).

1.1.2. Neuromuscular synapses

The *neuromuscular junction* or endplate (NMJ) is a synapse connecting cholinergic α -motor neurons with skeletal muscle cells, responsible for all voluntary muscle contraction. These junctions are supplied by thickly myelinated axons that conduct action potentials at high speed (A α fiber type). α -Motor axons are part of the peripheral nervous system, with their myelination being provided by *Schwann cells* that cover the arbor from *axon hillock* to NMJs in a continuous manner, being only periodically interrupted by *nodes of Ranvier* for action potential propagation. A node of Ranvier is constructed in a stereotypical manner: the unmyelinated area, i.e. the proper ‘node’ contains Na⁺ voltage-gated channels (Nav; Girault & Peles, 2002), while the myelinated regions that frame the ‘node’ are further subdivided into three regions (Poliak & Peles, 2003). (1) Two *paranodes* frame the ‘node’ and tightly attach each myelin lamella via paranodal ‘loops’ that contain anchoring proteins (e.g., caspr) to the axolemma, (2) two bilateral *juxtaparanodes*, which are located beneath the compact myelin next to the paranodes, and (3) the *internode*, which describes a long stretch of the axon that is covered by compact myelin between two nodes of Ranvier (Poliak & Peles, 2003). The segregation of these different domains depends on specific sorting and anchoring mechanisms via cell-adhesion molecules (CAMs) and specialized cytoskeletal elements, and may also involve molecular filters and barriers within the membrane (Eichel & Shen, 2022; Poliak & Peles, 2003). Both the first node (at the axon hillock) and the terminal nodes (at the NMJ) appear distinct from other nodes. Being myelinated on just one side, these regions contain only one paranodal specification and are, therefore, termed *heminodes*. While little is known about the terminal heminodes close to the junction, the proximal heminode has been well-characterized for its many unique features (Eichel & Shen, 2022). For example,

the axon hillock is thought to provide a diffusion barrier (Kobayashi et al., 1992; Nakada et al., 2003; Winckler et al., 1999) and control axonal transport by “selecting” the organelles that are allowed to pass between soma and axon (Farias et al., 2015; Koppers & Farias, 2021). (Girault & Peles, 2002; Poliak & Peles, 2003; Sanes & Lichtman, 2001)

The motor axons arise from the ventral horn of the spinal cord and travel through the body with little branching before diving into their target muscle. As a motor axon approaches a muscle cell (or *muscle fiber*), it divides into fine branches (**Figure 1.2**) that arrange themselves in so-called *end-plate bands* near the center of the muscle fibers. Right at its target muscle fiber, where the terminal branch loses its myelin sheath, forms a tripartite synaptic structure: (1) the presynaptic motor neuron connecting to the (2) postsynaptic muscle fiber, with the contact site being covered by (3) terminal non-myelinating Schwann cells. The connectivity pattern of motor neurons is characterized by high divergence: a single neuron connects to multiple muscle fibers that are excited all together, forming a so-called *motor unit*. Average motor unit size is muscle-specific: the smaller the motor units, the more precisely the muscle can be moved. During muscle action, neurons with small motor units are activated first, and only if the resulting force is insufficient for the task will neurons with larger units be recruited. This orderly recruitment pattern is also known as Henneman's size principle (Henneman et al., 1965). In adult mammals and most other vertebrates, each muscle fiber typically receives input from exactly one motor axon terminal. Most likely, the reason for this is to ensure that each muscle fiber does not get multiple contradictory inputs that have the possibility to cancel each other out due to the refractory period on the muscle membrane (Meirovitch et al., 2023). With just one input per muscle fiber, neuromuscular junction transmission must be fail-proof (all-or-nothing-principle). This is an important difference to cortical neurons, where multiple synaptic sites are formed between two neurons and where failure of a subset of the synaptic sites does not automatically pose a problem (Harris et al., 2012). (Rubenstein & Rakic, 2013; Sanes & Lichtman, 1999; Wood & Slater, 2001)

Motor neurons have, therefore, developed various safety mechanisms to ensure reliable neurotransmission (Wood & Slater, 2001). This is expressed as the so-called *safety factor*, which simply means that the postsynaptic membrane is depolarized by a much larger degree than is necessary for reaching the postsynaptic action potential threshold (Wood & Slater, 2001). This principle protects neurotransmission from failure even under prolonged muscle exercise, and is compromised in many motor diseases (Wood & Slater, 2001). Animals have developed different strategies to manifest a high safety factor. In most species, NMJs are gigantic structures when compared to most CNS synapses (300 μm^2 vs. 1 μm^2 ; Kleele et al., 2014; Sanes & Lichtman, 2001). This immense enlargement directly increases the quantal amount and thus the neurotransmitter amount that can be released per stimulus. Glutamatergic CNS synaptic boutons, on the other hand, are restricted to $\sim 1 \mu\text{m}$ to accommodate short diffusion distances to astrocytes for rapid glutamate clearance (Attwell & Gibb, 2005). (Wood & Slater, 2001)

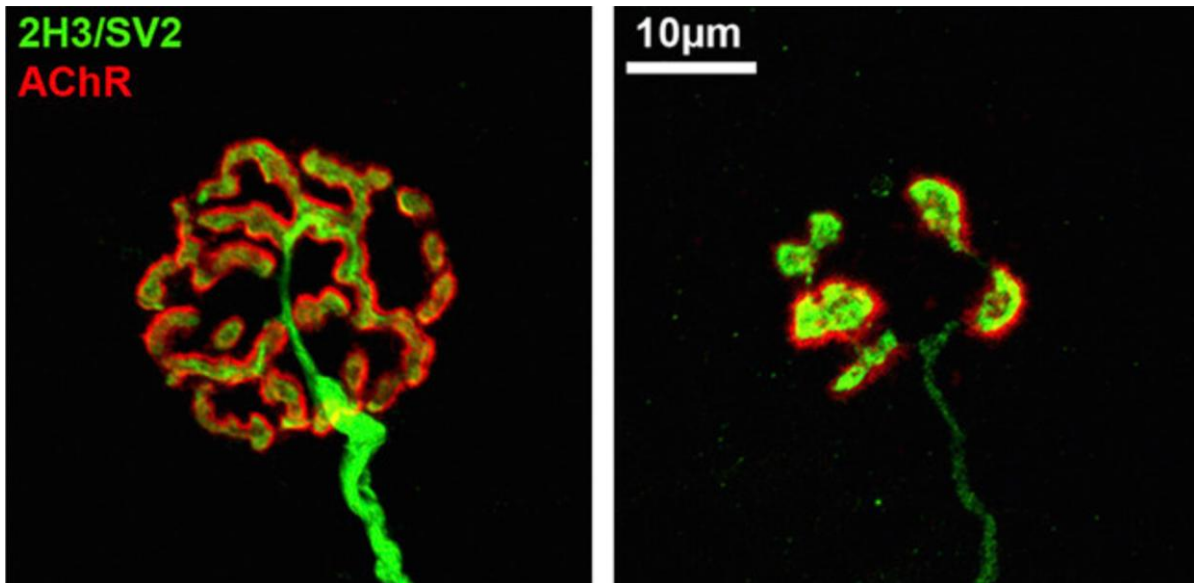


Figure 1.3 | Heterogeneity of neuromuscular junction morphology in different species. Left: mouse (*Mus musculus*), right: human junction. Green: presynaptic axon, red: postsynaptic membrane. The figure was adapted from Jones et al. (2017) under the Creative Commons license.

Paradoxically, smaller animals can sometimes maintain the largest NMJs (**Figure 1.3**). Rather than sizing NMJs up, larger animals opt for enhancing transmission efficacy on the postsynapse: the postsynaptic plaque is highly folded to increase the density of acetylcholine receptors (AChR). Synapses are generally considered to be areas that undergo high metabolic stress (Milton & Sweeney, 2012; Verma et al., 2022), with NMJs, in addition, having to withstand constant mechanical stress. Considering that nutrient commutes take much longer in axons of large animals, maintaining NMJs might become progressively uneconomical in these species. It seems that the geometry compels motor neurons to strike a balance between maximizing function and minimizing maintenance efforts (Wood & Slater, 2001). As a general principle, the nervous system strives to minimize the amount of consumed energy in ratio to transmitted information (Harris et al., 2012). (Wood & Slater, 2001)

The neuromuscular junction is a classic system that has served neuroscientists well for over a century to discover principles in synaptic physiology (Del Castillo & Katz, 1954; Tansey, 2006). Not only is it a well-established and characterized model system, but also highly accessible to *in vivo* imaging due to its placement and large size (Bianchi, 2018; Sanes & Lichtman, 2001). The conclusion that motor axon branches and their NMJs are highly vulnerable and disease-relevant structures that live “right on the edge” between fragility and stability (Bolam & Pissadaki, 2012) further underscores the high relevance of this model system for the study of axonal maintenance mechanisms.

1.2. Mitochondria

The 19th century featured the advent of light microscopy, the first tool that enabled the discovery of subcellular structures. The term ‘mitochondria’ was first coined by the pathologist Carl Benda to describe some peculiar intracellular granules (Greek *mitos*) forming threads (Greek *chondria*) that he observed upon staining cells with crystal violet (Benda, 1898). In earlier years, other microscopists had described similar structures: Richard Altmann observed ubiquitous subcellular structures he termed “bioblasts” (Altmann, 1890; **Figure 1.4**), which he noted for their similarity to bacteria, believing to have found metabolically and genetically autonomous entities that he considered the “elementary units of life”. (Cowdry, 1953; O'Rourke, 2010)

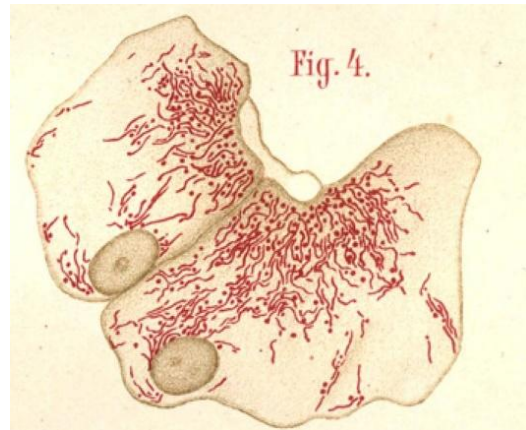


Figure 1.4 | Early accounts of mitochondria. Altmann’s drawing from the 19th century showing “bioblasts” in a frog liver cell (adapted from Altmann, 1890).

Indeed, mitochondria are small but vital organelles that reside in all but a few eukaryotic cells (Gronowicz et al., 1984; Karnkowska et al., 2016). From an evolutionary perspective, they are ancient cousins to bacteria, most likely originating from a symbiosis of oxidative proteobacteria that were engulfed by a nucleated, glycolytic host cell (Martijn et al., 2018; Roger et al., 2017; Sagan, 1967). Like their ancestors, mitochondria also procreate by division from one another and carry multiple copies of their own circular DNA (‘mtDNA’; Protasoni & Zeviani, 2021). However, most mitochondrial genes were ultimately transferred to the host nucleus, and a complex import machinery co-evolved to supply mitochondria with nuclear-encoded proteins (Dolezal et al., 2006; Neupert & Herrmann, 2007). Mitochondria became central to the life of a cell by serving as central hubs of metabolism and signaling (Shen et al., 2022). The most distinctive function of mitochondria is their unique ability to use oxygen in energy metabolism (*aerobic respiration*). Mitochondria contain *electron transport chain* (ETC) proteins on their inner membrane to generate a potential across the inner membrane and create a pH difference, which is used to drive *oxidative phosphorylation*: intermediates from the catabolism of carbohydrates are oxidized to form adenosine triphosphate (ATP), the main energy carrier in cells. (Hatefi, 1985)

As much as mitochondria form a dependency on their host, the reverse also holds true: both entities regulate each other’s functions in a bidirectional relationship (see the following chapters for more details). Specifically, cells employ two strategies for shaping their mitochondrial population: (1) cells optimize each mitochondrion’s function to meet the cells’ specific needs at a given time and location, (2) cells constantly check mitochondrial quality to maintain an adequate

number of healthy mitochondria, which is summed up by the term ‘mitostasis’ (mitochondrial homeostasis; Lopez-Domenech & Kittler, 2023; Misgeld & Schwarz, 2017).

- 1) *Mitochondrial dynamics*. The ability to fine-tune mitochondrial function is crucial for cells facing diverse functional demands within tissues (Mannella et al., 2013). For example, mitochondrial proteomes vary immensely among different cell types and tissues (Fecher et al., 2019; Pagliarini et al., 2008). Mitochondrial function is intimately linked to its structure, and tweaking one automatically affects the other (Benard et al., 2007; Bulthuis et al., 2019; Quintana-Cabrera & Scorrano, 2023). Functional diversity is accordingly reflected in the structural diversity across different cell types and tissues (Neupert, 2012). Besides cell-type specific expression patterns of mitochondrial proteins, cells also tailor mitochondrial structure and function via mitochondrial dynamics. For example, based on *fusion* and *fission*, mitochondria can form complex architectures that serve different purposes. In addition, mitochondria are *mobile*, which allows cells to distribute and *anchor* different mitochondria at different sites of need. (Misgeld & Schwarz, 2017)
- 2) *Mitochondrial turnover*. Mitochondria have a complex, semi-autonomous lifecycle. Mitochondria age over time due to accumulating damage: Reactive oxygen species, which are a toxic by-product of oxidative phosphorylation, are thought to damage multiple cellular components, but particularly mitochondria and their DNA (Balaban et al., 2005). Mitochondrial dysfunction is a major contributor to aging and, therefore, to age-associated diseases (Balaban et al., 2005; Brawek et al., 2010; Nicholls, 2004). Due to this, cells have developed extensive quality control mechanisms that ensure that damaged mitochondria can be discarded (*degradation*) and replaced by new, healthy ones (*biogenesis*; Ploumi et al., 2017; Popov, 2020).

1.2.1. Ultrastructure and function

Mitochondrial form and function are in a reciprocal relationship, and one cannot be fully understood without the other: Mitochondrial (dys)function alters the shape and organization of mitochondria, but the structure of a mitochondrion also affects its function (Benard et al., 2007; Bulthuis et al., 2019; Quintana-Cabrera & Scorrano, 2023). Mitochondrial shape is closely regulated at multiple scales: (1) internal structure (ultrastructure), (2) single organelle shape, and (3) at the mitochondrial network level (Glancy et al., 2020).

The internal architecture of mitochondria is fashioned according to a common blueprint. Mitochondria are compartmentalized organelles, which spatially segregate enzymes and metabolites to control biochemical reactions (Iovine et al., 2021). Specifically, this is achieved by two membrane encasements, the outer and inner membrane, which differ in function and origin (Glancy, 2020). The outer membrane is a semi-permeable barrier to the cytosol and contains

various signaling molecules allowing mitochondria to communicate with their environment. The inner membrane is very tortuous and has multiple dynamic invaginations, termed *cristae*, which fill the mitochondrial internal space (the matrix) to a large extent (Palade, 1952; Sjostrand, 1953). Mitochondria actively build an electrical proton gradient across the inner membrane, thereby storing energy that can be converted into ATP molecules. This energy conversion is established by the protein complexes of the *electron-transfer chain* (ETC), which lie within the cristae membranes. The cristae are a primary site of reactive oxygen species (ROS) production, a by-product of oxidative phosphorylation (Balaban et al., 2005). Single cristae can form functionally independent microcompartments with different membrane potentials (Wolf et al., 2019) and individualized synthesis of ETC proteins (Zorkau et al., 2021). The inner membrane potential is required for proper mitochondrial function—not only for energy production but also for mitochondrial protein import (Harbauer et al., 2014; Huang et al., 2002; Martin et al., 1991). (Glancy, 2020)

The *matrix* contains the mitochondrial genetic system and protein synthesis apparatus. Only 13 proteins (in humans) are encoded by mtDNA—the essential components of the respiratory complexes—thus retaining oxidative phosphorylation as the only process under direct mitochondrial control. Retaining these genes has either occurred to prevent ETC proteins from mislocalizing onto other organelles (Bjorkholm et al., 2017), or to enable the fine-tuning of these crucial complexes by feedback from local stress (Allen, 2015). The matrix also contains the enzymes of several essential metabolic pathways, such as lipid biosynthesis; furthermore, the matrix stores ions, such as Ca^{2+} , Fe, or Zn^{2+} , which are potent signaling agents and co-factors in chemical reactions (Garbincius & Elrod, 2022; Lill, 2009; Liu et al., 2021). Mitochondria buffer Ca^{2+} ions at contact sites with the endoplasmic reticulum (ER) and the plasma membrane (Rizzuto & Pozzan, 2006), which plays a large role in cell fate decisions (cell cycle, differentiation, death), as well as neurotransmission (Garbincius & Elrod, 2022). (Frey & Mannella, 2000; Mannella, 2006; Roger et al., 2017)

With mitochondrial function being so closely related to their ultrastructure, it is perhaps not surprising to find variations in mitochondrial ultrastructure reflecting the functional diversity of mitochondria in different cell types (for examples, see Glancy et al., 2020; Munn, 1974; Neupert, 2012). Cells such as liver cells, which have a greater demand for biosynthesis and signaling, prioritize a large matrix volume, while in muscle cells such as in the heart, the cristae are densely arranged, increasing their capacity for ATP production and ROS signaling (Glancy et al., 2020). In addition, the cristae themselves can take different shapes, regulated by MICOS and Opa1 (Glancy et al., 2020), and vary from tubular structures to complex lamellar/sheet-like structures (Neupert, 2012). With different components of the ETC having different preferences on their location within the cristae folds, cristae shape (e.g., curvature) also influences the assembly and stability of respiratory chain complexes to streamline respiration efficiency (Cogliati et al., 2013;

Glancy et al., 2020). Cristae can form microcompartments that are either functionally isolated from each other or functionally connected (Wolf et al., 2019). All these adaptations in mitochondrial morphology help cells to fine-tune mitochondria into becoming “specialists” that fill the individual needs of a cell. (Glancy et al., 2020)

The link between structure and function also allows the microscopist to spot pathological mitochondria with some confidence (Yoon, 2004). For example, loss in membrane potential, mitochondrial oxidative stress, and defects in respiration are strongly associated with aberrant mitochondrial shapes, such as spherically shaped mitochondria, as well as “blob-”, “vase-” or “donut-” shaped mitochondrial structures, potentially caused by stress-induced mitochondrial osmotic pressure or calcium stress (Ahmad et al., 2013; Glancy et al., 2020; Long et al., 2015; Nikic et al., 2011; Picard & McEwen, 2014). Fragmented mitochondria with disrupted ultrastructure are a common finding in pathological situations, such as cancer and in aging organisms (Duvezin-Caubet et al., 2006; Suomalainen, 1997; Thomsen et al., 2018; Toyama et al., 2016). In cell culture models of neurodegenerative diseases, mitochondria typically present as highly fragmented (Costa et al., 2010; Lutz et al., 2009; Nunnari & Suomalainen, 2012; Shirendeb et al., 2012; Song et al., 2011; Wang et al., 2009). (Glancy et al., 2020)

How mitochondria are arranged inside cells plays a significant role. Depending on the tissue, cell type, and position within a cell, mitochondria can vary in their appearance: either small spheres and threads can populate the cytosol, or mitochondria can form highly interconnected and branched structures by merging into a vast reticulum with contiguous inner and outer membranes (Misgeld & Schwarz, 2017). Mitochondrial networks can take different sizes and shapes, with high diversity between cell types (Johnson et al., 1980).

Why do mitochondria form networks? Geometrical features such as surface area and complexity have functional implications. For example, elongated mitochondria have higher bioenergetic efficiency than fragmented mitochondria (Liesa & Shirihai, 2013). Some neurons reflect nutrient levels by altering mitochondrial connectivity via changing the balance of fusion and fission, with the resulting shift in ATP production stimulating neuronal electrical activity (Dietrich et al., 2013). Furthermore, an expansive mitochondrial network can share and equilibrate membrane potential and matrix contents (ions, proteins, metabolites) more rapidly (Skulachev, 2001). In some cells, such as myocytes, those networks are necessary to provide fast, bioenergetic communication “routes” throughout the cell (Glancy et al., 2015). On the downside, networks are also more prone to spreading mitochondrial dysfunction, and pronounced damage to mitochondria usually leads to fragmentation and disconnecting of dysfunctional particles in small pieces for engulfment by degradative organelles (Glancy et al., 2020). The fusion-fission machinery is directly involved in regulating mitochondrial network

morphology, regulating mtDNA stability, replication, and nucleoid distribution (Bonekamp & Larsson, 2018; Chen et al., 2010; Westermann, 2002), as well as mitochondrial degradation.

1.3. Mitochondrial dynamics

Mitochondria are highly dynamic organelles that can alter their shape within seconds to minutes (Picard et al., 2013). Morphological transitions directly impact mitochondrial function and are necessary to meet the unique demands of cells over time (Hoppins, 2014). For this purpose, multiple mitochondrial ‘reshaping mechanisms’ have evolved (Eisner et al., 2018). Two examples are *fusion* and *fission* (divisions; Hoppins, 2014), which Lewis and Lewis (1914) already described accurately as mitochondria being “*seen to fuse together [...] [they] may unite into a complicated network, which in turn may again break down into threads*”. In addition, intracellular *transport* and *anchoring* (Hoppins, 2014) are important for organizing mitochondria across larger distances and distributing them to sites of need in a cell. The repertoire of reshaping mechanisms also includes cristae dynamics, intermitochondrial nanotunneling and junctions (Eisner et al., 2018).

The mitochondrial reshaping processes are mediated by specific molecular forces, which will be described in more detail in the following subsections. In general, fusion and fission are mediated by molecules from the family of dynamin-related proteins (DRPs; Ford & Chappie, 2019). Like dynamin, DRPs are GTPases that exert a mechanochemical force on membranes to channel membrane scission or tubulation (Praefcke & McMahon, 2004). Through GTP-dependent conformational shifts and self-assembly, they can form a molecular collar that pinches and ultimately severs the membrane (Hoppins & Nunnari, 2009). In contrast, mitochondrial motility and anchoring are mediated by proteins that bind the cytoskeleton (Maday et al., 2014). Different regulatory pathways have evolved that integrate the different forms of mitochondrial dynamism with each other and with cellular signaling pathways, although the links are not yet entirely clear (Hoppins, 2014).

1.3.1. Fission

During fission, a mitochondrion constricts and is severed to generate smaller organelles (Quintana-Cabrera & Scorrano, 2023). On the molecular level, dynamin-related protein 1 (DRP1) is the mechanoenzyme that mediates scission (Smirnova et al., 2001). Initially, DRP1 is recruited from the cytosol by different effector proteins that mark fission sites, such as Mdv1, Fis1, MFF, MiD49, and 51 (James et al., 2003; Loson et al., 2013; Otera et al., 2010; Palmer et al., 2011; Zhao et al., 2011). There, DRP1 assembles into a large spiral-like structure wrapping around the

mitochondrion, stimulating GTPase activity (Hoppins, 2014; Hoppins & Nunnari, 2009). Upon GTP hydrolysis, the helix constricts due to a conformational shift and divides the organelle (Faelber et al., 2011; Ford et al., 2011; Frohlich et al., 2013; Kalia et al., 2018; Macdonald et al., 2014; Mears et al., 2011). Fissions are key to many aspects of mitochondrial biology, including (1) mitochondrial biogenesis, (2) mitophagy, (3) mitochondrial motility, and (4) morphology, making fissions crucial for a healthy mitochondrial population. (Chan, 2020)

Biogenesis. Fissions that occur around the midzone of a mitochondrion are related to mitochondrial biogenesis (Kleele et al., 2021). These fissions are influenced by the position of the mtDNA nucleoids and are crucial in equally distributing mtDNA amongst daughter mitochondria (Hoppins, 2014). The adaptor MFF plays a role in attracting DRP1 to midzone fission sites (Kleele et al., 2021). Prior to this, ER tubules also wrap around fission sites (Friedman et al., 2011), to pre-constrict the mitochondrion via actin polymerization mediated by INF2 and myosin II (Korobova et al., 2014; Korobova et al., 2013).

Mitophagy. Fission also helps to segregate damaged mitochondria (Burman et al., 2017; Kleele et al., 2021; Twig et al., 2008). In this type of fission, a small mitochondrial particle containing damaged components is ejected (Kleele et al., 2021). In mammalian cells, the adaptor FIS1 (James et al., 2003) recruits DRP1 to mediate asymmetrical fissions (Kleele et al., 2021). FIS1 potentially also coordinates membrane contact with autophagosomes (Rojansky et al., 2016; Shen et al., 2014; Yamano et al., 2014), and the mitochondrial autophagy machinery can recruit the fission machinery (Mao et al., 2013). Evidence also indicates that autophagosomes preferably engulf mitochondria that are smaller in size, making prior fission a prerequisite to mitophagy (Kleele et al., 2021; Parone et al., 2008).

Motility and distribution. The transport of short mitochondria is easier than that of long mitochondria in neurites (Chan, 2020). Especially in neurons, a fission reaction may be required before mitochondria can be transported from the soma into the axon (Lewis et al., 2018; Misgeld & Schwarz, 2017).

Network morphology. Lastly, fission regulates mitochondrial size. Mitochondrial fusion and fission are thought to be two symbiotic forces, with their overall balance determining mitochondrial network morphology. For example, MFF regulates mitochondrial size in axons (Lewis et al., 2018).

1.3.2. Fusion

During fusion, two mitochondria merge to become a larger organelle, allowing an exchange of material between the individual organelles (Chen et al., 2003; Hoppins, 2014). Complete fusions can be readily observed if two mitochondria are marked with different matrix-targeted

fluorophores due to the diffusion and intermixing of the two colors (Hoppins & Nunnari, 2009). On the molecular level, fusion relies on the dynamin-related proteins OPA1 and mitofusin (MFN1 and MFN2; Chen et al., 2003; Ehses et al., 2009; Head et al., 2009; Song et al., 2007). In contrast to fission, relatively little is known about the molecular mechanisms underlying fusion (Gao & Hu, 2021; Hoppins, 2014). In particular, it is not understood how the properties of a DRP are harnessed to fuse membranes instead of severing them (Hoppins, 2014). Importantly, these DRPs also directly mediate other processes that work in synergy with fusion: bioenergetics, mitophagy, organelle transport, and interorganelle contacts (Dorn, 2019; Quintana-Cabrera & Scorrano, 2023). The DRPs have different isoforms and posttranslational modifications that potentially allow for this functional variability, although the mechanisms are not well understood (Hoppins, 2014).

Morphologically, fusion proceeds in discrete steps: (1) close apposition of the mitochondrial membranes, (2) tethering and merging of the outer mitochondrial membranes (OMMs), (3) merging of the inner mitochondrial membranes (IMMs), which ultimately leads to (4) merging of matrix space (Quintana-Cabrera & Scorrano, 2023). Distinct molecular mechanisms mediate these steps:

1 | Apposition. Mitochondria need to get in close contact before a fusion can begin (Quintana-Cabrera & Scorrano, 2023). *In vitro* assays use centrifugation to forcefully bring mitochondria together, while *in vivo*, this is most likely achieved by transport on the cytoskeleton (Hoppins & Nunnari, 2009). Moving mitochondria usually bump with their tip into another mitochondrion before a fusion occurs (Gatti et al., 2023; Liu et al., 2009). Moving mitochondria have a particular propensity for fusing: Liu et al. (2009) observed so-called ‘kiss-and-run’ fusions, where moving mitochondria quickly fused their outer membranes, then moved on. One of the many functions of mitofusins is being a molecular tether that links mitochondria to the transport machinery (the Miro/Milton complex; Misko et al., 2010). The reliance of fusion on motility is exploited when cells try to establish functionally distinct mitochondrial subpopulations. For example, lipid cells segregate mitochondria into subpopulations with distinct proteomes and metabolic capabilities by firmly anchoring mitochondria (to lipid droplets) to reduce their motility whilst keeping the fusion proteins intact (Benador et al., 2019).

2 | Outer membrane (OMM) fusion. In mammals, this step is mediated by the DRPs mitofusin (MFN) 1 and 2 (Chen et al., 2003; Santel & Fuller, 2001). Mitofusins are embedded at OMM contact sites; for fusion to occur, their presence is required on both mitochondria (Chen et al., 2005; Koshiba et al., 2004). There is still controversy around the proteins’ tertiary structure (Gao & Hu, 2021), and the exact mechanism of how mitofusins bind each other is not understood: most likely, self-assembly into larger oligomers and guanine nucleotide-dependent (dimerization and) tethering through trans interactions play a role (Cao et al., 2017; Koshiba et al., 2004; Qi et

al., 2016). In general, both mitofusins have highly homologous structures (Rojo et al., 2002) and make homo-oligomeric complexes as well as hetero-oligomeric complexes (MFN1–MFN2). Hetero-oligomeric complexes are more fusion-efficient, and indeed, both MFN1 and 2 are required for efficient fusion (Ishihara et al., 2004; Meeusen et al., 2004). Yet, the two mitofusins are not entirely redundant and have developed distinct roles for themselves (Chen et al., 2003). MFN2 has multiple functions outside of fusion, such as interacting with apoptosis proteins (Karbowski et al., 2006) and acting as a mitochondrial tether through its localization on the ER (de Brito & Scorrano, 2008). Another complementary function is the “switch” of Mfn2 from a fusion protein to a mitophagy receptor upon phosphorylation (Chen & Dorn, 2013).

3 | Inner membrane (IMM) fusion. An optional inner membrane fusion follows outer membrane fusion (Liu et al., 2009). Optic atrophy 1 (OPA1) is a DRP that is responsible for inner membrane fusion (Cipolat et al., 2004; Mishra et al., 2014; Song et al., 2009). OPA1 tethers and deforms two opposing membranes through interaction with cardiolipin (Mishra et al., 2014) and therefore only needs to be present on one of the two mitochondria to drive fusion (Song et al., 2009). Besides that, OPA1 is essential for maintaining cristae shape and has a role in mitochondrial respiration (Cogliati et al., 2013). How these distinct functions are mediated is not understood, although a possible way might be the existence of different OPA1 forms: ‘long’ isoforms of OPA1 (l-OPA1; Song et al., 2007) that localize to the inner membrane via a hydrophobic domain, as well as soluble ‘short’ isoforms (s-OPA1) that are generated by the proteases OMA1 and YME1L1 by cleavage from the long forms (Head et al., 2009). Both long and short forms are expressed at nearly equimolar amounts, and both are necessary for fusion (Ehse et al., 2009; Y. Ge et al., 2020; Head et al., 2009; Herlan et al., 2004; Herlan et al., 2003; Song et al., 2007). How exactly the long and short forms of OPA1 mediate inner membrane fusion remains controversial.

4 | Merging of matrix contents. Complete fusion allows mitochondria to share materials, such as mtDNA, lipids, proteins, metabolites, and ions (Chen et al., 2005; Ishihara et al., 2003; Nunnari et al., 1997; Quintana-Cabrera & Scorrano, 2023). Unlike the outer membrane, the cristae-forming inner membrane is more diffusion-restricted, so inner membrane components do not mix efficiently after fusion (Busch et al., 2006; Quintana-Cabrera & Scorrano, 2023). Additionally, the mixing of mtDNA nucleoids, which are large and most likely linked to the cristae membranes, seems limited (Gilkerson et al., 2008; Nunnari et al., 1997).

1.3.3. Motility and anchoring

Cells actively move and anchor mitochondria to specific positions, a process that has been studied most extensively in axons. A sophisticated, ATP-driven molecular machinery mediates mitochondrial transport (Hirokawa, 1982, 1998) that uses kinesin and dynein motors for long-

ranged transport on microtubule tracks (Schnapp et al., 1985; Vale, Reese, & Sheetz, 1985), and myosin motors for short-ranged transport on actin filaments (Chada & Hollenbeck, 2004; Morris & Hollenbeck, 1995; Sheng, 2014). In neurons, cargo can be transported in two directions: *anterograde transport* toward synaptic terminals and *retrograde transport* toward the soma (Allen et al., 1982; Brady et al., 1982; Hirokawa, 1998). In axons, this directionality of cargo is determined by the polarity of the microtubule network: kinesin motors move cargo in anterograde direction (Hurd & Saxton, 1996; Vale, Reese, & Sheetz, 1985; Vale, Schnapp, et al., 1985) towards the distally pointing microtubule plus ends (Baas et al., 2016; Vale, Schnapp, et al., 1985), while dynein motors drive retrograde transport (Hirokawa et al., 2010; Pilling et al., 2006) toward the microtubule minus ends pointing towards the soma (Schroer et al., 1989).

The transport of specific cargo is controlled by distinct molecular mechanisms and adaptors (Maday et al., 2014). In anterograde direction, mitochondrial transport is mostly mediated by three versions of the mammalian kinesin KIF5 (Hirokawa et al., 2010; Nakagawa et al., 1997; Nangaku et al., 1994; Tanaka et al., 1998), although in retrograde direction, all cargoes use cytoplasmic dynein 1 as the motor protein (Roberts et al., 2013). These motor proteins attach to mitochondria via the motor-adaptor complex Miro/Milton (TRAK1 and 2 in mammals; Brickley & Stephenson, 2011; Glater et al., 2006; Guo et al., 2005; Stowers et al., 2002). Mitochondrial speed is not constant, and most mitochondria move in a “saltatory” manner, frequently switching between movements (‘runs’) and stops (‘pauses’; Devireddy et al., 2015; Hollenbeck, 1996). Multiple molecular factors influence these mitochondrial motility patterns, a selection of which will be outlined below:

Motor protein number and distribution: The speed of an organelle depends on the total number of attached motors (Encalada et al., 2011; Hendricks et al., 2010), the proportion of attached kinesin versus dynein molecules (Derr et al., 2012), as well as whether these molecules are allowed to form cooperative microdomains on the mitochondrial surface (Rai et al., 2016; Rai et al., 2013), and the processivity of the motor proteins (Maday et al., 2014). For example, dynein is typically enhanced by dynactin (King & Schroer, 2000; Schroer, 2004).

Microtubule architecture: Motor protein processivity is also regulated by various microtubule-binding proteins and microtubule posttranslational modifications (PTMs; Baas et al., 2016; Janke & Bulinski, 2011). The organization of the cytoskeleton and its dynamics also determine mitochondrial transport (Kapitein & Hoogenraad, 2015; Yogev et al., 2016). For example, mitochondria continually have to pause at obstacles such as the end of a microtubule bundle or microtubule intersections (Balint et al., 2013; Yogev et al., 2016). At axonal branch points, microtubule-decorating proteins can also “guide” mitochondrial distribution (Tymanskyj et al., 2022; Tymanskyj & Ma, 2019; Tymanskyj et al., 2017; Tymanskyj et al., 2018). Damage to the cytoskeleton also reduces axonal transport (Baas & Ahmad, 2013; Brill et al., 2016).

Mitochondrial anchoring: The motor-adaptor protein Miro contains two regulatory EF-hand Ca^{2+} -binding domains (Fransson et al., 2003), which stop mitochondria in synapses during Ca^{2+} elevation (Macaskill et al., 2009; Saotome et al., 2008). Moreover, syntaphilin, an axon-specific docking protein (Kang et al., 2008), anchors mitochondria onto synaptic microtubules via Miro and Ca^{2+} ions (Chen & Sheng, 2013). Additionally, Milton is sensitive to glucose levels, stopping mitochondria through O-GlcNAcylation modification by the OGT enzyme (Iyer & Hart, 2003; Pekkurnaz et al., 2014) and allowing mitochondria to accumulate in glucose-enriched areas in neurons (Pekkurnaz & Wang, 2022). Similarly, BDNF arrests mitochondria via Miro1 binding Ca^{2+} ions, facilitating neurotransmitter release (Su et al., 2014). Moreover, the actin cytoskeleton also plays a role: for example, the motor myosin 19 anchors mitochondria to actin via Miro (Lopez-Domenech et al., 2018; Oeding et al., 2018; Quintero et al., 2009), and regulation of actin polymerization can also guide mitochondrial movement into microdomains such as filopodia and spines (Sung et al., 2008). Myosin 6 and syntaphilin were also found to anchor mitochondria on actin, triggered by synaptic activity through AMPK-mediated energy-sensing (Li et al., 2020). (Pekkurnaz & Wang, 2022)

1.4. Mitochondrial turnover

Mitochondria are subject to continual damage that accumulates throughout their life. Mitochondria produce reactive oxygen species (ROS) as by-products of oxidative phosphorylation, which can damage various subcellular components, particularly the mitochondria themselves (Balaban et al., 2005; Brawek et al., 2010; Nicholls, 2004). Resulting are mutations in mitochondrial DNA, loss of mitochondrial membrane potential with a drop in ATP production, damage in the protein import machinery, and hazardous levels of ROS production (Balaban et al., 2005; Brawek et al., 2010; Nicholls, 2004; Zhu et al., 2013). Multiple endogenic and exogenic factors—*inherited genetics, environmental toxins, and metabolic activity*—significantly speed up mitochondrial aging, making dysfunctional mitochondria a major contributor to cellular aging and age-associated diseases. In fact, all currently known cellular aging processes are linked to mitochondria (Lopez-Otin et al., 2023).

Cells have extensive quality control mechanisms that ensure that damaged mitochondrial components can be discarded (*degradation*) and replaced by new, healthy ones (*biogenesis*; Ploumi et al., 2017; Popov, 2020). The balance of these two processes controls the overall number of mitochondria and their quality inside the cell (Ploumi et al., 2017; Popov, 2020). The mitochondrial lifecycle is semi-autonomous, as their DNA can replicate independently of the cell cycle, which is advantageous for postmitotic cells like neurons (Popov, 2020; Tuppen et al., 2010).

1.4.1. Mitochondrial birth

Mitochondria are not made “*de novo*”, rather they are—in honor of their bacterial ancestry—reproduced by growth and division from preexisting organelles (Popov, 2020; Ryan & Hoogenraad, 2007). Mitochondrial growth involves replication of mtDNA, loading of phospholipids, as well as protein synthesis—the latter requiring the coordination of two genomes (nuclear and mitochondrial genomes; Hock & Kralli, 2009; Lopez-Lluch et al., 2008; McKenzie et al., 2009; Ventura-Clapier et al., 2008). The nuclear-encoded proteins are synthesized on cytosolic ribosomes and depend on specific targeting signals to reach the mitochondrial surface, from where they are placed into the correct mitochondrial subcompartments by a complex molecular import machinery (Baker et al., 2007; Harbauer et al., 2014; Pfanner et al., 2019).

Mitochondrial replication, called *biogenesis*, is difficult to spot directly: because biogenesis is continually countered by degradation, readouts that measure growth in mitochondrial content are difficult to interpret (Miller & Hamilton, 2012). In practice, biogenesis is therefore often studied by measuring the mitochondrial protein synthesis rate (Miller & Hamilton, 2012). Alternatively, assessing the import of biomolecules such as proteins and lipids, which is a central step in controlling biogenesis, might be meaningful (Harbauer et al., 2014). Expression levels of regulatory factors that govern biogenesis and mitochondrial DNA replication might be more ambiguous (Medeiros, 2008; Miller & Hamilton, 2012). Overall, these assays usually require a careful combination of different approaches for the correct interpretation (Medeiros, 2008), making mitochondrial biogenesis an elusive process that is difficult to study in any system, but especially in such a complex cell as the neuron (Lopez-Lluch et al., 2008).

Like in most cells, the co-transcriptional regulation factor PGC-1 α is a master regulator of mitochondrial biogenesis in neurons (Cardanho-Ramos & Morais, 2021; Hees & Harbauer, 2022; Lopez-Lluch et al., 2008; Wareski et al., 2009). PGC-1 α regulates mitochondrial density in dendrites, thereby affecting synaptic function and maintenance (Cheng et al., 2012). It stimulates the expression of many nuclear-encoded mitochondrial proteins, such as TFAM, which is essential for the transcription and replication of mtDNA (Jornayvaz & Shulman, 2010). PGC-1 α acts upon many physiological and pathological stimuli that indicate an increased demand for mitochondria via molecular signals like AMP/ATP or NAD⁺/NADH ratios, Ca²⁺ ion levels, or neurotrophins (Cardanho-Ramos & Morais, 2021; Hock & Kralli, 2009; Lopez-Lluch et al., 2008; Ryan & Hoogenraad, 2007). Remarkably, PGC-1 α null mice have a major neurodegenerative phenotype with striatal lesions (Lin et al., 2004), indicating that biogenesis is an important aspect of maintaining mitochondrial health in neurons. Similarly, pathways driving mitochondrial biogenesis are downregulated during aging (Lopez-Lluch et al., 2008; Yuan et al., 2016) and in many neurodegenerative diseases such as ALS, Parkinson’s disease, Huntington’s disease and

Alzheimer's disease (Golpich et al., 2017; Hees & Harbauer, 2022; Uittenbogaard & Chiaramello, 2014).

1.4.2. Mitochondrial degradation

Over time, damage accumulates in mitochondria due to aging and stress, thereby affecting mitochondrial function (Ploumi et al., 2017). Cells have developed a variety of mechanisms to repair the affected organelles (Ploumi et al., 2017). The majority of mitochondria are degraded via macroautophagy, although damaged matrix components may also be budded off in vesicles ('MDVs'; Soubannier et al., 2012) or even directly degraded in the inner membrane using the AAA protease system and the cytosolic ubiquitin-proteasome system (UPS) as first lines of defense (Ashrafi & Schwarz, 2013; Stavoe & Holzbaur, 2019).

Autophagy means 'self-eating' and describes a eukaryotic system for the degradation of various cellular components, including mitochondria, through incorporation into lysosomes or vacuoles (Ashford & Porter, 1962; De Duve & Wattiaux, 1966; Ohsumi, 1999). In adult animals, autophagy seems to serve two purposes on the cellular level: (1) non-selective degradation of cytosolic content during starvation for nutrient supply (via the TORC1-pathway), and (2) recycling of damaged proteins and organelles via 'selective autophagy', which mediates organelle quality control in cells (Evans & Holzbaur, 2019a; Julg et al., 2021; Stavoe & Holzbaur, 2019). The latter function is particularly important for neuronal health (Deng et al., 2017).

(Macro)autophagy is a coordinated, multi-step process that involves an isolation membrane (also called a phagophore) forming around the target to create a double-membrane vesicle, the autophagosome, which subsequently fuses with a lysosome or endosome for hydrolytic degradation (Julg et al., 2021; Ohsumi, 2014). The autophagosomal membrane formation is guided by an orderly recruitment of different ATG (autophagy-related) proteins (Ohsumi, 2014; Tanida, 2011). Atg8 (LC3 and GABARAP in mammals) is key for elongating the phagophore and can be used as an autophagosome marker as it eventually stays concentrated on the autophagosome (Julg et al., 2021). Selective autophagy exists for different organelles: mitophagy for mitochondria, pexophagy for peroxisomes, ER-phagy for the ER, etc. (Stavoe & Holzbaur, 2019). Mitophagy is thought to be the last line of defense that is primarily activated when mitochondria suffer irreversible damage (Narendra et al., 2010). On the molecular level, mitophagy is characterized by certain distinct elements: typically, proteins such as PINK1 and parkin can recognize damage on a mitochondrion and mark it with ubiquitin chains, which can be recognized by different 'autophagy adaptors' or 'receptors' that bind LC3 to link the mitochondrion to an autophagosomal membrane for engulfment (Evans & Holzbaur, 2019b; Julg et al., 2021). Importantly, the currently known mitophagy receptors are somewhat redundant: optineurin, SQSTM1, NDP52, TAX1BP1, and NBR1 (Evans & Holzbaur, 2019b). For example, a study

investigating these five mitophagy receptors in cell cultures found that only a knockout of all five genes (“Penta-KO”) resulted in visible mitophagy defects (Lazarou et al., 2015). Specific ubiquitin chains might recruit different mitophagy receptors; for example, optineurin has two ubiquitin-binding domains with a preference for K63-linked and M1 (also called linear) ubiquitin chains (Ryan & Tumbarello, 2018).

Optineurin is, in fact, a multifunctional protein, as it uses its ubiquitin-binding domain to selectively bind damaged mitochondria, protein aggregates, and intracellular pathogens (Heo et al., 2015; Lazarou et al., 2015; Wild et al., 2011; Wong & Holzbaur, 2014), but also creates a scaffolding platform during antiviral responses (Pourcelot et al., 2016) and protects neurons from necroptosis or apoptosis in an ALS-related pathway (Ito et al., 2016; Nakazawa et al., 2016). TBK1 and other kinases regulate optineurin’s functions via phosphorylation (Pilli et al., 2012; Richter et al., 2016). At a later stage during autophagy, optineurin binds to the actin-based motor protein myosin VI, which guides autophagosome maturation and fusion to lysosomes (Markovinovic et al., 2018; Tumbarello et al., 2012).

The PINK1/parkin pathway was one of the first pathways to be described in mitophagy. PINK1 is a kinase that recruits parkin, a ubiquitin-protein(E3)-ligase (Shimura et al., 2000), after accumulating on a depolarized mitochondrial membrane, for example, when CCCP is administered (Lazarou et al., 2012; Narendra et al., 2008; Narendra et al., 2010; Pickrell & Youle, 2015). PINK1 and parkin actually interlink mitophagy with many other mitostasis mechanisms: for example, PINK1 phosphorylates mitofusin 2, which allows this fusion protein to switch its usual function into recruiting and acting as a mitochondrial receptor for parkin (Chen & Dorn, 2013). Moreover, parkin mediates the elimination of the transcription factor parkin-interacting substrate (PARIS), which inhibits biogenesis via the PGC1 α pathway (Shin et al., 2011; Stevens et al., 2015). Finally, parkin can ubiquitinate outer mitochondrial proteins such as Miro, targeting them for the ubiquitin-proteasome system and preventing mitochondrial transport (Chan et al., 2011).

1.5. Neuronal mitostasis

Understanding the mechanisms that govern neuronal mitostasis is crucial, as disrupting mitostasis has detrimental effects on neuronal health. Neurons face unique challenges when trying to maintain their mitochondria:

- (1) *Neuronal architecture*: Neurons are highly compartmentalized cells, and synapses, axon, dendrites, and soma have different metabolic demands, resulting in very diverse mitochondrial populations (Collins et al., 2002; Craig & Banker, 1994; Monzel et al., 2023; Pekkurnaz & Wang, 2022; Turner et al., 2022; Wong-Riley, 1989). Yet, our knowledge

- about how neuronal geometry shapes mitostasis remains incomplete (Misgeld & Schwarz, 2017; Stavoe & Holzbaur, 2019). How is mitochondrial heterogeneity established to fit local demands? How is mitostasis coordinated on a global scale to balance the needs of areas that are far away from one another, like the soma and axonal endings? And how can all those mechanisms stay applicable to the wider variety of neuronal shapes stemming not only from their genetic programming but also experience-based neuronal plasticity (Misgeld & Schwarz, 2017)? (Lopez-Domenech & Kittler, 2023)
- (2) *Mitochondrial stress*: The brain oxidizes glucose at a higher rate than most other organs (Harris et al., 2012; Kety, 1957; Mink et al., 1981; Rolfe & Brown, 1997). High rates of oxidative phosphorylation are thought to result in higher production of reactive oxygen species (ROS) and thus faster mitochondrial aging (Balaban et al., 2005). How do neurons upscale mitochondrial turnover to deal with this challenge? How are “old” mitochondria adequately replaced with “new” ones in a compartment-specific manner?
- (3) *Glia coupling*: Glia serve to support neuronal function and form a functional unity with neurons. Defects in glial homeostasis also play a role in the development of neurodegenerative diseases (Ito et al., 2016; Strohm & Behrends, 2020). What influence do these cells wield on neuronal organelles and vice versa, and to which extent do they share components (Burdett & Freeman, 2014; Davis et al., 2014; Gainer et al., 1977; Gatzinsky et al., 1997; Licht-Mayer et al., 2022; Phinney et al., 2015)?
- (4) *Greater context*: Neurons, even when comparing those of the same neuronal subtypes, have specific functional outputs and play unique “roles” within a nervous circuit. How organelle regulation relates to the broader context of higher-brain functions is not trivial, and this question has recently gained more attention (Dietrich et al., 2013; Rosenberg et al., 2023).

1.5.1. Mitochondrial specialization in neurons

Neurons are primarily fueled by ATP, which they gain from oxidative phosphorylation within mitochondria (Kety, 1957; Sokoloff, 1960). Most of that energy (75%) is used on electrochemical signaling—establishing membrane potentials and neurotransmission (Harris et al., 2012). Neuronal energy expenditure correlates well with mitochondrial content: neurons that fire more or that have more synapses also have more mitochondria (Dorckenwald et al., 2017; Kageyama & Wong-Riley, 1985; Kageyama & Wong-Riley, 1982; Santuy et al., 2018; Wong-Riley & Carroll, 1984; Wong-Riley & Welt, 1980). In most cells, mitochondria do not fulfill their function uniformly throughout the cell, establishing instead unique subpopulations depending on their subcellular localization. In neurons, perhaps the most compelling sign of mitochondrial heterogeneity is the unique morphology of these organelles within different neuronal subcompartments (Collins et al.,

2002; Monzel et al., 2023; Pekkurnaz & Wang, 2022): In axons, mitochondria form small beads and spheres, whereas the somatodendritic area has more interconnected networks of larger and tubular mitochondria (Faitg et al., 2021; Lewis et al., 2018; Pekkurnaz & Wang, 2022; Popov et al., 2005; Turner et al., 2022; Xiao et al., 2018). Dendritic mitochondria in cortical neurons are more densely packed than axonal mitochondria, matching the higher ATP consumption of dendrites (Harris et al., 2012; Santuy et al., 2018; Wong-Riley, 1989). Interestingly, mitochondrial size progressively decreases along the axon, whereas dendritic mitochondria become larger with further distance from the soma (Turner et al., 2022). The purpose and mechanisms of mitochondria taking different shapes and distributions in different neuronal compartments still remain a mystery. Elongated mitochondria are more efficient in oxidative phosphorylation (Gomes et al., 2011), which may be related to higher membrane potentials of dendritic mitochondria (Overly et al., 1996) and to postsynaptic currents requiring more ATP than presynaptic currents (Harris et al., 2012). Further research will need to elucidate the functional diversity between these subpopulations and the mechanisms that specify mitochondrial heterogeneity (Pekkurnaz & Wang, 2022).

The functional specification of synaptic mitochondria has become a particular focal point of study (Devine & Kittler, 2018). In cortical neurons, more than half of ATP is produced for neurotransmission (Harris et al., 2012). ATP molecules must be locally synthesized at presynaptic sites to secure normal neurotransmission (Rangaraju et al., 2014). This includes the reversal of ion channel fluxes, endo/exocytosis of vesicles, as well as the synthesis and packaging of neurotransmitters into vesicles. In addition, ATP synthesis may also drive local macromolecule synthesis during synaptic plasticity (Rangaraju et al., 2019). The local presence of mitochondria increases synaptic efficacy and stability (Kwon et al., 2016; Lees et al., 2019; Smith et al., 2016; T. Sun et al., 2013), and mitochondrial enrichment occurs at synapses undergoing remodeling after injury (Briones et al., 2005). Axonal mitochondria are enriched at presynaptic boutons, where they are physically tethered to vesicle release sites (Rowland et al., 2000). Only up to half of the presynaptic boutons in the brain contain mitochondria (Chavan et al., 2015; Shepherd & Harris, 1998). While it may seem puzzling that not all boutons contain mitochondria, this number is not unexpected given that glutamatergic synapses have a preferred firing probability of 50% for energy efficiency reasons (Harris et al., 2012). Dendritic mitochondria are long (up to 100 μm ; Turner et al., 2022) and, therefore, not specifically “enriched” at postsynaptic sites, which may be related to the spatial-geometrical features of postsynaptic currents (postsynaptic currents are not ‘restricted’ to the synaptic sites but travel along the entire dendritic tree, and therefore may require different “mitochondrial coverage”). They do, however, seem to form microcompartments that locally support the dendritic spines in their vicinity (Rangaraju et al., 2019). Local protein synthesis may be a mechanism that allows synaptic mitochondria to develop specialized proteomes and regulate them during synaptic plasticity

(Dahlhaus et al., 2011; Piccoli et al., 2007; Rangaraju et al., 2017). Unfortunately, the unbiased approaches that tested proteomes, metabolomes, lipidomes and ETC activities of synaptic versus non-synaptic mitochondria are difficult to interpret (the “non-synaptic” population contained “everything else” in the brain, including different cell types; Battino et al., 1991; Davey et al., 1997; Kiebish et al., 2008; Stauch et al., 2014; Volgyi et al., 2015). A very recent proteomic approach compared synaptosomes from different neuronal cell types with each other, mostly hinting at mitochondrial diversification in terms of oxidative phosphorylation pathways (van Oostrum et al., 2023)

The enrichment of mitochondrial at presynaptic sites might also serve additional purposes, as typically, more mitochondria are present in axons and presynaptic terminals than would be predicted alone by the ATP consumption of these regions (although some argued that ATP consumption was underestimated in the calculation; Harris et al., 2012; Rangaraju et al., 2014). So far, it has been suggested that presynaptic mitochondria are necessary to regulate Ca^{2+} -levels in conjunction with the ER (Jung et al., 2020; Kwon et al., 2016), as these mitochondria have distinguishable Ca^{2+} -handling properties when compared to their non-synaptic counterparts (Brown et al., 2006). Mitochondrial calcium buffering can indeed enhance short-term synaptic plasticity (Billups & Forsythe, 2002; Kang et al., 2008; Kwon et al., 2016; Lee et al., 2007; Tang & Zucker, 1997). However, those studies mostly used high-frequency action potential trains, and the blocking of mitochondrial calcium buffering did not directly affect synaptic vesicle release (T. Sun et al., 2013; Verstreken et al., 2005). A direct involvement of presynaptic mitochondria in neurotransmission metabolism is another intriguing possibility (Guo et al., 2017). Considering the omnipresence of mitochondria in various pathways of neurotransmitter synthesis, it will be an intriguing possibility to dissect this in settings of neurodegenerative disease in the future. To name but a few examples, mitochondria are involved in GABA metabolism (Besse et al., 2015; Cavalcanti-de-Albuquerque et al., 2022) and mitochondrial enzymes are also involved in glutamate synthesis (Waagepetersen et al., 2003) and catecholamine degradation (Graves et al., 2020); furthermore, mitochondria synthesize cofactors for serotonin, melatonin, (nor)epinephrine and nitric oxide synthesis (Vasquez-Vivar et al., 2022).

1.5.2. Matching to local demands

While the regulation of mitochondrial genes via PGC-1 α can control mitochondrial content on a global level, it does not explain well if and how biogenesis adapts to local demand in the compartmentalized neuron (Hees & Harbauer, 2022). The canonic view presumes that mitochondrial biogenesis occurs in the cell body (Cardanho-Ramos & Morais, 2021; Hees & Harbauer, 2022), as 99% of the mitochondrial proteome is encoded by nuclear DNA (Rath et al., 2021). The idea of the necessity of axonal transport was already coined early in the days of

neuroscience, dating back to observations made by Ramon y Cajal that axons need trophic support from their somata (Ramon y Cajal, 1928). Later studies suggested that the majority of mitochondria reach the neuronal periphery via long-range microtubule-based transport (Chang & Reynolds, 2006; Griffin & Watson, 1988; Hollenbeck, 1996). A fission reaction is thought to free “freshly” manufactured mitochondria from the somatic mitochondrial reticulum (Lewis et al., 2018; Misgeld & Schwarz, 2017; Verstreken et al., 2005) before the mitochondria are distributed via anterograde transport into axons and dendrites (Cardanho-Ramos & Morais, 2021; Sheng, 2014; Sheng & Cai, 2012; Zheng et al., 2019).

In axons, most anterograde mitochondrial transport is thought to be targeted for high-energy consuming sites such as synapses (Chang & Reynolds, 2006; Hollenbeck, 1996). Local stimuli, such as Ca^{2+} -levels, are thought to recruit mitochondria to areas of enrichment, such as synaptic sites (Chen & Sheng, 2013) and perhaps axonal branch points (Couchet et al., 2013). However, in neurons with long processes, mitochondria also need to navigate through a large volume of the axon with many branch points before they can stop at their distal destinations. How mitochondrial delivery is regulated on this global scale to guarantee sufficient supply is not known. Specifically, does the axon hillock already “know” how many mitochondria are going to be needed in the periphery, and if yes, how? Is anterograde mitochondrial transport in the stem axon “matched” to the demand of the downstream sites (“à la carte” delivery; Lopez-Domenech & Kittler, 2023)? Alternative models suggest other mechanisms: For example, dense-core vesicles (DCV) continually circulate back and forth in surplus through the axon, with each synaptic site only picking organelles from the stream as they are needed (“conveyor-belt” or “running-sushi” model; Wong et al., 2012), however, this has not been explored yet for mitochondria in mammalian neurons. Another interesting idea might be something akin to a “bulk” or “slow wave” transport, where mitochondria slowly shift and push forward to fill up the axon as needed—resulting in a mitochondrial age gradient from proximal to distal (Ferree et al., 2013). The latter model could be particularly interesting for dendrites, where most mitochondria are very long (Turner et al., 2022), as this might pose a challenge to fast long-range transport.

The entire issue with most of these models is that axonal transport is not fast enough for short-lived mitochondrial proteins to survive the long axonal journey (Cardanho-Ramos & Morais, 2021; Hees & Harbauer, 2022). In support of a distal biogenesis model, studies have actually shown mtDNA replication (Amiri & Hollenbeck, 2008; Van Laar et al., 2018) and translation in axons (Kuzniewska et al., 2020; Yousefi et al., 2021). Further, nuclear-encoded mitochondrial transcripts were discovered in axons (Aschrafi et al., 2016; Briese et al., 2016; Gumy et al., 2011; Shigeoka et al., 2016; Zivraj et al., 2010), where they are locally translated via axonal ribosomes (Cioni et al., 2019; Cosker et al., 2016; Yoon et al., 2012). Messenger ribonucleoprotein (mRNP) granules facilitate axonal transport of these nuclear-encoded transcripts—interestingly, this may

occur as co-transport on organelles like mitochondria, thereby allowing protein translation to be targeted more precisely (Cohen et al., 2022; Harbauer et al., 2022).

Local translation could be an important mechanism for establishing intracellular mitochondrial diversity, although the cues that regulate local translation, especially in neurons, largely remain unknown (Hees & Harbauer, 2022). It has been shown that the local translation of mitochondrial proteins is important for axon development (Lee et al., 2022; Spillane et al., 2013), regeneration, and synaptic function (Kuzniewska et al., 2020). Concerning synaptic activity, an interesting hypothesis is that AMPK activity triggered by high ATP consumption stimulates mitochondrial biogenesis, either via a global activation of the PGC-1 α pathway or via activation of local mitochondrial biogenesis (Hees & Harbauer, 2022). This mechanism could explain the correlation of neuronal energy expenditure with mitochondrial density, as acute changes in anterograde mitochondrial transport do not occur upon altered axonal activity consistently *in vivo* (Faits et al., 2016; Sajic et al., 2013; Smit-Rigter et al., 2016; Zhang et al., 2010). In summary, while both possibilities are not mutually exclusive, the specific contribution of local translation to mitochondrial turnover and the nature of anterograde transport still remain incompletely understood and will need to be addressed experimentally in more detail.

1.5.3. Quality control in neurons

Similar to mitochondrial biogenesis, mitochondrial degradation is also thought to occur primarily in the neuronal soma: there are many reports of mature lysosomes being more densely arranged in the soma (Augenbraun et al., 1993; Cai et al., 2010; Cai et al., 2012; Cheng et al., 2018; Craig & Banker, 1994; Han et al., 2020; Lee et al., 2011; Lie et al., 2021; McWilliams et al., 2018; Parton & Dotti, 1993; Parton et al., 1992), potentially to reuse the degradation products directly as building blocks in the soma during biogenesis (e.g., released amino acids; Klionsky & Ohsumi, 1999). It is therefore assumed that mitochondria must travel to the soma for degradation and that this is the chief *raison d'être* for retrograde axonal transport (Cai et al., 2012; Chang & Reynolds, 2006; Lin et al., 2017; Sheng, 2014; Sheng & Cai, 2012; Ye et al., 2015). Some studies indeed found that retrogradely moving mitochondria are depolarized (Lin et al., 2017; Miller & Sheetz, 2004), although other studies did not find signs of mitochondrial damage in the retrograde population (Breckwoldt et al., 2014; Verburg & Hollenbeck, 2008).

Other reports have shown that it is not actual mitochondria but autophagosomes that are being retrogradely transported towards the soma: Several studies have now observed a constitutive, 'bulk' form of autophagy at the distal tips of axons (Kulkarni & Maday, 2018; Maday, 2016; Maday & Holzbaur, 2014, 2016; Maday et al., 2012; Neisch et al., 2017; Xie et al., 2015). In these reports, autophagosomes would continually form in the periphery before being retrogradely transported to the soma with their contents. On their retrograde journey, the autophagosomes matured, i.e.,

fused with late endosomes and lysosomes. While some have suggested such a model to be possible for the selective removal of mitochondria via mitophagy (Han et al., 2020; Xie et al., 2015), others insisted that mitophagy mainly occurred in the soma (Devireddy et al., 2015; Sung et al., 2016; Ye et al., 2015). The idea of mitophagy being restricted to the soma has also been challenged: For example, in one report, the authors showed that damaging mitochondria locally resulted in PINK1/parkin-mediated mitophagy in distal axons (Ashrafi et al., 2014).

Given that autophagy-related processes form in a compartmentalized manner (Stavoe & Holzbaur, 2019), it seems conceivable that different autophagy mechanisms are used in different neuronal compartments, perhaps via distinct molecular pathways. However, since most of the studied systems were cell culture systems, it remains unknown what the *in vivo* roles of many of these pathways (**Section 1.4.2**) are in neurons. Understanding this seems particularly important since autophagy is key to neuronal health, as evidenced by the variety of defects in this area that are associated with neurodegenerative disease (Chu, 2019; Covill-Cooke et al., 2018; Deng et al., 2017; Deus et al., 2020; Doblado et al., 2021; Evans & Holzbaur, 2019a; P. Ge et al., 2020; Lipinski et al., 2010; Minakaki et al., 2020; Palikaras et al., 2018) and aging (Carnio et al., 2014; Lipinski et al., 2010; Terman et al., 2006; Terman et al., 2010). Disrupting generic autophagy leads to severe phenotypes from neuronal degeneration (Felbor et al., 2002; Friedman et al., 2012; Hara et al., 2006; Komatsu et al., 2006; Yoshii et al., 2016). Some of the pathways that are thought to be involved in mitophagy are mutated in familial forms of Parkinson's disease (PINK1, parkin; Kitada et al., 1998; Valente et al., 2004), and Amyotrophic lateral sclerosis (optineurin, SQSTM1; Evans & Holzbaur, 2019a). Dozens of optineurin mutations alone have been linked to ALS and its related frontotemporal dementia (FTS) disease (Markovinic et al., 2017), with most of these mutations being loss-of-function. Given the importance of autophagy for neuronal health, it will be crucial to further explore the *in vivo* action of the different mitophagy pathways and their contributions to cell-type- or compartment-specific vulnerability in disease.

1.6. Aims of the thesis

Mitochondrial turnover—the exchange of old mitochondria with new ones—is a function of mitochondrial *biogenesis* and *degradation* (Ploumi et al., 2017; Popov, 2020). Neurons are thought to perform both these processes mainly in the soma and are canonically considered to rely on *anterograde* and *retrograde transport* to take over the majority of mitochondrial “turnover” in axons (Chang & Reynolds, 2006; Griffin & Watson, 1988; Hollenbeck, 1996; Sheng, 2014; Sheng & Cai, 2012).

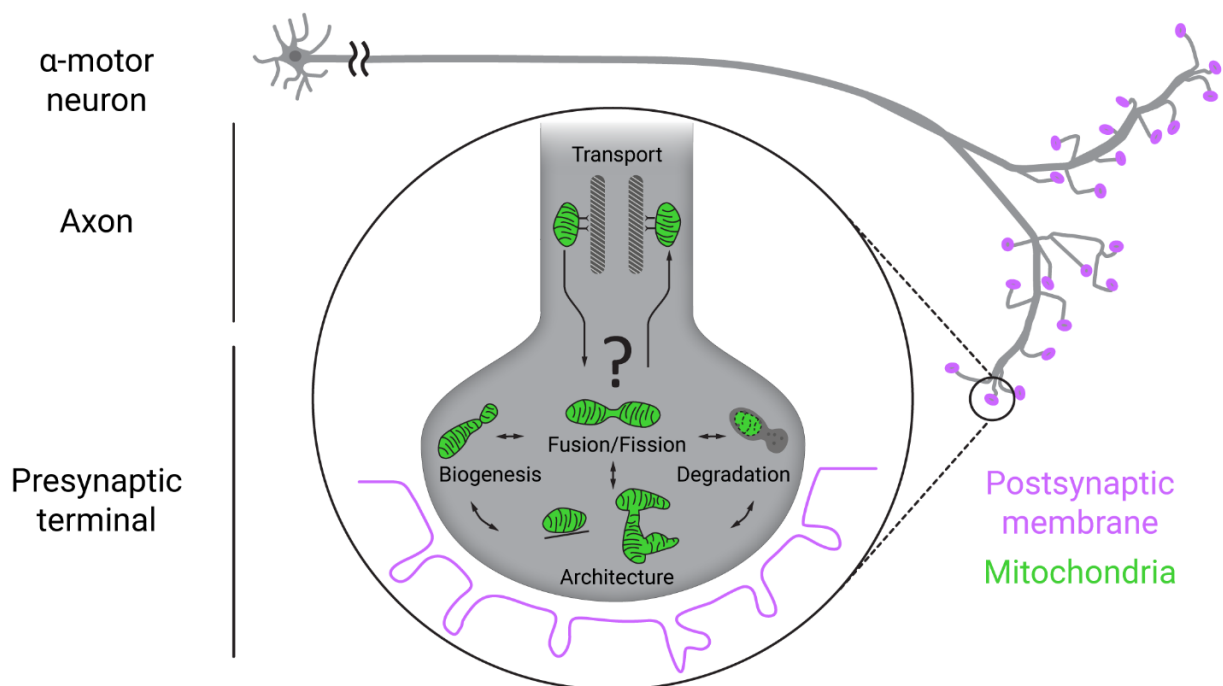


Figure 1.5 | The lifecycle of synaptic mitochondria in health and disease.

The fact that the importance of synaptic mitochondria for health and disease is often highlighted stands in contrast to how little is known about their actual behavior *in vivo*. This thesis aims to elucidate the individual steps of the mitochondrial “lifecycle” in mature synapses—first by comprehensively mapping out the physiological behavior of mitochondria, and then by interfering with these processes to investigate how mitochondrial disturbances relate to dying-back neurodegeneration. Specifically, the thesis aims to address the following questions to explore the intricate relationship between axonal transport and mitochondrial turnover (**Figure 1.5**):

1 | Mode of delivery of synaptic mitochondria: Is mitochondrial delivery matched to the demand of a neuron’s periphery, or are mitochondria selected on a “per need” basis (“à la carte” vs. “running sushi” models)? Are “new” mitochondria mainly supplied from the soma or by local biogenesis?

2 | Site and regulators of synaptic mitochondrial dynamics: What are the turnover rates of synaptic mitochondria? How do mitochondria that reach a synaptic site anchor and blend into the present peripheral pool? At which sites do peripheral mitochondria undergo fusion and fission?

3 | Site and regulators of mitochondrial degradation: Are “old” mitochondria removed from the synapse mainly by retrograde transport, or are mitochondria locally degraded? Which quality control mechanisms do mitochondria undergo in synapses?

In order to explore these and other questions in mature synapses of motor neurons, a novel optical pulse-chase imaging assay was developed based on transgenic mice that express photoswitchable proteins in neuronal mitochondria, which will be presented in the first section of the results chapter.

2. Materials and Methods

The methods described in this section are partially adapted from a manuscript that is being prepared for a peer-reviewed publication:

Working title: An optineurin-mediated retrograde transit filter controls mitostasis in distal axons.

Authors: Natalia Athanasia Marahori, Barbara Gailer, Martina Schifferer, Tatjana Kleele, Anna Iatroudi, Petros Avramopoulos, Stefan Engelhardt, Melike Lakadamyali, Monika Brill, and Thomas Misgeld

The work detailed here was performed by N. A. Marahori in the laboratory of T. Misgeld (TUM, Munich, Germany) unless specified otherwise.

2.1. Experimental animal models

Animal experiments were performed in accordance with national regulations and approved by the responsible federal agencies. The mice were kept in a maximum-barrier facility with quarterly Felasa monitoring (in accordance with EU Directive 2010/63 and §11 Abs. 1 Nr. 1 TSchG) and housed in individually ventilated cages (IVC, Techniplast, Euro-Standard III, 20 °C, group-housed at max. 5 adult mice) with dry food (ssniff), water *ad libitum* and enrichment. The cages were set to air conditioning with a humidity of $50 \pm 15\%$, a temperature of 22 ± 2 °C, and a light-dark cycle of 12 hours with a twilight phase. Transgenic mouse lines were interbred with C57BL/6N^{Ctrl} (Charles River) and C57BL/6J mice (<https://www.jax.org/strain/000664>) at regular intervals. For experiments, mice of both sexes (aged between 6 weeks and 24 months) were used, apart from the *Pink1*-KO and *Pink1-Parkin*-DKO datasets where indicated (postnatal days (P) 21–27), SOD1^{G93A} (P 14–21), and *Thy1*-(GA)149-CFP (5–6 weeks).

2.1.1. Transgenic reporter lines

Neuronal mitochondria were visualized by using a set of transgenic mice that express various (x) fluorescent proteins ('XFPs', coupled to a mitochondrial targeting sequence) under the well-established neuronal *Thy1*-promoter (termed '*Thy1*-mito-XFP' mouse lines; 'XFPs' in this study

were CFP, RFP, or Dendra2; Breckwoldt et al., 2014; Misgeld et al., 2007). In addition, the newly generated mouse lines *Thy1-mito-Dendra* and *Thy1-mito-paGFP* (see next section, cf. Magrane et al., 2014) were used to label subpopulations of mitochondria by photoswitching the fluorophore with a localized UV light pulse. Since paGFP is non-fluorescent in its native state (Patterson & Lippincott-Schwartz, 2002), *Thy1-mito-paGFP* were crossed to *Thy1-mito-RFP* mice (Breckwoldt et al., 2014) to visualize neuronal mitochondria in non-photoactivated areas. *In vivo* imaging of mitochondrial turnover was also performed in *Thy1-mito-Kaede* mice (Marinkovic et al., 2012).

Transgenic mice with expression of a fluorescent protein in neuronal cytoplasm (*Thy1-YFP-16*, -OFP3, or -CFP5 mice; Feng et al., 2000; Kay et al., 2011) were bred to colocalize dyes and staining patterns to axons. To study autophagosome dynamics, LC3-GFP mice were obtained (Mizushima et al., 2004) and crossed to *Thy1-mito-RFP* or *Thy1-OFP3* mice. Mice that express the enzyme Cre in cholinergic neurons ('ChAT-Cre' mice; Rossi et al., 2011) were crossed to ROSA-mito-GFP mice (Agarwal et al., 2017) to visualize mitochondria in motor neurons during TMRE incubation experiments. Mice that express the enzyme Cre in Schwann cells ('Plp-CreERT' mice ('Plp-CreERT' mice; Doerflinger et al., 2003) were crossed to ROSA-mito-Dendra mice (Pham et al., 2012) to visualize mitochondria in terminal Schwann cells. AAV injections were performed in either C57BL/6 mice (The Jackson Laboratory; Stock #000664) or the transgenic mouse lines expressing a fluorophore under the *Thy1*-promoter.

2.1.2. Knock-out and disease models

To elucidate the molecular mechanism of mitochondrial quality control in presynaptic terminals, the following knock-out (KO) mice and controls were used: *Pink1^{ko/ko}* × *Thy1-mito-Dendra* vs. *Pink1^{wt/wt}* × *Thy1-mito-Dendra* littermate controls ("Pink1-KO"; Glasl et al., 2012); *Prkn^{ko/ko}* × *Thy1-mito-Dendra* vs. *Prkn^{wt/wt}* × *Thy1-mito-Dendra* littermate controls ("Parkin-KO"; Itier et al., 2003); *Pink1^{ko/ko}* × *Prkn^{ko/ko}* × *Thy1-mito-Dendra* vs. *Pink1^{ko/ko}* × *Prkn^{wt/wt}* × *Thy1-mito-Dendra* littermate controls ("Pink1-Parkin-DKO"); ChAT-Cre^{mut/wt} × *Optn^{flox/flox}* × *Thy1-mito-Dendra* vs. ChAT-Cre^{wt/wt} × *Optn^{flox/flox}* × *Thy1-mito-Dendra* littermate controls ("Optn-cKO"; Munitic et al., 2013). Further, two animal models of Amyotrophic lateral sclerosis (ALS) were employed, with the following experimental and control groups: SOD1^{G93A +/-} (mut) × *Thy1-mito-Dendra* vs. SOD1^{G93A -/-} (wt) × *Thy1-mito-Dendra* littermate controls (Gurney et al., 1994), and *Thy1-(GA)149-CFP +/-* (mut) × *Thy1-mito-Dendra* vs. *Thy1-(GA)149-CFP (wt) -/-* × *Thy1-mito-Dendra* littermate controls (Schludi et al., 2017). The SOD1^{G93A +/-} breeder animals were monitored and scored weekly for the development of motor symptoms.

2.1.3. Generation of mouse lines

The *Thy1*-promoter was used to drive the expression of mito-Dendra and mito-paGFP selectively in neurons, as previously described (Marinkovic et al., 2015a; Misgeld et al., 2007). In brief, to create mito-Dendra and mito-paGFP fusion genes, an N-terminal in-frame fusion between the coding sequence of the fluorescent protein (Dendra2 or paGFP; Gurskaya et al., 2006; Patterson & Lippincott-Schwartz, 2002) and the mitochondrial targeting sequence from subunit VIII of the human cytochrome c oxidase gene (Clontech) was generated (Marinkovic et al., 2015b). After cloning the fusion gene into the *Thy1* vector, a standard pronuclear injection was performed to produce several independent founder lines, which were screened for expression patterns, levels, and photoconversion (Gailer, 2022; Marinkovic et al., 2015c). Two bright and broadly expressing lines were retained and used for further experiments (**Figure 3.2** and **3.3**, **Table 3.1**). Homozygotes of all lines bred normally and showed no neurological abnormalities.

2.2. Molecular biology

2.2.1. Genotyping

Transgenic mice were genotyped by PCR of tail or earlobe biopsies performed by animal caretakers and technicians. Adult mice were marked by ear tags (Hauptner & Herberholz) or ear holes; juvenile litters were marked by tattoos on the paws (Ketchum) for re-identification. For all comparative datasets (mutants and their genetic wildtype controls), an additional tail sample was taken after death to verify the initial PCR result. The DNA was isolated from the tissue using the following protocol:

		Final Concentration	Source	Program
10× Gitocher Buffer	15 µL	1×	see “ <i>Buffers and solutions</i> ”	55 °C: 5 h 95 °C: 5 min 4 °C: ∞
10% Triton™ X-100	7.5 µL	0.5%	Sigma-Aldrich, T8787	
2-Mercaptoethanol	1.5 µL	1%	Sigma-Aldrich, M6250	
Proteinase K (100 mg/mL)	0.75 µL	0.5 µg/µL	Roth, 7528.5	
H ₂ O	125.25 µL			
Total volume per tube	150 µL			

The following protocols were used for DNA amplification (Thermocycler, Eppendorf; for primers, see **Table 2.1**, p. 34):

“Kapa-HS”		Source	Program
GoTaq	10 μ L	Promega, M7421	95 °C: 2 min
Primers (10 pmol / μ L)	à 1 μ L	Metabion	<u>32 cycles:</u> 95 °C, 15 sec → 60 °C, 30 sec → 72 °C: 15 sec
DNA	1 μ L		72 °C: 5 min
H ₂ O	up to 20 μ L		4 °C: ∞

“Atg-Flox”-Touchdown		Source	Program
GoTaq	10 μ L	Promega, M7421	94 °C, 2 min
Primers (10 pmol / μ L)	à 1 μ L	Metabion	<u>10 cycles:</u> 94 °C, 15 sec → 65 °C, 30 sec (-0.5 °C per cycle decrease) → 72 °C, 120 sec
DNA	1 μ L		<u>20 cycles:</u> 94 °C: 15 sec → 65 °C: 30 sec → 72 °C: 120 sec
H ₂ O	up to 20 μ L		72 °C, 5 min 4 °C: ∞

“Chat-Cre” and “LC3-GFP”-Touchdown		Source	Program
GoTaq	10 μ L	Promega, M7421	94 °C: 2 min
Primers (10 pmol/ μ L)	à 1 μ L	Metabion	<u>10 cycles:</u> 94 °C, 20 sec → 65 °C. 15 sec (-0.5 °C per cycle decrease) → 68 °C: 10 sec
DNA	1 μ L		<u>28 cycles:</u> 94 °C, 15 sec → 60 °C, 15 sec → 72 °C, 10 sec
H ₂ O	up to 20 μ L		72 °C: 2 min 4 °C: ∞

The PCR reaction mix (20 μ L) was loaded on a 2% agarose/TAE gel (250 mL) together with 10 μ L of a 1K ladder (New England Biolabs, N0468L, N3200L) in the first well. The gel was submerged in 1 \times TAE buffer (Carl Roth, CL86.1) in a gel chamber, and electrophoresis was performed (DNA Pocket Block-UV gel chamber, Biozym Diagnostik). DNA bands were recorded under 312 nm light (Genoplex system, VWR).

2.2.2. Molecular cloning

mKeima-Red-Mito-7 was a gift from Michael Davidson (Addgene plasmid # 56018), and pAAV-hSyn-DIO-HA-hM3D(Gq)-IRES-mCitrine was a gift from Bryan Roth (Addgene plasmid # 50454). To generate the *hSyn*-mito-Keima construct for AAV9-production, mito-Keima was digested from the mKeima-Red-Mito-7 plasmid using NheI and NotI and ligated into a self-complementary AAV backbone plasmid. The human Synapsin promoter was amplified by PCR from the pAAV-hSyn-DIO-HA-hM3D(Gq)-IRES-mCitrine plasmid and then cloned before the mKeima-Red-Mito-7 using MluI and NheI. (P. Avramopoulos performed molecular cloning in the lab of S. Engelhardt, TUM; description adapted from the manuscript Marahori et al., in preparation)

Mouse line	Amplicon size (bp)	Primer name: oligonucleotide sequence (5'-3')	Source
<i>Thy1</i> -mito-paGFP	181	Mito-F: CGC CAA GAT CCA TTC GTT EYFP-R: GAA CTT CAG GGT CAG CTT GC	Marahori et al. (manuscript in preparation)
<i>Thy1</i> -mito-CFP	181	Mito-F: CGC CAA GAT CCA TTC GTT EYFP-R: GAA CTT CAG GGT CAG CTT GC	Misgeld et al. (2007); RRID:IMSR_JAX:007967
<i>Thy1</i> -mito-Dendra	230	Fw: CGC CAA GAT CCA TTC GTT Rev: TGG TCA GGA TGT CGT AGC TG	Marahori et al. (manuscript in preparation)
<i>Thy1</i> -mito-RFP	254	Mito-F: CGC CAA GAT CCA TTC GTT RFP-R: TTC TGC TGC CGT ACA TGA AG	Breckwoldt et al. (2014)
ROSA-mito-GFP	mut = 300 wt = 557	RosamitoGFP-F: GCA CTT GCT CTC CCA AAG TC RosamitoGFP-wt-R: CAT AGT CTA ACT CGC GAC ACT G RosamitoGFP-mut-R: GTT ATG TAA CGC GGA ACT CC	Agarwal et al. (2017) RRID:IMSR_JAX:021429
ROSA-mito-Dendra	mut = 175 wt = 604	RosamitoD wt-F: CCA AAG TCG CTC TGA GTT GTT ATC RosamitoD wt-R:mGAG CGG GAG AAA TGG ATA TG RosamitoD mut-F: CCC CAA CGA ATG GAT CTT G RosamitoD mut-R: TTC GAG GGA CCT AAT AAC TTC	Pham et al. (2012) RRID:IMSR_JAX:018385
<i>Thy1</i> -YFP-16	378	GFP-F: CAC ATG AAG CAG CAC GAC TT GFP-R: TGC TCA GGT AGT GGT TGT CG	Feng et al. (2000); RRID:IMSR_JAX:003782
<i>Thy1</i> -OFP	370	OFP3-F: TGC AGT TCG AAG ATG GTG GGT TC OFP3-R: ATG TTG CCT TCG GTT TTC CTG AC	Kay et al. (2011)
<i>Thy1</i> -CFP	378	GFP-F: CAC ATG AAG CAG CAC GAC TT GFP-R: TGC TCA GGT AGT GGT TGT CG	Feng et al. (2000); RRID:IMSR_JAX:003710
LC3-GFP	tg = 625 wt = 255	LC3-GFP-1: GGT GTT TGT TCC GTA CAC ATC ACC LC3-GFP-2: GGC AAA GCG GCA AAC AACCAT CAC LC3-GFP-3: GAG TGA AGC AGA ACG TGGGGC TCA CCT CGA	Mizushima et al. (2004); RRID:IMSR_RBRC00806
ChatCre	mut = 148 wt = 200	ChatCre mut-F: CAA AAG CGC TCT GAA GTT CCT ChatCre-WT-F: GCA AAG AGA CCT CAT CTG TGG A ChatCre-C-R: CAG GGT TAG TAG GGG CTG AC	Rossi et al. (2011); RRID:IMSR_JAX:006410
SOD1 ^{G93A}	236	SOD-F: CAT CAG CCC TAA TCC ATC TGA SOD-R: CGC GAC TAA CAA TCA AAG TGA	Gurney et al. (1994); RRID:IMSR_JAX:004435
<i>Thy1</i> -(GA)149-CFP	378	GFP-F: CAC ATG AAG CAG CAC GAC TT GFP-R: TGC TCA GGT AGT GGT TGT CG	Schludi et al. (2017)
<i>Optn</i> -flox	mut = 450 wt = 388	Optn-F: CCA TGC TCA GCC AGA GTT TC Optn-R: GAT ATA AAT GGC TTC AGG GAT GC	Munitic et al. (2013); RRID:IMSR_JAX:029708
<i>Pink1</i> -KO	ko = 583 wt = 781	Pink1-C-F: GAC AGT ACT TGC CTA GCG TAG Pink1-wt-R: CAG ACA CGC GCT TGG TTT TC Pink1-ko-R: GAG CAA TGC AGA AAG TCA GAG C	Glasl et al. (2012)
<i>Parkin</i> -KO	mut = 400 wt = 300	Parkin-ko-F: CAG CAG CCT CTG TTC CAC ATA CAC T Parkin-wt-F: TGC TCT GGG GTT CGT CCC CT Parkin-R: TGC CTG TCA CAT GCA ATG CAT ACC T	Itier et al. (2003)
<i>Plp</i> -CreErt	440	PlpCreErt-F: AGG TGG ACC TGA TCA TGGAG PlpCreErt-R: ATA CCG GAG ATC ATG CAA GC	Doerflinger et al. (2003) RRID:IMSR_JAX:005975

Table 2.1 | Mouse lines and genotyping primers.

2.2.3. Generation of adeno-associated virus (AAV) particles

For AAV9-*hSyn*-mito-Keima production, HEK293-T cells were grown in 10-tray Cell Factories (Thermo Fisher Scientific) using Dulbecco's modified essential medium (DMEM) containing 10% fetal bovine serum (Gibco) and 1% penicillin/streptomycin for 24 h before transfection. The transgene plasmid (420 µg of 'pAAV-*hSyn*-mito-Keima') and the helper plasmid (1.5 mg of pDP9rs, kindly provided by Roger Hajjar, Icahn School of Medicine at Mount Sinai, New York) were transfected into the HEK293-T cells using polyethylenimine (Polysciences). 72 h later, the cells were harvested, lysed, and benzonase-treated. The virus particles were purified by ultracentrifugation through an iodixanol density gradient (Optiprep, Progen). Iodixanol was replaced by Ringer lactate buffer (Braun) using Vivaspin 20 columns (Sartorius). The latter also aimed to concentrate the virus by decreasing the volume of the solution. Viral titers were determined by real-time PCR using SYBR Green Master Mix (Roche) to be in the range of 1×10^{13} – 2×10^{14} genome copies per milliliter. (AAV9-generation was performed by P. Avramopoulos in the lab of S. Engelhardt, TUM; description adapted from the manuscript Marahori et al., in preparation)

2.3. Surgery

2.3.1. Neonatal injection of AAV into brain ventricles

AAVs were injected into mice as described in Wang et al. (2021) and Marahori et al. (manuscript in preparation). The pups were anesthetized with ~32% isoflurane between postnatal days 2–3 and injected with 2 µL of AAV-particle suspension with a glass pipette on a nanoliter injector (30 nL/s; Micro4™ MicroSyringe Pump Controller and Nanoliter 2000, World Precision Instruments; pipette: 3.5" Drummonds #3-000-203-G/X) under ultrasound guidance (Vevo1100 Imaging System and Microscan MS550D transducer, Visualsonics) into the brain ventricle. After the procedure, the pups recovered on a heating mat (37 °C) before being returned to the mother. The injected mice were later sacrificed for live explant imaging or for histology, as described in **section 2.4 "Tissue preparation."**

2.3.2. Photoconversion of the intercostal nerve *in vivo*

To photoconvert a stretch of intercostal nerve, the tissue was exposed as previously described (Breckwoldt et al., 2014). Briefly, to expose an intercostal nerve, *Thy1*-mito-Dendra animals were anesthetized with ketamine/xylazine (KX) and the fur of the thorax was removed. After skin incision, the 3rd and 4th intercostal nerves were exposed, the pectoral muscle split, and the

intercostal space was carefully dissected without damaging the nerve. The intercostal nerve was then briefly illuminated with a 405 nm LED (using a BX51WI microscope and 20x objective) for 1 min. The pectoralis muscle and the skin were then sutured (6-0 monofilament) and cleaned with 80% ethanol. Mice were allowed to recover in a heating pad and monitored hourly for signs of discomfort. Triangularis sterni explants were prepared 4–8 hours days after photoconversion.

2.3.3. *In vivo* imaging in sternomastoid muscles

In vivo imaging of mitochondrial turnover was performed in the murine sternomastoid muscle as described previously (experiments performed by Dr. Melike Lakadamyali in the lab of J. Lichtman, Harvard University, USA; Turney et al., 2012). Briefly, the mouse was anesthetized with 0.10–0.15 mL of 17.4 mg/mL ketamine and 2.6 mg/mL xylazine in 0.9% NaCl solution (K/X) and intubated for ventilation. The sternomastoid muscle was exposed by a midline incision in the neck. The overlying skin and submandibular gland were fixed laterally with a retractor. A small spatula was inserted underneath the endplate zone in the center of the muscle. The muscle was slightly lifted on the spatula to isolate it from heartbeat-related motion artifacts. A low concentration (1 $\mu\text{g/mL}$) of fluorescently labeled α -bungarotoxin (Alexa647-BTX, Molecular Probes) was added for 30–60 seconds. The muscle was then washed extensively with lactated Ringer's solution, which was also used as an immersion medium during imaging. Confocal images were recorded using the FV1000 confocal system (Olympus, 20X/0.5 NA, and 100X/1.0 NA dipping-cone water immersion objectives). In order to avoid motion artifacts due to respiration, the ventilator was briefly switched off during imaging (< 30 seconds). The mice were placed on a heated pad, which was kept at around 30°C. After surgical closure of the wound, mice were injected with antisedan (atipamezole hydrochloride) for speeded recovery. The mice were subsequently injected with buprenorphine for analgesia.

2.4. Tissue preparation and microscopy

2.4.1. Acute nerve-muscle explants and widefield live microscopy

Thorax explants containing the triangularis sterni muscle and its associated intercostal nerves were dissected from mice using a modified protocol adapted from Kerschensteiner et al. (2008) and Brill et al. (2013). After lethal anesthesia with isoflurane (Abbott) and cervical dislocation of the mice, the explanted thoraces were prepared under a dissection microscope (Olympus SZ51). *Thy1-mito-Dendra* and *Thy1-mito-paGFP* thoraces were dissected in a dark room under red light to avoid premature photoswitching. The thorax was isolated from skin and pectoral muscles and

released from the animal cavity by quickly severing the ribs near the spine (< 1 min). The explanted tissue was transferred to a dish with oxygenated (bubbled with 95% O₂ / 5% CO₂) and cooled Ringer's solution (in mM: 125 NaCl, 2.5 KCl, 1.25 NaH₂PO₄, 26 NaHCO₃, 2 CaCl₂, 1 MgCl₂, 20 glucose) on ice, and any remaining inner organs were removed. The explant was pinned on a Sylgard-coated 3.5 cm dish with insect pins (Fine Science Tools, 26002-20) with the ventral side facing up. During the experiment, the explant was superfused with warmed, oxygenated Ringer's solution at 2–3 mL/min at temperatures between 33–36 °C in a heating ring (Warner instruments). Live image stacks and movies were recorded on μ Manager-controlled epifluorescence microscopes (Olympus BX51WI; www.micro-manager.org). Microscopes were equipped with $\times 4/0.5$ N.A. air-, $\times 20/0.5$ N.A. and $\times 100/1.0$ N.A. water-immersion dipping cone objectives, LED light source (pE-4000 CoolLED) or a mercury arc lamp (Olympus), a 405 nm LED (Thor Labs, #M405L1) or a 405 nm laser (Coherent), an automated filter wheel (Sutter), a CMOS camera (Andor Sona, low-noise mode) or a CCD camera (Retiga EXi, Qimaging) and a motorized stage (MMTP, Scientifica for xy-motility; Ludl, MAC 6000 for z-focus). Neutral density and infrared-blocking filters were used in the light path to guard against phototoxicity. The following multicolor filter sets were used: LED-DA/FI/TR/Cy5-B-000 (Semrock) or Triple-FITC/Cy3/Cy5 (Chroma #86016) for mito-Dendra; LED-CFP/YFP/mCherry-A-000 (Semrock) or Triple-ECFP/EYFP/mCherry (Chroma #89006) for mito-RFP and mito-paGFP signals; and GFP/Keima(pH)-3X2M-A-000 (Semrock) for mito-Keima (and associated mito-XFP fluorophores) imaging. For measurements of axonal transport in intercostal nerves (stem axons), time-lapse movies with 180–300 images were acquired at 1 Hz and exposure time of 300 ms. For synaptic transport measurements, movies were acquired for 30 min–2.5 h (0.5–0.33 Hz), usually at the “entry points” of terminal axon branches into superficial neuromuscular junctions (NMJs) of the triangularis sterni muscle. Only one or two NMJs were imaged per explant to keep the imaging time window within the limit of physiological transport rates (~3 h) unless specified otherwise in the text. After sample fixation, low-magnification stacks ($\times 20$ and $\times 4$) were taken to re-localize recorded synapses. (adapted from the manuscript Marahori et al., in preparation)

2.4.2. Photoswitching protocol

Photoswitching (photoactivation / -conversion) with 405 nm light was performed using a $\times 100/1.0$ N.A. water-immersion dipping cone objective. The 405 nm light was restrained to a ~40 μ m wide spot on the sample with a built-in aperture stop (Olympus). For time-lapse imaging, the smallest dose of 405 nm illumination that yielded adequate contrast was used to reduce potential phototoxicity (Dendra ~870 μ W*s, pa-GFP ~8.7 mW*s; see **Section 3.1**). In some mito-paGFP experiments, a 405 nm laser (Coherent) was used (0.1% laser power for 1 s). Photoactivation with two-photon lasers was performed on an Olympus FVMPE-RS microscope equipped with a

widefield live imaging setup similar to the one described above. Using a $\times 100/1.00$ N.A. water-immersion objective, mitochondria were photoactivated using the following settings: 60% laser power, 800 nm, ~ 6 s. (adapted from the manuscript Marahori et al., in preparation)

2.4.3. Vital dyes and live compounds

Acute nerve-muscle explants were incubated with mito-photo-DNP to depolarize mitochondria (Chalmers et al., 2012). The compound (Focus Biomolecules, 10-1580) was incubated as a bath application for 30 min (using the perfusion system described earlier; 20 μ M in prewarmed oxygenated Ringer's solution) in a dark room under red light (Glancy et al., 2015). In the experimental groups, mito-photo-DNP was photoactivated using a ~ 870 μ W*s UV dose right after washout with Ringer's for 7 min, while in the 'no depolarization' control groups, the UV dose was applied prior to mito-photo-DNP incubation, resulting in photoconversion of mito-Dendra for both groups, but photoactivation of mito-photo-DNP only in the experimental group.

To measure mitochondrial membrane potential, acute explants were isolated from ChAT-Cre \times ROSA-mito-GFP mice and then continually perfused at the widefield setup with 30 nM TMRE (non-quenching condition; diluted in oxy-Ringer's with 0.1% DMSO; Thermofisher, T669) at 30–33 $^{\circ}$ C, with imaging starting after at least 1 h of incubation. Stacks of junctions that were located in successfully TMRE-labelled muscle tissue were used for experiments. Then, neuromuscular junctions after photoactivation of mito-photo-DNP were acquired, and junctions with only UV illumination (control).

For LysoTracker experiments, acute triangularis sterni nerve-muscle explants were transferred either to a widefield setup (as described above) or an upright confocal setup equipped with $\times 100/1.0$ N.A. and $\times 20/0.5$ N.A. water-immersion objectives, a heated stage, and perfusion system (Olympus FV1000; 33–36 $^{\circ}$ C; 95% O_2 / 5% CO_2 bubbled Ringer's solution). The explants were incubated with LysoTracker Red DND-99 for 3 min (1:5000, Invitrogen, L7528) and Alexa-647-conjugated α -bungarotoxin for 15 min (1:50, Invitrogen, B-35450, 50 μ g/mL) added to perfusion media (Song et al., 2008). After wash-out, widefield or confocal image stacks (as indicated in figure legends) of superficial axon terminals were acquired at Nyquist resolution, and positions were mapped ($\times 20$ objective) to enable re-localization of the axons after sample fixation.

To visualize the myelin sheath during axonal transport measurements, acute nerve-muscle explants were briefly (15 min) stained with fluoromyelin red on a heated stage at a widefield setup equipped with a perfusion system (Thermofisher, F34652).

2.4.4. Tissue fixation and histology

Immunohistochemistry was performed using a modified protocol from Brill et al. (2016). Nerve-muscle explants were fixed in 4% paraformaldehyde (PFA; Sigma #P6148 or Electron Microscopy Sciences #15710) or 2% PFA for anti-ubiquitin stainings in 0.1 M phosphate buffer (PB) for 1–2 h on ice. Triangularis sterni muscles were dissected as whole mounts to leave the anatomy of motor axons and myocytes intact (Brill et al., 2013; Kerschensteiner et al., 2008). For some antibody stainings (anti-ubiquitin, anti-Dendra, anti-GFP, anti-tag-RFP), the muscles were permeabilized for 1 h at 37 °C with 5% CHAPS in H₂O (300 rpm; Roth #1479.3). For antibodies that were raised in mouse, blocking with mouse Fab-fragments (1:100 in PB) and then blocking solution was performed (each 1 h on a shaker, 60 rpm, at room temperature). Brains and spinal cords were collected from mice after lethal anesthesia with isoflurane and transcardial perfusion with 4% PFA in 0.01 M phosphate-buffered saline (PBS; pH 7.35). After postfixation by immersion overnight (4 °C), samples were mounted in 2% agarose and cut on a vibratome (Leica, 60 µm sections).

Samples were incubated overnight at 4 °C 60 rpm in the primary antibodies diluted in blocking solution (Muscle: 10% goat serum Millipore #S26, 1% BSA Sigma Aldrich A9647, 0.5% Triton X-100 Sigma-Aldrich T9284, in 0.1 M PB; Brain and spinal cord: 10% goat serum Sigma Aldrich G9023, 1% BSA Sigma Aldrich A9647, 0.5% Triton X-100 Sigma-Aldrich T9284, 0.05% NaN₃, Riedel de Haen 13412, in 0.01 M PBS). The following primary antibodies were used: anti-βIII-tubulin conjugated to Alexa-488 (mouse IgG2a, 1:200; Biolegend, #801203), to Alexa-555 (mouse IgG2a, 1:100; BD Biosciences #560339), to Alexa-594 (mouse IgG2a, 1:200; Biolegend #657408), or to Alexa-647 (mouse IgG2a, 1:200; Biolegend #657406); anti-Caspr (rabbit polyclonal, 1:500, Abcam, ab34151); anti-Dendra2 (rabbit polyclonal, 1:500, Evrogen, AB821); anti-GFP (rabbit polyclonal, 1:1000, Abcam, ab13970); anti-ubiquitin clone Ubi-1 (mouse IgG1, 1:10-1:20, Millipore, MAB1510). For labeling postsynaptic nicotinic acetylcholine receptors, Alexa-594-, Alexa-647- or biotin-conjugated α-bungarotoxin (1:20, Invitrogen, B-13423, B-35450, B1196; 50µg/mL in PBS) was added to the primary antibody staining. Brain and spinal cord sections were stained with Neurotrace 640/660 (Invitrogen N21483, 1:500). Samples were washed three times in 0.1 M PB (muscles) or 0.01 M PBS (vibratome sections) and then incubated for 2 h on a shaker (60 rpm, room temperature) with suitable secondary antibodies coupled to Alexa-Fluor dyes (raised in goat; Thermofisher and Jackson Immunoresearch) and/or streptavidin coupled to Alexa-405 (1:200, Invitrogen, S32351; 1mg/mL in PBS), then washed again. For mounting, glass slides covered in Vectashield (Vector Laboratories) or Fluoromount G (Thermofisher, #00-4958-02) were used. Muscles were flattened by placing them between glass slide and cover slip under magnetic pressure. (adapted from the manuscript Marahori et al., in preparation)

2.4.5. Confocal and Airy scan microscopy

Images in fixed samples were recorded using a confocal microscope equipped with $\times 10/0.40$ N.A. air-, $\times 20/0.8$ N.A., $\times 40/1.35$ and $\times 60/1.42$ N.A. oil-immersion (Olympus FV1000, Olympus FV3000), or $\times 10/0.45$ N.A. air-, $\times 20/0.8$ N.A. air-, and $\times 63/1.4$ N.A. oil-immersion objectives (Zeiss LSM980). NMJs that were live imaged before fixation on a widefield microscope were re-localized in the fixed sample using the surrounding microanatomy as fiducials (for example, using axon innervation and branching patterns, positions within the muscle). The samples were acquired using Nyquist sampling (for high-N.A. objectives), sequential scanning, and automated pinhole diameter. Airy Scan microscopy (LSM 800; LSM 980 with Airy Scan 2; Zeiss) was performed on samples that were mounted under ultra fine coverslips (Hecht Assistent, #41014521). Laser power and detector voltage were adjusted to neither under- nor oversaturate the fluorescence signals. The settings of quantitative datasets comparing experiments and controls were kept constant for comparability. Airy Scan stacks were processed with Zeiss ZEN Blue software using appropriate Wiener filter parameters, with constant settings between experiments and controls.

2.4.6. Electron microscopy

Triangularis sterni muscle explants were prepared as described above and transferred to cooled EM fixative (4% PFA, 2.5% glutaraldehyde, in 0.1 M sodium cacodylate) for 24 h at 4 °C. For correlative datasets, explants were first prepared for live imaging (described above, see figure legends), with fixation following immediately after image acquisition. The region containing the site of interest was punched using an asymmetrical shape and transferred to a glass slide. For correlative datasets, NMJs were re-localized and outlined by two asymmetrical shapes using two-photon laser burns (near-infrared branding “NIRB”; Bishop et al., 2011) on an Olympus FVMPE-RS microscope equipped with a $\times 25/1.05$ N.A. water-immersion multiphoton objective and GASP detectors (NIRB settings: 100% laser power, 920 nm, 30–60 s). Afterward, samples were post-fixed (48 h at 4 °C), and NIRB marks were re-localized on a dissection microscope. The triangularis sterni muscle layer was isolated before embedding as follows (by M. Schifferer, EM facility hub at DZNE Munich). A standard rOTO protocol was used for en bloc staining (Kislinger et al., 2023), and reduced osmium post-fixation (2% osmium tetroxide, 1.5% potassium ferrocyanide in 0.1 M sodium cacodylate buffer pH 7.4), TCH treatment (1% aqueous thiocarbohydrazide; Sigma, 223220-5G) and another osmium step (2% aqueous osmium) followed. The muscle was incubated overnight in 1% uranyl acetate at 4 °C, contrasted in 0.1% lead aspartate (silver nitrate, Alfa Aesar, A16345; L-aspartate, Sigma, A9256-100g), dehydrated, infiltrated with epon and embedded in a support tissue scaffold (mouse cortex). The block was trimmed by 200 μm to expose a rectangular block face with a TRIM90 knife (Diatome, Trim 90,

DTB90) on a PowerTome ultramicrotome (RMC). Consecutive sections were taken on an automated tape collecting ultramicrotome (ATUM) with a diamond ultra-knife (Diatome) at 50 nm thickness and collected on carbon-coated Kapton tape (kindly provided by Richard Schalek, Jeff Lichtman, Harvard; Schalek et al., 2012). The tape was plasma-treated (custom-built vacuum chamber based on the glow discharger easiGlow, PELCO) right before section collection (Kasthuri et al., 2015; Kislinger et al., 2023). The appearance of NIRB marks was monitored during sectioning and by light microscopic inspection of sample sections after methylene blue staining (Sigma, M9140). Kapton strips with the selected sections were assembled onto double-sided adhesive carbon tape (Science Services, P77819-25), mounted onto a 4-inch silicon wafer (Science Services, SC4CZp-525-01), and grounded with adhesive carbon tape strips (Science Services, 77816-25). Section images were acquired on a Crossbeam Gemini 340 SEM (Zeiss) in backscatter mode at 8 keV (high gain) at 7.0 mm WD and 60 μm aperture. Wafers were screened and selected for NIRB marks. In ATLAS5 Array Tomography (Fibics, Ottawa, Canada), the wafer was imaged at 6000 nm/pixel, followed by mapping and medium resolution (200 nm/pixel) imaging of individual tissue sections. The regions of interest were automatically acquired at 3 nm/pixel. The images were aligned semiautomatically using the *Fiji* TrakEM2 Plugin (Cardona et al., 2012) and annotated in IMOD for rendering by the author (<https://bio3d.colorado.edu/imod/>; Kremer et al., 1996). (adapted from the manuscript Marahori et al., in preparation)

2.5. Data analysis

Image analysis was performed with the ImageJ-based software *Fiji* unless indicated otherwise (<http://fiji.sc>) (Schindelin et al., 2012). To correct for movement during imaging, time-lapse movies were aligned to a region of interest prior to analysis ('Template matching' plugin; <https://sites.google.com/site/qingzongtseng/template-matching-ij-plugin>) (Tseng et al., 2011). Pixel intensity measurements were undertaken after background subtraction in each color channel.

2.5.1. Fluorescence intensity and UV-dose-response curves

To calculate the fluorescence intensity of photo-transformable proteins (paGFP and Dendra2), individual mitochondria were isolated in neuromuscular junctions (NMJs) by manually drawing regions of interest (ROI, 'freehand selection' tool). At least three measurements were taken per NMJ, and the average pixel intensity was calculated in *Fiji*. For dose-response curves, NMJs were illuminated with incremental steps of UV light, and measurements from each step were plotted against the corresponding cumulative duration of UV illumination. The ROIs were

repositioned manually to the selected mitochondria to account for sample drift. The intensity measurements were normalized to the initial value before UV illumination. In further experiments, mitochondria were considered to be ‘photoswitched’ (p.s.) if the ratio of the p.s./non-p.s. fluorescence intensity exceeded the mean before 405 nm illumination by at least 4 standard deviations.

2.5.2. Mitochondrial transport and shape

Axonal transport rates were measured by counting the fluorescent organelles which crossed a vertically placed line in either anterograde or retrograde direction, then divided by observation time (**Figure 2.1, a,b**; Marinkovic et al., 2012; Misgeld et al., 2007). Mitochondrial shape was manually annotated in *Fiji*: Length (l) and width (w) of individual moving mitochondria were measured with the ‘line’ tool; for area and perimeter, the mitochondria were outlined with the ‘freehand selection’ tool (**Figure 2.1, c**). Mitochondrial volume was calculated by assuming an ellipsoidal shape:

$$(1) \quad \frac{1}{6} \pi * l * w^2$$

In axon terminals, each mitochondrion was measured in three different time-lapse frames where possible, and the average was used for further analysis. Mitochondrial volume flux rates were calculated as the sum of transported mitochondrial volumes per time interval. Mitochondrial aspect ratio is given as mitochondrial length divided by width. Circularity is calculated as

$$(2) \quad 4 \pi \frac{area}{perimeter^2}$$

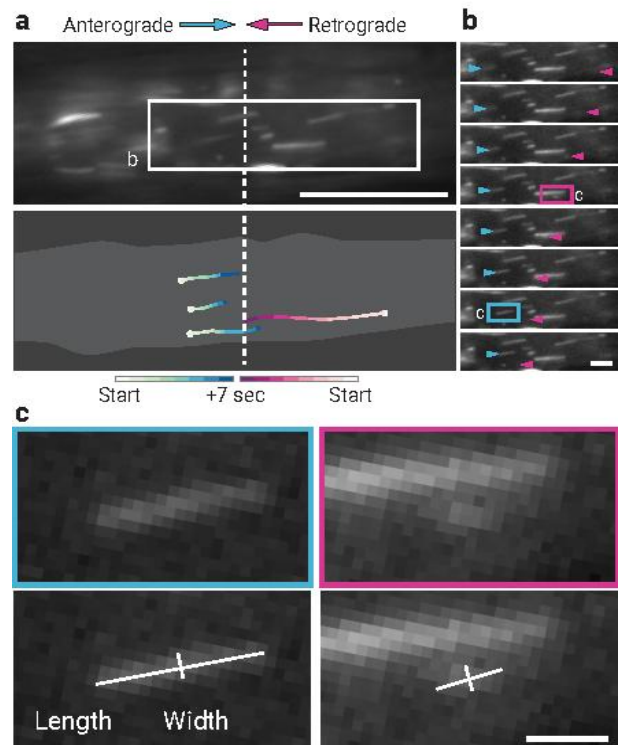


Figure 2.1 | Measuring the shape of moving mitochondria in intercostal nerve axons. **a**, Top: intercostal nerve axon showing mitochondria labeled with a fluorescent protein (*Thy1-mito-CFP* mouse). A time-lapse movie spanning 5 min in total was taken at this position (image shown was averaged over the time of 7 s). Bottom: moving mitochondria from the axon shown above were tracked over time (excerpt). The color scale indicates the position of the mitochondria at consecutive time points (frame rate, 1 Hz; the starting position is shown by a light circle, the final movement by the darkest shade). The color code represents mitochondria moving in anterograde (blue shades) or retrograde (magenta shades) directions. Transport rates were counted across the whole movie as the number of mitochondria traversing the vertically placed line, then divided by the total observation time. Usually, more mitochondria move in anterograde than in retrograde direction. **b**, Excerpt of a temporal image series; the position being indicated by the boxed area in **a**. The markers point to two moving mitochondria (blue: anterograde; magenta: retrograde) at consecutive time points (frame rate, 1 Hz). **c**, Average length and width of each mitochondrion traversing the line were obtained to calculate volume flux rates. Here, examples of two moving mitochondria are shown, their positions indicated by the boxed areas in **b** (left row: retrogradely moving mitochondrion, right row: anterogradely moving mitochondrion). Scale bars: **a**, 10 μm; **b**, 2 μm; **c**, 1 μm

Both shape factors represent a perfectly circular shape by the value of 1.

In Airy Scan image stacks, volume was calculated by outlining a mitochondrion's area in each z-section and multiplying the area sum with section thickness. A mitochondrion's area was defined as all cohesive pixels with intensity surpassing $\frac{1}{2}$ of the peak intensity in the corresponding line scans ('Plot Profile' *Fiji* function, example in **Figure 3.9, h**), multiplied by the resolution in xy. For widefield comparison, l and w were also defined by the distance between the $\frac{1}{2}$ maxima of fluorescence intensity in a line scan (**Figure 3.9, d**).

2.5.3. Tracking and organelle motility analysis

Organelles were tracked using the 'Manual Tracking' *Fiji* plugin. The organelle positions (x,y) for each time frame were extracted in a table, and the Euclidian distance between consecutive positions was calculated. Next, each track was divided into subsections of motility and pausing behavior. Pauses (= stops) were defined where a previously motile organelle was displaced by less than 2 pixels per frame ($\sim 0.09 \mu\text{m/s}$). Stops were registered as 'transient' if an organelle resumed motility again. Mitochondria that stopped for longer than 15 min remained in their position until they slowly disappeared or until the end of the movie (**Figure 3.17, c**), as these stops were never transient, they were instead marked as 'persistent'. For each organelle, the following motility parameters were extracted: average speed (total distance divided by total observation time), run speed (speed excluding time spent stopping), average pause duration (total time spent stopping divided by total number of stops), average duration of transient stops (pause duration excluding all stops at the start or end of the track), average pause rate (total number of stops divided by observation time).

For mitochondrial trackings in retrograde 'pulse-chase' experiments, each track was mapped onto the anatomy of its axon terminal. In these movies, the axon was outlined (based on a correlated β III-tubulin staining) and divided into the synaptic area (α -bungarotoxin), paranodal regions (anti-caspr), internodes and unmyelinated axon (only β III-tubulin). These compartments were sectioned further according to their relative size (from distal to proximal: 10 bins between the base and the apex of the synaptic branches, 10 bins along the internode, and 2 bins in between the heminode and synapse). Each mitochondrial position in time was assigned to the nearest bin, and then mitochondrial tracks and motility parameters were plotted relative to their position along the axonal compartments. The likelihood of a mitochondrion staying in the bin due to a permanent stop (only mitochondria were included that stopped at least 15 min before the end of the movie) was calculated after marking whether a mitochondrion passed the bin (Value 0) or whether the mitochondrion persistently stopped (Value 1). The mean over all mitochondria was then plotted per bin as a probability (**Figure 3.17, d**).

2.5.4. Mitochondrial capture experiments

Mitochondrial ‘capture’ was defined when mitochondria stopped persistently (> 15 min) in the synaptic exit point (or another node, depending on the experiment). The synaptic exit point was defined as the area between the proximal 1/10 of the presynapse and the heminode, which was corroborated by post hoc staining when possible. ‘Passing’ was defined when mitochondria moved through this region. In pie charts, the relative proportions of photoconverted mitochondria that were captured vs. passing were plotted (excluding mitochondria which entered the exit point within the last 15 min of the movie).

Mitochondrial volume flux rates were measured as described in **section 2.5.2**. Both photoconverted and non-photoconverted mitochondria were annotated through the ‘Merge’ color mode in *Fiji*. For ‘captured’ mitochondria, the last 15 min of the movie were excluded. The flux rates of ‘non-photoconverted’ captured mitochondria were estimated for each junction from the photoconverted flux by normalizing for the proportion of photoconverted synaptic area (**Figure 3.17, f**). For measuring synaptic areas, widefield image stacks before and after photoconversion were deconvolved (‘Subtract background’ *Fiji* Plugin, to remove unfocused scatter light) and maximum projected, and then the area was measured after thresholding of the mitochondrial signal (‘Otsu’ or ‘Li’ algorithms).

2.5.5. Lysosome distribution in axon terminals

Lysosome distributions were measured by creating a segmentation mask (mito-Keima: combined mask from the 438- and 556-nm channels after deconvolution with ‘Subtract background’ *Fiji* Plugin, manual thresholding and binarization; LysoTracker: manually thresholded and binarized cytoplasmic YFP channel) and using the mask to retain the pixels containing the lysosomal signal in the stack (after background subtraction). For mito-Keima, the resulting image stacks were additionally divided (556/438-nm) to create a ratiometric image. The stacks were then flattened by averaging the pixel values inside the mask across the z-dimension.

The axon terminals were sectioned into subcompartments using a correlated axon compartment staining (see above), and the pixel intensity profiles were plotted from each compartment by line scans (‘Plot Profile’ function in *Fiji*; the widths of the annotation lines were adjusted to cover the axon branches). The results were then averaged for each subcompartment of each bin. LysoTracker plots were additionally normalized to the internodal mean signal.

2.6. Image representation

For figure representation purposes, images were processed in *Fiji* and *Adobe Photoshop*. Different channels of an image series were combined in pseudo-colors using the ‘screen’ function in *Adobe Photoshop*. Maximum intensity projections were generated in *Fiji* and stitched in *Adobe Photoshop* (where needed). In most figures, images show maximum intensity projections of confocal or widefield image stacks. If single optical sections are shown, this was indicated in the figure legends. For representation, widefield stacks were deconvolved with the “Subtract background” Plugin in *Fiji* prior to maximum projection to remove unfocused scatter light (Conchello & Lichtman, 2005). Gamma settings were adjusted non-linearly in *Adobe Photoshop* to increase the visibility of low-intensity objects; however, gamma was not applied to panels that were used for pixel intensity quantification (e.g., ratiometric fluorophores like mito-Keima, protein staining quantifications like anti-ubiquitin). Images were placed on dark monochrome backgrounds where appropriate. For presentation purposes only, movies were denoised (e.g. Gaussian blur in *Fiji*, ‘dust and scratches’ in *Adobe Photoshop*, or ‘Candle’ algorithm in *MATLAB*; Coupe et al., 2012) and bleaching-corrected in *Fiji* using an exponential fit. Segmentations from electron microscopy stacks were rendered with *AMIRA* software. The relevant structures in electron micrographs were pseudo-colored by a transparent overlay.

2.7. Statistical analysis

For each dataset, measurements were taken from distinct entities, with the number of biological replicates being detailed in the corresponding figure legends. No statistical methods were used to predetermine sample sizes, but the chosen sizes were similar to previous measurements (Brill et al., 2016; Misgeld et al., 2007). The samples were not randomized during data collection since the mice were assigned to the experimental groups according to the given genotypes. However, comparative datasets were acquired and analyzed in a blinded manner.

Statistical analysis was performed with *GraphPad PRISM* software (Version 8). First, data were tested for a normal distribution using the D’Agostino-Pearson normality test unless the distribution was already known from previous, larger datasets. In datasets with normal distribution, significance was determined by a two-sided student’s *t*-test (unpaired unless indicated otherwise). Otherwise, significance was tested with a two-sided Mann-Whitney-U test. For paired analysis, a two-tailed Wilcoxon signed-rank test was used. A two-sided χ^2 -test was used for contingency analyses. A one-way or two-way ANOVA test with multiple comparisons was used to compare multiple (normally distributed) groups with each other. Not normally distributed data were analyzed using a Kruskal-Wallis-test and Dunn’s multiple comparisons test.

p values < 0.05 were considered significant and marked by “*”; p values < 0.01 were indicated by “**” and < 0.001 by “***.” Trendlines and R^2 values were generated in *Excel* based on a linear approximation. Boxplots show median, interquartile range, and whiskers 95th percentiles. Results written in the main text and the bars in bar plots indicate mean \pm s.e.m. The corresponding figure legends indicate the specific tests used in each dataset. Survival plots for fusion experiments were generated in *GraphPad PRISM* software.

2.8. Buffers and solutions

0.1 M Phosphate buffer (PB)

- Solution A – *alkaline* 0.1 M: 35.6 g Na_2HPO_4 dihydrate (Roth, 4984.1) in 2L dH_2O
- Solution B – *acidic* 0.1 M: 6.9 g NaH_2PO_4 monohydrate (Roth, K300.2) in 0.5L dH_2O
- Titrate the pH to 7.35 by mixing Solutions A and B:
 - approx. 200–250 mL Sol. B on 750 mL Sol. A
- Stir well (at least 30 min) on a magnetic stirrer with a hotplate.
- Store at RT.

10× Phosphate Buffered Saline (PBS)

Reagent	Quantity	Final Concentration	Source
NaH_2PO_4	2.56 g	18.6 mM	Riedel de Hän, 04270
Na_2HPO_4	11.94 g	84.1 mM	Sigma-Aldrich, S3264
NaCl	102.2	1750 mM	
H_2O	1 L		
<u>Total</u>	<u>1L</u>		

For experiments, 100 mL of 10× PBS was solved in 800 mL dH_2O , then pH was adjusted with HCl or NaOH solutions to 7.35, and then filled up with dH_2O to 1 L.

PFA in 0.1 M Phosphate buffer (PB)

Reagent	Quantity	Final Concentration	Source
Paraformaldehyde (PFA), EM grade, 16% aqueous solution	10 mL	4%	Electron microscopy sciences, 15710
0.2 M PB, pH 7.35	20 mL	0.1 M	see above
H_2O	10 mL		
<u>Total</u>	<u>40 mL</u>		

Keep at 4 °C. Prepare fresh before the experiment. Using 0.2 M PB, pH 7.35 for this recipe will yield a PFA mixture with pH 7.40.

Blocking Solution (10% GS, 1% BSA, 0.5% Tx) in PB

Reagent	Quantity	Final Concentration	Source
Goat Serum (GS)	10 mL	10%	Millipore, S26
Bovine serum albumin (BSA), pH 7	1 g	1%	Sigma-Aldrich, A9647
Triton™ X-100 (Tx)	0.5 mL	0.5%	Sigma-Aldrich, T8787
0.1 M PB, pH 7.35	up to 100 mL		

Blocking solutions were sterile filtered (0.45 µm), aliquoted, and stored at -20 °C.

Blocking Solution (10% GS, 1% BSA, 0.5% Tx) in PBS

Reagent	Quantity	Final Concentration	Source
Goat Serum (GS)	10 mL	10%	Millipore, S26
Bovine serum albumin (BSA), pH 7	1 g	1%	Sigma-Aldrich, A9647
Triton™ X-100 (Tx)	0.5 mL	0.5%	Sigma-Aldrich, T8787
1× PBS	up to 100 mL		

Blocking solutions were sterile filtered (0.45 µm), aliquoted, and stored at -20 °C.

Ringer's solution

Reagent	Quantity	Final Concentration	Source
1 M CaCl ₂	2 mL	2 mM	Sigma-Aldrich, C1016
1 M MgCl ₂	1 mL	1 mM	
H ₂ O	900 mL		
10× Ringer's solution	100 mL	20 mM	see below
Glucose	3.6 g		Sigma-Aldrich, 16301

Total volume 1 L. Stored at 4 °C.

Ringer's was bubbled with carbogen gas (95% O₂, 5% CO₂) at least 20 min before use.

10× Ringer's solution

Reagent	Quantity	Final Concentration	Source
NaHCO ₃	21.84 g	260 mM	Sigma-Aldrich, S6297
NaH ₂ PO ₄ * H ₂ O	1.72 g	12.5 mM	Riedel de Haen, 04270
KCl	1.86 g	25 mM	
NaCl	73.05 g	1.2 mM	

Total volume 1 L. Stored at 4 °C.

3. Results

The experiments described in this section were partially reported in a *bioRxiv*-preprint (which is currently being prepared for peer-reviewed publication):

Marahori, N. A., Gailer, B., Schifferer, M., Kleele, T., Iatroudi, A., Hannan, S. B., Avramopoulos, P., Engelhardt, S., Lakadamyali, M., Brill, M. S., & Misgeld, T. (2024). A retrograde transit filter mediated by optineurin controls mitostasis in distal axons. *bioRxiv*, DOI: 10.1101/2024.07.28.604753

The work detailed in this section was performed by N. A. Marahori in the laboratory of T. Misgeld (TUM, Munich, Germany) unless specified otherwise (contributions are detailed in the corresponding figure legends).

3.1. Optical pulse-chase imaging assay

Time-lapse microscopy is an effective tool to study the dynamics of neuronal mitochondria *in vivo* (Faits et al., 2016; Lewis et al., 2016; Marinkovic et al., 2012; Misgeld et al., 2007; Paquet et al., 2014; Plucinska et al., 2012; Smit-Rigter et al., 2016; Sorbara et al., 2014). Capturing mitochondrial dynamics, however, is challenging because (1) dynamic events are rare in fully mature neurons (Faits et al., 2016; Lewis et al., 2016; Misgeld & Schwarz, 2017; Smit-Rigter et al., 2016), and (2) because neurons, especially at synaptic sites, are often densely filled with mitochondria, up to the point where conventional light microscopy cannot resolve the space between individual organelles anymore. An ideal imaging assay should offer long observation times coupled with high temporal resolution (to capture these rare and fast events) and achieve the resolution down to a single mitochondrion (nm– μ m organelle size) yet follow its dynamics while it moves across the neuronal landscape (cm–m axon length; **Figure 3.1**).

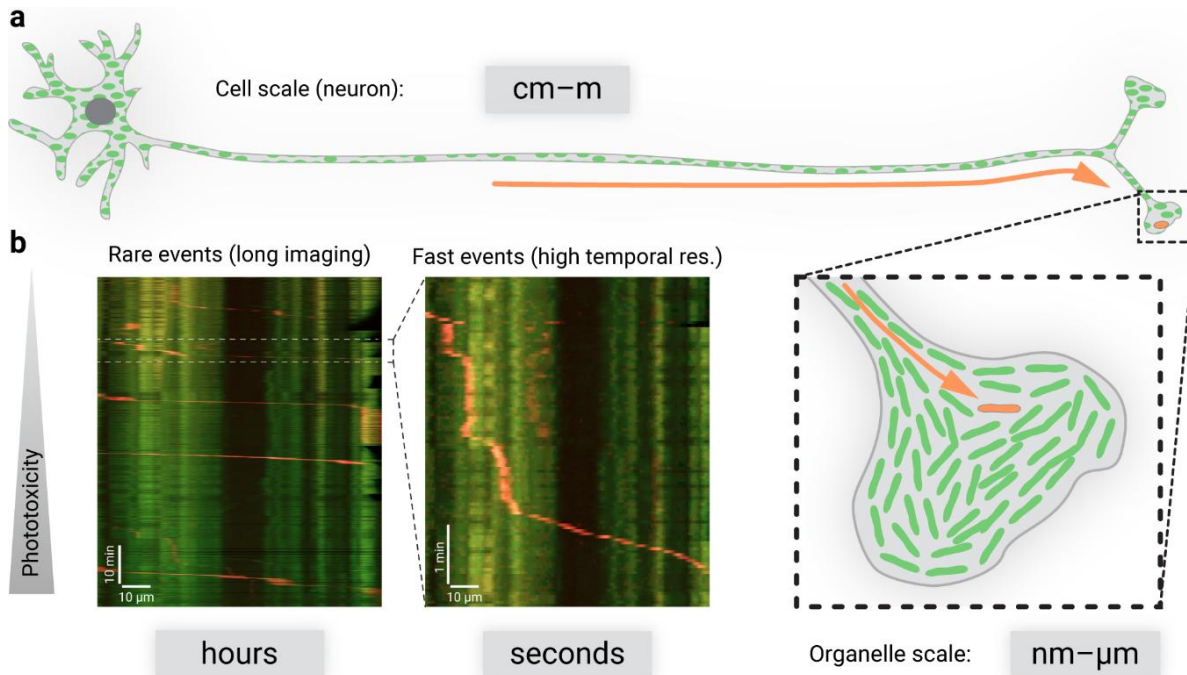


Figure 3.1 | Technical challenges of capturing the mitochondrial lifecycle in neurons. **a**, Spatial dimensions: mitochondria are densely clustered in motor neurons, and nm– μ m precision is necessary to discern the shapes and dynamics of individual mitochondria (red). However, mitochondria can travel distances that are way beyond a single field of view (cm–m). With conventional microscopy, bridging this chasm is challenging. **b**, Temporal dimensions: In axons, mitochondria move quickly (ms–s per μ m) but only occasionally (a few mitochondria per hour), which means long observation times need to be coupled with high frame rates. Both raise the total number of movie frames, increasing phototoxicity. The two images show kymographs of a mitochondrion (red) that moved anterogradely in a terminal motor axon branch (acute nerve-muscle explant of a *Thy1*-mito-Dendra mouse). A kymograph plots the fluorescent signal of an axon (horizontal axis) for each time frame of a movie (vertical axis). Stationary mitochondria, therefore, appear as vertical straight lines, and moving mitochondria as uneven lines. Left: The kymograph of the entire movie shows all events of moving mitochondria but is insufficient to view further details. Right: Enlarged view of the kymograph from the indicated time period, revealing more movement details. Experiment performed by the author.

Conventional widefield microscopy can combine high temporal resolution with long observation times more easily than optical sectioning microscopy, as it causes less phototoxicity, making it more suitable for imaging synaptic mitochondria *in situ* (Misgeld et al., 2007). However, widefield microscopy lacks spatial resolution and contrast, as it collects photons also outside the focal point (Conchello & Lichtman, 2005). The optical pulse-chase imaging assay that will be presented in this work was meant to tackle this and other issues. Using photoswitchable proteins that were targeted specifically to the mitochondrial matrix in neurons, this assay aimed at labeling individual subpopulations of mitochondria for studying the mitochondrial lifecycle *in vivo / in situ*:

- 1) Sparse-labelling mitochondria: visualizing single organelles against the dense pool of resident mitochondria with precision (for example, to measure shapes, transport parameters, and fusion events)
- 2) Proof of origin: labeling mitochondria in a certain neuronal compartment, then monitoring their appearance in another compartment further away, thus virtually expanding the available tracking range well beyond a single field of view
- 3) Time-stamping mitochondria: labeling a mitochondrial population at a certain time point and monitoring its exchange with “new” mitochondria (non-photoswitched), useful for measuring local mitochondrial turnover

Photoswitchable proteins are fluorophores that can change their color under (UV) light illumination (Zhou & Lin, 2013). To target neuronal mitochondria with these proteins, a set of transgenic mouse lines was generated in a collaborative effort (B. Gailer, M. Lakadamyali, M. Leischner, N. Marahori, T. Misgeld; see Gailer, 2022). In brief, the *Thy1*-promoter was used to drive the expression of photoswitchable proteins selectively in neurons, as previously described (see **Materials and Methods**; Marinkovic et al., 2015a, 2015b; Marinkovic et al., 2015c; Misgeld et al., 2007). Photoswitchable proteins are classified into various categories with different pros and cons (Zhou & Lin, 2013).

Line	Spinal cord		Retina			Cortex	Cerebellum			Hippocampus			Expres- sion level	Fixable with PFA?	2-Photon photoacti- vation	
	MN	DRG	RG	AC	BC		GC	MF	PC	DG	CA1	CA2				CA3
<i>Thy1</i> - mitoDen dra;4	+	+	+	±	-	±	-	+	+	-	-	+	-	bright	-	-
<i>Thy1</i> - mitopa GFP;N877	+	+	+	±	-	+	-	+	+	+	+	+	+	bright	+	+

Table 3.1 | Summary of expression patterns of the *Thy1*-mitopaGFP and *Thy1*-mitoDendra mouse lines using in this thesis. +: expression in most cells; subset (±): expression in < 80% of cells. AC: amacrine cells; BC: bipolar cells; CA: cornu ammonis; DG: dentate gyrus; DRG: dorsal root ganglion; GC: granule cells; L: cortical layer; MF: mossy fibers; MN: motor neurons; PC: Purkinje cells; RG: retinal ganglion cells (The characterization was partially adapted from Gailer, 2022, p. 36).

Two proteins from different classes were chosen to expand the variety for potential experimental designs: (1) the photoconvertible protein Dendra2, which can be switched from green to red fluorescence (Gurskaya et al., 2006), and (2) the photoactivateable protein paGFP, which is non-fluorescent in its native state and can be activated into green fluorescence (Patterson & Lippincott-Schwartz, 2002). From various founder lines, two bright and broadly expressing lines were retained and used for further experiments in this thesis (Table 3.1; Gailer, 2022). The properties of these two lines (*Thy1-mito-Dendra*;4 and *Thy1-mito-paGFP*;N877) regarding the expression patterns, levels, and photoconversion will be outlined below.

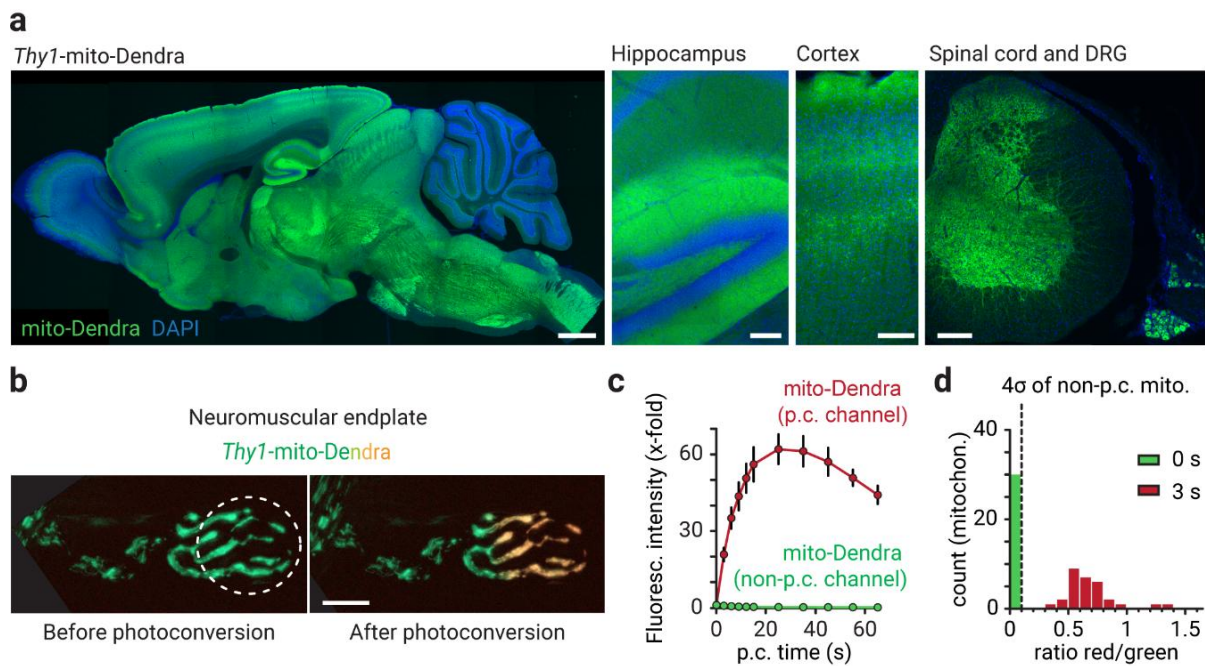


Figure 3.2 | Expression pattern and photoconversion properties in the *Thy1-mito-Dendra* transgenic mouse line. a, Expression of the mito-Dendra transgene throughout the nervous system (endogenous non-photoconverted Dendra fluorescence). Left to right: sagittal brain section, hippocampus, cerebral cortex, horizontal section of spinal cord and a dorsal root ganglion (DRG; modified from Gailer, 2022, p. 48). **b**, Widefield projections of motor axon terminals before and after photoconversion with 290 μ W 405 nm illumination in the circled region for 3 s (from green to red fluorescence; acute nerve-muscle explant). **c**, Photoconversion (p.c.) efficiency with 405 nm light (290 μ W; n = 10 NMJs, 2 *Thy1-mito-Dendra* mice). **d**, Distribution of Dendra-red/green ratio before and after p.c. (settings as in **b**; n = 30 mitochondria from the experiments in **d**). Dashed line indicates the 4x standard deviation distance from the mean of the non-p.c. mitochondria population. **c** shows mean \pm s.e.m. Scale bars in **a** (from left to right): 1 mm, 50 μ m, 50 μ m, 200 μ m; in **b** 10 μ m. The experiments in **b–d** were performed by the author. Figure and text were adapted from Marahori et al. (manuscript in preparation).

Thy1-mito-Dendra (line 4). In this line the cerebellar Purkinje and mossy fibers as well as a subset of cortical layers expressed the mito-Dendra construct brightly (Figure 3.2, a; Table 3.1). Most motor neurons (> 80%) also showed bright labeling (Figure 3.2, a,b; Table 3.1). In the triangularis sterni nerve-muscle explant, the maximum brightness of photoconversion was achieved with ~30 s of 290 μ W UV light illumination (70-fold increase), while further exposure only bleached the protein (Figure 3.2, c). However, 3 s illumination already yielded a ~20-fold

increase of Dendra-red (photoconverted) brightness, corresponding to a ~30-fold increase in Dendra-red/green ratio (**Figure 3.2, c**). Previously, a 30-fold (Lippincott-Schwartz & Patterson, 2003) or 10-fold increase (Karbowski et al., 2004; Karbowski et al., 2014) in fluorescence after photoactivation had been suggested to yield a useful contrast for imaging. Indeed, photoconversion with 3s resulted in Dendra-red/green fluorescence intensities of 405-nm-illuminated mitochondria that were more than 4 standard deviations away from the mean of non-illuminated mitochondrial populations (**Figure 3.2, d**), so this low dose was further used in live imaging experiments to minimize potential phototoxicity (Twig et al., 2006). (Gailer, 2022)

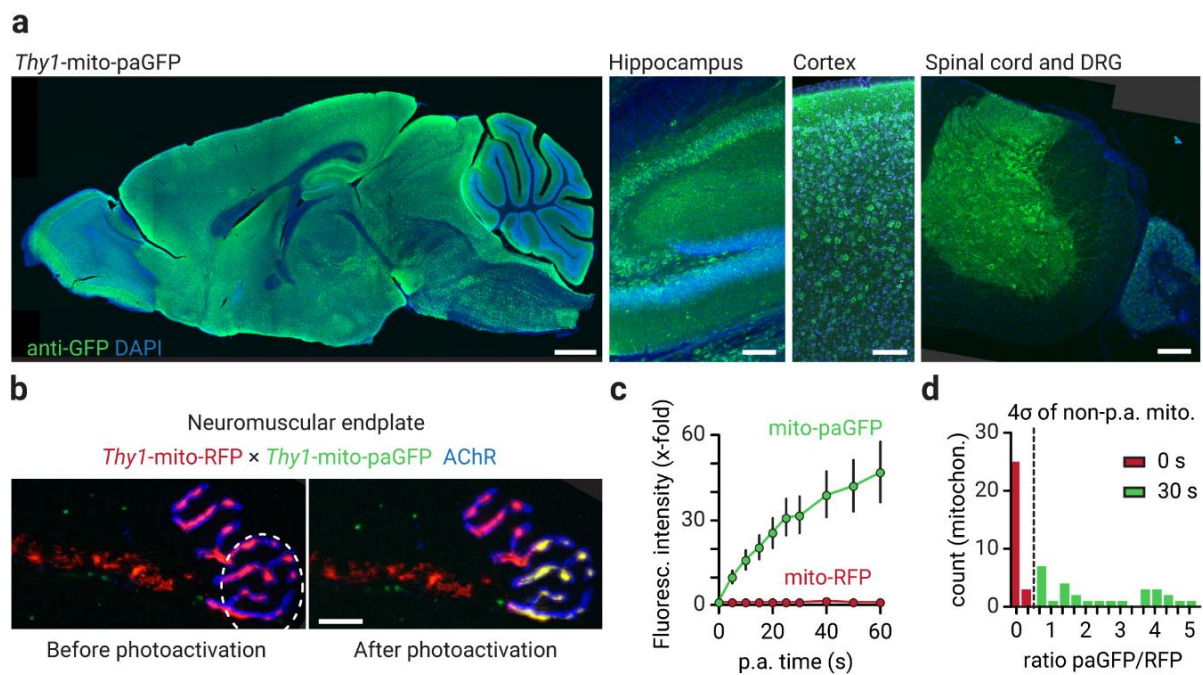


Figure 3.3 | Expression pattern and photoactivation properties in the *Thy1-mito-paGFP* transgenic mouse line. a, The mito-paGFP transgene is widely expressed throughout the central and peripheral nervous system (stained with anti-GFP-antibody). Left to right: sagittal brain section, hippocampus, cerebral cortex, horizontal section of the spinal cord, and a dorsal root ganglion (DRG; modified from Gailer, 2022, p. 37). **b**, Confocal projections of motor axon terminals before and after photoactivation with 290 μ W 405 nm light in the circled region for 30 s (acute nerve-muscle explant, *Thy1-mito-paGFP* × *Thy1-mito-RFP*; postsynaptic acetylcholine receptors stained with α -bungarotoxin, blue), image taken by the author. **c**, Photoactivation (p.a.) efficiency with ascending doses of 290 μ W 405 nm illumination ($n = 12$ NMJs from 4 *Thy1-mito-paGFP* × *Thy1-mito-RFP* mice). **d**, Distribution of paGFP/RFP fluorescence intensity ratio before and after p.a. (settings as in **b**; $n = 28$ mitochondria from the experiments in **c**). Dashed line indicates the 4x standard deviation distance from the mean of the non-p.a. mitochondria population. **c** shows mean \pm s.e.m. Scale bars in **a** (from left to right): 1 mm, 50 μ m, 50 μ m, 200 μ m; in **b** 10 μ m. The experiments in **c,d** were re-analyzed by the author from a dataset by Barbara Gailer (Gailer, 2022). Figure and text were adapted from Marahori et al. (manuscript in preparation).

Thy1-mito-paGFP (line N877). In the CNS of these mice, all layers of the cortex and hippocampus, as well as the cerebellar Purkinje cells and mossy fibers, were labeled (**Figure 3.3, a; Table 3.1**). Lower motor neurons showed bright and broad expression in the spinal cord and the neuromuscular junctions of the triangularis sterni muscle explant (**Figure 3.3, a,b; Table 3.1**). As paGFP is non-fluorescent in its native state, the line was usually crossed with *Thy1-mito-RFP* (Breckwoldt et al., 2014) for background labeling of mitochondria (**Figure 3.3, b**). With

increasing UV illumination, the brightness of photoactivated mito-paGFP steadily increased (**Figure 3.3, c**) and ultimately reached an asymptotic value (Gailer, 2022), providing a maximal ~50-fold increase in fluorescence (**Figure 3.3, c**). A ~30-fold increase in paGFP-fluorescence was achieved at 30s UV illumination (**Figure 3.3, c**), after which the paGFP/RFP ratios of the photoactivated mitochondria were more than 4 standard deviations apart from the mean of the non-photoactivated mitochondria (**Figure 3.3, d**). Concerning photoefficiency and -toxicity, the higher dose to reach ~30-fold contrast was considered a disadvantage for most live imaging experiments when compared to the *Thy1*-mito-Dendra line. (Gailer, 2022)

Unlike mito-Dendra, the photoactivated mito-paGFP was fixable with paraformaldehyde (and glutaraldehyde for 1 hour; **Figure 3.4, d**), making the *Thy1*-mito-paGFP line more useful for correlative histology and electron microscopy. Furthermore, paGFP is activatable by two-photon illumination (Das et al., 2012), which allowed targeting axonal mitochondria with precision on the single-organelle level (**Figure 3.5, d**).

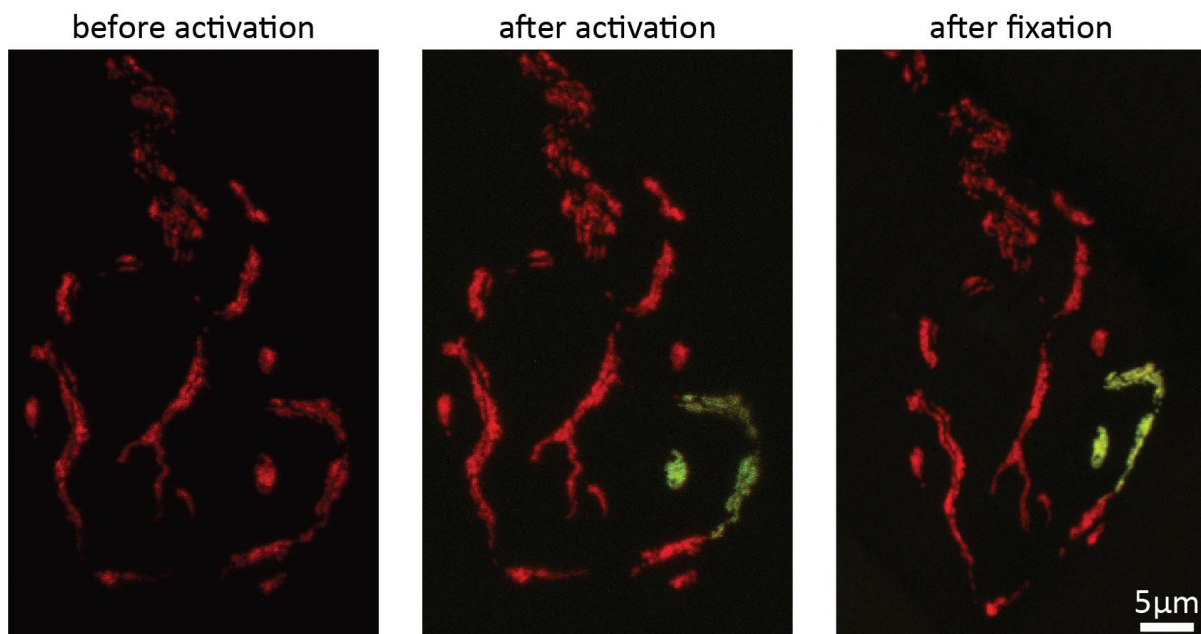


Figure 3.4 | Fixability of photoactivated mito-paGFP. Neuromuscular junction in a triangularis sterni muscle from a *Thy1*-mito-paGFP × *Thy1*-mito-RFP mouse (red: mito-RFP, green: photoactivated mito-paGFP). Left image: Live confocal projection before photoactivation (acute nerve-muscle explant). Center image: Live confocal projection after photoactivation. Right image: Confocal projection of the re-localized NMJ after fixation (2% PFA, 2% GA for 1 hour). Experiment was performed by the author together with Tatjana Kleele.

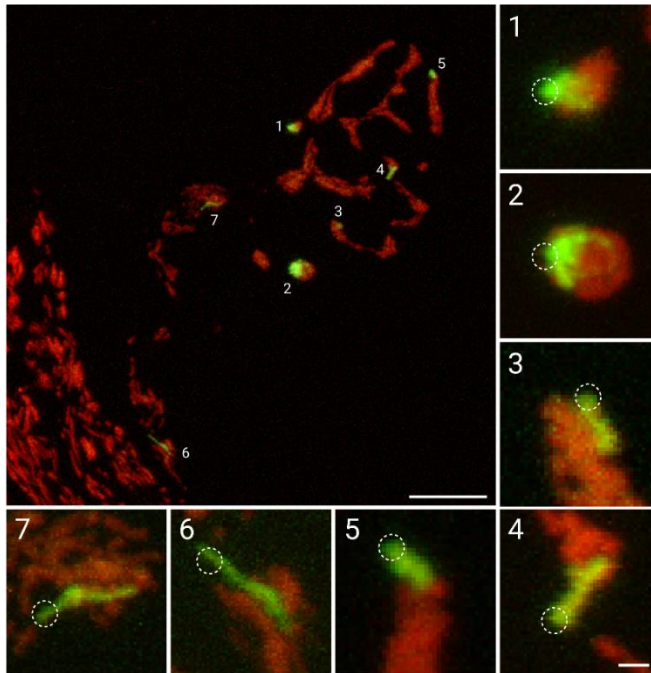


Figure 3.5 | Photoactivation of paGFP with a 2-Photon-laser. Neuromuscular junction in a nerve-muscle explant from a *Thy1-mito-paGFP* (green) × *Thy1-mito-RFP* (red) mouse (top left image). The mitochondria labeled by numbers were targeted for photoactivation by a two-photon laser that was placed in the areas indicated by dotted circles (surrounding images show magnified views of the areas). Scale bars: large image 10 μm , surrounding images 1 μm . The experiment was performed by the author.

3.2. Resolving mitochondrial shape

As described in **section 1.2.1**, mitochondria form networks of varying degrees, shapes, and sizes. The morphology of mitochondria can yield valuable information about their functional status. Unlike in the somatodendritic area, axonal mitochondria usually do not form networks and are described as short, with enrichment at the presynaptic sites. However, most of the reviewed studies have been performed in CNS neurons or cell cultures, while the architecture of mitochondria in α -motor axons and their synapses has not yet been explored in detail.

Fine structural elements of mitochondria, like the outer membrane and its continuity into networks, can be discerned using electron microscopy (EM; Palade, 1952). The tissue slices for EM are typically smaller than the diameter of most mitochondria so that a single section only shows cross-sections (of unknown orientation) and not the entire organelle in its continuity. **Figure 3.6** illustrates this, where presynaptic mitochondria were imaged in consecutive tissue sections: some slices show the mitochondrion throughout its entire length, while in other slices, the mitochondrion was only cut partially and falsely appears as two shorter objects. This suggests that a volume EM technique would be ideal to adequately discern mitochondrial shapes and features like network connectivity.

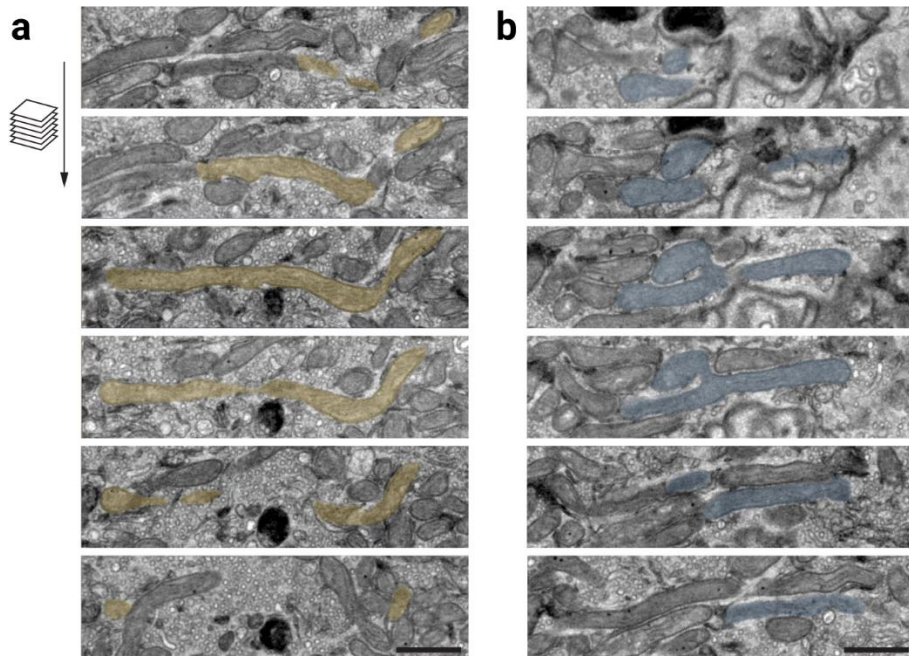


Figure 3.6 | Electron micrographs taken from serial ultrathin sections. Images from top to bottom show electron microscopy slices at various depths (z) in the stack. Two mitochondria (pseudo-colored orange in **a**, blue in **b**) in a neuromuscular junction of the triangularis sterni muscle were followed through the stack. Scale bars: 500 nm. Experiment was performed by the author together with Martina Schifferer.

Using a serial sectioning approach (ATUM; Kasthuri et al., 2015), volume electron microscopy stacks of adult neuromuscular junctions were acquired in the murine triangularis sterni muscle, and hundreds of presynaptic mitochondria were manually reconstructed (example in **Figure 3.7, a,b**, see **Materials and Methods**). The reconstructed NMJ branch in **Figure 3.7, a,b** shows a vast majority (90%) of the mitochondria being discrete and “stick”-shaped (200–3000 nm long), with the remaining mitochondria branching only into very basic bifurcated or trifurcated structures. As described for other types of axons, no extensive mitochondrial networks were found in α -motor axons (5 partial NMJs stacks from 4 mice). The sizes of the mitochondria were relatively uniformly distributed (fitted inverse Gaussian; **Figure 3.7, c**) and, surprisingly, very similar when the presynaptic site was compared to the myelinated axon branch (NMJ $0.03 \pm 0.02 \mu\text{m}^3$ vs. Axon $0.03 \pm 0.02 \mu\text{m}^3$, $p \geq 0.05$, Mann-Whitney-test, mean \pm s.e.m.; **Figure 3.7, c**).

Importantly, the experiments revealed how densely mitochondria are packed in the presynaptic junction: the distance between organelles could be just 4 nm (**Figure 3.8, a**), which is well below the diffraction limit of light. In the myelinated axon branch, however, mitochondria were more loosely arranged, which means that light microscopy could discern mitochondria with more confidence in this region (Airyscan, superresolution technique; **Figure 3.8, a**). The measurements of mitochondrial volume in the myelinated axon were comparable between Airyscan and EM (incl. 20–30% shrinkage through chemical fixation, communication by M. Schifferer; see **Figure 3.8, b**), suggesting that provided enough distance lies between the organelles (or a sparse label is employed), superresolution light microscopy can also be used to adequately quantify mitochondrial shapes in motor axons.

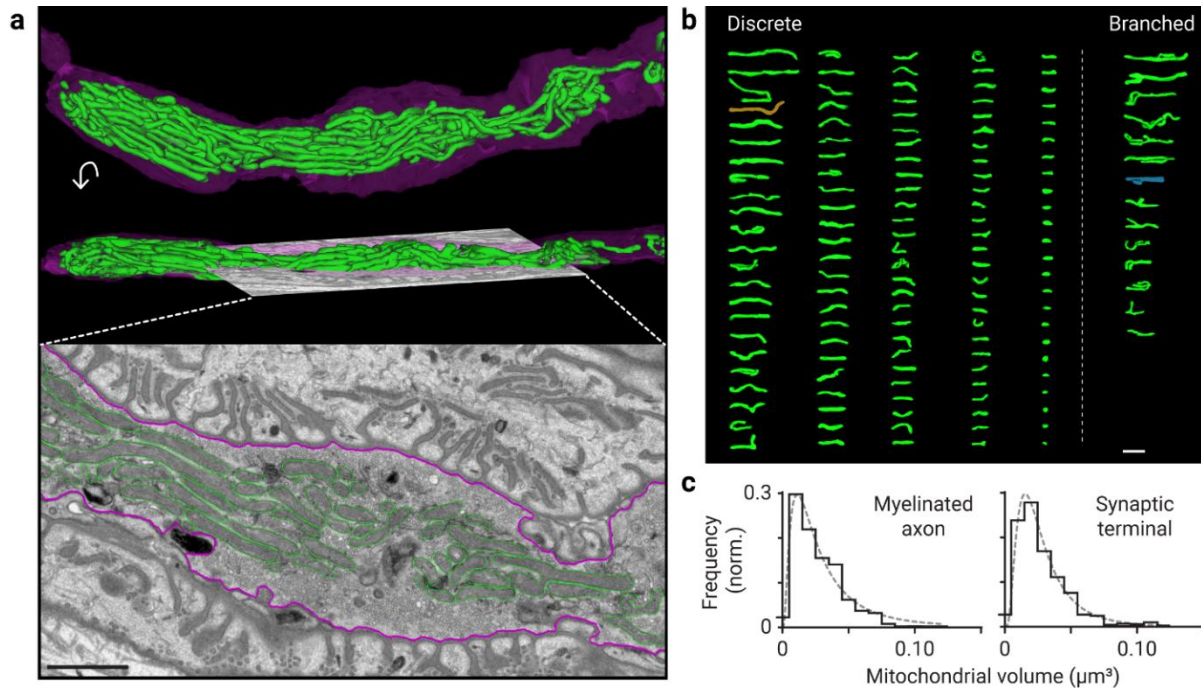


Figure 3.7 | Morphology of presynaptic mitochondria. **a**, Top: Reconstruction of an NMJ branch (violet) and its mitochondrial population (green) from an electron microscopic image stack, taken in the triangularis sterni muscle of a mouse. Middle: 90° Rotated view of the reconstruction. Bottom: Slice of the electron microscopy stack located at the indicated position; reconstructed mitochondria outlined in green, neuronal membrane in violet. **b**, All mitochondria reconstructions from **a** shown individually, sorted by size of the mitochondria. Left group: discrete (non-branched) organelles (orange: reconstruction of the mitochondrion in **Figure 3.6, a**), right group: branched organelles (blue: reconstruction of the mitochondrion in **Figure 3.6, b**). **c**, Distributions of mitochondrial volumes in the presynaptic terminal (right plot) and the adjacent myelinated axon branch, dotted line shows a fitted inverse Gaussian curve (left plot; $n = 345$ mitochondria in NMJ vs. $n = 203$ mitochondria in myelinated axon from 2 axon terminals, 1 mouse). Scale bars: **a, b** 1 μm . Experiments and analysis were performed by the author together with Martina Schifferer.

Unlike high-resolution techniques such as EM and Airyscan, conventional widefield microscopy cannot directly resolve 3-dimensional shapes of mitochondria because of its low depth (z) resolution. Previous investigations in the lab have taken advantage of the higher resolution in the xy -plane to measure the length and width of a mitochondrion, then—based on the assumption of a cylindrical or ellipsoidal shape—infer the mitochondrion’s volume (see **Materials and Methods**; Plucinska et al., 2012). As this study did not corroborate the validity of this assumption, a correlative experiment was designed to compare the mitochondrial volume measurements from widefield with Airyscan images. Airyscan microscopy, with its resolution of up to 90 nm in the xy -plane, can resolve fine details of mitochondrial morphology (Kondadi et al., 2020), and would therefore allow one to discern shape variations in the width dimension (typical mitochondrial diameters are close to the resolution limit of conventional light microscopy; **Figure 3.9, c, g**). When assuming a cylindrical or ellipsoid shape, imprecisions in width would have a particular impact on the result since mitochondrial volume scales exponentially with width but only linearly with length (see **Materials and Methods**). In the fixation-resilient mouse line *Thy1-mito-paGFP* \times *Thy1-mito-RFP*, an optical pulse-chase widefield experiment was performed to label

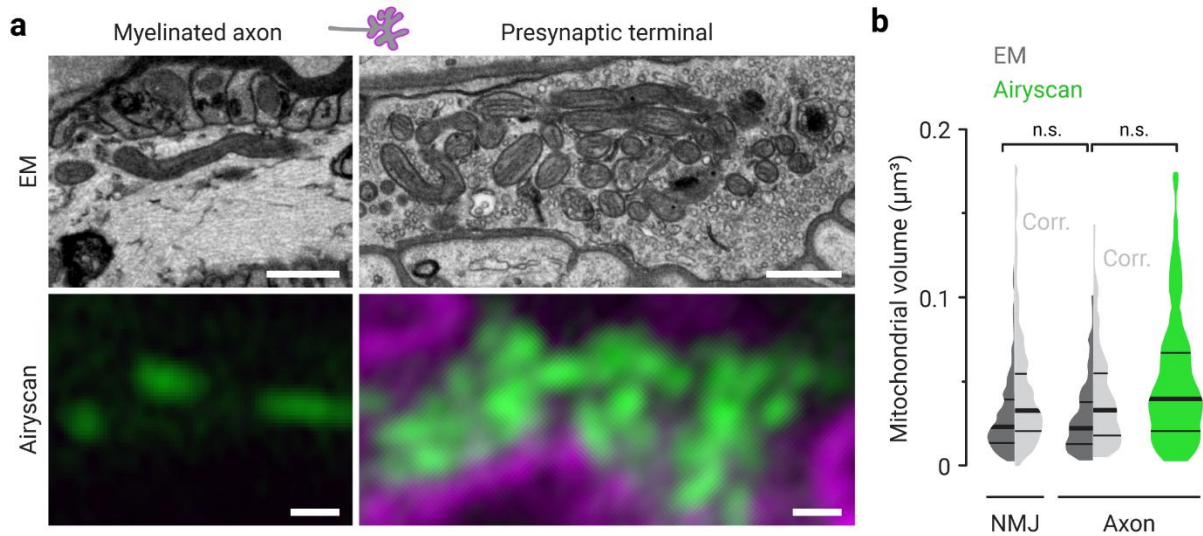


Figure 3.8 | Comparison of Airyscan microscopy with electron microscopy. **a**, Electron microscopy images (top row) and Airyscan images (bottom row; green: *Thy1*-mito-XFP, magenta: acetylcholine receptors) of mitochondria in the presynaptic terminal (right images) and in the adjacent myelinated terminal axon branch (left images) in triangularis sterni muscles. **b**, Quantification of mitochondrial volume in presynaptic terminal (NMJ) and myelinated axon from electron microscopy stacks (dark gray) and in axon from Airyscan stacks (green plot). “Corr(ected)”: Light gray side of the plots shows the quantification in EM after accounting for assumed tissue shrinkage (30%). EM-data: same dataset as in **Figure 3.7** (replotted). Airyscan data: $n = 88$ mitochondria from 10 axons, 5 *Thy1*-mito-XFP mice. $p \geq 0.05$ (between Airyscan and corrected EM results); one-way ANOVA test with Kruskal-Wallis multiple comparison test. Scale bars in **a** 500 nm. EM experiments were performed by the author together with Martina Schifferer, and all analysis and Airyscan microscopy were performed by the author.

anterogradely and retrogradely traveling mitochondria (Marinkovic et al., 2012) for re-identification on an Airyscan setup after fixation of the sample (experiment was performed in the large ‘stem’ intercostal nerve axons; see **Figure 3.9** for experimental setup). The correlated measurements proved mitochondrial size to be indistinguishable between Airyscan and widefield microscopy (based on an ellipsoidal approximation; **Figure 3.9, b–i**; Anterograde—Widefield $0.17 \pm 0.02 \mu\text{m}^3$ vs. Airyscan $0.14 \pm 0.02 \mu\text{m}^3$, $p \geq 0.05$, Mann-Whitney-U test; Retrograde—Widefield $0.14 \pm 0.02 \mu\text{m}^3$ vs. Airyscan $0.13 \pm 0.01 \mu\text{m}^3$, $p \geq 0.05$, Mann-Whitney-U test; mean \pm s.e.m., $n \geq 15$ axons from ≥ 3 mice). Overall, these results corroborate the validity of estimating mitochondrial volume from widefield time-lapse images (based on an ellipsoidal approximation).

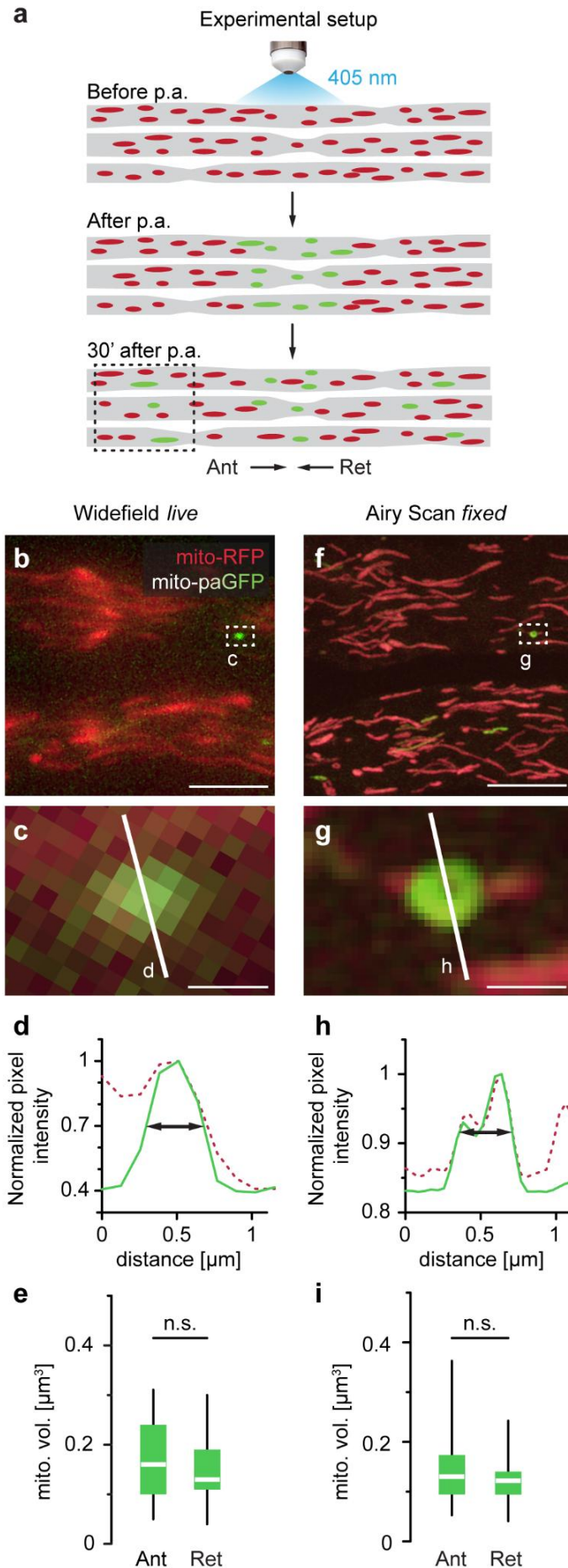


Figure 3.9 | Superresolution volume measurements of mitochondria undergoing axonal transport. **a**, Experimental setup: Axonal mitochondria marked with both (non-fluorescent) paGFP and (fluorescent, red) RFP were illuminated with UV (405 nm) light in a 200- μ m-stretch of intercostal nerve, thus photoactivating paGFP (green) and marking the mitochondria for later observation (acute nerve-muscle explants of *Thy1-mito-paGFP* \times *Thy1-mito-RFP* mice). 30 min after photoactivation (p.a.), single green-fluorescent mitochondria that underwent axonal transport were identified in regions adjacent to the photoactivation site (**b,c**). After fixation, the displaced mitochondria were re-localized and imaged with Airy Scan microscopy (**f,g**). **b**, Widefield live image adjacent to the photoactivation site (outlined by the dashed box in **a**). **c**, Individual photoactivated mitochondrion (position marked by the box in **b**). **d**, Pixel intensity profile of the mitochondrion shown in **c** (across the pixels indicated by the line in **c**; green: pa-GFP channel, red: RFP channel). Arrows show the width of the paGFP-intensity plot at half of its amplitude. **e**, Mitochondrial volume of photoactivated mitochondria that were transported in anterograde and retrograde directions, measured in widefield images ($n \geq 15$ axons, ≥ 4 mice). **f**, Overview of the region shown in **b** after sample fixation and re-location at the Airyscan setup. **g**, Airyscan image of the photoactivated mitochondrion shown in **c**; position of image outlined by box in **f**. **h**, Intensity profile of pixels along the line shown in **g**. Colors and symbols as in **d**. **i**, Mitochondrial volume of photoactivated mitochondria that moved in anterograde and retrograde directions measured in Airyscan image stacks (for calculation, see **Materials and Methods**; $n \geq 18$ axons, ≥ 3 mice). Scale bars in **b,f** 5 μ m, in **c,g** 500 nm. Box plots: median, quartile 1–quartile 3, whiskers 95th percentiles. Unpaired t-test was used to determine significance in **e** and Mann-Whitney test in **i**: n.s.: non-significant, $p \geq 0.05$). The author performed all experiments. Figure and text were adapted from Marahori et al. (manuscript in preparation).

3.3. Anterograde delivery of mitochondria to synapses

3.3.1. Mitochondrial turnover rate in synapses

Neurons are thought to perform most mitochondrial biogenesis in the soma, having developed anterograde axonal transport to supply their periphery with “new” mitochondria (Chang & Reynolds, 2006; Hollenbeck, 1996). However, the extent to which anterograde transport takes over mitochondrial “turnover” instead of local biogenesis is unknown. Previous reports have quantified axonal transport in adult animals *in vivo* and acute intercostal nerve-muscle explants, showing that ~5 mitochondria pass through an axonal cross-section per minute in anterograde direction (**Figure 3.16**; Misgeld et al., 2007). These transport rates decline in a proximal-to-distal manner as the stream of mitochondrial cargo divides proportionally at each axon branch point (Misgeld et al., 2007; see also **Figure 3.16**). For example, in terminal axon branches that supply neuromuscular junctions, only ~4 mitochondria move anterogradely per hour (**Figure 3.16**). This number suggests that the majority of anterograde mitochondrial transport in stem axons is targeted to the NMJs, given that a small motor unit as characteristic of the triangularis sterni muscle forms around 50 NMJs (Keller-Peck et al., 2001; Lu & Trussell, 2007). The mitochondrial pool of a neuromuscular junction contains ~300–500 mitochondria (counts measured in EM, **Section 3.2**), which, given an hourly entry of 4 mitochondria, would exchange the entire synaptic pool within 3 to 5 days. This is calculated under the assumption that new presynaptic mitochondria mostly originate from anterograde transport from the soma and not from local biogenesis. To test this, a “pulse-chase” experiment was performed by photoconverting presynaptic and axonal mitochondria in sternomastoid muscles of *Thy1-mito-Dendra* and *Thy1-mito-Kaede* mice, then tracking the fluorescent signal *in vivo* (by M. Lakadamyali; **Figure 3.10**). The photoconverted mito-Dendra signal remained highly stable and did not turn over for several days (**Figure 3.10, a,b**). The signal decayed over time and became hard to detect after 96 hours post-photoactivation (**Figure 3.10**). Together, the pulse-chase and the axonal transport data suggest that the majority of “new” mitochondrial material is delivered to NMJs from the soma (see also **Discussion**).

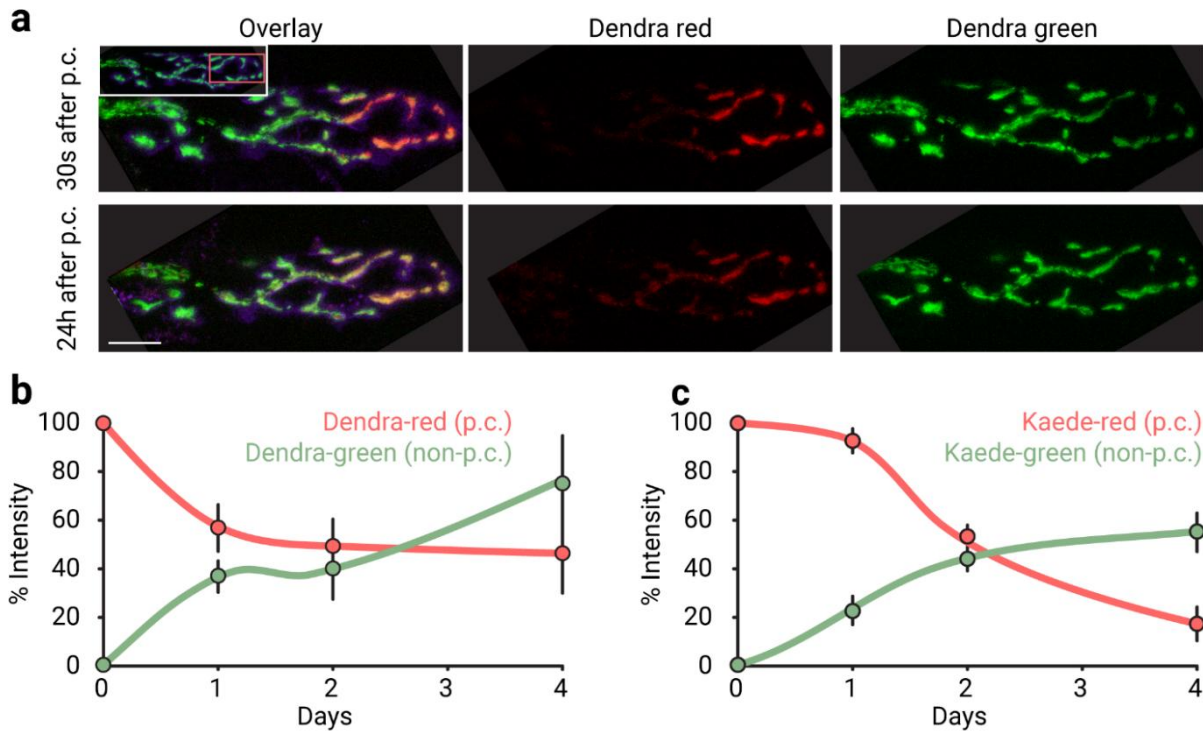


Figure 3.10 | Long-term monitoring of synaptic mitochondrial turnover *in vivo*. **a**, Confocal projections of an NMJ with mito-Dendra-labelled mitochondria (green, right column), which were identified *in vivo* in the surgically exposed sternomastoid muscle by the presence of acetylcholine receptors (violet). A small region of interest (red square) within the NMJ was illuminated with 405 nm laser light to induce photoconversion to red fluorescence (red, center column). Inset in the top left shows the NMJ before photoconversion. Imaging the same NMJ 24 hours later showed the presence of red mitochondria within the photo-converted region (lower row). **b**, Time-course of red and green fluorescence intensity of Kaede and Dendra in photoconverted synaptic territories. Intensities were measured from images obtained by repetitively recording NMJs using the same imaging parameters (n = 28 NMJs in *Thy1-mito-Kaede* and n = 9 NMJs in *Thy1-mito-Dendra* mice). The measurements were normalized to the intensities of a control NMJ that had not been photoconverted. Scale bar is 10 μ m. Experiments were performed by Dr. Melike Lakadamyali in the lab of J. Lichtman, Harvard University, USA.

3.3.2. Destination of anterograde transport

Mitochondria are typically enriched in presynaptic terminals, but the mechanism that drives this enrichment *in vivo* has not been investigated. Specific delivery to synaptic sites via anterograde transport, as suggested in the chapter before, is one possibility, with different mechanisms having been described in cell cultures, such as Ca^{2+} - or AMPK-driven anchoring of moving mitochondria at synaptic sites. Such (1) “targeted” mitochondrial delivery would require that mitochondria, in order to arrive at the synapses in the tips of the axonal tree, bypass many cm–m of the main axon trunk without stopping; this model would stand in contrast with other models, like (2) random likelihoods of stopping in any area of the axon or (3) a “slow wave” model, where mitochondria only slowly shift and push forward to fill up the axon (Ferree et al., 2013), similar to the sap of a tree.

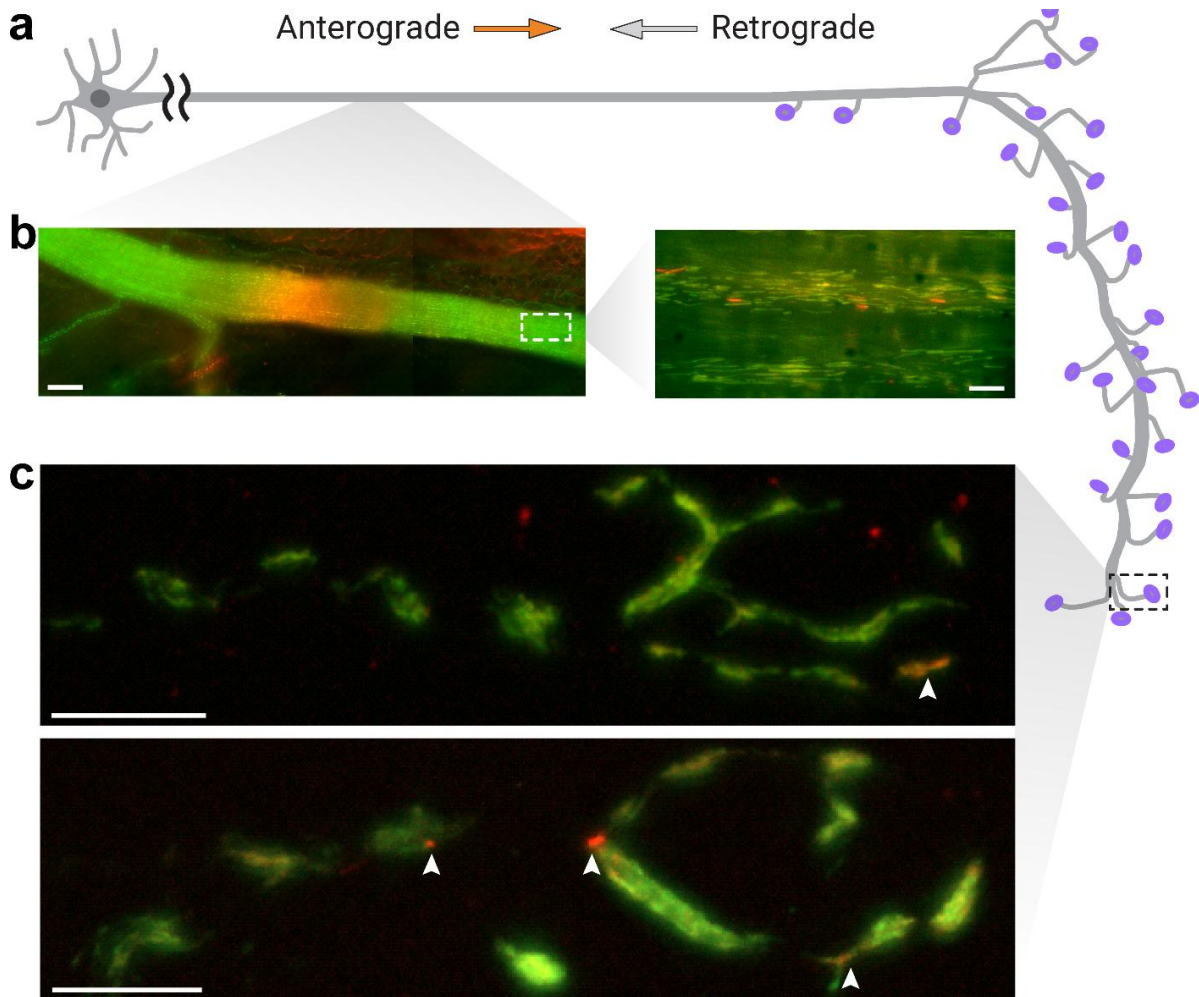


Figure 3.11 | In vivo pulse-chase experiment of mitochondrial transport in the triangularis sterni muscle in *Thy1-mito-Dendra* mice. **a**, Schematic of a motor neuron indicating experimental setup and positions of the imaging areas. **b**, Photoconversion of a stretch in the intercostal nerve after surgical exposure of the nerve and photoconversion with a 20× water objective for 1 min. The surgical site was closed after photoconversion, and images of the intercostal nerve were acquired 4–8h after photoconversion in acute nerve-muscle explants. Left: widefield overview of the intercostal nerve. Right: widefield image of axons positioned in anterograde direction from the photoconversion site (boxed area indicates the area from which the image was taken), showing photoconverted anterogradely moving mitochondria. **c**, Widefield projections from neuromuscular junctions indicating photoconverted mitochondria by arrows. Scale bars in **b** 100 μm (left) and 10 μm (right), in **c** 10 μm . Experiments were performed by the author together with Dr. Tatjana Kleele.

To test whether anterogradely moving mitochondria traverse the intercostal nerve in a “straightforward” manner, stretches of intercostal nerve were photoconverted in *Thy1-mito-Dendra* mice. Assuming a peak velocity of mitochondria of $\sim 1 \mu\text{m/s}$ (Misgeld et al., 2007), mitochondria could arrive at the neuromuscular junctions at the axon tips earliest 3–6 h after photoconversion (the stem axon imaging site is $\sim 1\text{--}2\text{cm}$ away from the NMJs). As this timespan surpasses the lifetime of the nerve-muscle explant, the photoconversion was performed *in vivo* after surgical exposure of the intercostal nerve (see **Materials and Methods**), and then the explant was prepared for imaging between 4–8h after photoconversion. In a preliminary dataset of this experiment, single photoconverted mitochondria were indeed readily observed in neuromuscular junctions at this point in time (**Figure 3.11**), suggesting that these mitochondria

had directly moved to this location without any detours or longer stops on their way. A similar experiment was conducted using an alternative approach: Using a Cre-driven system (ROSA-mito-GFP mice), the expression of a mitochondrial matrix GFP was induced in the motor neuron somata via injection of an AAV9-iCre virus into neonatal mice (the ‘pulse’). The appearance of mito-GFP was then monitored over time (‘chase’) in different compartments of the neuron: somata, stem axons, and neuromuscular junctions. In this exploratory experiment, GFP-containing mitochondria were initially observed most densely at the synaptic junctions (**Figure 3.12**, 5 dpi), while over time, both axon and junction slowly increased their density of GFP-expressing mitochondria. This experiment suggests that indeed, mitochondria are transported in a “straightforward” manner towards junctions. However, this experiment would need to be repeated in mice with a background labeling of all mitochondria (e.g., *Thy1*-mito-RFP) to fully appreciate the proportion of mitochondrial delivery.

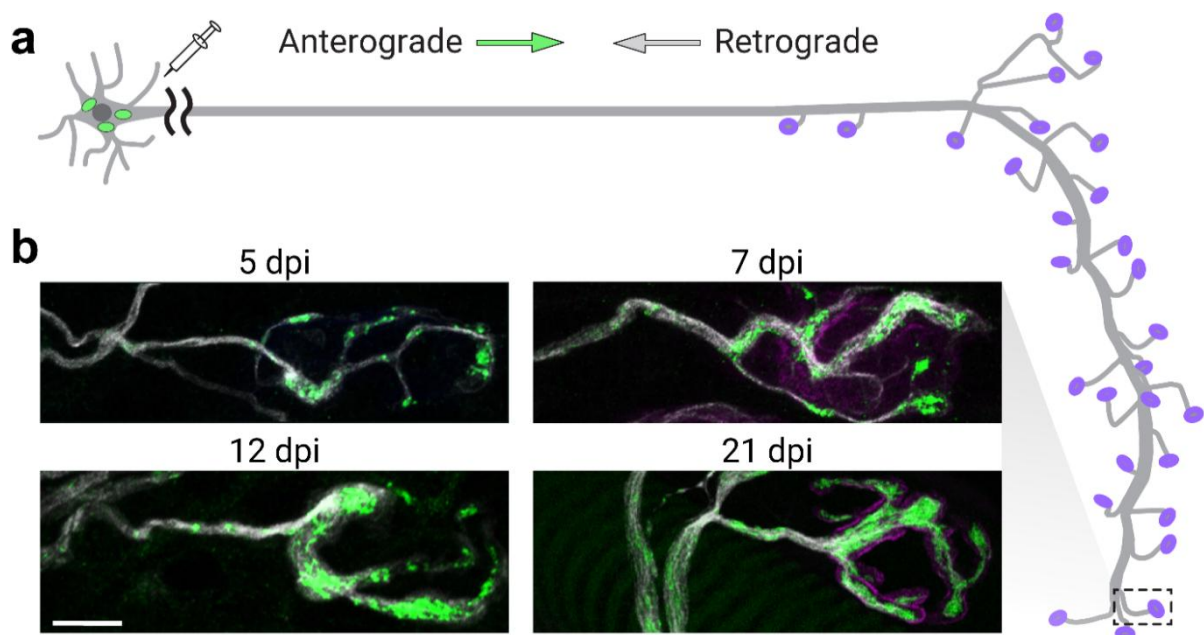


Figure 3.12 | *In vivo* pulse-chase experiment of mitochondrial transport in the triangularis sterni muscle in ROSA-mito-GFP mice injected with an AAV9-iCre virus. **a**, Schematic of a motor neuron indicating experimental setup and positions of the imaging areas. **b**, Confocal projections of neuromuscular junctions at different days post injections (dpi). Axons are labeled with a β III-tubulin-antibody (grey), anti-GFP-antibody (green), and, on the right side, with bungarotoxin (magenta). Scale bar in **b** 10 μ m for all images. Experiments were performed by the author.

3.3.3. Modes of mitochondrial delivery

Different mechanisms have been suggested to explain how mitochondrial delivery to specific axonal sites is regulated on a global scale inside the cell (**Section 1.5.2**). According to the “running-sushi-belt” model, mitochondria profusely circulate throughout the axon to be picked up locally by synaptic sites that need them (Wong et al., 2012). The mitochondria that were not

needed anywhere will make a turn at the axon end to continue scouting in the opposite direction (Wong et al., 2012). An alternative model, however, suggests that axons already “know” the actual demand of downstream located axonal sites and are able to “match” the anterograde transport rate precisely to this need, thereby avoiding any (energy-wasting) redundancy in mitochondrial transport.

The following experiment was designed to test which model best describes the mode of mitochondrial delivery to neuromuscular junctions, as this has not yet been explored *in vivo*. Using the transgenic mouse line *Thy1-mito-Dendra*, neuromuscular junctions (NMJs) were located in acute nerve-muscle explants on a widefield setup; then suitable NMJs were selected for time-lapse imaging of mitochondrial transport in the synaptic entry point and terminal axon branch (see **Materials and Methods**). The term ‘synaptic entry point’ describes the region where the terminal motor axon branch loses its myelin sheath to transition into the synaptic territory. Just prior to the start of the movie, the mitochondria on both sides of the entry point were marked by different labels: all mitochondria that resided in the synaptic territory were labeled by photoconversion to exhibit red fluorescence, while all other axonal mitochondria were left in their non-photoconverted (green) state (**Figure 3.13, a–c**). Thus, it could be easily determined whether anterogradely moving mitochondria (coming from the axon, they would appear green) ever made a “U-turn” inside the junction to continue scouting the axon in retrograde direction, as would be predicted by the ‘running-sushi-belt’ model (**Figure 3.13, a**). Alternatively, the ‘matched delivery’ model (“à la carte”) would predict that no anterogradely moving (green) mitochondria turned around, which means that all retrogradely moving mitochondria would rather have red fluorescence (**Figure 3.13, a**).

During time-lapse imaging over a total of ~32 hours (‘axon imaging hours’), the vast majority of retrograde transport was indeed photoconverted (97% of 98 retrogradely moving mitochondria, **Figure 3.13, d–f**). However, in this experiment, each junction was only imaged for up to 2 hours after photoconversion, as fluorescence bleaching would prevent further imaging. To exclude that mitochondria simply took a longer time to turn around in the synapse, the experiment was repeated, but with transport imaging starting at 2 hours after the photoconversion was initially performed until the lifetime of the explant preparation was reached (approximately 4 hours).

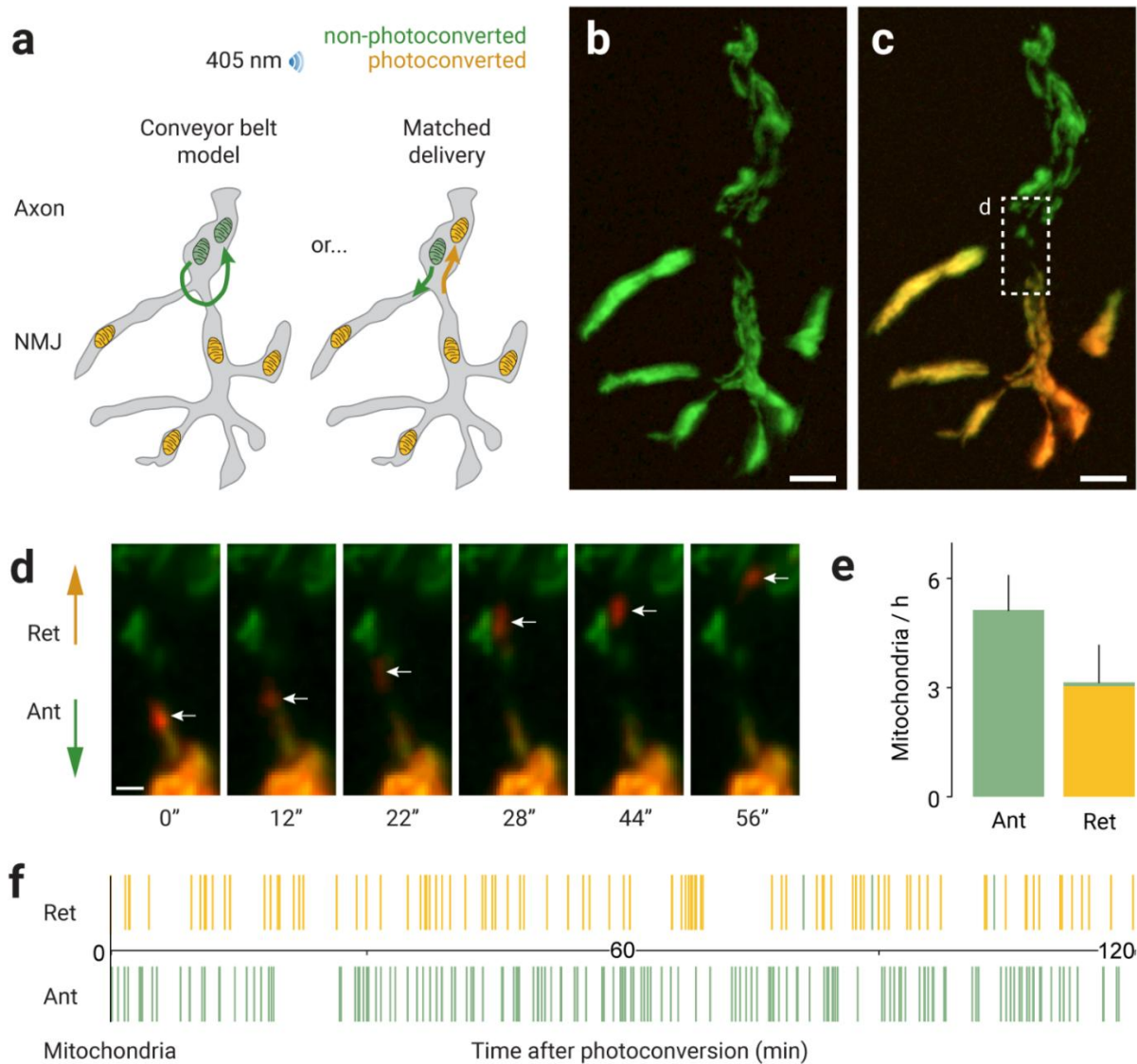


Figure 3.13 | Mitochondrial delivery is matched to the “need” of the presynaptic terminal. **a**, Experimental setup: presynaptic mitochondria were photoconverted from green to red fluorescence to distinguish between two models of mitochondrial delivery. Left: Conveyor belt (or “running sushi belt”) model predicts non-photoconverted mitochondria returning from the junction in retrograde direction, contrary to the “matched delivery” model (right), which predicts that “new” mitochondria which enter the junction anterogradely do not immediately turn around, rather, retrograde mitochondrial flux consists of “old” (thus photoconverted) mitochondria. **b,c** Widefield projections of neuromuscular junctions in a triangularis sterni muscle live explant of a *Thy1-mito-Dendra* mouse, before (**b**) and after (**c**) illumination of the synaptic mitochondria with 405 nm light. **d**, Mitochondrial transport was time-lapse imaged in the area indicated by a box in **c**. White arrows show a photoconverted mitochondrion at different time points, as it moves retrogradely from the junction towards the axon. **e,f** Mitochondrial transport in anterograde and retrograde direction, with color-code showing whether the moving mitochondria were photoconverted (orange) or non-photoconverted (green; $n = 24$ axons, from 23 *Thy1-mito-Dendra* mice): **e**, Average mitochondrial transport rates and **f**, transported mitochondria from all experiments listed individually (as “ticks” in either anterograde and retrograde direction), sorted by the time of event occurrence (time after photoconversion; $n = 159$ anterogradely and $n = 98$ retrogradely moving mitochondria). Scale bars: $5 \mu\text{m}$ in **b,c** and $1 \mu\text{m}$ in **d**. All experiments were performed by the author.

During a total of ~20 axon imaging hours of this modified experiment, most anterogradely moving mitochondria were still retained in the junction, with ~95% of retrogradely transported

mitochondria being photoconverted ($n_{\text{ant}} = 78$ and $n_{\text{ret}} = 37$ mitochondria, from 10 axons in 7 *Thy1-mito-Dendra* mice).

Potential damage to mitochondria by UV phototoxicity (Twig et al., 2006) could be a confounding factor, even though care was taken to use the lowest possible dose of UV light for photoconversion (see **Section 3.1**). To exclude that photodamage to the synapse affected the results, an “inverse” experiment was designed, where a portion of the axon that supplies anterogradely moving mitochondria to a junction was targeted by UV light (**Figure 3.14, a,b**). In this experiment, time-lapse imaging at the synapse showed that no photoconverted mitochondria that moved anterogradely towards the synapse returned; instead, all retrograde transport was non-photoconverted ($n = 60$ retrogradely moving mitochondria, 26 ‘axon imaging hours’; **Figure 3.14, c–e**). Thus, any effects of putative phototoxicity on the mode of mitochondrial delivery to junctions were excluded.

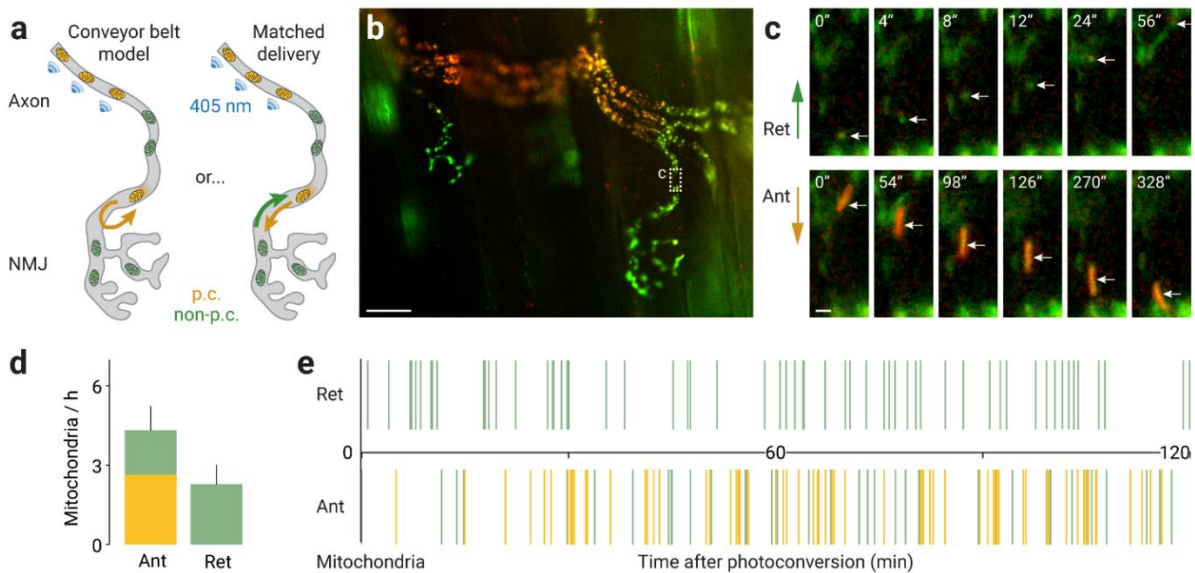


Figure 3.14 | Mitochondrial delivery being matched to the “need” of the presynaptic terminal is not an artifact of photoconversion-induced toxicity. **a**, Experimental setup: mitochondria in the axon supplying a neuromuscular junction were photoconverted from green to red fluorescence to “catch” anterogradely moving mitochondria. Thus, a similar experiment could be performed as in **Figure 3.13**, but without exposing the synapse to potentially toxic UV light. Left: Here, the conveyor belt (or “running sushi belt”) model predicts that photoconverted mitochondria can return retrogradely, whereas the “matched delivery” model (right) predicts that only non-photoconverted mitochondria leave the junction. **b**, Widefield image of neuromuscular junctions in a triangularis sterni muscle live explant of a *Thy1-mito-Dendra* mouse, after illumination of the supplying axon bundle with 405 nm light. **c**, Mitochondrial transport was time-lapse imaged in the area indicated by a box in **b**. White arrows show a non-photoconverted (top row) and a photoconverted (bottom row) mitochondrion at different time points as they move in retrograde and anterograde direction. **d,e** Mitochondrial transport in anterograde and retrograde direction, color-code showing whether the moving mitochondria were photoconverted (orange) or non-photoconverted (green; $n = 13$ axons, from 10 *Thy1-mito-Dendra* mice): **d**, Average mitochondrial transport rates and **e**, transported mitochondria from all experiments listed individually (as “ticks” in either anterograde and retrograde direction), sorted by the time of event occurrence (time after photoconversion; $n = 112$ anterogradely and $n = 60$ retrogradely moving mitochondria). Only a subset of the anterogradely moving mitochondria were photoconverted ($n = 69$) since only a limited portion (~1000 μm) of the entire axon was targeted for photoconversion. Scale bars: 10 μm in **b** and 1 μm in **c**. The author performed all experiments.

To summarize, these results show that most mitochondria that are transported to neuromuscular junctions are retained there for up to 4 hours (the duration of the observation), thereby refuting the ‘running sushi belt’ model in favor of a ‘matched delivery’ model for motor neurons. Furthermore, the results suggest a distinct purpose and identity of retrogradely moving mitochondria, as this population originates from an older population of resident synaptic mitochondria.

3.3.4. Mitochondrial fusions in synapses

Studies that had been performed *in vitro* on mitochondrial transport showed that transported mitochondria are anchored at synapses in a Ca^{2+} -dependent manner to support neurotransmission (Chen & Sheng, 2013). To investigate how anchoring occurred *in vivo*, anterogradely moving mitochondria were followed by time-lapse imaging in neuromuscular junctions of *Thy1-mito-Dendra* mice. Similar to the experimental setup in **Figure 3.14**, anterogradely moving mitochondria were labeled by photoconverting a portion of the axon that supplied the junction of interest. Upon entering a junction from the axon, the photoconverted mitochondria were randomly distributed throughout the junction and eventually halted for a protracted time upon reaching their final positions, potentially suggesting some form of anchoring or capturing mechanism similar to the one that has been described in cell cultures.

Surprisingly, anterogradely moving mitochondria showed a unique behavior that was otherwise very atypical for stationary synaptic and axonal mitochondria: within 15 minutes of having entered the junction, half of the followed mitochondria had fused into the stationary synaptic pool (**Figure 3.15**). Upon complete fusion between a photoconverted and a non-photoconverted mitochondrion, the process becomes visible due to the diffusion of the two colors after matrix content intermixing (**Figure 3.15**). In a control performed with stationary mitochondria, fusions were rare: using a two-photon laser, individual stationary mitochondria were photoactivated in the densely populated synaptic junction (*Thy1-mito-paGFP* × *Thy1-mito-RFP* line), with only 1 of 30 studied mitochondria fusing with another stationary mitochondrion within the observation time (**Figure 3.15, d; Figure 3.5**). Interestingly, in a similar experiment performed in terminal Schwann cells, which cover NMJs, mitochondria were regularly observed to show fuse with each other (mitochondrial half-life was 15 minutes). These results argue that mitochondrial fusion is a highly regulated process in motor neurons that is only available to some mitochondria but not others. Interestingly, stationary mitochondria were not incapable of fusion, as this process was possible when they were confronted with a mitochondrion that had newly entered the junction. Further work will need to establish the purpose and the mechanisms of the observed selective fusions, as well as determine if the control over this mechanism affects synaptic function (see **Discussion**).

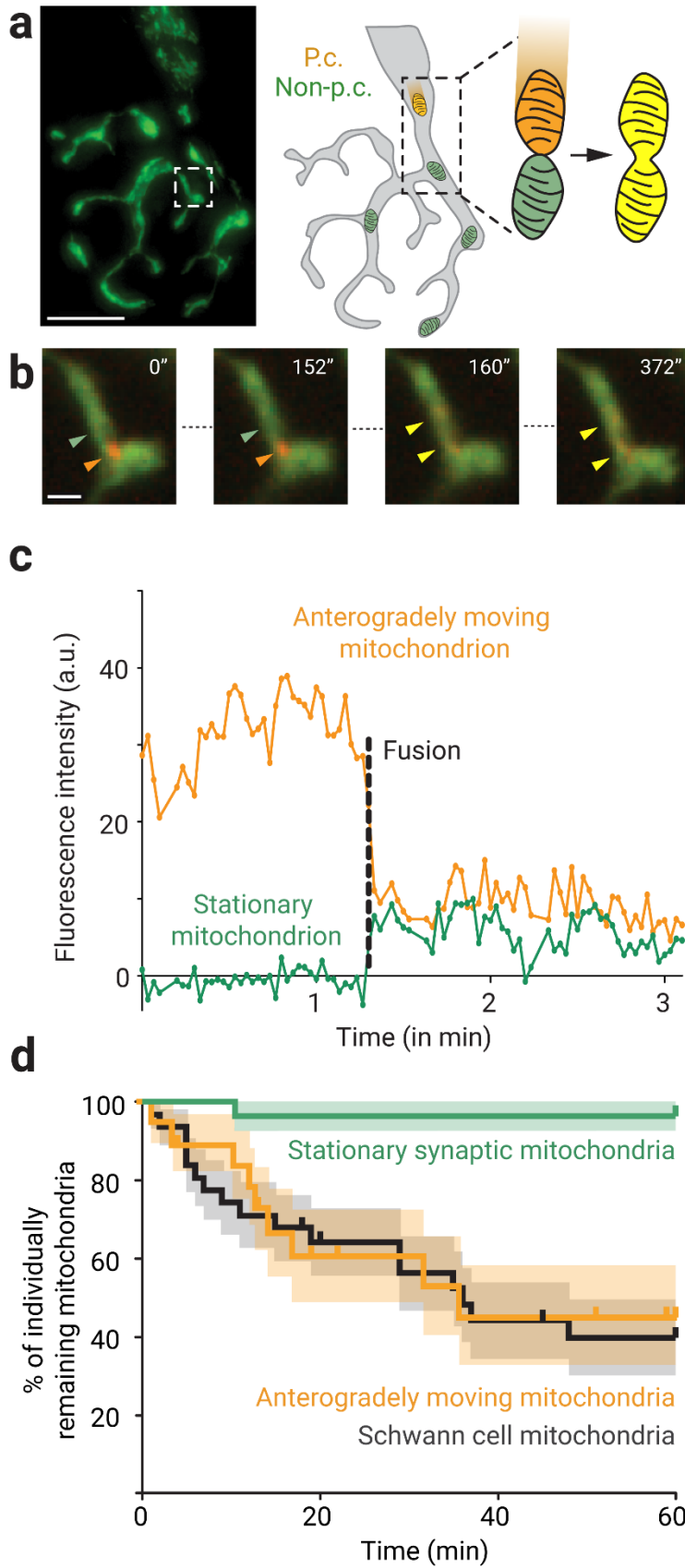


Figure 3.15 | Photoconverted anterogradely moving mitochondria fuse into the synaptic pool shortly after entering the neuromuscular junction. **a**, Wide-field projection of a neuromuscular junction that has been photoconverted (p.c.) upstream in its supplying axon (not shown, see **Figure 3.14** for p.c. setup; acute nerve muscle explants from *Thy1-mito-Dendra* mice). Schematic: p.c. anterogradely moving mitochondria enter the synaptic junction, upon which a fusion with non-p.c. resident mitochondria would be visible as a merging of the two colors. **b**, Time-lapse of the area indicated in the box in **a**. A p.c. anterogradely moving mitochondrion (orange arrow) has stopped in the junction (1st and 2nd images), and after a few minutes, it fused with a synaptic mitochondrion (green then yellow arrows). **c**, Pixel intensity plots of the two mitochondria shown in **b** during the time-lapse. The dissipation of the p.c. occurred suddenly, as would be expected of fusion, not gradually, as would be expected of bleaching. **d**, Quantification of mitochondrial “life lives” (survival plots): Orange plot shows the proportion of individually remaining p.c. mitochondria that had entered the NMJ by anterograde transport (time shown after entering the NMJ; 20 mitochondria in *Thy1-mito-Dendra* mice). Green plot: Proportion of stationary synaptic mitochondria that had remained individually (i.e., unfused; time shown after photoactivation; Two-photon laser activation of $n = 28$ single mitochondria in *Thy1-mito-paGFP* × *Thy1-mito-RFP* mice (see **Figure 3.5** for experimental setup). Black curve: Proportion of individually remaining (unfused) Schwann cell mitochondria (time shown after p.c.; $n = 31$ mitochondria in *Plp-Cre* × *ROSA-mito-Dendra* mice). Upticks: indicate when follow-up of a mitochondrion ended earlier, e.g., due to the end of observation time. Shown is mean ± s.e.m. Scale bars: 10 μm in **a** and 1 μm in **b**. The author performed all experiments.

3.4. Mitochondrial degradation in synaptic terminals

3.4.1. Synaptic mitochondria are partly removed by retrograde transport

Neurons are thought to perform most lysosomal degradation in the soma, with old mitochondria being “removed” from the periphery by retrograde transport along the axon (Chang & Reynolds, 2006; Griffin & Watson, 1988; Hollenbeck, 1996; Sheng, 2014; Sheng & Cai, 2012). Previous reports have quantified, however, that fewer mitochondria are returning retrogradely toward the soma than are transported anterogradely in adult animals *in vivo*, and this phenomenon is observed in multiple species and neuronal subpopulations (Chen et al., 2016; Misgeld et al., 2007; Misgeld & Schwarz, 2017; Xu et al., 2017). In acute intercostal nerve-muscle explants, only ~3 mitochondria per minute move in retrograde direction (compared to ~5/min anterogradely; **Figure 3.16, b**), and only ~2/h in terminal axon branches at the NMJs (compared to ~4/h anterogradely; **Figure 3.16, c**; Misgeld et al., 2007). Despite this surplus of anterograde transport, mice typically maintain a stable mitochondrial volume in mature neuromuscular junctions (NMJs, ≥ 6 weeks; Marinkovic et al., 2012). This suggests that mitochondria are degraded in the axonal periphery, although the actual mechanism of this degradation remains unknown. An alternative explanation might be that anterogradely moving mitochondria are simply smaller than retrogradely moving ones. Previous reports did not include a size correction for mitochondria (Misgeld & Schwarz, 2017), so that mitochondrial size was now measured in widefield microscopy movies (see **Materials and Methods**; **Figure 3.9**, **Figure 3.16, d,e**). Indeed, retrogradely moving mitochondria were not larger than anterogradely moving ones (if anything, at the NMJ, the retrogradely moving ones were actually smaller, **Figure 3.9**, **Figure 3.16, d,e**). The calculated mitochondrial volume (see **Section 3.2** and **Materials and Methods**) was combined with the measurements of mitochondrial transport (**Figure 3.16, b,c**) to generate a “mitochondrial volume flux” value (**Figure 3.16, f,g**). Mitochondrial volume flux was recorded in the proximal stem of the axon, within the intercostal nerve (ICN) before peripheral branches diverge off and in the most distal terminal branches, where axons enter the presynaptic terminal (**Figure 3.16, a–c**). Indeed, on average, significantly more mitochondrial volume was transported anterogradely than retrogradely in stem axons, but the most dramatic difference was found in terminal branches close to the synaptic junctions (**Figure 3.16, f,g**; ICN 1.9-fold vs. NMJ 3.4-fold difference from averaged transport rates, 2.2 and 29 total ‘axon imaging hours’, respectively). In summary, those results suggest that in the axonal periphery, retrograde transport towards the soma does not account for the entire removal of mitochondria; instead, mitochondrial turnover may be complemented by a yet unknown degradative mechanism.

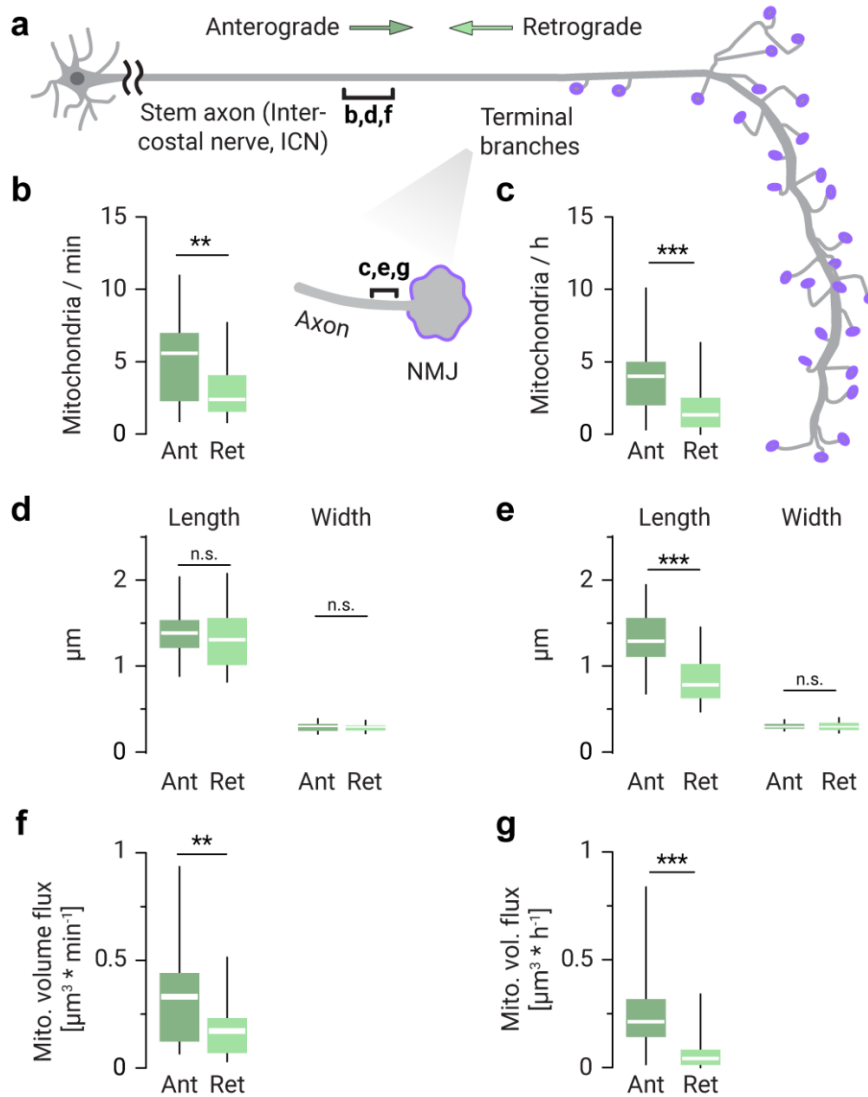


Figure 3.16 | Most mitochondria delivered to distal motor axon branches vanish in synapses. **a**, Schematic illustrating the geometry of mature α -motor neuron projections. Brackets show live imaging positions in acute intercostal nerve-muscle explants, where measurements **b–g** were taken (NMJ: neuromuscular junction). Measurements of anterogradely ('Ant') and retrogradely ('Ret') transported mitochondria in **b,d,f**, stem axons (29 axons from 14 *Thy1*-mito-XFP transgenic mice; 'XFP' were various fluorescent tags, see Methods) and in **c,e,g**, distal axon branches with synaptic terminals (25 axons, 16 *Thy1*-mito-XFP mice). Measurements in **b,c** of mitochondrial transport rates, in **d,e** of mitochondrial size (length and width as indicated), and in **f,g** mitochondrial volume flux rates. Statistical significance was determined in **b,c,f,g** with a Mann-Whitney-U test and in **d,e** with an unpaired *t*-test. Experiments were performed by the author. Figure was adapted from Marahori et al. (manuscript in preparation).

3.4.2. Synaptic mitochondria are captured before exiting the NMJ

The apparent “overflow” of mitochondria already occurred at the most distal sites—right before the terminal branches enter the NMJs—, which suggests that mitochondria were degraded somewhere within the confines of the NMJs. To discern single moving mitochondria against the dense pool of synaptic mitochondria, a pulse-chase experiment was designed: about half of the synaptic mitochondrial pool was photoconverted from green to red fluorescence in nerve-muscle explants of *Thy1*-mito-Dendra mice (**Figure 3.17, a**), then individual photoconverted mitochondria were followed by time-lapse imaging as they dispatched from the stationary synaptic pool and initiated retrograde movement. These retrogradely moving mitochondria were then tracked and the track coordinates were mapped to anatomical landmarks after fixation of the sample (see **Figure 3.17, a,b**). Interestingly, most mitochondria behaved in two distinct

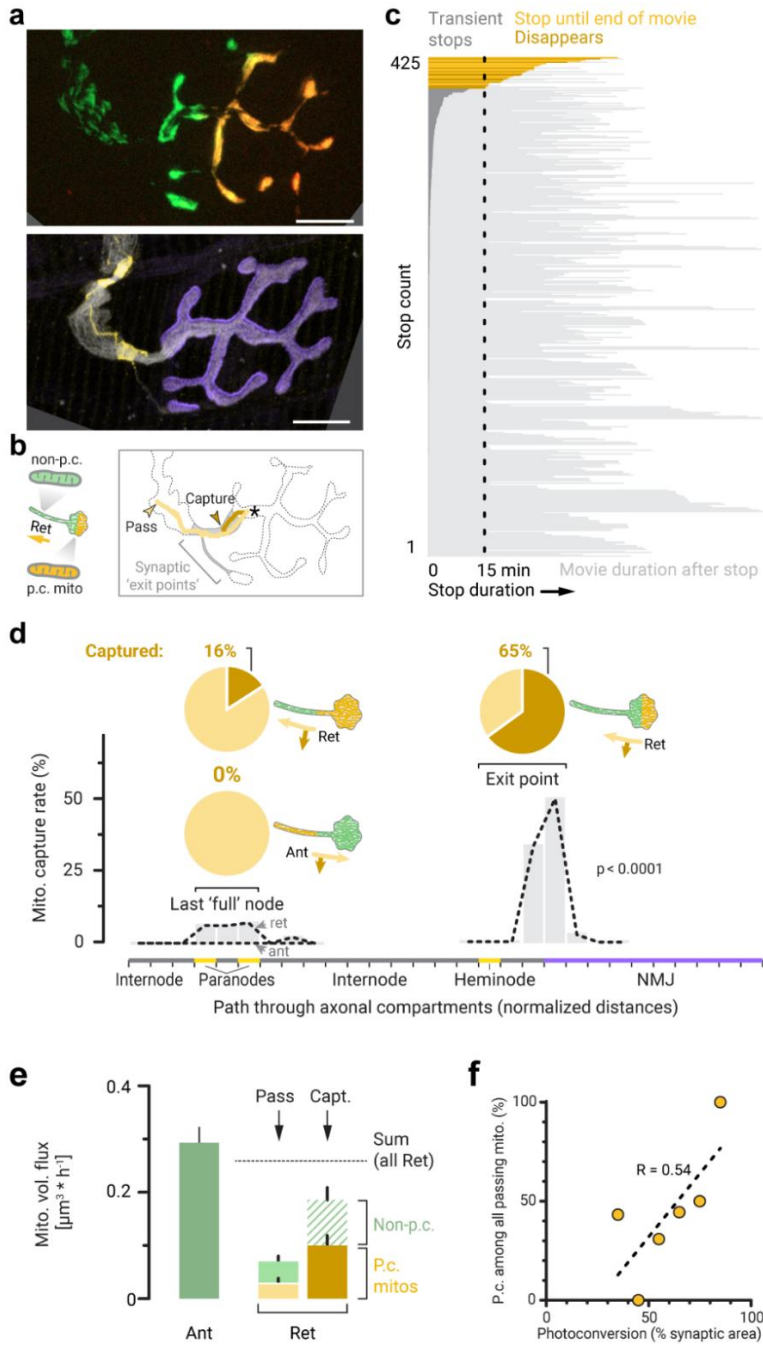


Figure 3.17 | Retrogradely moving mitochondria are captured in terminal axon branches.

a, Top: Widefield projection of motor axon terminal with Dendra-tagged mitochondria that were photoconverted (p.c.) from green to red fluorescence (*Thy1*-mito-Dendra mouse line). Bottom: Confocal projection of a post hoc staining of the same junction with marked acetylcholine receptors (α -bungarotoxin, magenta), nodes of Ranvier (paranodal components, anti-Caspr-antibody, yellow), and neuronal microtubules (BIII-tubulin-antibody, gray). **b**, Left: Schematic showing the experimental setup (p.c. presynaptic mitochondria that started retrograde movement were followed on the non-p.c. background). Right: Trackings of two p.c. mitochondria. Star: start of the tracks; dark orange: mitochondrion stop permanently ('captured') in synaptic exit point (gray area), light orange: continued into axon ('pass'). **c**, All registered pauses of the retrogradely moving p.c. mitochondria that were tracked in through the synaptic exit point ($n = 425$ stops; from experiments in **e**) sorted underneath one another from longest to shortest pause. 'Persistent' pauses (oranges) were either observed until the end of the movie or until the fluorescent signal slowly disappeared, whereas after 'transient' pauses, mitochondria resumed movement (see **Materials and Methods**). **d**, Graph indicating the probability that p.c. mitochondria stop permanently while traversing through different axon regions: internodes, paranodes/heminode, and NMJ (for binning, see **Materials and Methods**). Mitochondria from various locations and directions were tracked (indicated in schematics): right plot, retrogradely

moving synaptic mitochondria; left plots: mitochondria moving anterogradely or retrogradely through the preterminal 'full' nodes. Pie charts: proportion of tracks that ended in 'capture' (%). ($n \geq 19$ mitochondria from ≥ 4 axons, ≥ 3 *Thy1*-mito-Dendra mice per group for 'full' nodes; $n = 40$ mitochondria for exit points, from experiments in **e**). **e**, Average mitochondrial volume flux rates at synaptic exit points. Rates of 'captured' and 'passing' mitochondria are stacked to visualize the sum: p.c. (orange) and non-p.c. (green) populations, hatched: non-p.c. 'captured' flux was estimated as described in **Materials and Methods** ($n = 32$ NMJs, 20 *Thy1*-mito-Dendra mice, pooled with *Thy1*-mito-Dendra mice that expressed a ChAT-Cre-recombinase, but did not contain any floxed genes). **f**, Relationship of the fraction of p.c. synaptic area and the fraction of p.c. mitochondria in the overall stream of retrogradely 'passing' mitochondria, with a linear trendline (shown are means per 10%-bin; $n = 28$ NMJs, 19 *Thy1*-mito-Dendra mice from the dataset in **e**). Scale bars, 10 μm . A χ^2 -test was used to determine significance in **f** ('Ret' synaptic exit point $p < 0.001$; 'Ant' and 'Ret' last node of Ranvier $p \geq 0.05$). All experiments were performed by the author. Figure was adapted from Marahori et al. (manuscript in preparation).

manners: while some left the junction to progress into the axon towards the soma ('passed' mitochondria, 35%), other stopped along their route without moving away for the rest of the observation time ('captured' mitochondria, 65%; **Figure 3.17, c**, and **Figure 3.17, d**, righthand plot; $n = 40$ mitochondria observed from 32 'axon-imaging hours'). The probability of being captured was highest for retrogradely moving mitochondria in a particular spot: in the transition area that separates the junction from the distal-most internode, which is close to the distal heminode (termed synaptic 'exit point'; **Figure 3.17, c**; χ^2 -test, $p < 0.001$). The volume flux of captured mitochondria accounted for the difference between anterograde and retrograde volume flux, which indicates that 'captured' mitochondria may constitute the "missing" population mentioned in the previous section (**Figure 3.17, e**; Ant. $0.28 \pm 0.03 \mu\text{m}^3/\text{h}$, Ret. passed $0.07 \pm 0.01 \mu\text{m}^3/\text{h}$, captured $0.19 \pm 0.04 \mu\text{m}^3/\text{h}$; $n = 32$ NMJs from 20 mice; values were corrected for the partial photoconversion of the NMJs, **Figure 3.17, f**).

3.4.3. Mitochondrial capture occurs at distal nodes of Ranvier

Since mitochondrial capture was specifically occurring in the synaptic exit point, which lies close to the terminal heminode, it prompted the question of which structural component of the heminode 'captures' these mitochondria. During development, nodes of Ranvier develop different components in a time-sequential manner (Girault & Peles, 2002). For example, compact myelin formation and the anchoring of the node to the actin cytoskeleton are among the final steps (Girault & Peles, 2002). To test whether mitochondrial capture depended on the presence of a fully mature heminode, an experiment was performed in the developing axons of young mice. Indeed, in axons that were not yet fully developed (not myelinated up to the exit point), a smaller "mismatch" of anterograde vs. retrograde transport ('net' transport rates; **Figure 3.18**) was observed than in fully myelinated axons. These results suggest that while myelination itself does not determine capture (unmyelinated axons still showed a mismatch in transport, albeit smaller), another structure that is more often associated with myelin may (such as a nodal component that develops earlier than myelin sheaths). Further studies will need to probe these heminodal components further.

Since the terminal heminode is a particular node of Ranvier, the question arose whether mitochondrial 'captures' occur at any node when mitochondria attempt to pass it. Previous reports, for example, showed a general reduction in speed when mitochondria pass through the nodes of Ranvier to nurture the nodes with energy (Ohno et al., 2011). To test this, retrogradely moving, photoconverted mitochondria were also tracked across other nodes, such as the preterminal nodes (so 'full' nodes that are located upstream of the heminodal exit point, **Figure 3.17, d**) and in the stem axons of the intercostal nerve. Indeed, 'capture' was observed in the most distal 'full' nodes but with much lower frequency than in the heminode (**Figure 3.17, d**, 16%

probability of capture in distal ‘full’ nodes vs. 65% in heminode; $p \geq 0.05$, χ^2 -test; $n = 69$ mitochondria observed from 9 total ‘axon imaging hours’ vs. NMJ measurements detailed in the section above). In stem axon nodes, the ‘capture’ phenomenon was not encountered at all (0% ‘capture’, $n \geq 30$ mitochondria observed from 3 total ‘axon imaging hours’, 3 axons from 3 *Thy1*-mito-Dendra mice). This suggests that either synaptic retrogradely moving mitochondria are “different” than axonal mitochondria from more proximal locations or that distal nodes of Ranvier have a special ability to capture mitochondria.

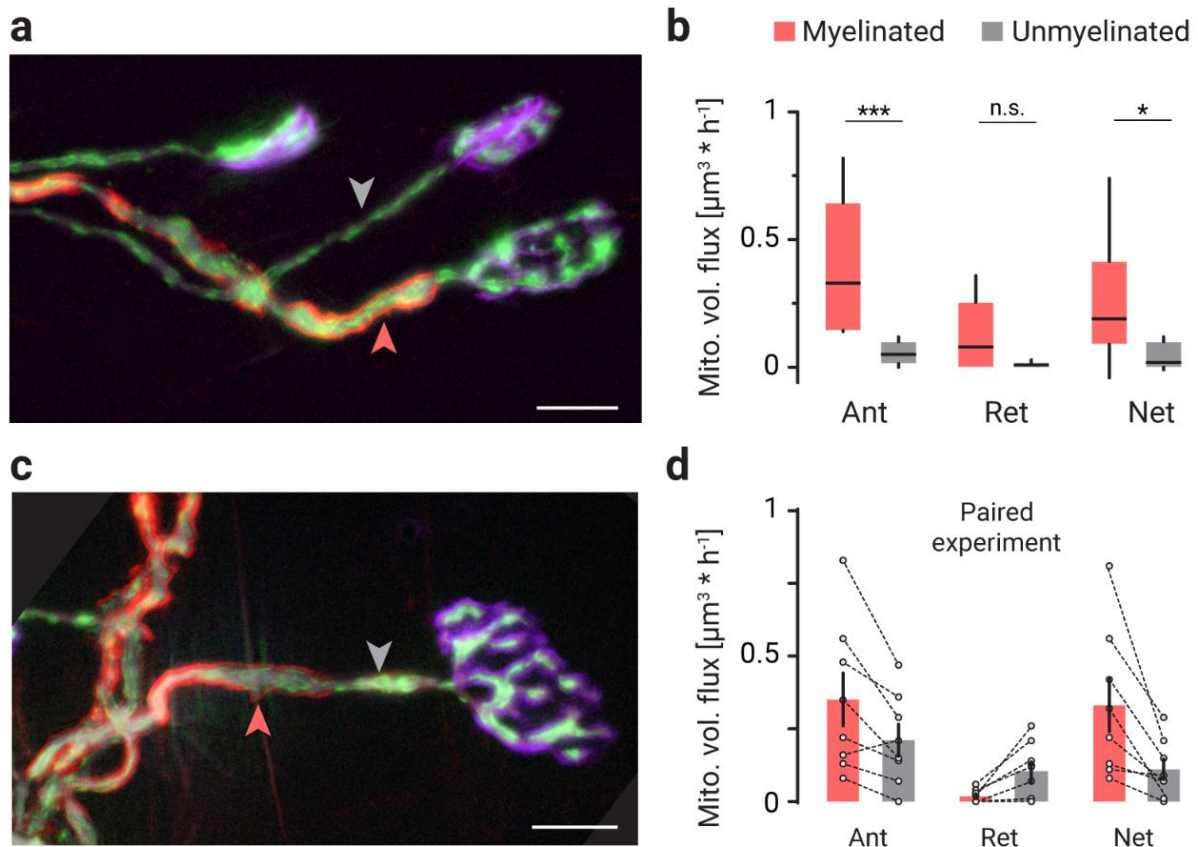


Figure 3.18 | Transport rates in developing, unmyelinated terminal axon branches. Myelination is fully developed at 3 weeks of age. In young *Thy1*-YFP-16 (axon label, grey in **a,c**) \times *Thy1*-mito-CFP (line K; mitochondria label, green in **a,c**) mice (2 weeks old) terminal branches with and without myelination were identified using a myelin vital dye (fluoromyelin red in **a,c**); acetylcholine receptors labeled with bungarotoxin 647 (magenta in **a,c**). **a**, Widefield projection shows a myelinated (red arrow) and an unmyelinated (grey arrow) terminal axon branch in acute nerve-muscle explants. **b**, Mitochondrial volume flux measured in myelinated and unmyelinated axon branches, flux shown in anterograde and retrograde direction, as well as net flux (ant minus ret; ≥ 9 axons from ≥ 3 mice per group). **c**, Widefield projection shows a myelinated (red arrow) and an unmyelinated (grey arrow) section of the same terminal axon branch in acute nerve-muscle explants. **d**, Mitochondrial volume flux measured in myelinated and unmyelinated portions on the same axon branch, flux shown in anterograde and retrograde direction, and net flux (8 axons from 5 mice). Scale bars, 10 μm . Significance was determined in **b** by a Mann-Whitney-U test and in **d** by a Wilcoxon paired test. Experiments performed by the author.

Moreover, anterogradely moving mitochondria were not captured at distal nodes (**Figure 3.17, d**; 0% capture, $n = 19$ mitochondria from 6 total ‘axon imaging hours’). With the mentioned reduced motility around the nodes of Ranvier (Ohno et al., 2011) having been bidirectional, these results seem to exclude previously reported factors as the specific cause for captures. The axon

caliber constrictions around the distal nodes of Ranvier are also symmetric (diameter, $54 \pm 6\%$ of preceding internode in anterograde vs. $43 \pm 3\%$ in retrograde direction; $p \geq 0.05$, Mann-Whitney-U test, **Figure 3.19, a,b**), excluding asymmetric spatial constraints as another potential cause that might explain why mitochondrial captures occur more often in retrograde direction. Overall, the data point to a selective mechanism that acts only on a particular population of mitochondria.

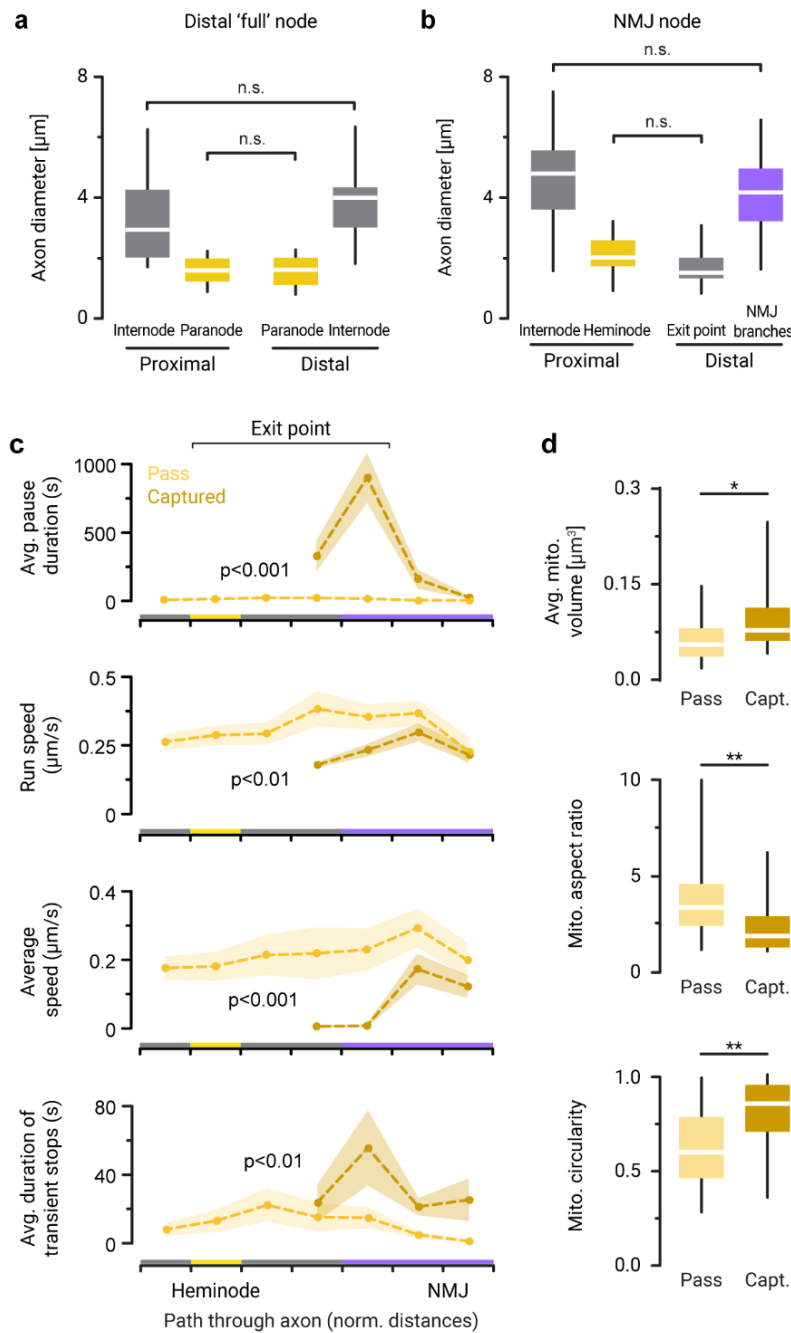


Figure 3.19 | 'Captured' mitochondria have unique characteristics when compared to 'passing' mitochondria. **a,b**, Axonal constriction around nodes of Ranvier in α -motor axon endings from triangularis sterni muscle muscles ($n \geq 11$ axons from ≥ 8 *Thy1*-mito-Dendra mice): **a**, axon calibers around the distal 'full' nodes, and **b**, around the synaptic exit point and heminode (for NMJ branches and for exit points the sum of the individual branch calibers is shown). **c**, Movements parameters of 'passing' and 'captured' mitochondria while traveling through particular axon subcompartments (for legend, see description in **Figure 3.17**; 49 mitochondria tracked in 21 NMJs from 16 *Thy1*-mito-Dendra mice). **d**, Morphology of 'passing' and 'captured' mitochondria ($n \geq 19$ mitochondria per group, from the experiments in **Figure 3.17**), from top to bottom: average organelle volume, aspect ratio, and circularity (see **Materials and Methods**). One-way ANOVA test with multiple comparisons was used to determine significance in **a,b**, a two-way ANOVA test in **c**, and Mann Whitney U tests for **d**. In **c**, mean (circles) \pm s.e.m. (shaded) are shown. The author performed all experiments. Figure was adapted from Marahori et al. (manuscript in preparation).

In fact, mitochondria that were later captured slowed down when approaching the synaptic exit point compared to ‘passing’ mitochondria (**Figure 3.19, c**; reduced average run speed of captured mitochondria in exit point by 56%; $n = 49$ mitochondria). Furthermore, ‘captured’ mitochondria were of a spherical, “blown-up” shape when compared to passing mitochondria (**Figure 3.19, d**), possibly indicating a dysfunctional state (Ferree et al., 2013; Nikic et al., 2011; Zick et al., 2009). This indicates that ‘captured’ mitochondria originate from a diverse population of synaptic mitochondria that is potentially specifically recognized at the exit point.

3.4.4. Damaged mitochondria are preferentially captured

The previous experiments described how in murine motor axon endings, a distinct portion of synaptic mitochondria that embarks on its retrograde journey to exit the neuromuscular junction is instead hindered from doing so at the synaptic ‘exit point,’ by a process termed ‘capture.’ The experiments further showed that ‘captured’ mitochondria have distinct properties compared to ‘passing’ mitochondria, indicating that ‘captured’ mitochondria might be dysfunctional organelles that are prohibited from further spreading throughout the axon, potentially to be targeted instead for local degradation in the junctions. As typical biosensors that are used to measure mitochondrial membrane depolarization (a hallmark of dysfunctional organelles), such as TMRE, cannot be used concurrently with mito-Dendra due to spectral overlap, an experiment was instead designed to damage synaptic mitochondria with a photo-caged uncoupling agent, then observe whether this treatment amplifies mitochondrial capture rates. To this end, the photoactivatable compound photo-mito-DNP was used to reduce the membrane potential of synaptic mitochondria in a local manner (Chalmers et al., 2012). Acute nerve-muscle explants were thus incubated with photo-mito-DNP (Glancy et al., 2015), which specifically reduced the fluorescence of the potential-sensitive dye TMRE compared to the control group (see **Materials and Methods; Figure 3.20, a,b**), suggesting that this protocol can depolarize synaptic mitochondrial populations selectively.

In experiments with explants from *Thy1*-mito-Dendra mice, photo-depolarization of synaptic mitochondria drastically elevated the proportion of captured mitochondria at the exit point (85%), compared to the ‘sham’ control where photo-mito-DNP was only applied after UV exposure (33%; capture fraction increased 2.5-fold, $n \geq 12$ mitochondria from ≥ 6 ‘NMJ imaging hours’ per group, $p = 0.003$, χ^2 -test; **Figure 3.20, d**). In absolute numbers, fewer mitochondria were allowed to pass through the exit points upon depolarization, as shown by comparative volume flux measurements (**Figure 3.20, c**; Control: $0.20 \pm 0.07 \mu\text{m}^3/\text{h}$ vs. Depolarized: $0.02 \pm 0.01 \mu\text{m}^3/\text{h}$; $p < 0.05$, Mann-Whitney-U test). Depolarized NMJs tended to also show an absolute increase in captured mitochondrial volume flux when compared to the control (**Figure 3.20, c**; Control: 0.15

$\pm 0.08 \mu\text{m}^3/\text{h}$ vs. Depolarized: $0.28 \pm 0.08 \mu\text{m}^3/\text{h}$; $p \geq 0.05$, Mann-Whitney-U test), indicating that the mitochondria which did not pass were instead captured.

To exclude unspecific compound toxicity affecting the transport machinery, anterograde transport rates were also measured. Unlike the retrogradely moving population, anterogradely moving mitochondria were not significantly affected in the photo-depolarized group, indicating that the observed effects were specific to the depolarization-targeted mitochondria (**Figure 3.20, e**; Control: $0.39 \pm 0.21 \mu\text{m}^3/\text{h}$ vs. Depolarized: $0.29 \pm 0.08 \mu\text{m}^3/\text{h}$; $p \geq 0.05$, Mann-Whitney-U test).

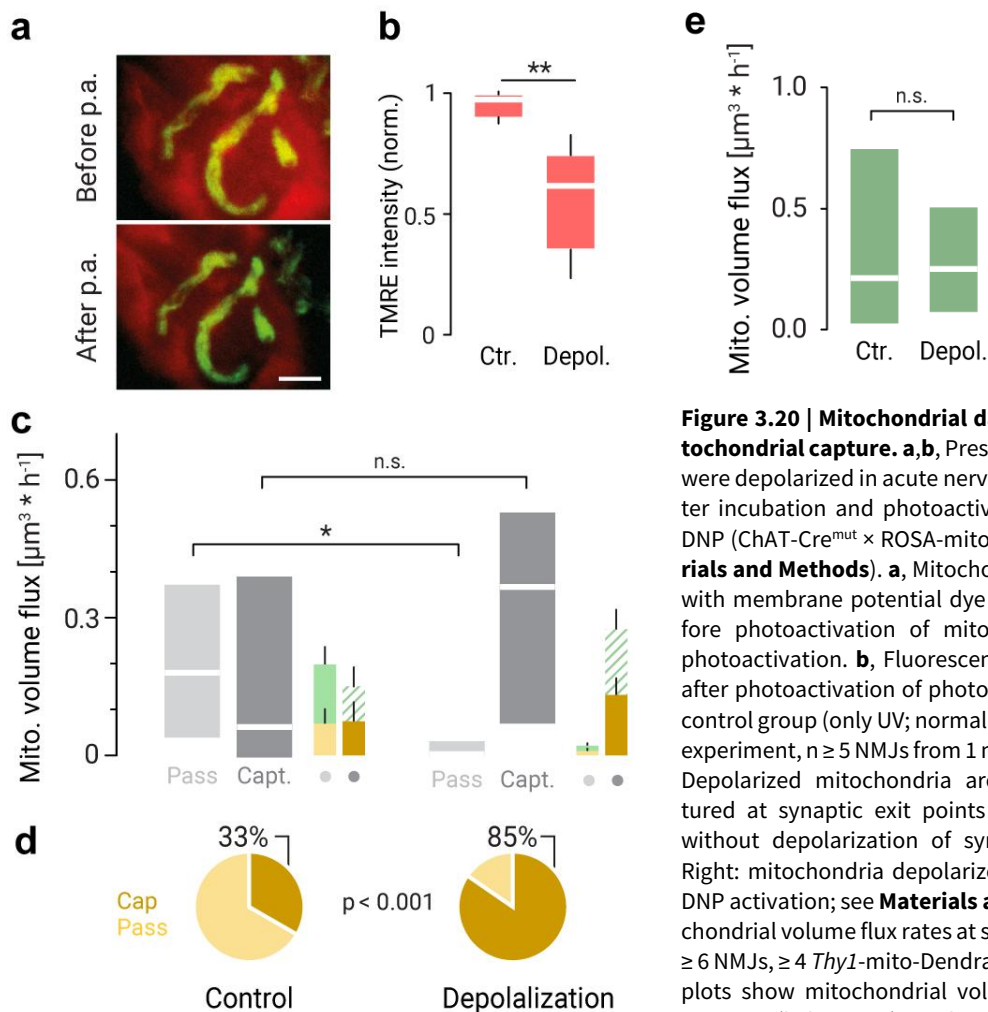


Figure 3.20 | Mitochondrial damage amplifies mitochondrial capture.

a,b, Presynaptic mitochondria were depolarized in acute nerve–muscle explants after incubation and photoactivation of photo-mito-DNP (ChAT-Cre^{mut} × ROSA-mito-GFP mice, see **Materials and Methods**). **a**, Mitochondria (green) labeled with membrane potential dye TMRE (red). Top: before photoactivation of mito-DNP, Bottom: after photoactivation. **b**, Fluorescence intensity of TMRE after photoactivation of photo-mito-DNP and in the control group (only UV; normalized to the start of the experiment, $n \geq 5$ NMJs from 1 mouse per group). **c,d**, Depolarized mitochondria are preferentially captured at synaptic exit points (Left: control group without depolarization of synaptic mitochondria; Right: mitochondria depolarized using photo-mito-DNP activation; see **Materials and Methods**) **c**, Mitochondrial volume flux rates at synaptic exit points, ($n \geq 6$ NMJs, ≥ 4 *Thy1*-mito-Dendra mice per group). Box plots show mitochondrial volume flux rates of all passing (light grey) and captured (dark grey) mitochondria. Miniature bar graphs show stacked mean values for both p.c. (orange) and non-p.c. populations (green) measured in the passing (light shades) and captured (dark shades) populations (similar to the experimental setup in **Figure 3.17**). **d**, Pie charts representing fractions of p.c. captured mitochondria (%; dark orange; $n \geq 12$ mitochondria per group, from the same mice as in **c**). **e**, Anterograde volume flux from the same movies as **c**. Scale bar in **a** 10 μm . Mann-Whitney test was used to determine significance in **b,c**; a χ^2 -test was used in pie charts (**d**, $p = 0.003$). The author performed all experiments. Figure was adapted from Marahori et al. (manuscript in preparation).

In summary, these results suggest that a cascade of perinodal checkpoints “filters out” and removes damaged mitochondria from the retrograde motile pool to prevent such mitochondria from spreading throughout the axon. The results further indicate that this system can respond to acute mitochondrial damage at the junction by increasing mitochondrial capture rates quickly.

3.4.5. Mitochondrial capture in motor neuron disease

The fact that depolarized mitochondria were captured more frequently at exit points further prompted to ask if disease-related damage would also amplify mitochondrial capture. To test this, two mouse models of motor neuron disease were employed, *SOD1^{G93A}* and *Thy1*-(GA)149-CFP ("GA-CFP"; Gurney et al., 1994; Schludi et al., 2017). Mutations in the gene encoding Cu/Zn superoxide dismutase-1 (SOD1) are responsible for ~20% of familial ALS cases, and expression of mutant SOD1 in transgenic mice leads to a progressive motor neuron disease in these mice, characterized, for example, by dying-back denervation (Fischer et al., 2004) with destruction of the nodal architecture at symptomatic stages (**Figure 3.21, a**). Therefore, to exclude secondary unspecific effects of axon degeneration, the experiments were performed in pre-symptomatic stages: in *SOD1^{G93A} +/-* × *Thy1*-mito-Dendra mice, mitochondrial capture was monitored at two weeks of age (before the onset of the global axon transport deficits previously reported in the intercostal nerve; Marinkovic et al., 2012). In mice expressing the pathogenic *SOD1^{G93A}* mutation (+), mitochondrial capture fractions in exit points indeed increased by 1.9-fold compared to healthy littermates (**Figure 3.21, c**; $n \geq 48$ mitochondria from ≥ 19 'axon imaging hours' per genotype, $p < 0.001$, χ^2 -test). Similarly, at a presymptomatic age (5–6 weeks old), *GA-CFP^{+/-}* ×

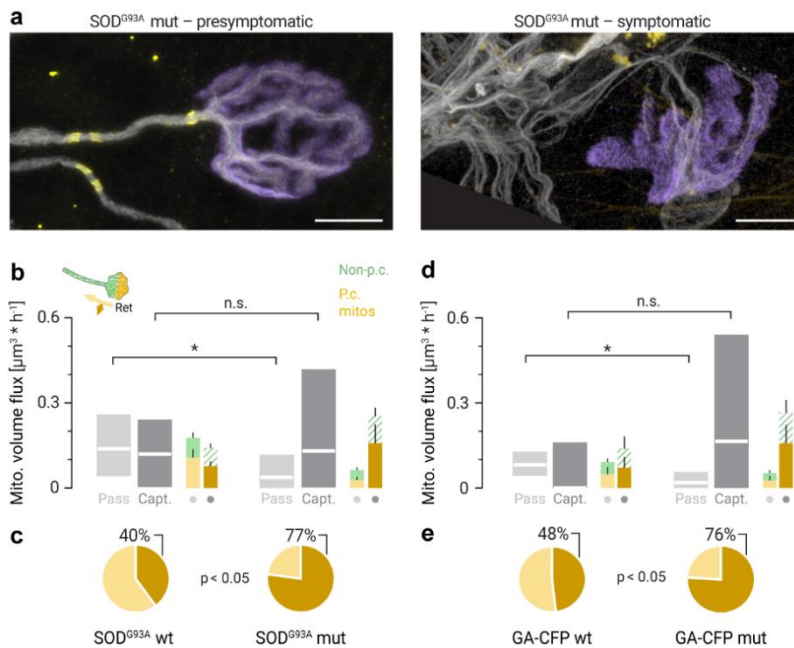


Figure 3.21 | In presymptomatic mouse models of Amyotrophic lateral sclerosis, mitochondria are more frequently captured when compared to healthy littermate controls (wt). **a**, Maximum confocal projections of motor axon terminals in triangularis sterni muscles of ALS-related mice (*SOD1^{G93A}* mutation); Left: a presymptomatic, 2-week-old mouse with intact NMJ architecture, Right: Denervation in a 20-week-old, symptomatic mouse with destruction of the nodal architecture (anti-Caspr antibody, yellow; α -bungarotoxin, magenta; anti- β III-tubulin, white). **b,c**, Synaptic mitochondria in presymptomatic *SOD1^{G93A} +/-* ("mut") mice are preferentially captured at synaptic exit points (experimental setup as in **Figure 3.17**; Right: experimental group with two-week-old

SOD1^{G93A} +/- ("mut") × *Thy1*-mito-Dendra mice; Left: healthy *SOD1^{G93A} -/-* ("wt") × *Thy1*-mito-Dendra littermates; $n \geq 13$ mice per genotype). **b**, Mitochondrial volume flux at synaptic exit points ($n \geq 19$ NMJs per genotype). **c**, Fractions of p.c. captured mitochondria ($n \geq 48$ mitochondria per genotype). **d,e**, Mitochondria in presymptomatic *GA-CFP^{+/-}* mice are preferentially captured at synaptic exit points (Right: experimental group with 5-week-old *GA-CFP^{+/-}* ("mut") × *Thy1*-mito-Dendra mice; Left: healthy *GA-CFP^{-/-}* ("wt") × *Thy1*-mito-Dendra littermates; $n \geq 11$ mice per genotype). **d**, Mitochondrial volume flux at synaptic exit points ($n \geq 19$ NMJs per genotype). **e**, Fractions of p.c. captured mitochondria ($n \geq 26$ mitochondria per genotype). Legends: as in **Figure 3.17** Scale bars in **a** 10 μm . Mann-Whitney test was used to determine significance in **b,d**; a χ^2 -test was used in pie charts (**c**, $p < 0.001$; **e**, $p = 0.047$). The author performed all experiments. Figure was adapted from Marahori et al. (manuscript in preparation).

Thy1-mito-Dendra mice expressing the dipeptide repeat protein C9orf72 showed a ~1.6-fold increased fraction of captured mitochondria (**Figure 3.21, e**; $n \geq 26$ mitochondria from ~19 NMJ imaging hours per genotype, $p = 0.047$, χ^2 -test). In both mouse models, the ‘passing’ volume flux rates were significantly decreased compared to healthy littermate controls **Figure 3.21, b,d**). Overall, these results indicate that beyond “filtering out” damaged mitochondria in healthy axons, this system of mitochondrial capture at perinodal checkpoints can also be adjusted and upregulated in degenerative axonopathies.

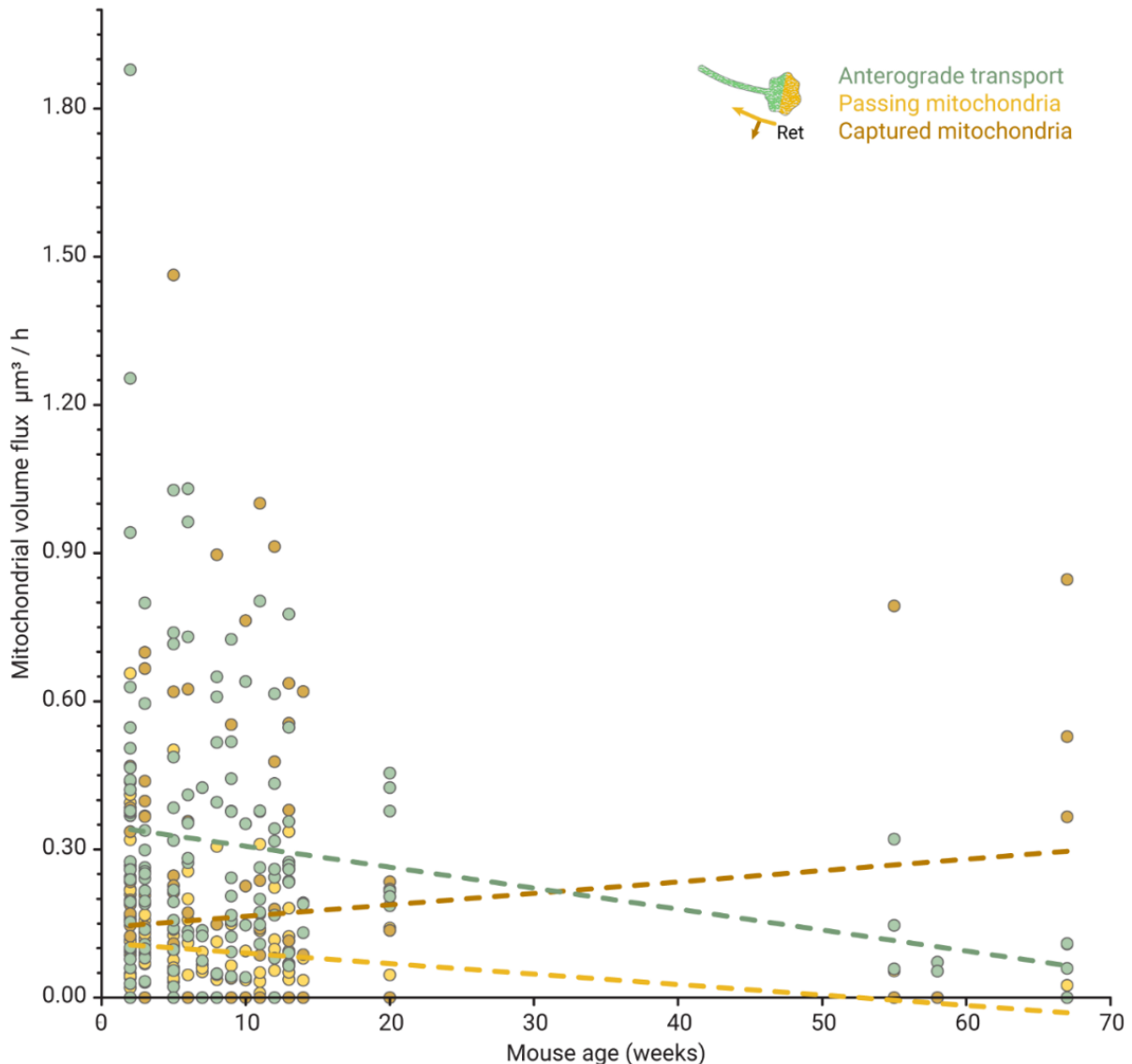


Figure 3.22 | Changes in mitochondrial transport in motor axon terminals over mouse age. This graph shows the transport data measured in “capture experiments” (see **Figure 3.17** for experimental setup) pooled from all wildtype controls used in this thesis (specifically, the wildtypes in **Figure 3.17, 3.21, 3.29** and floxed animals that were negative for ChAT-Cre, **Figure 3.31**); additionally, a preliminary dataset with aged animals was included (9 NMJs from 5 *Thy1*-mito-Dendra mice, ages 55-67 weeks). The dotted lines show trendlines through the data based on linear approximation. Experiments were performed by the author.

Moreover, mitochondrial damage is known to accumulate with age under physiological conditions. This has been previously suggested as a factor contributing to aging becoming a risk factor for developing neurodegenerative disease. To analyze whether mitochondrial capture is indeed amplified with age, the mitochondrial volume flux results of healthy mice were sorted by mouse age (**Figure 3.22**). Wildtype mice from 2 weeks up to 67 weeks of age were analyzed (equivalent to an age span of ~4–55 human years; Dutta & Sengupta, 2016). Interestingly, both anterograde and retrograde ('passing') volume flux showed a decreasing trend with age (**Figure 3.22**). A global drop-off in axonal transport of mitochondria has been previously shown in other model systems (Lewis et al., 2016). However, 'captured' mitochondrial volume flux rates showed the opposite trend, tending to increase with age (**Figure 3.22**). These data suggest that mitochondrial 'capture' may also be upregulated during normal aging to maintain mitochondrial quality in distal axons.

3.4.6. Hotspots of lysosomal activity in axon terminals

The fact that, on average, ‘captured’ mitochondrial volume flux roughly amounts to the mitochondrial population that is “missing” in axonal transport rates (**Figure 3.17, e, Section 3.4.1**), suggests that ‘captured’ mitochondria may be targeted for degradation in synaptic exit points. To explore this, mice were injected with an adeno-associated virus (AAV) to express a mitophagy indicator under a synapsin promoter in neurons (AAV9-*hSyn*-mito-Keima; see **Materials and Methods**).

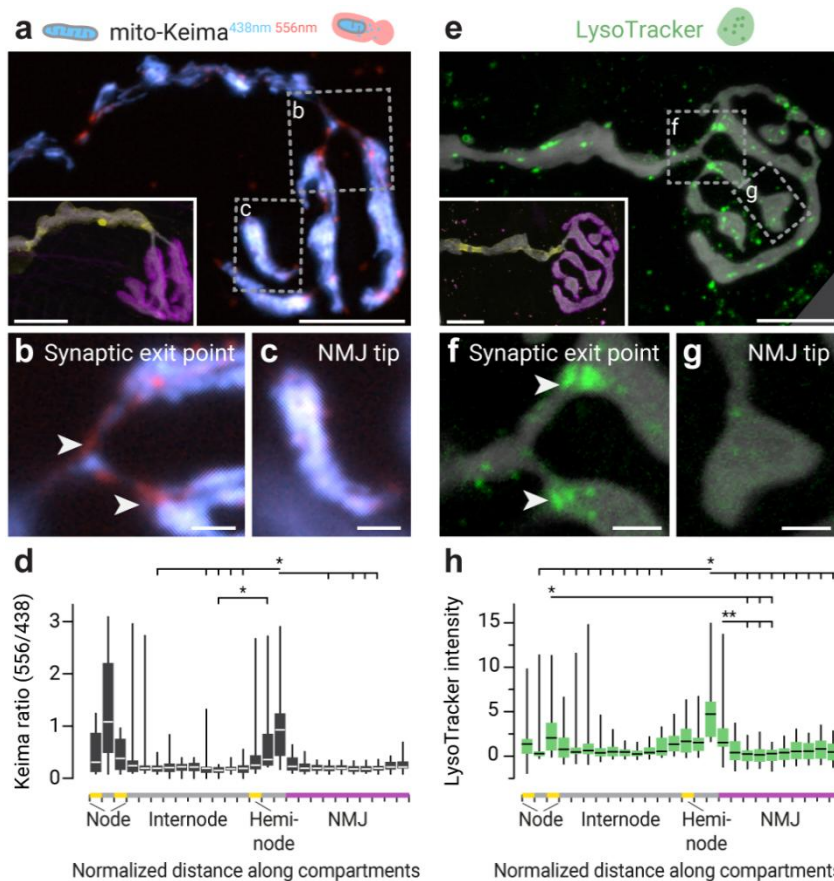


Figure 3.23 | Degradative organelles accumulate at distal nodes of Ranvier of motor axons, i.e., at mitochondrial ‘capture’ sites. **a–d**, Mitolysosomes in AAV9-*hSyn*-mito-Keima expressing mice (live experiments in acute nerve–muscle explants). **a**, Widefield projection of mito-Keima-expressing axon terminal, after excitation with 438 ± 12 nm (blue pseudo-colored) and 556 ± 10 nm light (red). Inset: correlated staining after sample fixation showing axon microanatomy (anti-Caspr, yellow; α -bungarotoxin, magenta; anti- β III-tubulin, white). Boxes indicate positions of widefield images (single sections) in **b**, Synaptic exit point with mitolysosome accumulations (high 556/438 ratio; arrowheads), and **c**, axon terminal tip. **d**, Mito-Keima signal ratio at 556/438 nm excitation along different subcompartments of motor axon terminals (NMJ, magenta; heminode and paranodes, yellow; internode, gray; $n = 14$ axons, 7 AAV9-injected *Thy1*-

mito-CFP and C57BL/6 mice). **e–h**, Staining with acidophilic vital dyes (LysoTracker) to visualize degradative organelles (live experiments in acute nerve–muscle explants). **e**, Confocal projection of LysoTracker staining (green) in a YFP-expressing neuron (white, *Thy1*-YFP-16 line). Inset: correlated post-hoc staining, anti-Caspr (yellow), α -bungarotoxin (magenta). Boxes indicate positions of single optical sections through the synaptic exit point (**f**) and tips (**g**), with LysoTracker accumulations (arrowheads) shown within the exit point. **h**, LysoTracker fluorescence intensity inside axon terminals (normalized to signals in internodes; $n = 20$ axons, 3 *Thy1*-YFP-16 mice). Scale bars in **a,e** 10 μ m; **b,c,f,g** 2 μ m. Statistical significance was determined using a Kruskal-Wallis-test (**d,h**) with Dunn’s multiple comparisons test. The author performed all experiments. Figure was adapted from Marahori et al. (manuscript in preparation).

Mito-Keima is a ratiometric indicator that allows visualizing mitochondria (neutral pH) as well as lysosomes that are degrading mitochondria (‘mitolysosomes’, due to Keima’s shift in spectrum under acidic pH; Katayama et al., 2011). In nerve–muscle explants of injected mice, mitolysosomes were thus observed along the entire motor axon terminal; however, the signal

was strongly enriched in synaptic exit points and near paranodes (**Figure 3.23, a–d**), revealing that mitochondrial capture sites are, in fact, “hotspots” of mitochondrial degradation.

In a similar experiment, explants were incubated with LysoTracker (**Figure 3.23, e–h**), an acidophilic vital dye that labels lysosomes and late endosomes (Song et al., 2008). LysoTracker accumulated at synaptic exit points (**Figure 3.23, e–h**) and also colocalized in correlated 3-dimensional electron microscopy with heterogeneous, electron-dense organelles (**Figure 3.24**), which is a characteristic appearance of degradative lysosomes.

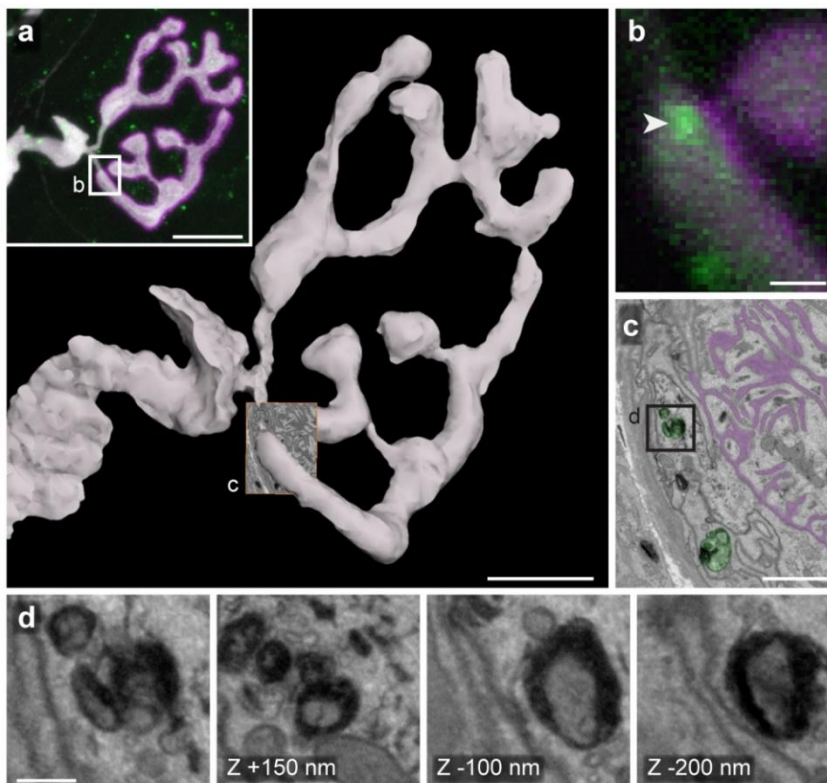


Figure 3.24 | Correlative electron microscopy of LysoTracker-stained organelles. **a**, Three-dimensional rendering based on tracings in serial electron micrographs, which were acquired from a re-localized axon terminal after a LysoTracker live experiment in an acute nerve–muscle explant was performed. Inset: Confocal projection of the axon terminal before fixation, stained with LysoTracker (green; α -bungarotoxin, magenta; *Thy1*-YFP-16, white). **b**, Confocal single optical section through the synaptic exit point showing the accumulation of LysoTracker-stained organelle(s), indicated by an arrowhead; section position indicated by box in the inset in **a**. **c**, Ultrathin section through the targeted organelles (pseudo-colored green; post-synaptic folds: pseudo-colored magenta; section

position shown in rendering, **a**). **d**, Micrograph of electron-dense organelles at the position of the box in **c** (image on the very left; the other micrographs are taken from different sections in the 3D-stack at the same xy-position, with displacement in z-axis indicated in images). Scale bars in **a** 10 μ m; **b,c** 1 μ m; **d** 200 nm. The experiment was performed by the author together with M. Schifferer (EM facility, DZNE). Figure was adapted from Marahori et al. (manuscript in preparation).

Most LysoTracker-stained organelles colocalized with Keima labeled mitolysosomes (91% of 415 particles; **Figure 3.25, a–c**), which were not marked or marked only dimly with “regular” mitochondrial matrix labels (*Thy1*-mito-XFP mice; **Figure 3.25, d,e**), suggesting an actively digestive state of mitolysosomes in synaptic exit points.

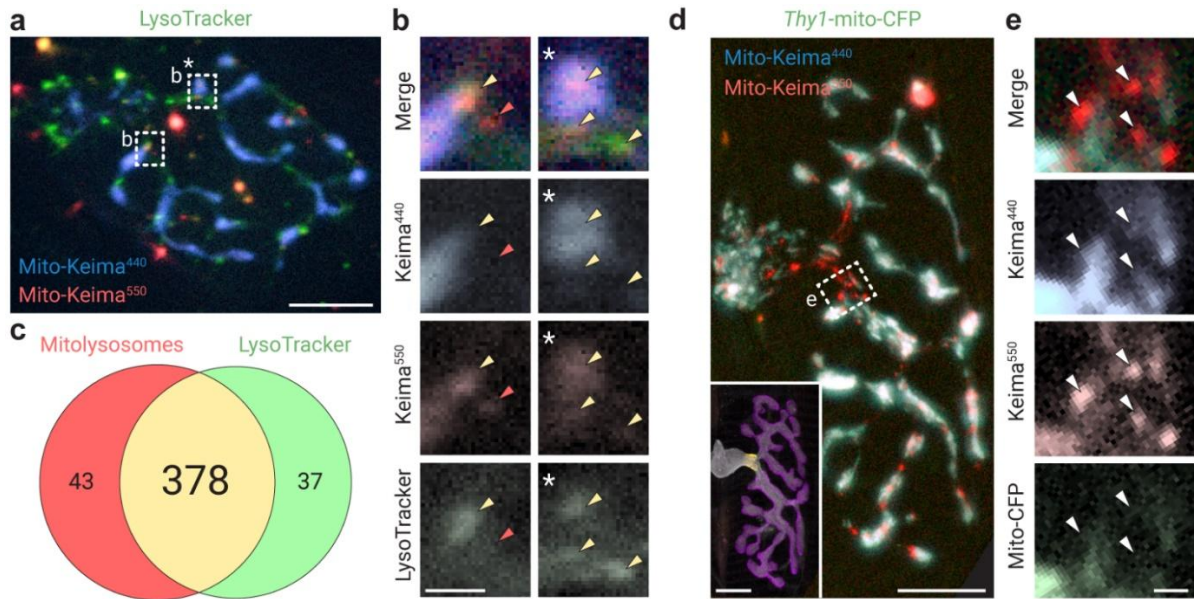


Figure 3.25 | Parallel labeling and colocalization of mitochondrial and lysosomal markers. a–c, Mitolysosomes and LysoTracker colocalize in acute nerve–muscle explants. **a,** Widefield projection of a neuromuscular junction expressing AAV9-hSyn-mito-Keima (blue, neutral Keima-440; red, acidic Keima-550) with concurrent LysoTracker labeling (green). **b,** Widefield optical sections of mitolysosomes (high Keima-550 signal) in the synaptic exit point (two positions are shown, indicated by the two boxes in **a**, the box marked with an asterisk refers to the series of images on the righthand side). The same area is shown in all three channels (blue, neutral Keima-440; red, acidic Keima-550; green, LysoTracker). Yellow arrows point to mitolysosomes that are colocalizing with LysoTracker, red arrows point to mitolysosome lacking LysoTracker signal. **c,** Venn diagram quantifying colocalization of LysoTracker and mitolysosomes, $n = 458$ particles from 10 NMJs in 3 C57BL/6 mice. **d,e,** Mitolysosomes lack regular mitochondrial matrix markers (*Thy1*-mito-CFP) in acute nerve–muscle explants. **d,** Widefield projection of a neuromuscular junction of a *Thy1*-mito-CFP mouse labeled with AAV9-*hSyn*-mito-Keima. Inset shows post-hoc correlated staining (anti-Caspr, yellow; α -bungarotoxin, magenta; anti- β III-tubulin, white). **e,** Widefield single optical sections of mitolysosomes in the synaptic exit point (position of image indicated by a box in **d**). The same area is shown in all three channels (blue, neutral Keima-440; red, acidic Keima-550; green, mito-CFP). Arrows point to mitolysosomes (high Keima-550 signal) that are lacking in Mito-CFP fluorescence. Scale bars in **a,d** 10 μ m; **b** 2 μ m; **e** 1 μ m. The author performed the experiments. Figure was adapted from Marahori et al. (manuscript in preparation).

3.4.7. Mitophagy dynamics in axon terminals

For long-ranged retrograde transport of mitochondria towards the soma, different models have been proposed to describe the dynamic transition of mitochondria into autophago-lysosomal degradation. These models range from (1) ‘bona fide’ mitochondria being transported towards the soma (Mandal et al., 2021) for degradation (Sheng, 2014), (2) to models that suggest that progressively maturing autophagosomes and endolysosomes engulf mitochondria on their axonal journey (Maday, 2016). To further explore the specific relationship between mitochondrial captures and lysosomal digestion at the synaptic exit point, an experiment was performed where the distal portions of NMJs were photoactivated in *Thy1*-mito-paGFP mice (injected with AAV9-*hSyn*-mito-Keima) to monitor the acidity of retrogradely moving photoactivated mitochondria at various locations along their route. The aim of this experiment was to determine whether

'captured' mitochondria actually constitute 'bona fide' mitochondria or if these entities had already been enclosed in a (pre-)degradative organelle during their journey to the exit point.

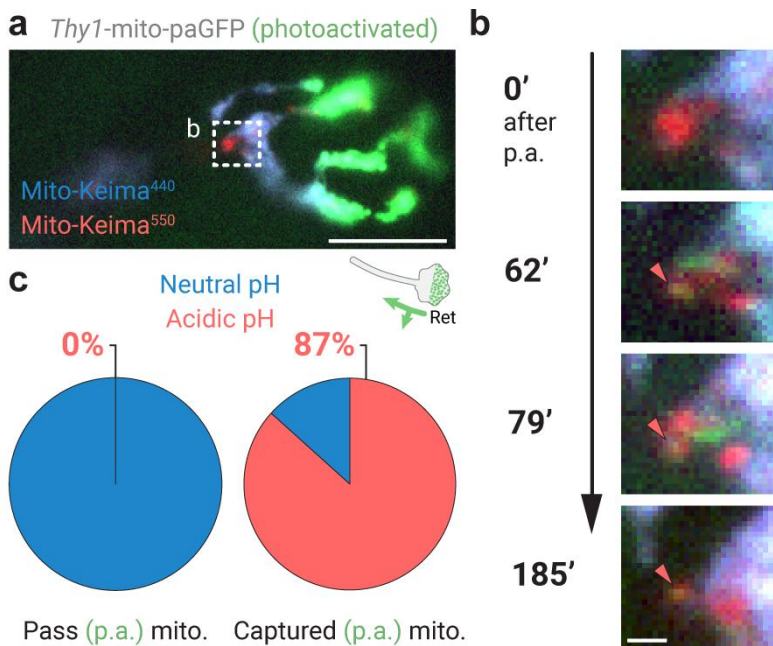


Figure 3.26 | Colocalization of mitotlysosomes and captured mitochondria over time. **a**, Mitochondria were photoactivated (p.a.) from non-fluorescent to green fluorescence in the distal half of neuromuscular junctions in acute nerve-muscle explants of *Thy1*-mito-paGFP mice expressing AAV9-*hSyn*-mito-Keima (widefield image section; blue, neutral Keima-440; red, acidic Keima-550). After photoactivation, the synaptic exit point (boxed area) was monitored routinely for p.a. 'captured' mitochondria and the proximal axon for p.a. 'passed' mitochondria (stacks ca. every 10–15 min to avoid photobleaching). **b**, Widefield image sections from the location indicated in **a**, taken at different time intervals as indicated next to each image (min after p.a.). A 'captured' p.a. mitochondrion

(green fluorescence) colocalizing with a mitotlysosome (high Keima-550/Keima-440 ratio), indicated by a red arrow in each time point. **c**, Proportion of 'passing' and 'captured' mitochondria that colocalized with mitotlysosomes (red) within the duration of the experiment ($n = 9$ 'passing' and $n = 15$ 'captured' mitochondria from 10 NMJs, 5 mice). Scale bars: 10 μm in **a**, 1 μm in **b**. The experiments were performed by the author. Figure was adapted from Marahori et al. (manuscript in preparation).

Neither 'captured' nor 'passing' mitochondria were seen to colocalize with an acidic mito-Keima signal whilst moving, however, many 'captured' mitochondria (87%) turned acidic after reaching the exit point (**Figure 3.26**). Moreover, mitotlysosomes had distinct properties when compared to 'captured' mitochondria: mitotlysosomes were more circular and smaller (**Figure 3.27, a**) and moved faster than 'captured' mitochondria (**Figure 3.27, b**). Also, mitotlysosomes showed movement behaviors that were uncharacteristic of 'captured' mitochondria, such as frequently attaching and detaching from exit points with bouts of fast bidirectional movement in between ('captured' mitochondria usually show unidirectional movement and do not 'detach' from exit points after stopping there). Overall, these findings suggest that 'bona fide' dysfunctional mitochondria were recognized and captured at synaptic exit points in order to meet lysosomal degradation.

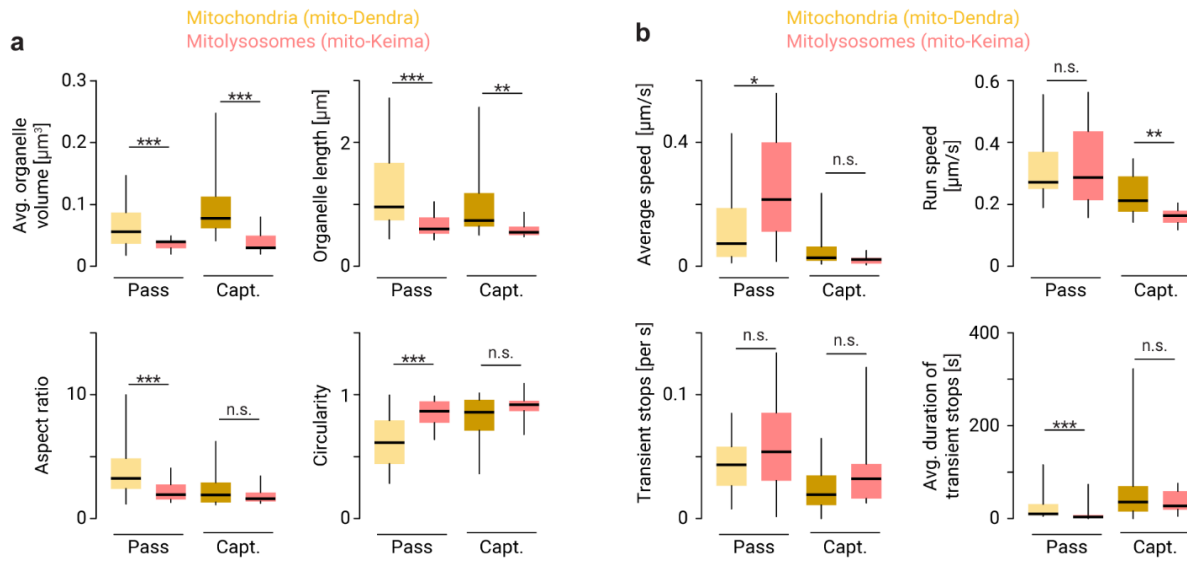


Figure 3.27 | Comparing organelle properties of ‘captured’ mitochondria and mitolysosomes. Mitochondrial properties (analysis from the dataset in **Figure 3.19, c,d** replotted, *Thy1*-mito-Dendra mice) are compared against mitolysosomal properties (movies acquired in ≥ 4 NMJs from ≥ 3 mice per group; *Thy1*-mito-CFP mice injected with AAV9-*hSyn*-mito-Keima). **a**, Mitochondrial morphology measurements from **Figure 3.19, d** are compared against measurements in mitolysosome movies (‘pass’: $n = 20$ mitolysosomes and ‘captured’: $n = 11$ mitolysosomes). **b**, Mitochondrial movement parameters from tracks in **Figure 3.19, c** are compared against mitolysosome movement parameters (‘pass’: $n = 22$ mitolysosomes and ‘captured’: $n = 8$ mitolysosomes). Mann-Whitney-U test was used to determine significance. The author performed the experiments. Figure was adapted from Marahori et al. (manuscript in preparation).

3.4.8. The PINK1/parkin pathway is not essential for mitochondrial capture

The results implied a selective mechanism of capturing dysfunctional mitochondria at synaptic exit points, and different mitophagy-mediating proteins have indeed been shown to interact with the axonal transport machinery. For example, PINK1 and parkin, which label mitochondria with polyubiquitin chains for mitophagy (Geisler et al., 2010; Matsuda et al., 2010; Narendra et al., 2008; Narendra et al., 2010; Vives-Bauza et al., 2010), can detach damaged mitochondria from the transport machinery to facilitate local axonal mitophagy in neuronal cell cultures (Ashrafi et al., 2014; Wang et al., 2011).

To test whether the PINK1/parkin pathway mediates mitochondrial capture, the retrograde pulse-chase experiment at the synaptic junction was repeated in *Pink1*-*Parkin*-double knockout (dKO) mice. However, triangularis sterni muscles from adult animals surprisingly showed a marked denervation phenotype (**Figure 3.28, a–c**, red arrows and stars), which has been previously published (Rogers et al., 2017). In addition to the denervation phenotype, dKO mice also has severely reduced retrograde transport of mitochondria in stem axons (**Figure 3.28, e**), which was not observed in mice that had been knocked out for PINK1 alone (**Figure 3.28, d**).

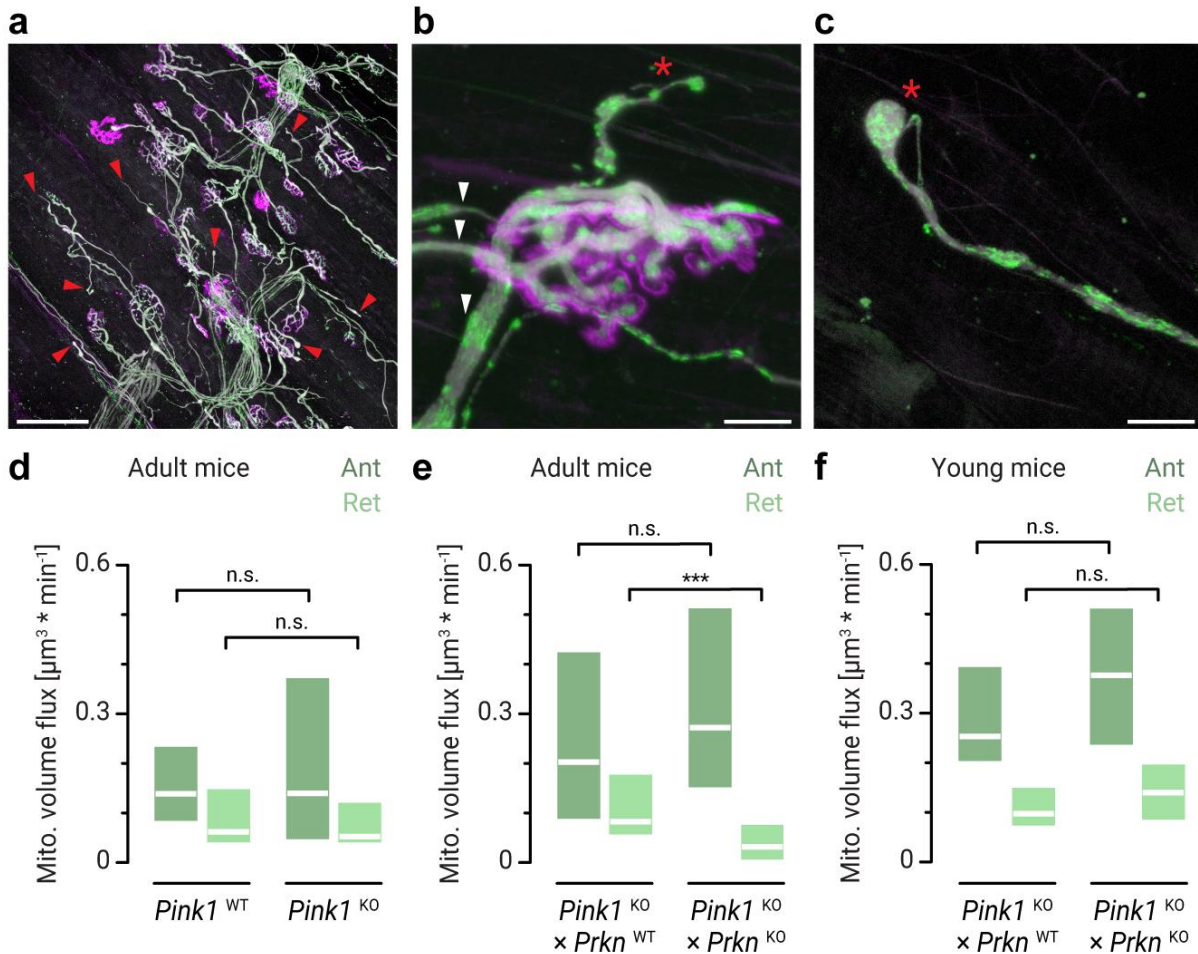


Figure 3.28 | Neuromuscular phenotype of *Pink1-Parkin*-dKO mice. **a-c**, Neuromuscular junctions of an adult *Pink1-Parkin*-double KO (dKO) mouse (*Pink1*^{ko/ko} \times *Prkn*^{ko/ko} \times *Thy1*-mito-Dendra; mitochondria, green; β III-tubulin antibody, grey; AChR labeled by bungarotoxin, magenta): **a** shows a confocal maximum projection of the neuromuscular endplate band in the triangularis sterni muscle, red arrows point to multiple axon sprouts (axon “stumps” that do not form a synapse), in **b** confocal projection of a junction that is multi-innervated (three axons indicated by arrows supply the synaptic territory), star indicates axon sprout, in **c** confocal projection of axon sprout (star) with fragmented mitochondria. **d-f**, Mitochondrial volume flux measured in stem axons (intercostal nerve) of acute-nerve muscle explants in **d**, adult single *Pink1*-KO compared to *Pink1*-WT (Exp: *Pink1*^{ko/ko} \times *Thy1*-mito-Dendra; Ctr: *Pink1*^{wt/wt} \times *Thy1*-mito-Dendra littermates; $n \geq 15$ axons from $n \geq 2$ mice per group); **e**, adult *Pink1-Parkin*-double KO (dKO) compared to single *Pink1*-KO (Exp: *Pink1*^{ko/ko} \times *Prkn*^{ko/ko} \times *Thy1*-mito-Dendra; Ctr: *Pink1*^{ko/ko} \times *Prkn*^{wt/wt} \times *Thy1*-mito-Dendra littermates; $n \geq 42$ axons from $n \geq 3$ mice per group); **f**, juvenile (3-week-old) *Pink1-Parkin*-double KO (dKO) compared to single *Pink1*-KO (Exp: *Pink1*^{ko/ko} \times *Prkn*^{ko/ko} \times *Thy1*-mito-Dendra; Ctr: *Pink1*^{ko/ko} \times *Prkn*^{wt/wt} \times *Thy1*-mito-Dendra littermates; $n \geq 30$ axons from $n \geq 3$ mice per group). Scale bars in **a** 100 μm , in **b,c** 10 μm . Mann-Whitney-U test was used to determine significance. The author performed the experiments. Figure was adapted from Marahori et al. (manuscript in preparation).

To test whether the mitochondrial capture mechanism at the synaptic exit point depends on the PINK1/parkin pathway in a causal manner, the imaging was therefore performed at an earlier age (3-week-old mice), before the onset of the transport phenotype in stem axons (**Figure 3.28**, **f**; Mann-Whitney-tests for mitochondrial volume flux: Anterograde, $p \geq 0.05$; Retrograde $p \geq 0.05$). In this setting, mitochondrial volume flux rates and the proportion of captured mitochondria were unchanged when comparing *Pink1-Parkin*-dKO and *Pink1*-KO mice to wildtype mice

(**Figure 3.29**; Ctr: 54% capture, DKO: 62% capture; per group ≥ 29 tracked mitochondria during $20 \geq$ 'NMJ hours', χ^2 -test $p \geq 0.05$).

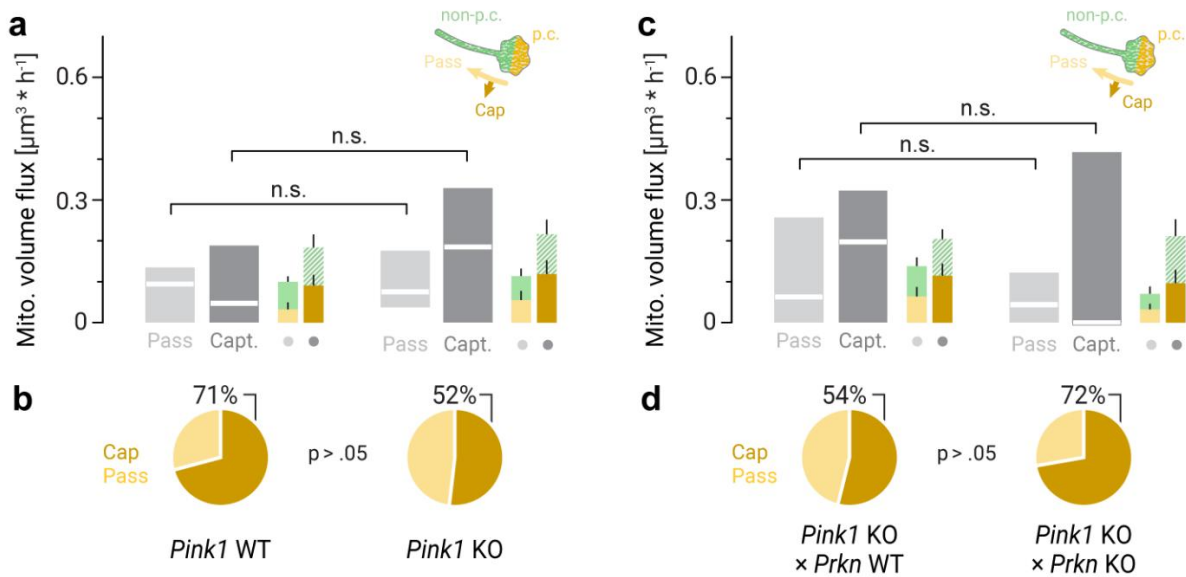


Figure 3.29 | The PINK1/parkin pathway is not essential for mitochondrial capture. **a–b**, Mitochondrial capture experiment in juvenile *Pink1*-KO mice (see **Figure 3.17** for experimental setup and legends; Exp: *Pink1*^{ko/ko} × *Thy1*-mito-Dendra; Ctr: *Pink1*^{wt/wt} × *Thy1*-mito-Dendra littermates): **a**, Mitochondrial volume flux at synaptic exit points ($n \geq 15$ axons from ≥ 8 mice per group); **b**, Mitochondrial capture fractions of retrogradely moving p.c. mitochondria in synaptic exit points ($n \geq 24$ mitochondria per group, measured from the movies in **a**). **c–d**, Mitochondrial capture experiment in juvenile *Pink1*-*Parkin*-double KO (dKO) mice (Exp: *Pink1*^{ko/ko} × *Prkn*^{ko/ko} × *Thy1*-mito-Dendra; Ctr: *Pink1*^{ko/ko} × *Prkn*^{wt/wt} × *Thy1*-mito-Dendra littermates): **c**, Mitochondrial volume flux ($n \geq 15$ axons from ≥ 10 mice per group); **d**, Mitochondrial capture fractions ($n \geq 18$ mitochondria from the movies in **c**). Mann-Whitney-U test was used to determine significance in **a** and **c**, a χ^2 -test was used in pie charts (**b**, $p \geq 0.05$; **d**, $p \geq 0.05$). The author performed all experiments. Figure was adapted from Marahori et al. (manuscript in preparation).

This argues that the PINK1/parkin pathway is not essentially involved in mitochondrial capture at the synaptic exit point, a function that is perhaps taken by another ubiquitin-E3-ligase, such as MITOL (Yonashiro et al., 2006). In favor of this, immunostainings against ubiquitin do indeed reveal an accumulation of ubiquitin at the synaptic exit point compared to the rest of the synaptic terminal (**Figure 3.30**). It cannot be entirely excluded that the PINK1/parkin pathway plays a role in mitochondrial capture, as developmental compensation might take place in knockout mice, especially if the PINK1/parkin pathway is essential for mitophagy. So far, however, the data suggest that the PINK1/parkin pathway is not absolutely required for distal mitophagy, although it likely plays alternative roles in the motor neuron, resulting in the observed degenerative phenotype.

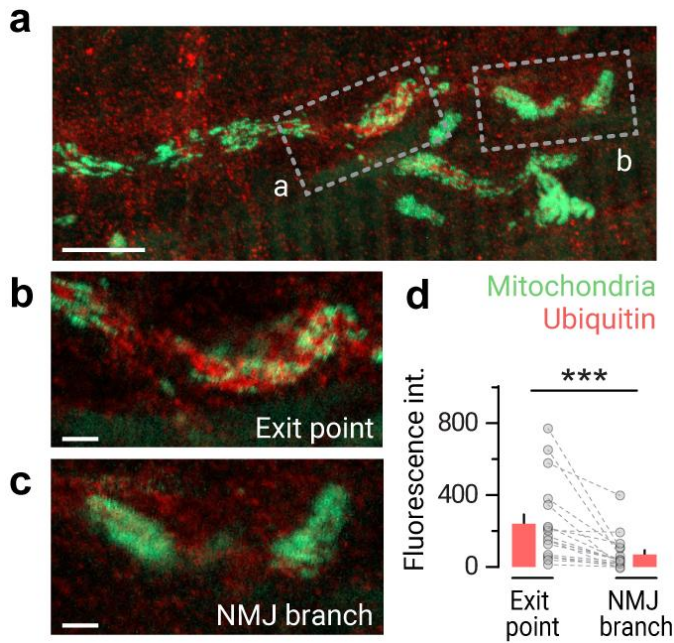


Figure 3.30 | Ubiquitin enrichment in synaptic exit points. **a–c**, An antibody staining against ubiquitin was applied to fixed triangularis sterni muscles isolated from *Thy1-mito-Dendra* mice (staining shown in red; green: mitochondria). **a**, Confocal projection of a neuromuscular junction, **b**, Single optical section of the synaptic exit point and from **c**, an NMJ branch; locations of **b** and **c** are indicated by boxes in **a**. **d**, Quantification of ubiquitin staining brightness in synaptic exit points and NMJ branches ($n = 18$ axon terminals from 2 mice). Scale bars in **a** 10 μm , in **b,c** 2 μm . A Wilcoxon (paired) test was used to determine significance. The author performed the experiments. Figure was adapted from Marahori et al. (manuscript in preparation).

3.4.9. Optineurin mediates mitochondrial capture

In addition to ubiquitinating proteins, mitophagy also depends on so-called mitophagy adaptor proteins. Those proteins interlink ubiquitin-tagged mitochondria with the autophagosomal membrane, facilitating autophagosomal engulfment. In this study, optineurin was chosen as a candidate due to its involvement in motor neuron disease. Indeed, cell-type specific deletion of optineurin in motor neurons selectively reduced mitochondrial capture significantly (from 76% in the control to 34% in the *Optn*-cKO; **Figure 3.31, b**, $p < 0.01$, χ^2 -test; $n \geq 38$ tracked mitochondria per group; ChAT-Cre^{mut/wt} \times *Optn*^{flox/flox} mice compared to ChAT-Cre^{wt/wt} \times *Optn*^{flox/flox} littermate controls). The volume flux of ‘passing’ mitochondria was increased 4-fold in the conditional knockout (**Figure 3.31, a**; Controls: $0.04 \pm 0.01 \mu\text{m}^3/\text{h}$, cKO: $0.16 \pm 0.06 \mu\text{m}^3/\text{h}$, $p < 0.05$, Mann-Whitney-U-test), suggesting that when motor neurons lack optineurin, mitochondria that would otherwise be captured are instead able to pass the synaptic exit point. In line with this, ‘passing’ mitochondria were also rounder in the knockout than in littermate controls, appearing more similar to their normally captured counterparts, suggesting that these are indeed mitochondria that “slipped through” the filter (**Figure 3.31, c,d**). Retrograde mitochondrial volume flux in intercostal nerve stem axons was not significantly different between knockouts and littermate controls (**Figure 3.31, e**; Ctr: $0.15 \pm 0.02 \mu\text{m}^3/\text{min}$, KO: $0.17 \pm 0.04 \mu\text{m}^3/\text{min}$, $p > 0.05$, Mann-Whitney-U-test), suggesting that optineurin is specifically active in mitostasis at synaptic terminals, but not other areas of the axons. Together, these data reveal a previously unknown, non-canonical mechanism of neuronal mitophagy responsible for most of mitochondrial turnover in distal motor axons.

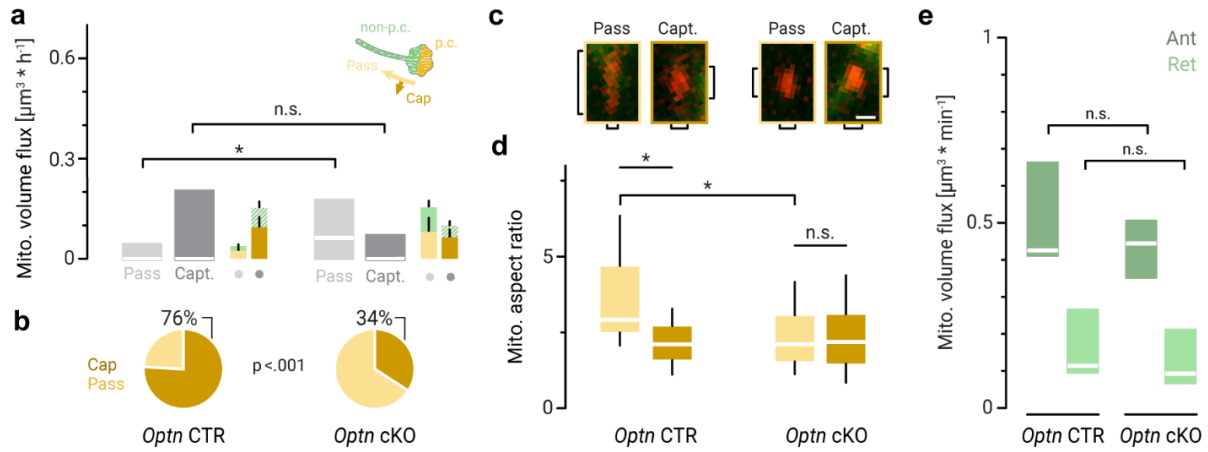


Figure 3.31 | Optineurin mediates mitochondrial capture in synaptic exit points. **a–b**, Mitochondrial capture experiment in *Optn*-c(onditional)KO mice (see **Figure 3.17** for experimental setup and legends; Exp: ChAT-Cre^{mut/wt} × *Optn*^{fllox/fllox} × *Thy1*-mito-Dendra mice; Controls: ChAT-Cre^{wt/wt} × *Optn*^{fllox/fllox} × *Thy1*-mito-Dendra littermates); **a**, Mitochondrial volume flux at synaptic exit points ($n \geq 29$ axons from ≥ 18 mice per group); **b**, Mitochondrial capture fractions of retrogradely moving p.c. mitochondria in synaptic exit points ($n \geq 29$ mitochondria per genotype, analyzed from the movies in **a**). **c–d**, Morphological properties of ‘captured’ and ‘passed’ mitochondria in *Optn*-cKO and control mice (analyzed from the movies in **a**); **c** shows retrogradely moving p.c. mitochondria (red) in the synaptic exit point from each genotype and mitochondrial ‘class’ (left pair: *Optn* control, right pair: *Optn*-cKO). Vertical brackets represent mitochondrial length, horizontal brackets mitochondrial width, to illustrate how the measurements in **d** were taken. **d**, Mitochondrial aspect ratio, which denotes the ratio of mitochondrial length and width, for retrogradely moving p.c. mitochondria from each genotype and class ($n \geq 13$ mitochondria per group; from the movies in **a**). **e**, Anterograde and retrograde mitochondrial volume flux in stem axons measured in acute nerve-muscle explants of *Optn*-cKO mice (right pair: Exp: ChAT-Cre^{mut/wt} × *Optn*^{fllox/fllox} × *Thy1*-mito-Dendra mice; left pair: ChAT-Cre^{wt/wt} × *Optn*^{fllox/fllox} × *Thy1*-mito-Dendra littermate controls; $n \geq 19$ axons from 3 mice per group). Scale bar in **c** 500 nm (for all shown images). Mann-Whitney-U test was used to determine significance in **a** and **e**, a χ^2 -test was used in **b**, $p = 0.0006$. A Kruskal Wallis test with multiple comparisons correction was used to determine significance in **d**. The author performed all experiments. Figure was adapted from Marahori et al. (manuscript in preparation).

4. Discussion

The text in this section was written by N. A. Marahori and in parts, elaborates on ideas from a manuscript that is being prepared for a peer-reviewed publication:

Working title: An optineurin-mediated retrograde transit filter controls mitostasis in distal axons.

Authors: Natalia Athanasia Marahori, Barbara Gailer, Martina Schifferer, Tatjana Kleele, Anna Iatroudi, Petros Avramopoulos, Stefan Engelhardt, Melike Lakadamyali, Monika Brill, and Thomas Misgeld

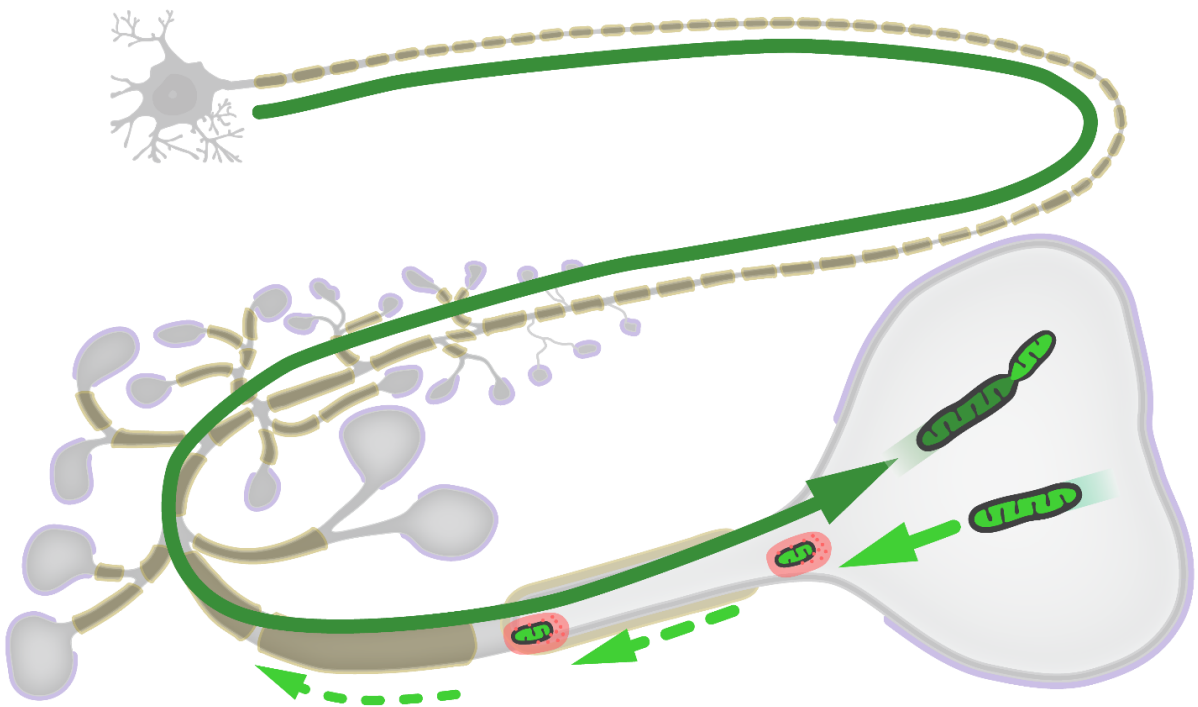


Figure 4.1 | Model how anterograde and retrograde transport contribute to synaptic mitostasis *in vivo*. Schematic of a lower motor neuron; dark green: anterograde mitochondrial transport from the soma; light green: retrograde mitochondrial transport; red: mitophagy at distal nodes of Ranvier (yellow: myelin sheaths, violet: synaptic sites).

Mitostasis—mitochondrial homeostasis—is a fundamental process that sustains cellular health in many tissues, but especially in the nervous system, as evidenced by the fact that defects in mitostasis are closely linked to neurodegeneration (De Vos et al., 2008; Hafezparast et al., 2003; Maday et al., 2014; Mariano et al., 2018; Nunnari & Suomalainen, 2012; Rugarli & Langer, 2012). Yet, why defects in mitostasis manifest in this manner remains poorly understood. So far, most aspects of mitostasis have been studied in cell culture systems, which lack the specific properties and morphology of mature neurons as are formed *in vivo*. Such studies have not fully elucidated many basic aspects of mitostasis: What are the major sites of mitochondrial degradation and biogenesis in neurons? How does axonal transport relate to mitostasis? How do mitostatic processes map onto the complex geometry of mature neurons? How is intracellular mitochondrial heterogeneity and functional specification established, and in which ways do compartmentalized mitostatic pathways contribute? Especially, how do these processes maintain mitochondria at the synapse, which is the main functional site of a neuron that is also most prone to disease? What characterizes the lifecycle of a “typical” synaptic mitochondrion? The lack of this knowledge is, to a large degree, due to a lack of *in vivo* imaging methods that can visualize the dynamism and turnover of neuronal mitochondria in a complex mammalian tissue context. In this work, numerous *in situ* imaging assays have been developed for measuring mitochondrial shapes, dynamics, turnover, and mitophagy, most centrally an optical pulse-chase approach that allows tagging small subpopulations of mitochondria with photoswitched proteins. This specific labeling of mitochondrial subpopulations can be useful for tracking the fate of individual organelles and measuring mitochondrial turnover and has allowed to perform the first in-depth *in situ* characterizations of synaptic mitostasis in both physiological and disease-related settings. The main findings of this study are twofold: (1) in lower motor neurons, “new” synaptic mitochondria are provided to distal axonal sites by targeted anterograde transport from the soma and share their contents with the residual pool via fusions; (2) the bulk (75%) of mitochondrial degradation occurs directly at the synapse via optineurin-mediated mitophagy, refuting the canonical textbook view that long-range retrograde transport is responsible for most mitochondrial elimination. This leads to the conclusion that *in situ*, mitostasis is a highly compartmentalized process with implications for cell type- and compartment-specific vulnerability in neurodegenerative diseases.

4.1. Methods to study mitochondrial fate *in vivo*

Elucidating the “life” of neuronal mitochondria is an important undertaking, yet the process has remained enigmatic for scientists. Historically, attempts at measuring mitochondrial turnover—the rate and the conditions at which mitochondria are replaced—have been made with radioisotope pulse-chase experiments (Miwa et al., 2010). After *in vivo* labeling of mitochondrial metabolites such as mtDNA, amino acids, or lipids (the “pulse”), mitochondria were isolated and

protein turnover rates were inferred from the kinetics of label disappearance over time (“chase”; Miwa et al., 2010). In the brains of rodents, the reported half-lives were quite variable—ranging from a few days to multiple months (Cuzner et al., 1966; Gross et al., 1969; Huemer et al., 1971; Khan & Wilson, 1965; Menzies & Gold, 1971, 1972; Miwa et al., 2010; Pasquini et al., 1973; Von Hungen et al., 1968). The high variability has been mostly attributed to the problematic technical issues inherent to this technique (re-usage of radioisotope-labeled amino acids by the cells; Bakalkin et al., 1978; Miwa et al., 2010). Metabolic labeling assays also lacked resolution at the cellular level (Trudeau et al., 2014), making it impossible to infer mitochondrial half-lives in neurons from these studies.

The discovery of fluorescent proteins (such as GFP; Chalfie et al., 1994; Tsien, 1998) and their application to neuronal cell cultures has circumvented many of the drawbacks of pulse-chase radiolabeling techniques, allowing to directly visualize mitochondrial transport and further elucidate mechanistic details on an organelle-based level (Roy, 2020). Transgenic animals containing these proteins in neuronal mitochondria have further greatly advanced the studies of mitochondrial biology in neurons *in vivo* (Breckwoldt et al., 2014; Fecher et al., 2019; Magrane et al., 2014; Misgeld et al., 2007; Pilling et al., 2006; Plucinska & Misgeld, 2016; Plucinska et al., 2012). *In vivo* imaging studies, however, also began to face several important restrictions (see introduction of **Section 3.1**).

The optical pulse-chase assay developed in this work aimed at combining the benefits from both worlds. Two transgenic mouse lines containing the photoswitchable proteins Dendra and paGFP were generated (for similar mice, see Magrane et al., 2014; Marinkovic et al., 2012; Pham et al., 2012), which allowed labeling a specific subpopulation of mitochondria with UV light (the “pulse”) and following these mitochondria over time (“chase”), with the additional feature of live imaging these organelles at specific points in time and space. Practically speaking, this approach served various experimental purposes (**Figure 3.1**), which will be elaborated below.

Mitochondrial turnover. Mitochondria should not be considered as individual organelles of defined size and nature but rather as a dynamic syncytium constantly undergoing fusion and fission (Ryan & Hoogenraad, 2007) so that instead of describing mitochondrial turnover by counting individual organelles, it is often rather given by globally measuring lifetimes of mitochondrial proteins or lipids. Inspired by the radioisotope pulse-chase experiments in living animals (Miwa et al., 2010), a similar experiment was designed where synaptic mitochondria were irradiated with UV light (“pulse”), and then the disappearance of the photoswitched (and replacement by non-photoswitched) mitochondria was quantified over time (“chase”, **Figure 3.10, a**). This *in vivo* experiment yielded that the majority of photoswitched mitochondria were replaced after ~4 days, which is in line with previously reported mitochondrial half-lives reported in cell cultures (Dorrbaum et al., 2018). Compared to radioisotope experiments, “optical” pulse-

chase experiments should yield more reliable measurements of mitochondrial half-life, as the photoswitchable labels are large, complex proteins that, unlike the radiolabeled basic metabolites, cannot be reused after their degradation. Photoswitching of mito-Dendra is irreversible (Gurskaya et al., 2006) and should not spontaneously revert to its non-photoswitched state or diffuse into the cytoplasm. Likely confounders could be inadvertently “slow” photoswitching unless care is taken to minimize exposure of the experimental area to blue light (Dempsey et al., 2015), and photobleaching also needs to be controlled and corrected (see **Materials and Methods** for experimental measures). The results do, however, come under the assumption that mito-Dendra is a suitable long-lived protein to measure mitochondrial lifetime, which further studies will have to determine.

Mitochondrial age: In an optical pulse-chase experiment, the mitochondrial population that is labeled by photoswitching has been effectively “time-stamped,” which allowed the experiments in **Figure 3.13** and **3.14** to distinguish between “new” from “old” synaptic mitochondria. Because of the lifetime of the nerve-muscle preparation, only mitochondrial “ages” up to 4 h were distinguished; however, taken *in vivo*, such an approach could potentially be even expanded. An alternative tool to study mitochondrial age is mito-Timer (Trudeau et al., 2014). Mito-Timer initially fluoresces green (young protein) and shifts to red (old) over time. The overall ratio of green and red fluorescence in a cell depends on factors such as mitochondrial biogenesis, fusion, and degradation. It has, therefore, been suggested as a readout for mitochondrial turnover, or “age.” Important differences between mito-Timer and pulse-chase methods are: (1) no specific, only relative rates of turnover can be determined with mito-Timer, unlike in pulse-chase assays; (2) mito-Timer gives a gradual and not binary readout about age; (3) mito-Timer is limited to its 12–18h maturation window. (Trudeau et al., 2014)

Mitochondrial morphology: Superresolution techniques or electron microscopy are often needed to resolve the fine details of mitochondrial structure and network morphology. Widefield microscopy can also resolve the general shape of a mitochondrion, provided that the mitochondrion is sparsely labeled or isolated from other surrounding mitochondria (**Figure 3.9**). In cell cultures, photoswitching of individual organelles has been used to resolve finer details of mitochondrial shape: for example, visualizing fine structures such as mitochondrial nanotunnels (Huang et al., 2013). In this work, photoswitching allowed not only to disambiguate the fine morphology of both resident and moving synaptic mitochondria (**Section 3.2**) but also to track the fine details of their movements and stops in between hundreds of other organelles (**Figure 3.19**).

Mitochondrial fusion: Photoswitching can be used in a mitochondrial fusion assay due to the fusion of two differentially colored mitochondria resulting in a visible merging of the two colors (Hoppins & Nunnari, 2009). In primary neuron cultures, partial photoactivation of a mito-paGFP-

labelled cell was redistributed throughout the cell, while in Mfn2 mutated cells, this redistribution was severely impaired (Baloh et al., 2007). Photoswitching assays have been widely used in more cell culture photoactivation assays since (Karbowski et al., 2004; Karbowski et al., 2014; Magrane et al., 2012). This work successfully identified mitochondrial fusions in a setting that would otherwise prohibit such observations with regular tools (**Figure 3.15**). While most exchange of mitochondrial matrix is thought to occur via complete fusions, the assay cannot formally distinguish other forms of matrix exchange, such as mitochondrial nanotunnels (Eisner et al., 2018), which can interconnect even distant (8 μm) mitochondria (Huang et al., 2013; Lavorato et al., 2017).

Long-range transport. Time-lapse imaging mitochondria after photoswitching has two advantages when compared to a “standard” approach with monochrome mitochondrial labels: First, moving mitochondria can be tracked with high spatial precision, even in optically dense areas (Marinkovic et al., 2012). A similar approach has been taken successfully for sparsely labeling and visualizing the transport of cytosolic proteins with photoactivated GFP (Roy et al., 2011). (2) Single photoswitched mitochondria can be tracked across large distances—up to many cm in axons—that would otherwise exceed a typical field of view. With the photoswitching assay providing a “proof of origin” for mitochondria (Marinkovic et al., 2012), mitochondrial dynamics can be followed and compared even across different neuronal subcompartments *in vivo*—while retaining an imaging modality that still operates at Nyquist resolution. Indeed, photoactivated mitochondria were identified in *in vivo* labeling experiments after they had passed many cm of the intercostal nerve (**Figure 3.11**). Unlike other approaches that have tried to tackle the problem of long-distance (e.g., “orbital tracking” microscopy (Wehnekamp et al., 2019), photoswitchable-based assays do not require highly specialized setups and are implementable on most microscopes.

To summarize, optical pulse-chase methods are versatile tools, allowing us to observe precisely how the various aspects of the mitochondrial lifecycle relate to each other—namely, mitochondrial turnover, age, morphology, transport, and fusion in neurons.

4.2. Renewal of synaptic mitochondria

The chief *raison d’être* of anterograde mitochondrial transport is thought to be supplying distal axon locations with “fresh” organelles, given that most biogenesis is thought to occur in the soma. Indeed, in typical NMJs with ~ 4 mitochondria being transported anterogradely per hour, the turnover of the presynaptic pool was predicted to occur within 3–5 days. This number is remarkably similar to the results from the *in vivo* turnover experiment (~ 4 days), where the decay of photoconverted mito-Dendra was tracked over time (**Figure 3.10**). This suggests that the

majority of mitochondria are delivered to the junction directly from the soma, and not locally generated. The long-range *in vivo* pulse-chase experiments also suggest this to be true, as labeled mitochondria seemed to move directly toward the axon tips without detours (**Section 3.3.2**). An interesting experiment to corroborate these findings could be the imaging of mito-Timer in motor terminals (Ferree et al., 2013; Hernandez et al., 2013). Given the reported maturation times of mito-Timer of about 12–18 h and the estimated mitochondrial turnover at the NMJ of ~4 days, an experiment with mito-Timer would most likely result in a “red” mitochondrial resident population at the synapse, while anterogradely moving mitochondria, if they indeed move directly from the soma to the junction, would appear rather “green”.

It is also well-known that the lifetime of mitochondrial proteins is extremely variable: in some tissues, considerable interprotein differences were observed with half-lives spanning from hours to months (~60 d; Kim et al., 2012). Both mitochondria- and nuclear-encoded transcripts are translated on axonal ribosomes, indicating a substantial amount of mitochondrial biogenesis in axons (Aschrafi et al., 2016; Briese et al., 2016; Cioni et al., 2019; Cosker et al., 2016; Gumy et al., 2011; Kuzniewska et al., 2020; Shigeoka et al., 2016; Yoon et al., 2012; Yousefi et al., 2021; Zivraj et al., 2010). A possibility that combines these findings would be that anterograde transport delivers something akin to “generic building blocks” to the periphery, i.e., mitochondrial packages that mainly contain structural or essential proteins, and that these mitochondria will only be further decorated with more proteins after they reached their final destination. A study recently reported a set of incredibly long-lived mitochondrial proteins in the brain that persist for many months (LLPs) for providing long-term architectural stability within cells due to their association with cristae membranes (Bomba-Warczak et al., 2021). It is possible that these anterograde “delivery packages” not only supply such structures but also a continual stream of “fresh” mitochondrial transcripts to the resident synaptic pool of mitochondria. For example, transcripts encoding short-lived proteins, which are delivered on organelles via “hitchhiking” (Harbauer et al., 2022), might be shared with the resident mitochondrial pool via fusions that were observed between anterogradely moving and resident synaptic mitochondria in pulse-chase experiments (**Figure 3.15**). Further studies will have to determine exactly what constitutes anterogradely moving mitochondria and how they differ from resident (“old”) synaptic mitochondria in more detail.

4.3. Distribution by anterograde transport

Another important aspect that needs to be addressed in the future is understanding how neurons distribute their mitochondria appropriately. For example, mitochondria being enriched in synapses suggests that there is either a preferred delivery system to these sites or high rates of local biogenesis. The experiments in this thesis strongly suggest regulated delivery mechanisms

to synaptic sites via anterograde transport (**Section 3.3**). Such “targeted” mitochondrial delivery would require that mitochondria bypass the main axon trunk without stopping to arrive at the synapses. While studies in cellular systems suggest that moving mitochondria can “sense” a variety of local cues at synapses (Pekkurnaz & Wang, 2022), this cannot explain how mitochondria would “know” from a distance where to go or where to turn at branch points. This information might be carried in axon caliber, microtubule cytoskeleton, or retrograde signaling (Cardanho-Ramos & Morais, 2021; Tymanskyj et al., 2022; Tymanskyj et al., 2018). Multiple levels of decision-making are conceivable: (1) at branch points, (2) at the axon hillock, (3) anterogradely moving mitochondria destined for synapses carrying a “tag.”

Moreover, how mitochondrial enrichment is regulated to correlate with the metabolic demand of a neuron type or neuronal subcompartment is not well understood. Studies showed that mitochondria produce the majority of ATP that is generated in response to increased neuronal activity (Hall et al., 2012; Lin et al., 2010). However, in several studies, short-term changes in neuronal activity did not change mitochondrial transport rates, suggesting that neurons do not have to react to increased metabolic demands by sending more mitochondria. An alternative mechanism for enriching mitochondria might be the regulation of biogenesis or turnover: for example, via acetylcholine levels (L. Sun et al., 2013) or molecular signals like AMP/ATP or NAD⁺/NADH ratios, Ca²⁺ ion levels, or neurotrophins (Cardanho-Ramos & Morais, 2021; Hock & Kralli, 2009; Lopez-Lluch et al., 2008; Ryan & Hoogenraad, 2007). However, as anterograde transport has not been measured yet under chronic changes in neuronal activity (Misgeld & Schwarz, 2017), it remains open whether any of the specific targeting mechanisms for anterogradely moving mitochondria are related to the metabolic need of the periphery.

4.4. Linking fusion and anterograde transport

Anterogradely moving mitochondria that entered a neuromuscular junction had a particular propensity to fuse with other mitochondria of the synaptic pool, thereby sharing their contents with the synaptic mitochondria, which was a very unusual behavior for resident axonal mitochondria otherwise (**Figure 3.15**). It implies that either (1) anterogradely moving mitochondria are “special” to carry a particular molecular factor that allows them to fuse, while stationary mitochondria lack this factor, or (2) anterogradely moving mitochondria are, in fact, regular mitochondria, and there rather is a restrictive factor that prevents stationary mitochondria from fusing, or (3) both.

The question of whether anterogradely moving mitochondria form a distinct mitochondrial pool with unique functional, architectural, and proteomic features is important, as mentioned already in the previous chapters. It might be possible that anterogradely moving mitochondria carry a

specific fusion protein that works asymmetrically; for example, OPA1 (Song et al., 2009) or OPA1-regulating protein. Another likely possibility is that the distinguishing factor is mobility (Gatti et al., 2023; Liu et al., 2009). The kinetic energy that results from mitochondrial movement can catalyze mitochondrial fusion (Hoppins & Nunnari, 2009). Similarly, multiple fusion and transport proteins interact with each other to facilitate fusion: For example, Mitofusin 2 is necessary for axonal transport and interacts with the Miro/Milton complex (Misko et al., 2010), and Miro2 is required for mitochondrial nanotunneling along microtubules, a process akin to fusion (Cao et al., 2019).

Remarkably, the fusion rates of anterogradely moving mitochondria are similar to fusion rates of terminal Schwann cell mitochondria, which were used as a control (**Figure 3.15**). This might, in fact, indicate that a restrictive factor prevents synaptic mitochondria from fusing. It was surprising that resident mitochondria do not fuse, considering how most of these organelles are just a few nanometers spaced apart (**Figure 3.8**). Synaptic mitochondria are highly organized, being kept in a special subsynaptic compartment that is located just above the synaptic vesicle zone, with all mitochondria facing neatly in the same direction (**Figure 3.7**). In the EM images, nothing specific seemed to be holding these mitochondria apart; however, the actin cytoskeleton would not be visible with this EM technique. Actin cages have indeed been described to immobilize and separate mitochondria in the cytosol, abolishing their ability to fuse (Quintana-Cabrera & Scorrano, 2023). Mostly, these cages are formed around damaged mitochondria to prevent them from spreading their matrix contents (Quintana-Cabrera & Scorrano, 2023). Actin is indeed an important structural protein that fulfills many specific functions in synapses, including axonal transport (Bingham et al., 2023; Morris & Hollenbeck, 1995; Roy, 2020; Sato et al., 2022; Venkatesh et al., 2020). The idea of an actin cage holding synaptic mitochondria in the synapse could be tested experimentally, for example, by using actin depolymerization tools (Muller-Deku et al., 2020).

Mitochondrial fusion plays an important role in maintaining synaptic health: for example, MFN modulates spine density and synaptic plasticity by shaping the kinetics of Ca^{2+} ion transients (Li et al., 2010). Indeed, Charcot-Marie-Tooth type 2A is caused by mutations in the human MFN2 gene, and disease models again showed that mitochondrial dysmotility, dysfunction, and impaired fusion were closely linked in the pathogenesis of this disease (Baloh et al., 2007; Misko et al., 2010; Misko et al., 2012; Rocha et al., 2018). Understanding the role that mitochondrial transport and fusion play in synaptic mitostasis, as well as elucidating how these processes are regulated to fill synaptic needs will be an important next step.

4.5. Compartmentalized mitophagy pathways

The experiments in the second half of this thesis also revealed a novel organellar quality control mechanism in motor axons (**Section 3.4**). Specifically, a distal site of neuronal mitophagy was revealed that relies on short-ranged axonal transport to local hotspots of degradative activity. The model proposes that mitochondria moving in axon endings are constantly checked for their health. Specifically, a retrogradely moving mitochondrion will stop at predefined checkpoint areas, where the mitochondrion will be prohibited from moving any further if it is deemed dysfunctional, a process that was termed mitochondrial ‘capture.’ Mitochondria then undergo engulfment by local lysosomes at these “checkpoints,” which are located near distal nodes of Ranvier of motor neuron axons and characterized by hotspots of local degradative activity.

Mitophagy and retrograde transport were cross-coordinated at the distal nodes of Ranvier, which had previously been reported to mediate degradative processes by a paranodal Schwann cell network (Gatzinsky et al., 1997) or glial transmitophagy (Burdett & Freeman, 2014; Davis et al., 2014; Phinney et al., 2015). While it is possible that degradative material leaves the nodal cytoplasm and is transferred to the Schwann cell, such displacement of mitolysosomes was not clearly observed in mito-Keima time-lapses (**Figure 3.27**), neither did others observe mitochondrial uptake into junctional Schwann cells (Bishop et al., 2004), indicating that most lysosomal material is rather recycled inside the axon, perhaps to supply ingredients for local biogenesis (Klionsky & Ohsumi, 1999). On a further note, nodes of Ranvier have a specialized, actin-rich cytoskeleton (Lopez-Domenech et al., 2018), via that optineurin, having a myosin-binding domain (Ryan & Tumbarello, 2018), might mediate mitochondrial captures. The organelle-sorting mechanism at the axon hillock heminode indeed also involves myosin V- and actin-related arrest of cargo from microtubule transporters (Koppers & Farias, 2021). Unfortunately, while the proximal heminode at the axon hillock has been extensively studied (Eichel & Shen, 2022), little is known about the structure of the distal heminode, so that most insights on why these sites are hotspots for mitochondrial captures remain speculative.

These distal nodes supply a sequential array of perinodal “checkpoints” that control the health of passing mitochondria in a presumably consecutive manner, in addition to enriching locally passing lysosomes in these areas. This mechanism supplies each axon terminal with a semi-autonomous system that degrades at least 75% of aged presynaptic mitochondrial volume. Considering that the overall amount of synaptic mitochondrial content surpasses somatic content by a multitude (~15000 mitochondria for the triangularis sterni, versus ~300 somatic mitochondria; Lin et al., 2019; Misgeld & Schwarz, 2017; Tamada, 2023), this results in an extensive amount of mitochondrial turnover occurring in presynaptic compartments. The advantage of this local homeostatic mechanism would be that it is inherently scalable, its capacity relying directly on the number of axon terminals. Such a system would be inherently more

adaptable to the individual geometrical conformation that naturally results from remodeling and plasticity (Sanes & Lichtman, 1999), making it particularly beneficial for perhaps large neuron types with extensive distal arborizations.

Overall, whether a similar quality control mechanism is implemented in other neurons, especially other projection-type neurons, remains open. While lower motor neurons are incredibly disease-relevant, their large terminal synapses and thickly myelinated axons are not typical compared to most CNS neurons. However, autophagic defects are also known to affect CNS neurons (Stavoe & Holzbaur, 2019), and mitochondria are known to accumulate in branch points in these axons (Courchet et al., 2013; Plucinska et al., 2012; Spillane et al., 2013)—which are often nodes of Ranvier (if myelinated) and synaptic boutons. While these studies have suggested that mitochondria stop at CNS branch points to provide for them, it cannot be excluded at this point whether these sites also feature lysosomal activity.

In motor axons, the results support the notion of a mechanistic link between defects in mitochondrial transport and degradation, both of which have been observed in neurodegenerative disease (Abeliovich & Gitler, 2016). While this model describes a hitherto unknown mechanism, it involves several aspects of previously published models of mitophagy that have been gathered from neuronal cell cultures. Specifically, the results are in line with autophago-lysosomal degradation involving retrograde motility that initiates distally in axon tips (Kulkarni & Maday, 2018; Maday, 2016; Maday & Holzbaur, 2014, 2016; Maday et al., 2012; Neisch et al., 2017; Xie et al., 2015). However, the work refutes the notion that broken mitochondria move primarily to the soma for degradation, and this being the chief purpose of retrograde mitochondrial transport (Cai et al., 2012; Chang & Reynolds, 2006; Griffin & Watson, 1988; Hollenbeck, 1996; Lin et al., 2017; Miller & Sheetz, 2004; Sheng, 2014; Sheng & Cai, 2012; Ye et al., 2015), instead strengthening the idea that mitochondria that engage in long-ranged retrograde transport are relatively healthy organelles (Breckwoldt et al., 2014; Verburg & Hollenbeck, 2008) and that mitochondria are rather displaced from the transport machinery once they are damaged (Ashrafi et al., 2014; Wang et al., 2011). Moreover, this work argued against the classical notion that active lysosomes execute their functions mainly in the soma (Augenbraun et al., 1993; Cai et al., 2010; Cai et al., 2012; Cheng et al., 2018; Craig & Banker, 1994; Han et al., 2020; Lee et al., 2011; Lie et al., 2021; McWilliams et al., 2018; Parton & Dotti, 1993; Parton et al., 1992), as there was rather an abundance of apparently degrading organelles in NMJs, most likely lysosomes (**Figure 3.23**). It is likely that many studies have reached this conclusion because lysosomes are very densely arranged in somata, whereas in axons, they do not belong to the majority of the resident organelles (e.g., compared to mitochondria, **Figure 3.23**), thus they are more loosely arranged. Particularly in small-caliber axons, the absolute number of lysosomes is, therefore, most likely much smaller and less noticeable than in the large motor axon terminals.

This work leaves two aspects open: the origin of the ‘captured’ mitochondria and the fate of the ‘passing’ mitochondria. ‘Captured’ mitochondria, for example, could be individual synaptic organelles that have grown dysfunctional, or they could result from material sorting and asymmetric fission of a damaged particle (Kleele et al., 2021). As most synaptic mitochondria ($0.05 \pm 0.03 \mu\text{m}^3$ corrected for 30% tissue shrinkage in EM reconstructions) are not much larger than ‘captured’ mitochondria ($0.09 \pm 0.01 \mu\text{m}^3$), however, such a fission event would most likely have to follow a fusion event. Alternatively, the large size and circular shape of the ‘captured’ mitochondria might be a result of losing internal structure and osmotic swelling of the mitochondrial particle (Nikic et al., 2011).

‘Passing’ mitochondria might be relatively healthy organelles that are destined to be “redistributed” to other areas of need, such as other synapses or axon areas (Mandal et al., 2021; Wong et al., 2012), or they might indeed be part of a constitutive ‘bulk’ autophagy pathway that moves this material retrogradely into the soma. However, redistribution to other NMJs does not occur in this system (observations from the mitochondrial transport dataset at branchpoints, in Brill et al., 2016), and ‘passing’ mitochondria did not co-localize with degradative markers (**Figure 3.26**). Furthermore, the ‘passing’ mitochondria at terminal branches were much smaller than in stem axons (**Figure 3.16**), suggesting that this is not the same population and that synaptic mitochondria mostly do not reach the stem axon. Instead, they are perhaps taken up by one of the consecutive nodes of Ranvier for degradation. This would argue that the “fate” of retrogradely moving synaptic mitochondria is entirely different from that of more proximally moving mitochondria. Alternatively, they might be remodeled by fusions with axonal mitochondria into differently looking mitochondria, or “larger” resident mitochondria from the stem axon could progressively join the retrograde stream in significant amounts over time. This would make an argument of a contiguous “baseline stream” of retrogradely moving organelles that are targeted, e.g., for unselective ‘bulk’ autophagy. Alternatively, some of the mitochondria undergoing long-range transport might be part of a retrograde signal about the distal synaptic pool towards the soma (Rishal & Fainzilber, 2014), or they might return to the soma for a “health upgrade” to receive new structural proteins, RNAs, etc., to bring back to the periphery. Regardless of this “baseline stream’s” specific purpose, it seems reasonable to consider that neurons employ multiple quality control mechanisms. For example, the peripheral quality control mechanism at the distal nodes of Ranvier would augment such “baseline” systems, as it is more attuned to neuronal geometry and acute changes in mitochondrial health. Employing such a combination of multiple quality control mechanisms might be a backup mechanism for overcoming acute distress, aging, or disruption in certain pathways. For example, the fact that mitophagy adaptors could potentially rescue each other (Lazarou et al., 2015) would explain why defects in mitostasis typically only manifest as slowly progressive problems.

Distal mitochondrial degradation systems might indeed serve as a “first line of defense” and prevent extremely damaged organelles from spreading throughout the axon and into the soma, thus protecting the genome from excessive oxidative damage. The failure of optineurin could indeed result in the “spreading” of hazardous organelles towards the soma, which could manifest as a disease. To summarize, the scale of this distal mitochondrial degradative system might reflect these regions’ high vulnerability to motor neuron diseases. With an overabundance of stress—disease, age, disruption of relevant pathways such as optineurin—those compartments might be the first to be “overwhelmed” with local turnover. In motor neurons, the distal degradative mechanism employs optineurin (**Figure 3.31**) but not PINK1 and parkin (**Figure 3.29**), which is paralleled by ALS being caused by human optineurin mutations (Cirulli et al., 2015; Maruyama et al., 2010), unlike Parkinson’s disease, which is rather associated with PINK1 and parkin (Pickrell & Youle, 2015). Peripheral systems of mitostasis could, therefore, potentially explain several features of mitochondria-associated neurodegeneration: cell-type specificity, compartment-specificity (‘dying-back’ pattern), and slow progression.

4.6. Mitochondrial diversity and neuronal compartmentalization

Initially, the life cycle of mitochondria was imagined as a singular cycle encompassing all mitochondria equally (Benador et al., 2019), however, work on mitochondrial heterogeneity has increasingly added to the emerging principle that many cells, especially polarized and extended ones such as neurons, employ highly compartmentalized and specialized cell biological machinery to maintain their mitochondria. Specifically, neurons control mitochondrial shapes, functions, dynamics, and turnover precisely to fit the individual needs of a cell type or neuronal subcompartment.

Axonal and synaptic mitochondria are stick-shaped and do not form extensive networks (**Figure 3.7**), suggesting that they fuse little with each other. Indeed, the fact that the photoconversion experiments successfully labeled subpopulations of synaptic mitochondria without dissipating immediately as would happen in cultured cells argues for the existence of stably distinct organelles in the synapse rather than a mitochondrial network with regular fusion-fission. In a similar experiment in motor neuron somata, the photoconverted color also remained relatively stable, although it began to diffuse slightly within a few hours (Magrane et al., 2012). It seems rather puzzling that neurons have high fusion-fission rates, given that defects in mitochondrial fusion and fission proteins are associated with neurodegenerative diseases: for example, Drp1 mutations are lethal with severe neurodevelopmental defects (Kageyama et al., 2012; Waterham et al., 2007; Zhang et al., 2012) and OPA1 and MFN2 mutations have severe neurodegenerative phenotypes (Itoh et al., 2013). Potentially, these proteins serve other important functions

(mitochondrial size has been suggested to be important for the Ca^{2+} handling properties of synaptic mitochondria; Lewis et al., 2018). However, restriction of mitochondrial fusion might be necessary in motor neurons to uphold the specification of neuronal mitochondria into metabolically distinct subpopulations. This would indeed require that mitochondria do not randomly intermix their matrix contents. In other cell types, selective mitochondrial fusions (via limiting their motility) indeed result in functional compartmentalization within the cells (Benador et al., 2019; Twig et al., 2008), and disruption of fusion enhances mitochondrial heterogeneity in cells (Chen et al., 2005). Likely, neurons actively restrict fusion-fission only to the mitochondria that actually need them (for example, anterogradely moving mitochondria), and it might be the first step in allowing neurons to establish mitochondrial intracellular heterogeneity. How neurons do that and what decides which mitochondria are allowed to fuse and which are not, remains to be addressed in the future.

Similarly, targeted mitochondrial transport or controlled local biogenesis are likely key to establishing compartmentalized mitochondrial diversity. As discussed earlier, an attractive model would be that anterogradely moving mitochondria are “basic” mitochondrial delivery packages that are further specialized by local control of mitochondrial transcripts and their transport to specific neuronal sites (Hees & Harbauer, 2022). However, the results from this work also leave open the possibility that anterogradely moving mitochondria have “special” properties that target them to synapses. The results from the pulse-chase experiments in this thesis argue that both anterograde transport and local biogenesis are crucial for establishing heterogeneous mitochondrial pools. Exploring mitochondrial targeting mechanisms in the future will yield important insights into how mitochondrial diversity is established in the nervous system.

Last, but not least, the work in this thesis and others (Evans & Holzbaur, 2019b) show that autophagy is not equally distributed throughout the neuron but concentrated at specific sites. Instead of being delivered to the soma, most mitochondria were locally degraded in terminal synapses in mouse motor axons by a distal optineurin-mediated mechanism, which seemed to be an important protective mechanism for establishing homeostasis in motor disease settings. However, the study leaves it open to understand the purpose of other mitophagy pathways that might act in parallel. For example, the PINK1/parkin pathway did seem to have an effect on motor neurons (**Section 3.4.8**), albeit not on degradation of damaged synaptic mitochondria. Perhaps there are also other pathways with the purpose of establishing mitochondrial functional specification at certain sites by selectively degrading specific mitochondrial proteins in a local manner. Future work will have to address the potential role of other degradation pathways in motor neurons.

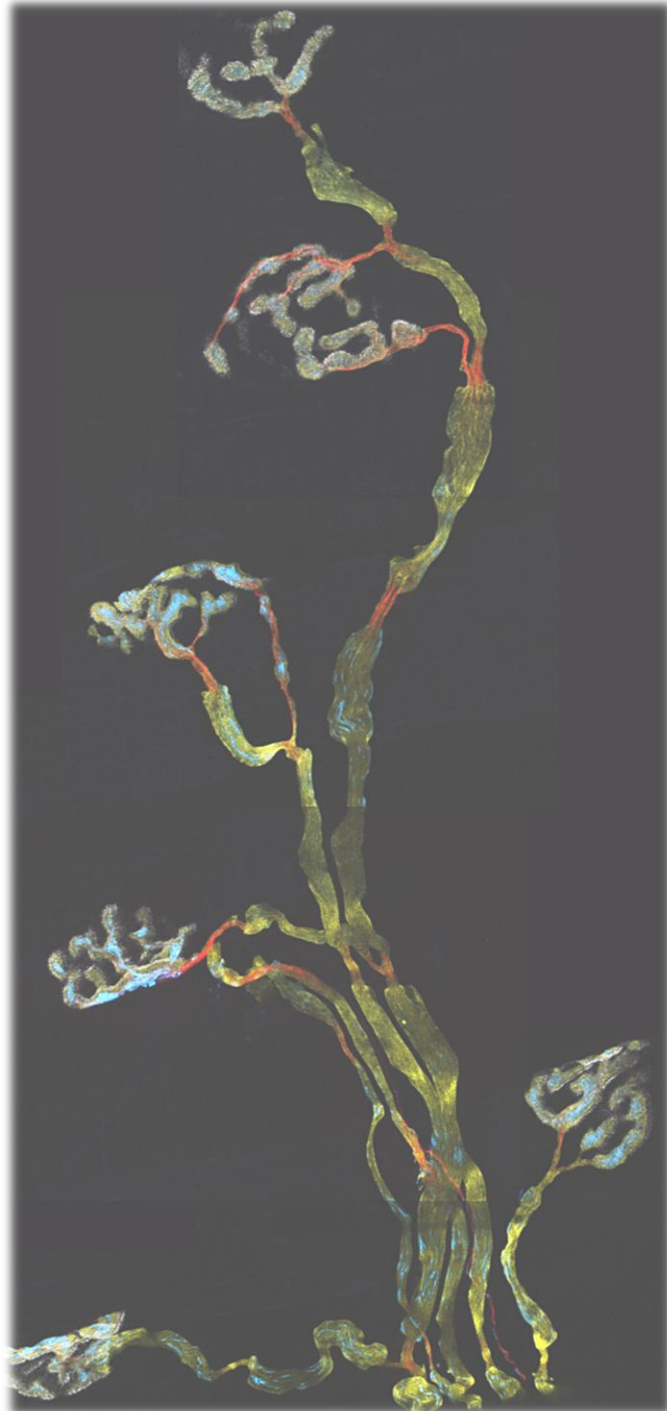
To summarize, the work in this thesis exemplifies the vital role of site-specific molecular pathways for organelle homeostasis in highly compartmentalized cells such as neurons. The fact

that neurons establish semi-autonomous processes on a local level while still coordinating them on a global level suggests that neurons have extensive retrograde communication signaling between synapses and the soma, which remains poorly understood for mitochondria (Cardanho-Ramos & Morais, 2021). Further work will hopefully address this topic further and dissect the role of regional mitostasis pathways in selective vulnerability during neurodegenerative diseases.

4.7. Future directions

Mitochondria are fascinating organelles that are essential to all living organisms. Aging progressively deteriorates an organism's physiological state and is a natural process that cannot be stopped. Behind the macroscopic presentation of aging lie very complex cell biological processes, all of which have been linked to mitochondrial biology so far (Lopez-Otin et al., 2023). Many pathological cellular processes found in neurodegenerative disease are also common hallmarks of aging, only that in a disease setting, this “aging” occurs at an accelerated pace in selective cell types due to specific intrinsic or extrinsic stressors for those cells (Saxena & Caroni, 2011). For example, the mitochondrial quality control mechanism discovered in this work for distal murine motor axons is indeed highly active in aged mice (**Figure 3.22**), whereas in models of motor neuron disease, increased mitochondrial capture already occurs at younger ages than normal (**Figure 3.21**). Naturally, aging-associated diseases are difficult to understand due to their multifactorial nature, making them difficult to treat.

One of the most effective ingredients for delaying aging is caloric restriction, which is thought to restrict the generation of reactive oxygen species in mitochondria due to lower rates of oxidative phosphorylation (Flanagan et al., 2020). “Boosting” mitochondrial health has therefore become a popular field of study, making mitochondrial science a highly disease-relevant section of cell biology (Andreux et al., 2013; Monzel et al., 2023; O'Brien & Tian, 2021). However, our understanding of what mitochondrial “function” constitutes versus mitochondrial “dysfunction” is still rudimentary, and some authors still have reservations about whether this approach will be misleading unless it captures the actual *in vivo* complexity and diversity of mitochondrial biology—calling for more research that is focused on understanding the cell-type and compartment specificity of mitochondrial homeostasis mechanisms, especially in neuroscience (Misgeld & Schwarz, 2017; Monzel et al., 2023; Nikolettou & Tavernarakis, 2018). This approach will likely not only have to include mitochondria but also other pieces that are part of neurodegenerative disease, such as synaptic excitotoxicity, defects in neuronal calcium handling, axonal translation, microtubules, the ER, and many more (Saxena & Caroni, 2011).



5. Danksagung

Diese Doktorarbeit wäre ohne die Hilfe und Unterstützung mehrerer Personen nicht möglich gewesen. Mein erster Dank geht an meinen Doktorvater Thomas Misgeld für seine Betreuung und Lehre, für seinen kreativen Input, sowie für die beständige und optimistische Unterstützung insbesondere in stressigen Zeiten. Ich bin sehr dankbar, dass ich diese prägende Zeit unter seiner Anleitung verbringen konnte. Desweiteren möchte ich meinen Kollegen am Lehrstuhl danken, insbesondere Tatjana, Martina, Lorena und Polina für die konstruktive Zusammenarbeit und Begeisterung an den hier vorgestellten Projekten, sowie für Hilfe und/oder Rat. Ich danke Monika Brill-Leischner, von der ich viele meiner Fähigkeiten gelernt habe, für ihre Unterstützung, sowie Angelika Harbauer und Christian Behrends für ihren Rat in meinem TAC-Komitee und außerhalb. Ich möchte mich außerdem bei Dr. Kristine Kellermann, Manuela, Nebi, Daniela und Matea herzlich für die Hilfe bei der Tierversorgung, sowie Kristina, Yvonne und Moni S. für die technische und administrative Unterstützung bedanken. Die hier vorgestellten Projekte wurden von auch von unseren Studenten technisch unterstützt: vielen Dank Anna, Ela, Elizabeth, Jan-Niklas, Noah, Oliver, Philip und Theo! Eine Doktorarbeit ist wie ein Marathon und ich möchte mich deshalb auch bei meinen Freunden, insbesondere bei Willi, Melinda, Sarah, Eva und Fabi bedanken, die mir während dieser Zeit den Rücken gestärkt haben. Mein größter und ganz besonderer Dank geht an meine Eltern Lucyna und Vassilios, die meine Ausbildung mit aller Kraft unterstützt haben und mir immer zur Seite standen. Die Wissenschaft ist ein gemeinsames Unterfangen und ohne diese Unterstützung wäre ich nicht so weit gekommen, vielen Dank an alle und all diejenigen, die ich hier nicht explizit genannt habe.

6. References

- Abeliovich, A., & Gitler, A. D. (2016). Defects in trafficking bridge Parkinson's disease pathology and genetics. *Nature*, 539(7628), 207-216. <https://doi.org/10.1038/nature20414>
- Adalbert, R., & Coleman, M. P. (2013). Review: Axon pathology in age-related neurodegenerative disorders. *Neuropathol Appl Neurobiol*, 39(2), 90-108. <https://doi.org/10.1111/j.1365-2990.2012.01308.x>
- Agarwal, A., Wu, P. H., Hughes, E. G., Fukaya, M., Tischfield, M. A., Langseth, A. J., Wirtz, D., & Bergles, D. E. (2017). Transient Opening of the Mitochondrial Permeability Transition Pore Induces Microdomain Calcium Transients in Astrocyte Processes. *Neuron*, 93(3), 587-605 e587. <https://doi.org/10.1016/j.neuron.2016.12.034>
- Ahmad, T., Aggarwal, K., Pattnaik, B., Mukherjee, S., Sethi, T., Tiwari, B. K., Kumar, M., Micheal, A., Mabalirajan, U., Ghosh, B., Sinha Roy, S., & Agrawal, A. (2013). Computational classification of mitochondrial shapes reflects stress and redox state. *Cell Death Dis*, 4(1), e461. <https://doi.org/10.1038/cddis.2012.213>
- Alhindi, A., Boehm, I., & Chaytow, H. (2021). Small junction, big problems: Neuromuscular junction pathology in mouse models of amyotrophic lateral sclerosis (ALS). *J Anat*. <https://doi.org/10.1111/joa.13463>
- Allen, J. F. (2015). Why chloroplasts and mitochondria retain their own genomes and genetic systems: Colocation for redox regulation of gene expression. *Proc Natl Acad Sci U S A*, 112(33), 10231-10238. <https://doi.org/10.1073/pnas.1500012112>
- Allen, R. D., Metzuzals, J., Tasaki, I., Brady, S. T., & Gilbert, S. P. (1982). Fast axonal transport in squid giant axon. *Science*, 218(4577), 1127-1129. <https://www.ncbi.nlm.nih.gov/pubmed/6183744>
- Altmann, R. (1890). *Die Elementarorganismen und ihre Beziehungen zu den Zellen*. Veit.
- Amiri, M., & Hollenbeck, P. J. (2008). Mitochondrial biogenesis in the axons of vertebrate peripheral neurons. *Dev Neurobiol*, 68(11), 1348-1361. <https://doi.org/10.1002/dneu.20668>
- Andreux, P. A., Houtkooper, R. H., & Auwerx, J. (2013). Pharmacological approaches to restore mitochondrial function. *Nat Rev Drug Discov*, 12(6), 465-483. <https://doi.org/10.1038/nrd4023>
- Aschrafi, A., Kar, A. N., Gale, J. R., Elkahloun, A. G., Vargas, J. N., Sales, N., Wilson, G., Tompkins, M., Gioio, A. E., & Kaplan, B. B. (2016). A heterogeneous population of nuclear-encoded mitochondrial mRNAs is present in the axons of primary sympathetic neurons. *Mitochondrion*, 30, 18-23. <https://doi.org/10.1016/j.mito.2016.06.002>
- Ashford, T. P., & Porter, K. R. (1962). Cytoplasmic components in hepatic cell lysosomes. *J Cell Biol*, 12, 198-202. <https://www.ncbi.nlm.nih.gov/pubmed/13862833>
<http://jcb.rupress.org/content/jcb/12/1/198.full.pdf>
- Ashrafi, G., Schlehe, J. S., LaVoie, M. J., & Schwarz, T. L. (2014). Mitophagy of damaged mitochondria occurs locally in distal neuronal axons and requires PINK1 and Parkin. *J Cell Biol*, 206(5), 655-670. <https://doi.org/10.1083/jcb.201401070>
- Ashrafi, G., & Schwarz, T. L. (2013). The pathways of mitophagy for quality control and clearance of mitochondria. *Cell Death Differ*, 20(1), 31-42. <https://doi.org/10.1038/cdd.2012.81>
- Attwell, D., & Gibb, A. (2005). Neuroenergetics and the kinetic design of excitatory synapses. *Nat Rev Neurosci*, 6(11), 841-849. <https://doi.org/10.1038/nrn1784>

- Attwell, D., & Laughlin, S. B. (2001). An energy budget for signaling in the grey matter of the brain. *J Cereb Blood Flow Metab*, 21(10), 1133-1145. <https://doi.org/10.1097/00004647-200110000-00001>
- Augenbraun, E., Maxfield, F. R., St Jules, R., Setlik, W., & Holtzman, E. (1993). Properties of acidified compartments in hippocampal neurons. *Eur J Cell Biol*, 61(1), 34-43. <https://www.ncbi.nlm.nih.gov/pubmed/8223706>
- Baas, P. W., & Ahmad, F. J. (2013). Beyond taxol: microtubule-based treatment of disease and injury of the nervous system. *Brain*, 136(Pt 10), 2937-2951. <https://doi.org/10.1093/brain/awt153>
- Baas, P. W., Rao, A. N., Matamoros, A. J., & Leo, L. (2016). Stability properties of neuronal microtubules. *Cytoskeleton (Hoboken)*, 73(9), 442-460. <https://doi.org/10.1002/cm.21286>
- Bakalkin, G. Y., Kalnov, S. L., Galkin, A. V., Zubatov, A. S., & Luzikov, V. N. (1978). The lability of the products of mitochondrial protein synthesis in *Saccharomyces cerevisiae*. A novel method for protein half-life determination. *Biochem J*, 170(3), 569-576. <https://doi.org/10.1042/bj1700569>
- Baker, M. J., Frazier, A. E., Gulbis, J. M., & Ryan, M. T. (2007). Mitochondrial protein-import machinery: correlating structure with function. *Trends Cell Biol*, 17(9), 456-464. <https://doi.org/10.1016/j.tcb.2007.07.010>
- Balaban, R. S., Nemoto, S., & Finkel, T. (2005). Mitochondria, oxidants, and aging. *Cell*, 120(4), 483-495. <https://doi.org/10.1016/j.cell.2005.02.001>
- Balint, S., Verdeny Vilanova, I., Sandoval Alvarez, A., & Lakadamyali, M. (2013). Correlative live-cell and superresolution microscopy reveals cargo transport dynamics at microtubule intersections. *Proc Natl Acad Sci U S A*, 110(9), 3375-3380. <https://doi.org/10.1073/pnas.1219206110>
- Baloh, R. H., Schmidt, R. E., Pestronk, A., & Milbrandt, J. (2007). Altered axonal mitochondrial transport in the pathogenesis of Charcot-Marie-Tooth disease from mitofusin 2 mutations. *J Neurosci*, 27(2), 422-430. <https://doi.org/10.1523/JNEUROSCI.4798-06.2007>
- Battino, M., Bertoli, E., Formiggini, G., Sassi, S., Gorini, A., Villa, R. F., & Lenaz, G. (1991). Structural and functional aspects of the respiratory chain of synaptic and nonsynaptic mitochondria derived from selected brain regions. *J Bioenerg Biomembr*, 23(2), 345-363. <https://doi.org/10.1007/BF00762227>
- Benador, I. Y., Veliova, M., Liesa, M., & Shirihai, O. S. (2019). Mitochondria Bound to Lipid Droplets: Where Mitochondrial Dynamics Regulate Lipid Storage and Utilization. *Cell Metab*, 29(4), 827-835. <https://doi.org/10.1016/j.cmet.2019.02.011>
- Benard, G., Bellance, N., James, D., Parrone, P., Fernandez, H., Letellier, T., & Rossignol, R. (2007). Mitochondrial bioenergetics and structural network organization. *J Cell Sci*, 120(Pt 5), 838-848. <https://doi.org/10.1242/jcs.03381>
- Benda, C. (1898). Ueber die Spermatogenese der Vertebraten und höherer Evertebraten, II. Theil: Die Histiogenese der Spermien. *Archiv für Anatomie und Physiologie*, 73, 393-398.
- Besse, A., Wu, P., Bruni, F., Donti, T., Graham, B. H., Craigen, W. J., McFarland, R., Moretti, P., Lalani, S., Scott, K. L., Taylor, R. W., & Bonnen, P. E. (2015). The GABA transaminase, ABAT, is essential for mitochondrial nucleoside metabolism. *Cell Metab*, 21(3), 417-427. <https://doi.org/10.1016/j.cmet.2015.02.008>
- Bianchi, L. (2018). *Developmental neurobiology*. Garland Science, Taylor & Francis Group, LLC.
- Billups, B., & Forsythe, I. D. (2002). Presynaptic mitochondrial calcium sequestration influences transmission at mammalian central synapses. *J Neurosci*, 22(14), 5840-5847. <https://doi.org/10.1523/JNEUROSCI.22-14-05840.2002>

- Bingham, D., Jakobs, C. E., Wernert, F., Boroni-Rueda, F., Jullien, N., Schentarra, E. M., Friedl, K., Da Costa Moura, J., van Bommel, D. M., Caillol, G., Ogawa, Y., Papandreou, M. J., & Leterrier, C. (2023). Presynapses contain distinct actin nanostructures. *J Cell Biol*, 222(10). <https://doi.org/10.1083/jcb.202208110>
- Bishop, D., Nikic, I., Brinkoetter, M., Knecht, S., Potz, S., Kerschensteiner, M., & Misgeld, T. (2011). Near-infrared branding efficiently correlates light and electron microscopy. *Nat Methods*, 8(7), 568-570. <https://doi.org/10.1038/nmeth.1622>
- Bishop, D. L., Misgeld, T., Walsh, M. K., Gan, W. B., & Lichtman, J. W. (2004). Axon branch removal at developing synapses by axosome shedding. *Neuron*, 44(4), 651-661. <https://doi.org/10.1016/j.neuron.2004.10.026>
- Bjorkholm, P., Ernst, A. M., Hagstrom, E., & Andersson, S. G. (2017). Why mitochondria need a genome revisited. *FEBS Lett*, 591(1), 65-75. <https://doi.org/10.1002/1873-3468.12510>
- Boillee, S., Vande Velde, C., & Cleveland, D. W. (2006). ALS: a disease of motor neurons and their nonneuronal neighbors. *Neuron*, 52(1), 39-59. <https://doi.org/10.1016/j.neuron.2006.09.018>
- Bolam, J. P., & Pissadaki, E. K. (2012). Living on the edge with too many mouths to feed: why dopamine neurons die. *Mov Disord*, 27(12), 1478-1483. <https://doi.org/10.1002/mds.25135>
- Bomba-Warczak, E., Edassery, S. L., Hark, T. J., & Savas, J. N. (2021). Long-lived mitochondrial cristae proteins in mouse heart and brain. *J Cell Biol*, 220(9). <https://doi.org/10.1083/jcb.202005193>
- Bonekamp, N. A., & Larsson, N. G. (2018). SnapShot: Mitochondrial Nucleoid. *Cell*, 172(1-2), 388-388 e381. <https://doi.org/10.1016/j.cell.2017.12.039>
- Braak, H., & Del Tredici, K. (2009). Neuroanatomy and pathology of sporadic Parkinson's disease. *Adv Anat Embryol Cell Biol*, 201, 1-119. <https://www.ncbi.nlm.nih.gov/pubmed/19230552>
- Brady, S. T., Lasek, R. J., & Allen, R. D. (1982). Fast axonal transport in extruded axoplasm from squid giant axon. *Science*, 218(4577), 1129-1131. <https://www.ncbi.nlm.nih.gov/pubmed/6183745>
- Brawek, B., Loffler, M., Wagner, K., Huppertz, H. J., Wendling, A. S., Weyerbrock, A., Jackisch, R., & Feuerstein, T. J. (2010). Reactive oxygen species (ROS) in the human neocortex: role of aging and cognition. *Brain Res Bull*, 81(4-5), 484-490. <https://doi.org/10.1016/j.brainresbull.2009.10.011>
- Breckwoltd, M. O., Pfister, F. M., Bradley, P. M., Marinkovic, P., Williams, P. R., Brill, M. S., Plomer, B., Schmalz, A., St Clair, D. K., Naumann, R., Griesbeck, O., Schwarzlander, M., Godinho, L., Bareyre, F. M., Dick, T. P., Kerschensteiner, M., & Misgeld, T. (2014). Multiparametric optical analysis of mitochondrial redox signals during neuronal physiology and pathology in vivo. *Nat Med*, 20(5), 555-560. <https://doi.org/10.1038/nm.3520>
- Brickley, K., & Stephenson, F. A. (2011). Trafficking kinesin protein (TRAK)-mediated transport of mitochondria in axons of hippocampal neurons. *J Biol Chem*, 286(20), 18079-18092. <https://doi.org/10.1074/jbc.M111.236018>
- Briese, M., Saal, L., Appenzeller, S., Moradi, M., Baluapuri, A., & Sendtner, M. (2016). Whole transcriptome profiling reveals the RNA content of motor axons. *Nucleic Acids Res*, 44(4), e33. <https://doi.org/10.1093/nar/gkv1027>
- Brill, M. S., Kleele, T., Ruschkies, L., Wang, M., Marahori, N. A., Reuter, M. S., Hausrat, T. J., Weigand, E., Fisher, M., Ahles, A., Engelhardt, S., Bishop, D. L., Kneussel, M., & Misgeld, T. (2016). Branch-Specific Microtubule Destabilization Mediates Axon Branch Loss during Neuromuscular Synapse Elimination. *Neuron*. <https://doi.org/10.1016/j.neuron.2016.09.049>

- Brill, M. S., Marinkovic, P., & Misgeld, T. (2013). Sequential photo-bleaching to delineate single Schwann cells at the neuromuscular junction. *J Vis Exp*(71), e4460. <https://doi.org/10.3791/4460>
- Briones, T. L., Suh, E., Jozsa, L., Rogozinska, M., Woods, J., & Wadowska, M. (2005). Changes in number of synapses and mitochondria in presynaptic terminals in the dentate gyrus following cerebral ischemia and rehabilitation training. *Brain Res*, 1033(1), 51-57. <https://doi.org/10.1016/j.brainres.2004.11.017>
- Brown, M. R., Sullivan, P. G., & Geddes, J. W. (2006). Synaptic mitochondria are more susceptible to Ca²⁺ overload than nonsynaptic mitochondria. *J Biol Chem*, 281(17), 11658-11668. <https://doi.org/10.1074/jbc.M510303200>
- Bruijn, L. I., Miller, T. M., & Cleveland, D. W. (2004). Unraveling the mechanisms involved in motor neuron degeneration in ALS. *Annu Rev Neurosci*, 27, 723-749. <https://doi.org/10.1146/annurev.neuro.27.070203.144244>
- Bulthuis, E. P., Adjobo-Hermans, M. J. W., Willems, P., & Koopman, W. J. H. (2019). Mitochondrial Morphofunction in Mammalian Cells. *Antioxid Redox Signal*, 30(18), 2066-2109. <https://doi.org/10.1089/ars.2018.7534>
- Burdett, T. C., & Freeman, M. R. (2014). Neuroscience. Astrocytes eyeball axonal mitochondria. *Science*, 345(6195), 385-386. <https://doi.org/10.1126/science.1258295>
- Burman, J. L., Pickles, S., Wang, C., Sekine, S., Vargas, J. N. S., Zhang, Z., Youle, A. M., Nezich, C. L., Wu, X., Hammer, J. A., & Youle, R. J. (2017). Mitochondrial fission facilitates the selective mitophagy of protein aggregates. *J Cell Biol*, 216(10), 3231-3247. <https://doi.org/10.1083/jcb.201612106>
- Busch, K. B., Bereiter-Hahn, J., Wittig, I., Schagger, H., & Jendrach, M. (2006). Mitochondrial dynamics generate equal distribution but patchwork localization of respiratory Complex I. *Mol Membr Biol*, 23(6), 509-520. <https://doi.org/10.1080/09687860600877292>
- Cai, Q., Lu, L., Tian, J. H., Zhu, Y. B., Qiao, H., & Sheng, Z. H. (2010). Snapin-regulated late endosomal transport is critical for efficient autophagy-lysosomal function in neurons. *Neuron*, 68(1), 73-86. <https://doi.org/10.1016/j.neuron.2010.09.022>
- Cai, Q., Zakaria, H. M., Simone, A., & Sheng, Z. H. (2012). Spatial parkin translocation and degradation of damaged mitochondria via mitophagy in live cortical neurons. *Curr Biol*, 22(6), 545-552. <https://doi.org/10.1016/j.cub.2012.02.005>
- Cao, Y., Xu, C., Ye, J., He, Q., Zhang, X., Jia, S., Qiao, X., Zhang, C., Liu, R., Weng, L., Liu, Y., Liu, L., & Zheng, M. (2019). Miro2 Regulates Inter-Mitochondrial Communication in the Heart and Protects Against TAC-Induced Cardiac Dysfunction. *Circ Res*, 125(8), 728-743. <https://doi.org/10.1161/CIRCRESAHA.119.315432>
- Cao, Y. L., Meng, S., Chen, Y., Feng, J. X., Gu, D. D., Yu, B., Li, Y. J., Yang, J. Y., Liao, S., Chan, D. C., & Gao, S. (2017). MFN1 structures reveal nucleotide-triggered dimerization critical for mitochondrial fusion. *Nature*, 542(7641), 372-376. <https://doi.org/10.1038/nature21077>
- Cappello, V., & Francolini, M. (2017). Neuromuscular Junction Dismantling in Amyotrophic Lateral Sclerosis. *Int J Mol Sci*, 18(10). <https://doi.org/10.3390/ijms18102092>
- Cardanho-Ramos, C., & Morais, V. A. (2021). Mitochondrial Biogenesis in Neurons: How and Where. *Int J Mol Sci*, 22(23). <https://doi.org/10.3390/ijms222313059>
- Cardona, A., Saalfeld, S., Schindelin, J., Arganda-Carreras, I., Preibisch, S., Longair, M., Tomancak, P., Hartenstein, V., & Douglas, R. J. (2012). TrakEM2 software for neural circuit reconstruction. *PLoS One*, 7(6), e38011. <https://doi.org/10.1371/journal.pone.0038011>
- Carnio, S., LoVerso, F., Baraibar, M. A., Longa, E., Khan, M. M., Maffei, M., Reischl, M., Canepari, M., Loeffler, S., Kern, H., Blaauw, B., Friguet, B., Bottinelli, R., Rudolf, R., & Sandri, M. (2014).

- Autophagy impairment in muscle induces neuromuscular junction degeneration and precocious aging. *Cell Rep*, 8(5), 1509-1521. <https://doi.org/10.1016/j.celrep.2014.07.061>
- Cavalcanti-de-Albuquerque, J. P., de-Souza-Ferreira, E., de Carvalho, D. P., & Galina, A. (2022). Coupling of GABA Metabolism to Mitochondrial Glucose Phosphorylation. *Neurochem Res*, 47(2), 470-480. <https://doi.org/10.1007/s11064-021-03463-2>
- Chada, S. R., & Hollenbeck, P. J. (2004). Nerve growth factor signaling regulates motility and docking of axonal mitochondria. *Curr Biol*, 14(14), 1272-1276. <https://doi.org/10.1016/j.cub.2004.07.027>
- Chalfie, M., Tu, Y., Euskirchen, G., Ward, W. W., & Prasher, D. C. (1994). Green fluorescent protein as a marker for gene expression. *Science*, 263(5148), 802-805. <https://doi.org/10.1126/science.8303295>
- Chalmers, S., Caldwell, S. T., Quin, C., Prime, T. A., James, A. M., Cairns, A. G., Murphy, M. P., McCarron, J. G., & Hartley, R. C. (2012). Selective uncoupling of individual mitochondria within a cell using a mitochondria-targeted photoactivated protonophore. *J Am Chem Soc*, 134(2), 758-761. <https://doi.org/10.1021/ja2077922>
- Chan, D. C. (2020). Mitochondrial Dynamics and Its Involvement in Disease. *Annu Rev Pathol*, 15, 235-259. <https://doi.org/10.1146/annurev-pathmechdis-012419-032711>
- Chan, N. C., Salazar, A. M., Pham, A. H., Sweredoski, M. J., Kolawa, N. J., Graham, R. L., Hess, S., & Chan, D. C. (2011). Broad activation of the ubiquitin-proteasome system by Parkin is critical for mitophagy. *Hum Mol Genet*, 20(9), 1726-1737. <https://doi.org/10.1093/hmg/ddr048>
- Chang, D. T., & Reynolds, I. J. (2006). Mitochondrial trafficking and morphology in healthy and injured neurons. *Prog Neurobiol*, 80(5), 241-268. <https://doi.org/10.1016/j.pneurobio.2006.09.003>
- Chavan, V., Willis, J., Walker, S. K., Clark, H. R., Liu, X., Fox, M. A., Srivastava, S., & Mukherjee, K. (2015). Central presynaptic terminals are enriched in ATP but the majority lack mitochondria. *PLoS One*, 10(4), e0125185. <https://doi.org/10.1371/journal.pone.0125185>
- Chen, H., Chomyn, A., & Chan, D. C. (2005). Disruption of fusion results in mitochondrial heterogeneity and dysfunction. *J Biol Chem*, 280(28), 26185-26192. <https://doi.org/10.1074/jbc.M503062200>
- Chen, H., Detmer, S. A., Ewald, A. J., Griffin, E. E., Fraser, S. E., & Chan, D. C. (2003). Mitofusins Mfn1 and Mfn2 coordinately regulate mitochondrial fusion and are essential for embryonic development. *J Cell Biol*, 160(2), 189-200. <https://doi.org/10.1083/jcb.200211046>
- Chen, H., Vermulst, M., Wang, Y. E., Chomyn, A., Prolla, T. A., McCaffery, J. M., & Chan, D. C. (2010). Mitochondrial fusion is required for mtDNA stability in skeletal muscle and tolerance of mtDNA mutations. *Cell*, 141(2), 280-289. <https://doi.org/10.1016/j.cell.2010.02.026>
- Chen, J., & Herrup, K. (2008). Selective vulnerability of neurons in primary cultures and in neurodegenerative diseases. *Rev Neurosci*, 19(4-5), 317-326. <https://doi.org/10.1515/revneuro.2008.19.4-5.317>
- Chen, M., Li, Y., Yang, M., Chen, X., Chen, Y., Yang, F., Lu, S., Yao, S., Zhou, T., Liu, J., Zhu, L., Du, S., & Wu, J. Y. (2016). A new method for quantifying mitochondrial axonal transport. *Protein Cell*, 7(11), 804-819. <https://doi.org/10.1007/s13238-016-0268-3>
- Chen, Y., & Dorn, G. W., 2nd. (2013). PINK1-phosphorylated mitofusin 2 is a Parkin receptor for culling damaged mitochondria. *Science*, 340(6131), 471-475. <https://doi.org/10.1126/science.1231031>
- Chen, Y., & Sheng, Z. H. (2013). Kinesin-1-syntrophin coupling mediates activity-dependent regulation of axonal mitochondrial transport. *J Cell Biol*, 202(2), 351-364. <https://doi.org/10.1083/jcb.201302040>

- Cheng, A., Wan, R., Yang, J. L., Kamimura, N., Son, T. G., Ouyang, X., Luo, Y., Okun, E., & Mattson, M. P. (2012). Involvement of PGC-1alpha in the formation and maintenance of neuronal dendritic spines. *Nat Commun*, *3*, 1250. <https://doi.org/10.1038/ncomms2238>
- Cheng, X. T., Xie, Y. X., Zhou, B., Huang, N., Farfel-Becker, T., & Sheng, Z. H. (2018). Characterization of LAMP1-labeled nondegradative lysosomal and endocytic compartments in neurons. *J Cell Biol*, *217*(9), 3127-3139. <https://doi.org/10.1083/jcb.201711083>
- Chin, J. H., & Vora, N. (2014). The global burden of neurologic diseases. *Neurology*, *83*(4), 349-351. <https://doi.org/10.1212/WNL.0000000000000610>
- Chu, C. T. (2019). Mechanisms of selective autophagy and mitophagy: Implications for neurodegenerative diseases. *Neurobiol Dis*, *122*, 23-34. <https://doi.org/10.1016/j.nbd.2018.07.015>
- Chung, T., Park, J. S., Kim, S., Montes, N., Walston, J., & Hoke, A. (2017). Evidence for dying-back axonal degeneration in age-associated skeletal muscle decline. *Muscle Nerve*, *55*(6), 894-901. <https://doi.org/10.1002/mus.25267>
- Cioni, J. M., Koppers, M., & Holt, C. E. (2018). Molecular control of local translation in axon development and maintenance. *Curr Opin Neurobiol*, *51*, 86-94. <https://doi.org/10.1016/j.conb.2018.02.025>
- Cioni, J. M., Lin, J. Q., Holtermann, A. V., Koppers, M., Jakobs, M. A. H., Azizi, A., Turner-Bridger, B., Shigeoka, T., Franze, K., Harris, W. A., & Holt, C. E. (2019). Late Endosomes Act as mRNA Translation Platforms and Sustain Mitochondria in Axons. *Cell*, *176*(1-2), 56-72 e15. <https://doi.org/10.1016/j.cell.2018.11.030>
- Cipolat, S., Martins de Brito, O., Dal Zilio, B., & Scorrano, L. (2004). OPA1 requires mitofusin 1 to promote mitochondrial fusion. *Proc Natl Acad Sci U S A*, *101*(45), 15927-15932. <https://doi.org/10.1073/pnas.0407043101>
- Cirulli, E. T., Lasseigne, B. N., Petrovski, S., Sapp, P. C., Dion, P. A., Leblond, C. S., Couthouis, J., Lu, Y. F., Wang, Q., Krueger, B. J., Ren, Z., Keebler, J., Han, Y., Levy, S. E., Boone, B. E., Wimbish, J. R., Waite, L. L., Jones, A. L., Carulli, J. P., . . . Goldstein, D. B. (2015). Exome sequencing in amyotrophic lateral sclerosis identifies risk genes and pathways. *Science*, *347*(6229), 1436-1441. <https://doi.org/10.1126/science.aaa3650>
- Cogliati, S., Frezza, C., Soriano, M. E., Varanita, T., Quintana-Cabrera, R., Corrado, M., Cipolat, S., Costa, V., Casarin, A., Gomes, L. C., Perales-Clemente, E., Salviati, L., Fernandez-Silva, P., Enriquez, J. A., & Scorrano, L. (2013). Mitochondrial cristae shape determines respiratory chain supercomplexes assembly and respiratory efficiency. *Cell*, *155*(1), 160-171. <https://doi.org/10.1016/j.cell.2013.08.032>
- Cohen, B., Altman, T., Golani-Armon, A., Savulescu, A. F., Ibraheem, A., Mhlanga, M. M., Perlson, E., & Arava, Y. S. (2022). Co-transport of the nuclear-encoded Cox7c mRNA with mitochondria along axons occurs through a coding-region-dependent mechanism. *J Cell Sci*, *135*(16). <https://doi.org/10.1242/jcs.259436>
- Collins, T. J., Berridge, M. J., Lipp, P., & Bootman, M. D. (2002). Mitochondria are morphologically and functionally heterogeneous within cells. *EMBO J*, *21*(7), 1616-1627. <https://doi.org/10.1093/emboj/21.7.1616>
- Conchello, J. A., & Lichtman, J. W. (2005). Optical sectioning microscopy. *Nat Methods*, *2*(12), 920-931. <https://doi.org/10.1038/nmeth815>
- Cosker, K. E., Fenstermacher, S. J., Pazyra-Murphy, M. F., Elliott, H. L., & Segal, R. A. (2016). The RNA-binding protein SFPQ orchestrates an RNA regulon to promote axon viability. *Nat Neurosci*, *19*(5), 690-696. <https://doi.org/10.1038/nn.4280>
- Costa, V., Giacomello, M., Hudec, R., Lopreiato, R., Ermak, G., Lim, D., Malorni, W., Davies, K. J., Carafoli, E., & Scorrano, L. (2010). Mitochondrial fission and cristae disruption increase the response

- of cell models of Huntington's disease to apoptotic stimuli. *EMBO Mol Med*, 2(12), 490-503. <https://doi.org/10.1002/emmm.201000102>
- Coupe, P., Munz, M., Manjon, J. V., Ruthazer, E. S., & Collins, D. L. (2012). A CANDLE for a deeper in vivo insight. *Med Image Anal*, 16(4), 849-864. <https://doi.org/10.1016/j.media.2012.01.002>
- Courchet, J., Lewis, T. L., Jr., Lee, S., Courchet, V., Liou, D. Y., Aizawa, S., & Polleux, F. (2013). Terminal axon branching is regulated by the LKB1-NUAK1 kinase pathway via presynaptic mitochondrial capture. *Cell*, 153(7), 1510-1525. <https://doi.org/10.1016/j.cell.2013.05.021>
- Covill-Cooke, C., Howden, J. H., Birsa, N., & Kittler, J. T. (2018). Ubiquitination at the mitochondria in neuronal health and disease. *Neurochem Int*, 117, 55-64. <https://doi.org/10.1016/j.neuint.2017.07.003>
- Cowdry, E. V. (1953). Historical background of research on mitochondria. *J Histochem Cytochem*, 1(4), 183-187. <https://doi.org/10.1177/1.4.183>
- Craig, A. M., & Banker, G. (1994). Neuronal polarity. *Annu Rev Neurosci*, 17, 267-310. <https://doi.org/10.1146/annurev.ne.17.030194.001411>
- Cuzner, M. L., Davison, A. N., & Gregson, N. A. (1966). Turnover of brain mitochondrial membrane lipids. *Biochem J*, 101(3), 618-626. <https://doi.org/10.1042/bj1010618>
- Dadon-Nachum, M., Melamed, E., & Offen, D. (2011). The "dying-back" phenomenon of motor neurons in ALS. *J Mol Neurosci*, 43(3), 470-477. <https://doi.org/10.1007/s12031-010-9467-1>
- Dahlhaus, M., Li, K. W., van der Schors, R. C., Saiepour, M. H., van Nierop, P., Heimel, J. A., Hermans, J. M., Loos, M., Smit, A. B., & Levelt, C. N. (2011). The synaptic proteome during development and plasticity of the mouse visual cortex. *Mol Cell Proteomics*, 10(5), M110 005413. <https://doi.org/10.1074/mcp.M110.005413>
- Das, S., Hajnoczky, N., Antony, A. N., Csordas, G., Gaspers, L. D., Clemens, D. L., Hoek, J. B., & Hajnoczky, G. (2012). Mitochondrial morphology and dynamics in hepatocytes from normal and ethanol-fed rats. *Pflugers Arch*, 464(1), 101-109. <https://doi.org/10.1007/s00424-012-1100-4>
- Davey, G. P., Canevari, L., & Clark, J. B. (1997). Threshold effects in synaptosomal and nonsynaptic mitochondria from hippocampal CA1 and paramedian neocortex brain regions. *J Neurochem*, 69(6), 2564-2570. <https://doi.org/10.1046/j.1471-4159.1997.69062564.x>
- Davis, C. H., Kim, K. Y., Bushong, E. A., Mills, E. A., Boassa, D., Shih, T., Kinebuchi, M., Phan, S., Zhou, Y., Bihlmeyer, N. A., Nguyen, J. V., Jin, Y., Ellisman, M. H., & Marsh-Armstrong, N. (2014). Transcellular degradation of axonal mitochondria. *Proc Natl Acad Sci U S A*, 111(26), 9633-9638. <https://doi.org/10.1073/pnas.1404651111>
- de Brito, O. M., & Scorrano, L. (2008). Mitofusin 2 tethers endoplasmic reticulum to mitochondria. *Nature*, 456(7222), 605-610. <https://doi.org/10.1038/nature07534>
- De Duve, C., & Wattiaux, R. (1966). Functions of lysosomes. *Annu Rev Physiol*, 28, 435-492. <https://doi.org/10.1146/annurev.ph.28.030166.002251>
- De Vos, K. J., Grierson, A. J., Ackerley, S., & Miller, C. C. (2008). Role of axonal transport in neurodegenerative diseases. *Annu Rev Neurosci*, 31, 151-173. <https://doi.org/10.1146/annurev.neuro.31.061307.090711>
- Del Castillo, J., & Katz, B. (1954). Quantal components of the end-plate potential. *J Physiol*, 124(3), 560-573. <https://www.ncbi.nlm.nih.gov/pubmed/13175199>
- Dempsey, W. P., Georgieva, L., Helbling, P. M., Sonay, A. Y., Truong, T. V., Haffner, M., & Pantazis, P. (2015). In vivo single-cell labeling by confined primed conversion. *Nat Methods*, 12(7), 645-648. <https://doi.org/10.1038/nmeth.3405>

- Deng, Z., Purtell, K., Lachance, V., Wold, M. S., Chen, S., & Yue, Z. (2017). Autophagy Receptors and Neurodegenerative Diseases. *Trends Cell Biol*, 27(7), 491-504. <https://doi.org/10.1016/j.tcb.2017.01.001>
- Derr, N. D., Goodman, B. S., Jungmann, R., Leschziner, A. E., Shih, W. M., & Reck-Peterson, S. L. (2012). Tug-of-war in motor protein ensembles revealed with a programmable DNA origami scaffold. *Science*, 338(6107), 662-665. <https://doi.org/10.1126/science.1226734>
- Deus, C. M., Yambire, K. F., Oliveira, P. J., & Raimundo, N. (2020). Mitochondria-Lysosome Crosstalk: From Physiology to Neurodegeneration. *Trends Mol Med*, 26(1), 71-88. <https://doi.org/10.1016/j.molmed.2019.10.009>
- Devine, M. J., & Kittler, J. T. (2018). Mitochondria at the neuronal presynapse in health and disease. *Nat Rev Neurosci*, 19(2), 63-80. <https://doi.org/10.1038/nrn.2017.170>
- Devireddy, S., Liu, A., Lampe, T., & Hollenbeck, P. J. (2015). The Organization of Mitochondrial Quality Control and Life Cycle in the Nervous System In Vivo in the Absence of PINK1. *J Neurosci*, 35(25), 9391-9401. <https://doi.org/10.1523/JNEUROSCI.1198-15.2015>
- Dietrich, M. O., Liu, Z. W., & Horvath, T. L. (2013). Mitochondrial dynamics controlled by mitofusins regulate AgRP neuronal activity and diet-induced obesity. *Cell*, 155(1), 188-199. <https://doi.org/10.1016/j.cell.2013.09.004>
- Doblado, L., Lueck, C., Rey, C., Samhan-Arias, A. K., Prieto, I., Stacchiotti, A., & Monsalve, M. (2021). Mitophagy in Human Diseases. *Int J Mol Sci*, 22(8). <https://doi.org/10.3390/ijms22083903>
- Doerflinger, N. H., Macklin, W. B., & Popko, B. (2003). Inducible site-specific recombination in myelinating cells. *Genesis*, 35(1), 63-72. <https://doi.org/10.1002/gene.10154>
- Dolezal, P., Likic, V., Tachezy, J., & Lithgow, T. (2006). Evolution of the molecular machines for protein import into mitochondria. *Science*, 313(5785), 314-318. <https://doi.org/10.1126/science.1127895>
- Dorkenwald, S., Schubert, P. J., Killinger, M. F., Urban, G., Mikula, S., Svara, F., & Kornfeld, J. (2017). Automated synaptic connectivity inference for volume electron microscopy. *Nat Methods*, 14(4), 435-442. <https://doi.org/10.1038/nmeth.4206>
- Dorn, G. W., 2nd. (2019). Evolving Concepts of Mitochondrial Dynamics. *Annu Rev Physiol*, 81, 1-17. <https://doi.org/10.1146/annurev-physiol-020518-114358>
- Dorrbaum, A. R., Kochen, L., Langer, J. D., & Schuman, E. M. (2018). Local and global influences on protein turnover in neurons and glia. *Elife*, 7. <https://doi.org/10.7554/eLife.34202>
- Dutta, S., & Sengupta, P. (2016). Men and mice: Relating their ages. *Life Sci*, 152, 244-248. <https://doi.org/10.1016/j.lfs.2015.10.025>
- Duvezin-Caubet, S., Jagasia, R., Wagener, J., Hofmann, S., Trifunovic, A., Hansson, A., Chomyn, A., Bauer, M. F., Attardi, G., Larsson, N. G., Neupert, W., & Reichert, A. S. (2006). Proteolytic processing of OPA1 links mitochondrial dysfunction to alterations in mitochondrial morphology. *J Biol Chem*, 281(49), 37972-37979. <https://doi.org/10.1074/jbc.M606059200>
- Ehse, S., Raschke, I., Mancuso, G., Bernacchia, A., Geimer, S., Tondera, D., Martinou, J. C., Westermann, B., Rugarli, E. I., & Langer, T. (2009). Regulation of OPA1 processing and mitochondrial fusion by m-AAA protease isoenzymes and OMA1. *J Cell Biol*, 187(7), 1023-1036. <https://doi.org/10.1083/jcb.200906084>
- Eichel, K., & Shen, K. (2022). The function of the axon initial segment in neuronal polarity. *Dev Biol*, 489, 47-54. <https://doi.org/10.1016/j.ydbio.2022.05.016>
- Eisner, V., Picard, M., & Hajnoczky, G. (2018). Mitochondrial dynamics in adaptive and maladaptive cellular stress responses. *Nat Cell Biol*, 20(7), 755-765. <https://doi.org/10.1038/s41556-018-0133-0>

- Encalada, S. E., Szpankowski, L., Xia, C. H., & Goldstein, L. S. (2011). Stable kinesin and dynein assemblies drive the axonal transport of mammalian prion protein vesicles. *Cell*, 144(4), 551-565. <https://doi.org/10.1016/j.cell.2011.01.021>
- Evans, C. S., & Holzbaur, E. L. F. (2019a). Autophagy and mitophagy in ALS. *Neurobiol Dis*, 122, 35-40. <https://doi.org/10.1016/j.nbd.2018.07.005>
- Evans, C. S., & Holzbaur, E. L. F. (2019b). Quality Control in Neurons: Mitophagy and Other Selective Autophagy Mechanisms. *J Mol Biol*. <https://doi.org/10.1016/j.jmb.2019.06.031>
- Faelber, K., Posor, Y., Gao, S., Held, M., Roske, Y., Schulze, D., Haucke, V., Noe, F., & Daumke, O. (2011). Crystal structure of nucleotide-free dynamin. *Nature*, 477(7366), 556-560. <https://doi.org/10.1038/nature10369>
- Faitg, J., Lacefield, C., Davey, T., White, K., Laws, R., Kosmidis, S., Reeve, A. K., Kandel, E. R., Vincent, A. E., & Picard, M. (2021). 3D neuronal mitochondrial morphology in axons, dendrites, and somata of the aging mouse hippocampus. *Cell Rep*, 36(6), 109509. <https://doi.org/10.1016/j.celrep.2021.109509>
- Faits, M. C., Zhang, C., Soto, F., & Kerschensteiner, D. (2016). Dendritic mitochondria reach stable positions during circuit development. *Elife*, 5, e11583. <https://doi.org/10.7554/eLife.11583>
- Farias, G. G., Guardia, C. M., Britt, D. J., Guo, X., & Bonifacino, J. S. (2015). Sorting of Dendritic and Axonal Vesicles at the Pre-axonal Exclusion Zone. *Cell Rep*, 13(6), 1221-1232. <https://doi.org/10.1016/j.celrep.2015.09.074>
- Fecher, C., Trovo, L., Muller, S. A., Snaidero, N., Wettmarshausen, J., Heink, S., Ortiz, O., Wagner, I., Kuhn, R., Hartmann, J., Karl, R. M., Konnerth, A., Korn, T., Wurst, W., Merkler, D., Lichtenthaler, S. F., Perocchi, F., & Misgeld, T. (2019). Cell-type-specific profiling of brain mitochondria reveals functional and molecular diversity. *Nat Neurosci*, 22(10), 1731-1742. <https://doi.org/10.1038/s41593-019-0479-z>
- Felbor, U., Kessler, B., Mothes, W., Goebel, H. H., Ploegh, H. L., Bronson, R. T., & Olsen, B. R. (2002). Neuronal loss and brain atrophy in mice lacking cathepsins B and L. *Proc Natl Acad Sci U S A*, 99(12), 7883-7888. <https://doi.org/10.1073/pnas.112632299>
- Feng, G., Mellor, R. H., Bernstein, M., Keller-Peck, C., Nguyen, Q. T., Wallace, M., Nerbonne, J. M., Lichtman, J. W., & Sanes, J. R. (2000). Imaging neuronal subsets in transgenic mice expressing multiple spectral variants of GFP. *Neuron*, 28(1), 41-51. <https://www.ncbi.nlm.nih.gov/pubmed/11086982>
- Ferree, A. W., Trudeau, K., Zik, E., Benador, I. Y., Twig, G., Gottlieb, R. A., & Shirihai, O. S. (2013). MitoTimer probe reveals the impact of autophagy, fusion, and motility on subcellular distribution of young and old mitochondrial protein and on relative mitochondrial protein age. *Autophagy*, 9(11), 1887-1896. <https://doi.org/10.4161/auto.26503>
- Fischer, L. R., Culver, D. G., Tennant, P., Davis, A. A., Wang, M., Castellano-Sanchez, A., Khan, J., Polak, M. A., & Glass, J. D. (2004). Amyotrophic lateral sclerosis is a distal axonopathy: evidence in mice and man. *Exp Neurol*, 185(2), 232-240. <https://doi.org/10.1016/j.expneurol.2003.10.004>
- Fischer, L. R., & Glass, J. D. (2007). Axonal degeneration in motor neuron disease. *Neurodegener Dis*, 4(6), 431-442. <https://doi.org/10.1159/000107704>
- Flanagan, E. W., Most, J., Mey, J. T., & Redman, L. M. (2020). Calorie Restriction and Aging in Humans. *Annu Rev Nutr*, 40, 105-133. <https://doi.org/10.1146/annurev-nutr-122319-034601>
- Ford, M. G., Jenni, S., & Nunnari, J. (2011). The crystal structure of dynamin. *Nature*, 477(7366), 561-566. <https://doi.org/10.1038/nature10441>
- Ford, M. G. J., & Chappie, J. S. (2019). The structural biology of the dynamin-related proteins: New insights into a diverse, multitasking family. *Traffic*, 20(10), 717-740. <https://doi.org/10.1111/tra.12676>

- Fransson, A., Ruusala, A., & Aspenstrom, P. (2003). Atypical Rho GTPases have roles in mitochondrial homeostasis and apoptosis. *J Biol Chem*, 278(8), 6495-6502. <https://doi.org/10.1074/jbc.M208609200>
- Frey, T. G., & Mannella, C. A. (2000). The internal structure of mitochondria. *Trends Biochem Sci*, 25(7), 319-324. [https://doi.org/10.1016/s0968-0004\(00\)01609-1](https://doi.org/10.1016/s0968-0004(00)01609-1)
- Friedman, J. R., Lackner, L. L., West, M., DiBenedetto, J. R., Nunnari, J., & Voeltz, G. K. (2011). ER tubules mark sites of mitochondrial division. *Science*, 334(6054), 358-362. <https://doi.org/10.1126/science.1207385>
- Friedman, L. G., Lachenmayer, M. L., Wang, J., He, L., Poulouse, S. M., Komatsu, M., Holstein, G. R., & Yue, Z. (2012). Disrupted autophagy leads to dopaminergic axon and dendrite degeneration and promotes presynaptic accumulation of alpha-synuclein and LRRK2 in the brain. *J Neurosci*, 32(22), 7585-7593. <https://doi.org/10.1523/JNEUROSCI.5809-11.2012>
- Frohlich, C., Grabiger, S., Schwefel, D., Faelber, K., Rosenbaum, E., Mears, J., Rocks, O., & Daumke, O. (2013). Structural insights into oligomerization and mitochondrial remodelling of dynamin 1-like protein. *EMBO J*, 32(9), 1280-1292. <https://doi.org/10.1038/emboj.2013.74>
- Fu, H., Hardy, J., & Duff, K. E. (2018). Selective vulnerability in neurodegenerative diseases. *Nat Neurosci*, 21(10), 1350-1358. <https://doi.org/10.1038/s41593-018-0221-2>
- Gailer, B. (2022). *Pulse-chase imaging of neuronal mitochondria* [Technical University Munich]. Munich.
- Gainer, H., Tasaki, I., & Lasek, R. J. (1977). Evidence for the glia-neuron protein transfer hypothesis from intracellular perfusion studies of squid giant axons. *J Cell Biol*, 74(2), 524-530. <https://doi.org/10.1083/jcb.74.2.524>
- Gan, L., Cookson, M. R., Petrucelli, L., & La Spada, A. R. (2018). Converging pathways in neurodegeneration, from genetics to mechanisms. *Nat Neurosci*, 21(10), 1300-1309. <https://doi.org/10.1038/s41593-018-0237-7>
- Gao, S., & Hu, J. (2021). Mitochondrial Fusion: The Machineries In and Out. *Trends Cell Biol*, 31(1), 62-74. <https://doi.org/10.1016/j.tcb.2020.09.008>
- Garbincius, J. F., & Elrod, J. W. (2022). Mitochondrial calcium exchange in physiology and disease. *Physiol Rev*, 102(2), 893-992. <https://doi.org/10.1152/physrev.00041.2020>
- Gatti, P., Schiavon, C., Manor, U., & Germain, M. (2023). Mitochondria- and ER-associated actin are required for mitochondrial fusion. *bioRxiv*. <https://doi.org/10.1101/2023.06.13.544768>
- Gatzinsky, K. P., Persson, G. H., & Berthold, C. H. (1997). Removal of retrogradely transported material from rat lumbosacral alpha-motor axons by paranodal axon-Schwann cell networks. *Glia*, 20(2), 115-126. [https://doi.org/10.1002/\(sici\)1098-1136\(199706\)20:2<115::aid-glia3>3.0.co;2-8](https://doi.org/10.1002/(sici)1098-1136(199706)20:2<115::aid-glia3>3.0.co;2-8)
- GBD Neurology Collaborators. (2019). Global, regional, and national burden of neurological disorders, 1990-2016: a systematic analysis for the Global Burden of Disease Study 2016. *Lancet Neurol*, 18(5), 459-480. [https://doi.org/10.1016/S1474-4422\(18\)30499-X](https://doi.org/10.1016/S1474-4422(18)30499-X)
- Ge, P., Dawson, V. L., & Dawson, T. M. (2020). PINK1 and Parkin mitochondrial quality control: a source of regional vulnerability in Parkinson's disease. *Mol Neurodegener*, 15(1), 20. <https://doi.org/10.1186/s13024-020-00367-7>
- Ge, Y., Shi, X., Boopathy, S., McDonald, J., Smith, A. W., & Chao, L. H. (2020). Two forms of Opa1 cooperate to complete fusion of the mitochondrial inner-membrane. *Elife*, 9. <https://doi.org/10.7554/eLife.50973>
- Geisler, S., Holmstrom, K. M., Skujat, D., Fiesel, F. C., Rothfuss, O. C., Kahle, P. J., & Springer, W. (2010). PINK1/Parkin-mediated mitophagy is dependent on VDAC1 and p62/SQSTM1. *Nat Cell Biol*, 12(2), 119-131. <https://doi.org/10.1038/ncb2012>

- Ghosh-Choudhary, S. K., Liu, J., & Finkel, T. (2021). The role of mitochondria in cellular senescence. *FASEB J*, 35(12), e21991. <https://doi.org/10.1096/fj.202101462R>
- Gilkerson, R. W., Schon, E. A., Hernandez, E., & Davidson, M. M. (2008). Mitochondrial nucleoids maintain genetic autonomy but allow for functional complementation. *J Cell Biol*, 181(7), 1117-1128. <https://doi.org/10.1083/jcb.200712101>
- Girault, J. A., & Peles, E. (2002). Development of nodes of Ranvier. *Curr Opin Neurobiol*, 12(5), 476-485. [https://doi.org/10.1016/s0959-4388\(02\)00370-7](https://doi.org/10.1016/s0959-4388(02)00370-7)
- Glancy, B. (2020). Visualizing Mitochondrial Form and Function within the Cell. *Trends Mol Med*, 26(1), 58-70. <https://doi.org/10.1016/j.molmed.2019.09.009>
- Glancy, B., Hartnell, L. M., Malide, D., Yu, Z. X., Combs, C. A., Connelly, P. S., Subramaniam, S., & Balaban, R. S. (2015). Mitochondrial reticulum for cellular energy distribution in muscle. *Nature*, 523(7562), 617-620. <https://doi.org/10.1038/nature14614>
- Glancy, B., Kim, Y., Katti, P., & Willingham, T. B. (2020). The Functional Impact of Mitochondrial Structure Across Subcellular Scales. *Front Physiol*, 11, 541040. <https://doi.org/10.3389/fphys.2020.541040>
- Glasl, L., Kloos, K., Giesert, F., Roethig, A., Di Benedetto, B., Kuhn, R., Zhang, J., Hafen, U., Zerle, J., Hofmann, A., de Angelis, M. H., Winkhofer, K. F., Holter, S. M., Vogt Weisenhorn, D. M., & Wurst, W. (2012). Pink1-deficiency in mice impairs gait, olfaction and serotonergic innervation of the olfactory bulb. *Exp Neurol*, 235(1), 214-227. <https://doi.org/10.1016/j.expneurol.2012.01.002>
- Glater, E. E., Megeath, L. J., Stowers, R. S., & Schwarz, T. L. (2006). Axonal transport of mitochondria requires milton to recruit kinesin heavy chain and is light chain independent. *J Cell Biol*, 173(4), 545-557. <https://doi.org/10.1083/jcb.200601067>
- Golpich, M., Amini, E., Mohamed, Z., Azman Ali, R., Mohamed Ibrahim, N., & Ahmadiani, A. (2017). Mitochondrial Dysfunction and Biogenesis in Neurodegenerative diseases: Pathogenesis and Treatment. *CNS Neurosci Ther*, 23(1), 5-22. <https://doi.org/10.1111/cns.12655>
- Gomes, L. C., Di Benedetto, G., & Scorrano, L. (2011). During autophagy mitochondria elongate, are spared from degradation and sustain cell viability. *Nat Cell Biol*, 13(5), 589-598. <https://doi.org/10.1038/ncb2220>
- Graves, S. M., Xie, Z., Stout, K. A., Zampese, E., Burbulla, L. F., Shih, J. C., Kondapalli, J., Patriarchi, T., Tian, L., Brichta, L., Greengard, P., Krainc, D., Schumacker, P. T., & Surmeier, D. J. (2020). Dopamine metabolism by a monoamine oxidase mitochondrial shuttle activates the electron transport chain. *Nat Neurosci*, 23(1), 15-20. <https://doi.org/10.1038/s41593-019-0556-3>
- Griffin, J. W., & Watson, D. F. (1988). Axonal transport in neurological disease. *Ann Neurol*, 23(1), 3-13. <https://doi.org/10.1002/ana.410230103>
- Gronowicz, G., Swift, H., & Steck, T. L. (1984). Maturation of the reticulocyte in vitro. *J Cell Sci*, 71, 177-197. <https://doi.org/10.1242/jcs.71.1.177>
- Gross, N. J., Getz, G. S., & Rabinowitz, M. (1969). Apparent turnover of mitochondrial deoxyribonucleic acid and mitochondrial phospholipids in the tissues of the rat. *J Biol Chem*, 244(6), 1552-1562. <https://www.ncbi.nlm.nih.gov/pubmed/5773057>
- Guedes-Dias, P., & Holzbaur, E. L. F. (2019). Axonal transport: Driving synaptic function. *Science*, 366(6462). <https://doi.org/10.1126/science.aaw9997>
- Gumy, L. F., Yeo, G. S., Tung, Y. C., Zivraj, K. H., Willis, D., Coppola, G., Lam, B. Y., Twiss, J. L., Holt, C. E., & Fawcett, J. W. (2011). Transcriptome analysis of embryonic and adult sensory axons reveals changes in mRNA repertoire localization. *RNA*, 17(1), 85-98. <https://doi.org/10.1261/rna.2386111>

- Guo, L., Tian, J., & Du, H. (2017). Mitochondrial Dysfunction and Synaptic Transmission Failure in Alzheimer's Disease. *J Alzheimers Dis*, 57(4), 1071-1086. <https://doi.org/10.3233/JAD-160702>
- Guo, X., Macleod, G. T., Wellington, A., Hu, F., Panchumarthi, S., Schoenfield, M., Marin, L., Charlton, M. P., Atwood, H. L., & Zinsmaier, K. E. (2005). The GTPase dMiro is required for axonal transport of mitochondria to Drosophila synapses. *Neuron*, 47(3), 379-393. <https://doi.org/10.1016/j.neuron.2005.06.027>
- Gurney, M. E., Pu, H., Chiu, A. Y., Dal Canto, M. C., Polchow, C. Y., Alexander, D. D., Caliendo, J., Hentati, A., Kwon, Y. W., Deng, H. X., & et al. (1994). Motor neuron degeneration in mice that express a human Cu,Zn superoxide dismutase mutation. *Science*, 264(5166), 1772-1775. <https://doi.org/10.1126/science.8209258>
- Gurskaya, N. G., Verkhusha, V. V., Shcheglov, A. S., Staroverov, D. B., Chepurnykh, T. V., Fradkov, A. F., Lukyanov, S., & Lukyanov, K. A. (2006). Engineering of a monomeric green-to-red photoactivatable fluorescent protein induced by blue light. *Nat Biotechnol*, 24(4), 461-465. <https://doi.org/10.1038/nbt1191>
- Hafezparast, M., Klocke, R., Ruhrberg, C., Marquardt, A., Ahmad-Annur, A., Bowen, S., Lalli, G., Witherden, A. S., Hummerich, H., Nicholson, S., Morgan, P. J., Oozageer, R., Priestley, J. V., Averill, S., King, V. R., Ball, S., Peters, J., Toda, T., Yamamoto, A., . . . Fisher, E. M. (2003). Mutations in dynein link motor neuron degeneration to defects in retrograde transport. *Science*, 300(5620), 808-812. <https://doi.org/10.1126/science.1083129>
- Hagemann, C., Moreno Gonzalez, C., Guetta, L., Tyzack, G., Chiappini, C., Legati, A., Patani, R., & Serio, A. (2022). Axonal Length Determines Distinct Homeostatic Phenotypes in Human iPSC Derived Motor Neurons on a Bioengineered Platform. *Adv Healthc Mater*, 11(10), e2101817. <https://doi.org/10.1002/adhm.202101817>
- Hall, C. N., Klein-Flugge, M. C., Howarth, C., & Attwell, D. (2012). Oxidative phosphorylation, not glycolysis, powers presynaptic and postsynaptic mechanisms underlying brain information processing. *J Neurosci*, 32(26), 8940-8951. <https://doi.org/10.1523/JNEUROSCI.0026-12.2012>
- Han, S., Jeong, Y. Y., Sheshadri, P., Su, X., & Cai, Q. (2020). Mitophagy regulates integrity of mitochondria at synapses and is critical for synaptic maintenance. *EMBO Rep*, 21(9), e49801. <https://doi.org/10.15252/embr.201949801>
- Hara, T., Nakamura, K., Matsui, M., Yamamoto, A., Nakahara, Y., Suzuki-Migishima, R., Yokoyama, M., Mishima, K., Saito, I., Okano, H., & Mizushima, N. (2006). Suppression of basal autophagy in neural cells causes neurodegenerative disease in mice. *Nature*, 441(7095), 885-889. <https://doi.org/10.1038/nature04724>
- Harbauer, A. B., Hees, J. T., Wanderoy, S., Segura, I., Gibbs, W., Cheng, Y., Ordonez, M., Cai, Z., Cartoni, R., Ashrafi, G., Wang, C., Perocchi, F., He, Z., & Schwarz, T. L. (2022). Neuronal mitochondria transport Pink1 mRNA via synaptotagmin 2 to support local mitophagy. *Neuron*, 110(9), 1516-1531 e1519. <https://doi.org/10.1016/j.neuron.2022.01.035>
- Harbauer, A. B., Zahedi, R. P., Sickmann, A., Pfanner, N., & Meisinger, C. (2014). The protein import machinery of mitochondria—a regulatory hub in metabolism, stress, and disease. *Cell Metab*, 19(3), 357-372. <https://doi.org/10.1016/j.cmet.2014.01.010>
- Harris, J. J., Jolivet, R., & Attwell, D. (2012). Synaptic energy use and supply. *Neuron*, 75(5), 762-777. <https://doi.org/10.1016/j.neuron.2012.08.019>
- Hatefi, Y. (1985). The mitochondrial electron transport and oxidative phosphorylation system. *Annu Rev Biochem*, 54, 1015-1069. <https://doi.org/10.1146/annurev.bi.54.070185.005055>
- Head, B., Griparic, L., Amiri, M., Gandre-Babbe, S., & van der Blik, A. M. (2009). Inducible proteolytic inactivation of OPA1 mediated by the OMA1 protease in mammalian cells. *J Cell Biol*, 187(7), 959-966. <https://doi.org/10.1083/jcb.200906083>

- Hees, J. T., & Harbauer, A. B. (2022). Metabolic Regulation of Mitochondrial Protein Biogenesis from a Neuronal Perspective. *Biomolecules*, 12(11). <https://doi.org/10.3390/biom12111595>
- Hendricks, A. G., Perlson, E., Ross, J. L., Schroeder, H. W., 3rd, Tokito, M., & Holzbaur, E. L. (2010). Motor coordination via a tug-of-war mechanism drives bidirectional vesicle transport. *Curr Biol*, 20(8), 697-702. <https://doi.org/10.1016/j.cub.2010.02.058>
- Henneman, E., Somjen, G., & Carpenter, D. O. (1965). Functional Significance of Cell Size in Spinal Motoneurons. *J Neurophysiol*, 28, 560-580. <https://doi.org/10.1152/jn.1965.28.3.560>
- Henstridge, C. M., Pickett, E., & Spires-Jones, T. L. (2016). Synaptic pathology: A shared mechanism in neurological disease. *Ageing Res Rev*, 28, 72-84. <https://doi.org/10.1016/j.arr.2016.04.005>
- Heo, J. M., Ordureau, A., Paulo, J. A., Rinehart, J., & Harper, J. W. (2015). The PINK1-PARKIN Mitochondrial Ubiquitylation Pathway Drives a Program of OPTN/NDP52 Recruitment and TBK1 Activation to Promote Mitophagy. *Mol Cell*, 60(1), 7-20. <https://doi.org/10.1016/j.molcel.2015.08.016>
- Herlan, M., Bornhovd, C., Hell, K., Neupert, W., & Reichert, A. S. (2004). Alternative topogenesis of Mgm1 and mitochondrial morphology depend on ATP and a functional import motor. *J Cell Biol*, 165(2), 167-173. <https://doi.org/10.1083/jcb.200403022>
- Herlan, M., Vogel, F., Bornhovd, C., Neupert, W., & Reichert, A. S. (2003). Processing of Mgm1 by the rhomboid-type protease Pcp1 is required for maintenance of mitochondrial morphology and of mitochondrial DNA. *J Biol Chem*, 278(30), 27781-27788. <https://doi.org/10.1074/jbc.M211311200>
- Hernandez, G., Thornton, C., Stotland, A., Lui, D., Sin, J., Ramil, J., Magee, N., Andres, A., Quarato, G., Carreira, R. S., Sayen, M. R., Wolkowicz, R., & Gottlieb, R. A. (2013). MitoTimer: a novel tool for monitoring mitochondrial turnover. *Autophagy*, 9(11), 1852-1861. <https://doi.org/10.4161/auto.26501>
- Hippocrates. (ca. 400 BC). *The Sacred Disease* (J. Chadwick & W. N. Mann, Trans.; G. E. R. Lloyd, Ed.) [Essay]. Hippocratic writings (London 1983), Penguin Books, pp. 249-251.
- Hirokawa, N. (1982). Cross-linker system between neurofilaments, microtubules, and membranous organelles in frog axons revealed by the quick-freeze, deep-etching method. *J Cell Biol*, 94(1), 129-142. <https://www.ncbi.nlm.nih.gov/pubmed/6181077>
- Hirokawa, N. (1998). Kinesin and dynein superfamily proteins and the mechanism of organelle transport. *Science*, 279(5350), 519-526. <https://www.ncbi.nlm.nih.gov/pubmed/9438838>
- Hirokawa, N., Niwa, S., & Tanaka, Y. (2010). Molecular motors in neurons: transport mechanisms and roles in brain function, development, and disease. *Neuron*, 68(4), 610-638. <https://doi.org/10.1016/j.neuron.2010.09.039>
- Hock, M. B., & Kralli, A. (2009). Transcriptional control of mitochondrial biogenesis and function. *Annu Rev Physiol*, 71, 177-203. <https://doi.org/10.1146/annurev.physiol.010908.163119>
- Hollenbeck, P. J. (1996). The pattern and mechanism of mitochondrial transport in axons. *Front Biosci*, 1, d91-102. <https://www.ncbi.nlm.nih.gov/pubmed/9159217>
- Hoppins, S. (2014). The regulation of mitochondrial dynamics. *Curr Opin Cell Biol*, 29, 46-52. <https://doi.org/10.1016/j.ceb.2014.03.005>
- Hoppins, S., & Nunnari, J. (2009). The molecular mechanism of mitochondrial fusion. *Biochim Biophys Acta*, 1793(1), 20-26. <https://doi.org/10.1016/j.bbamcr.2008.07.005>
- Howarth, C., Gleeson, P., & Attwell, D. (2012). Updated energy budgets for neural computation in the neocortex and cerebellum. *J Cereb Blood Flow Metab*, 32(7), 1222-1232. <https://doi.org/10.1038/jcbfm.2012.35>

- Huang, S., Ratliff, K. S., & Matouschek, A. (2002). Protein unfolding by the mitochondrial membrane potential. *Nat Struct Biol*, 9(4), 301-307. <https://doi.org/10.1038/nsb772>
- Huang, X., Sun, L., Ji, S., Zhao, T., Zhang, W., Xu, J., Zhang, J., Wang, Y., Wang, X., Franzini-Armstrong, C., Zheng, M., & Cheng, H. (2013). Kissing and nanotunneling mediate intermitochondrial communication in the heart. *Proc Natl Acad Sci U S A*, 110(8), 2846-2851. <https://doi.org/10.1073/pnas.1300741110>
- Huemer, R. P., Lee, K. D., Reeves, A. E., & Bickert, C. (1971). Mitochondrial studies in senescent mice. II. Specific activity, buoyant density, and turnover of mitochondrial DNA. *Exp Gerontol*, 6(5), 327-334. [https://doi.org/10.1016/0531-5565\(71\)90001-5](https://doi.org/10.1016/0531-5565(71)90001-5)
- Hunn, B. H., Cragg, S. J., Bolam, J. P., Spillantini, M. G., & Wade-Martins, R. (2015). Impaired intracellular trafficking defines early Parkinson's disease. *Trends Neurosci*, 38(3), 178-188. <https://doi.org/10.1016/j.tins.2014.12.009>
- Hurd, D. D., & Saxton, W. M. (1996). Kinesin mutations cause motor neuron disease phenotypes by disrupting fast axonal transport in Drosophila. *Genetics*, 144(3), 1075-1085. <https://www.ncbi.nlm.nih.gov/pubmed/8913751>
- Imbriani, P., Schirinzi, T., Meringolo, M., Mercuri, N. B., & Pisani, A. (2018). Centrality of Early Synaptopathy in Parkinson's Disease. *Front Neurol*, 9, 103. <https://doi.org/10.3389/fneur.2018.00103>
- Iovine, J. C., Claypool, S. M., & Alder, N. N. (2021). Mitochondrial compartmentalization: emerging themes in structure and function. *Trends Biochem Sci*, 46(11), 902-917. <https://doi.org/10.1016/j.tibs.2021.06.003>
- Ishihara, N., Eura, Y., & Mihara, K. (2004). Mitofusin 1 and 2 play distinct roles in mitochondrial fusion reactions via GTPase activity. *J Cell Sci*, 117(Pt 26), 6535-6546. <https://doi.org/10.1242/jcs.01565>
- Ishihara, N., Jofuku, A., Eura, Y., & Mihara, K. (2003). Regulation of mitochondrial morphology by membrane potential, and DRP1-dependent division and FZO1-dependent fusion reaction in mammalian cells. *Biochem Biophys Res Commun*, 301(4), 891-898. [https://doi.org/10.1016/s0006-291x\(03\)00050-0](https://doi.org/10.1016/s0006-291x(03)00050-0)
- Itier, J. M., Ibanez, P., Mena, M. A., Abbas, N., Cohen-Salmon, C., Bohme, G. A., Laville, M., Pratt, J., Corti, O., Pradier, L., Ret, G., Joubert, C., Periquet, M., Araujo, F., Negroni, J., Casarejos, M. J., Canals, S., Solano, R., Serrano, A., . . . Garcia de Yébenes, J. (2003). Parkin gene inactivation alters behaviour and dopamine neurotransmission in the mouse. *Hum Mol Genet*, 12(18), 2277-2291. <https://doi.org/10.1093/hmg/ddg239>
- Ito, Y., Ofengeim, D., Najafov, A., Das, S., Saberi, S., Li, Y., Hitomi, J., Zhu, H., Chen, H., Mayo, L., Geng, J., Amin, P., DeWitt, J. P., Mookhtiar, A. K., Florez, M., Ouchida, A. T., Fan, J. B., Pasparakis, M., Kelliher, M. A., . . . Yuan, J. (2016). RIPK1 mediates axonal degeneration by promoting inflammation and necroptosis in ALS. *Science*, 353(6299), 603-608. <https://doi.org/10.1126/science.aaf6803>
- Itoh, K., Nakamura, K., Iijima, M., & Sesaki, H. (2013). Mitochondrial dynamics in neurodegeneration. *Trends Cell Biol*, 23(2), 64-71. <https://doi.org/10.1016/j.tcb.2012.10.006>
- Iyer, S. P., & Hart, G. W. (2003). Roles of the tetratricopeptide repeat domain in O-GlcNAc transferase targeting and protein substrate specificity. *J Biol Chem*, 278(27), 24608-24616. <https://doi.org/10.1074/jbc.M300036200>
- James, D. I., Parone, P. A., Mattenberger, Y., & Martinou, J. C. (2003). hFis1, a novel component of the mammalian mitochondrial fission machinery. *J Biol Chem*, 278(38), 36373-36379. <https://doi.org/10.1074/jbc.M303758200>

- Janke, C., & Bulinski, J. C. (2011). Post-translational regulation of the microtubule cytoskeleton: mechanisms and functions. *Nat Rev Mol Cell Biol*, 12(12), 773-786. <https://doi.org/10.1038/nrm3227>
- Johnson, L. V., Walsh, M. L., & Chen, L. B. (1980). Localization of mitochondria in living cells with rhodamine 123. *Proc Natl Acad Sci U S A*, 77(2), 990-994. <https://doi.org/10.1073/pnas.77.2.990>
- Jones, R. A., Harrison, C., Eaton, S. L., Llaverro Hurtado, M., Graham, L. C., Alkhamash, L., Oladiran, O. A., Gale, A., Lamont, D. J., Simpson, H., Simmen, M. W., Soeller, C., Wishart, T. M., & Gillingwater, T. H. (2017). Cellular and Molecular Anatomy of the Human Neuromuscular Junction. *Cell Rep*, 21(9), 2348-2356. <https://doi.org/10.1016/j.celrep.2017.11.008>
- Jornayvaz, F. R., & Shulman, G. I. (2010). Regulation of mitochondrial biogenesis. *Essays Biochem*, 47, 69-84. <https://doi.org/10.1042/bse0470069>
- Julg, J., Strohm, L., & Behrends, C. (2021). Canonical and Noncanonical Autophagy Pathways in Microglia. *Mol Cell Biol*, 41(3), e0038920. <https://doi.org/10.1128/MCB.00389-20>
- Jung, H., Kim, S. Y., Canbakis Cecen, F. S., Cho, Y., & Kwon, S. K. (2020). Dysfunction of Mitochondrial Ca(2+) Regulatory Machineries in Brain Aging and Neurodegenerative Diseases. *Front Cell Dev Biol*, 8, 599792. <https://doi.org/10.3389/fcell.2020.599792>
- Kageyama, G. H., & Wong-Riley, M. (1985). An analysis of the cellular localization of cytochrome oxidase in the lateral geniculate nucleus of the adult cat. *J Comp Neurol*, 242(3), 338-357. <https://doi.org/10.1002/cne.902420304>
- Kageyama, G. H., & Wong-Riley, M. T. (1982). Histochemical localization of cytochrome oxidase in the hippocampus: correlation with specific neuronal types and afferent pathways. *Neuroscience*, 7(10), 2337-2361. [https://doi.org/10.1016/0306-4522\(82\)90199-3](https://doi.org/10.1016/0306-4522(82)90199-3)
- Kageyama, Y., Zhang, Z., Roda, R., Fukaya, M., Wakabayashi, J., Wakabayashi, N., Kensler, T. W., Reddy, P. H., Iijima, M., & Sesaki, H. (2012). Mitochondrial division ensures the survival of postmitotic neurons by suppressing oxidative damage. *J Cell Biol*, 197(4), 535-551. <https://doi.org/10.1083/jcb.201110034>
- Kalia, R., Wang, R. Y., Yusuf, A., Thomas, P. V., Agard, D. A., Shaw, J. M., & Frost, A. (2018). Structural basis of mitochondrial receptor binding and constriction by DRP1. *Nature*, 558(7710), 401-405. <https://doi.org/10.1038/s41586-018-0211-2>
- Kandel, E. R., Koester, J., Mack, S., & Siegelbaum, S. (2021). *Principles of neural science* (Sixth edition. ed.). McGraw Hill.
- Kang, J. S., Tian, J. H., Pan, P. Y., Zald, P., Li, C., Deng, C., & Sheng, Z. H. (2008). Docking of axonal mitochondria by syntaphilin controls their mobility and affects short-term facilitation. *Cell*, 132(1), 137-148. <https://doi.org/10.1016/j.cell.2007.11.024>
- Kann, O., & Kovacs, R. (2007). Mitochondria and neuronal activity. *Am J Physiol Cell Physiol*, 292(2), C641-657. <https://doi.org/10.1152/ajpcell.00222.2006>
- Kapitein, L. C., & Hoogenraad, C. C. (2015). Building the Neuronal Microtubule Cytoskeleton. *Neuron*, 87(3), 492-506. <https://doi.org/10.1016/j.neuron.2015.05.046>
- Karbowski, M., Arnoult, D., Chen, H., Chan, D. C., Smith, C. L., & Youle, R. J. (2004). Quantitation of mitochondrial dynamics by photolabeling of individual organelles shows that mitochondrial fusion is blocked during the Bax activation phase of apoptosis. *J Cell Biol*, 164(4), 493-499. <https://doi.org/10.1083/jcb.200309082>
- Karbowski, M., Cleland, M. M., & Roelofs, B. A. (2014). Photoactivatable green fluorescent protein-based visualization and quantification of mitochondrial fusion and mitochondrial network complexity in living cells. *Methods Enzymol*, 547, 57-73. <https://doi.org/10.1016/B978-0-12-801415-8.00004-7>

- Karbowski, M., Norris, K. L., Cleland, M. M., Jeong, S. Y., & Youle, R. J. (2006). Role of Bax and Bak in mitochondrial morphogenesis. *Nature*, 443(7112), 658-662. <https://doi.org/10.1038/nature05111>
- Karnkowska, A., Vacek, V., Zubacova, Z., Treitli, S. C., Petrzalkova, R., Eme, L., Novak, L., Zarsky, V., Barlow, L. D., Herman, E. K., Soukal, P., Hroudova, M., Dolezal, P., Stairs, C. W., Roger, A. J., Elias, M., Dacks, J. B., Vlcek, C., & Hampl, V. (2016). A Eukaryote without a Mitochondrial Organelle. *Curr Biol*, 26(10), 1274-1284. <https://doi.org/10.1016/j.cub.2016.03.053>
- Kasthuri, N., Hayworth, K. J., Berger, D. R., Schalek, R. L., Conchello, J. A., Knowles-Barley, S., Lee, D., Vazquez-Reina, A., Kaynig, V., Jones, T. R., Roberts, M., Morgan, J. L., Tapia, J. C., Seung, H. S., Roncal, W. G., Vogelstein, J. T., Burns, R., Sussman, D. L., Priebe, C. E., ... Lichtman, J. W. (2015). Saturated Reconstruction of a Volume of Neocortex. *Cell*, 162(3), 648-661. <https://doi.org/10.1016/j.cell.2015.06.054>
- Katayama, H., Kogure, T., Mizushima, N., Yoshimori, T., & Miyawaki, A. (2011). A sensitive and quantitative technique for detecting autophagic events based on lysosomal delivery. *Chem Biol*, 18(8), 1042-1052. <https://doi.org/10.1016/j.chembiol.2011.05.013>
- Kay, J. N., De la Huerta, I., Kim, I. J., Zhang, Y., Yamagata, M., Chu, M. W., Meister, M., & Sanes, J. R. (2011). Retinal ganglion cells with distinct directional preferences differ in molecular identity, structure, and central projections. *J Neurosci*, 31(21), 7753-7762. <https://doi.org/10.1523/JNEUROSCI.0907-11.2011>
- Keller-Peck, C. R., Walsh, M. K., Gan, W. B., Feng, G., Sanes, J. R., & Lichtman, J. W. (2001). Asynchronous synapse elimination in neonatal motor units: studies using GFP transgenic mice. *Neuron*, 31(3), 381-394. <https://www.ncbi.nlm.nih.gov/pubmed/11516396>
[http://www.cell.com/neuron/pdf/S0896-6273\(01\)00383-X.pdf](http://www.cell.com/neuron/pdf/S0896-6273(01)00383-X.pdf)
- Kerschensteiner, M., Reuter, M. S., Lichtman, J. W., & Misgeld, T. (2008). Ex vivo imaging of motor axon dynamics in murine triangularis sterni explants. *Nat Protoc*, 3(10), 1645-1653. <https://doi.org/10.1038/nprot.2008.160>
- Kety, S. S. (1957). The general metabolism of the brain in vivo. In D. Richter (Ed.), *Metabolism of the nervous system* (pp. 221-237). Pergamon <https://doi.org/https://doi.org/10.1016/B978-0-08-009062-7.50026-6>
- Khan, A. A., & Wilson, J. E. (1965). Studies of Turnover in Mammalian Subcellular Particles: Brain Nuclei, Mitochondria and Microsomes. *J Neurochem*, 12, 81-86. <https://doi.org/10.1111/j.1471-4159.1965.tb11942.x>
- Kiebish, M. A., Han, X., Cheng, H., Lunceford, A., Clarke, C. F., Moon, H., Chuang, J. H., & Seyfried, T. N. (2008). Lipidomic analysis and electron transport chain activities in C57BL/6J mouse brain mitochondria. *J Neurochem*, 106(1), 299-312. <https://doi.org/10.1111/j.1471-4159.2008.05383.x>
- Kim, T. Y., Wang, D., Kim, A. K., Lau, E., Lin, A. J., Liem, D. A., Zhang, J., Zong, N. C., Lam, M. P., & Ping, P. (2012). Metabolic labeling reveals proteome dynamics of mouse mitochondria. *Mol Cell Proteomics*, 11(12), 1586-1594. <https://doi.org/10.1074/mcp.M112.021162>
- King, S. J., & Schroer, T. A. (2000). Dynactin increases the processivity of the cytoplasmic dynein motor. *Nat Cell Biol*, 2(1), 20-24. <https://doi.org/10.1038/71338>
- Kislinger, G., Niemann, C., Rodriguez, L., Jiang, H., Fard, M. K., Snaidero, N., Schumacher, A. M., Kerschensteiner, M., Misgeld, T., & Schifferer, M. (2023). Neurons on tape: Automated Tape Collecting Ultramicrotomy-mediated volume EM for targeting neuropathology. *Methods Cell Biol*, 177, 125-170. <https://doi.org/10.1016/bs.mcb.2023.01.012>
- Kitada, T., Asakawa, S., Hattori, N., Matsumine, H., Yamamura, Y., Minoshima, S., Yokochi, M., Mizuno, Y., & Shimizu, N. (1998). Mutations in the parkin gene cause autosomal recessive juvenile parkinsonism. *Nature*, 392(6676), 605-608. <https://doi.org/10.1038/33416>

- Kleele, T., Marinkovic, P., Williams, P. R., Stern, S., Weigand, E. E., Engerer, P., Naumann, R., Hartmann, J., Karl, R. M., Bradke, F., Bishop, D., Herms, J., Konnerth, A., Kerschensteiner, M., Godinho, L., & Misgeld, T. (2014). An assay to image neuronal microtubule dynamics in mice. *Nat Commun*, 5, 4827. <https://doi.org/10.1038/ncomms5827>
- Kleele, T., Rey, T., Winter, J., Zaganelli, S., Mahecic, D., Perreten Lambert, H., Ruberto, F. P., Nemir, M., Wai, T., Pedrazzini, T., & Manley, S. (2021). Distinct fission signatures predict mitochondrial degradation or biogenesis. *Nature*, 593(7859), 435-439. <https://doi.org/10.1038/s41586-021-03510-6>
- Klionsky, D. J., & Ohsumi, Y. (1999). Vacuolar import of proteins and organelles from the cytoplasm. *Annu Rev Cell Dev Biol*, 15, 1-32. <https://doi.org/10.1146/annurev.cellbio.15.1.1>
- Kneysnberg, A., Combs, B., Christensen, K., Morfini, G., & Kanaan, N. M. (2017). Axonal Degeneration in Tauopathies: Disease Relevance and Underlying Mechanisms. *Front Neurosci*, 11, 572. <https://doi.org/10.3389/fnins.2017.00572>
- Kobayashi, T., Storrie, B., Simons, K., & Dotti, C. G. (1992). A functional barrier to movement of lipids in polarized neurons. *Nature*, 359(6396), 647-650. <https://doi.org/10.1038/359647a0>
- Komatsu, M., Waguri, S., Chiba, T., Murata, S., Iwata, J., Tanida, I., Ueno, T., Koike, M., Uchiyama, Y., Kominami, E., & Tanaka, K. (2006). Loss of autophagy in the central nervous system causes neurodegeneration in mice. *Nature*, 441(7095), 880-884. <https://doi.org/10.1038/nature04723>
- Kondadi, A. K., Anand, R., Hansch, S., Urbach, J., Zobel, T., Wolf, D. M., Segawa, M., Liesa, M., Shirihai, O. S., Weidtkamp-Peters, S., & Reichert, A. S. (2020). Cristae undergo continuous cycles of membrane remodelling in a MICOS-dependent manner. *EMBO Rep*, 21(3), e49776. <https://doi.org/10.15252/embr.201949776>
- Koppers, M., & Farias, G. G. (2021). Organelle distribution in neurons: Logistics behind polarized transport. *Curr Opin Cell Biol*, 71, 46-54. <https://doi.org/10.1016/j.ceb.2021.02.004>
- Korobova, F., Gauvin, T. J., & Higgs, H. N. (2014). A role for myosin II in mammalian mitochondrial fission. *Curr Biol*, 24(4), 409-414. <https://doi.org/10.1016/j.cub.2013.12.032>
- Korobova, F., Ramabhadran, V., & Higgs, H. N. (2013). An actin-dependent step in mitochondrial fission mediated by the ER-associated formin INF2. *Science*, 339(6118), 464-467. <https://doi.org/10.1126/science.1228360>
- Koshiba, T., Detmer, S. A., Kaiser, J. T., Chen, H., McCaffery, J. M., & Chan, D. C. (2004). Structural basis of mitochondrial tethering by mitofusin complexes. *Science*, 305(5685), 858-862. <https://doi.org/10.1126/science.1099793>
- Kremer, J. R., Mastronarde, D. N., & McIntosh, J. R. (1996). Computer visualization of three-dimensional image data using IMOD. *J Struct Biol*, 116(1), 71-76. <https://doi.org/10.1006/jsbi.1996.0013>
- Kulkarni, V. V., & Maday, S. (2018). Neuronal endosomes to lysosomes: A journey to the soma. *J Cell Biol*, 217(9), 2977-2979. <https://doi.org/10.1083/jcb.201806139>
- Kuzniewska, B., Cysewski, D., Wasilewski, M., Sakowska, P., Milek, J., Kulinski, T. M., Winiarski, M., Kozielowicz, P., Knapska, E., Dadlez, M., Chacinska, A., Dziembowski, A., & Dziembowska, M. (2020). Mitochondrial protein biogenesis in the synapse is supported by local translation. *EMBO Rep*, 21(8), e48882. <https://doi.org/10.15252/embr.201948882>
- Kwon, S. K., Sando, R., 3rd, Lewis, T. L., Hirabayashi, Y., Maximov, A., & Polleux, F. (2016). LKB1 Regulates Mitochondria-Dependent Presynaptic Calcium Clearance and Neurotransmitter Release Properties at Excitatory Synapses along Cortical Axons. *PLoS Biol*, 14(7), e1002516. <https://doi.org/10.1371/journal.pbio.1002516>
- Lavorato, M., Iyer, V. R., Dewight, W., Cupo, R. R., Debattisti, V., Gomez, L., De la Fuente, S., Zhao, Y. T., Valdivia, H. H., Hajnoczky, G., & Franzini-Armstrong, C. (2017). Increased mitochondrial

- nanotunneling activity, induced by calcium imbalance, affects intermitochondrial matrix exchanges. *Proc Natl Acad Sci U S A*, 114(5), E849-E858. <https://doi.org/10.1073/pnas.1617788113>
- Lazarou, M., Jin, S. M., Kane, L. A., & Youle, R. J. (2012). Role of PINK1 binding to the TOM complex and alternate intracellular membranes in recruitment and activation of the E3 ligase Parkin. *Dev Cell*, 22(2), 320-333. <https://doi.org/10.1016/j.devcel.2011.12.014>
- Lazarou, M., Sliter, D. A., Kane, L. A., Sarraf, S. A., Wang, C., Burman, J. L., Sideris, D. P., Fogel, A. I., & Youle, R. J. (2015). The ubiquitin kinase PINK1 recruits autophagy receptors to induce mitophagy. *Nature*, 524(7565), 309-314. <https://doi.org/10.1038/nature14893>
- Lee, D., Lee, K. H., Ho, W. K., & Lee, S. H. (2007). Target cell-specific involvement of presynaptic mitochondria in post-tetanic potentiation at hippocampal mossy fiber synapses. *J Neurosci*, 27(50), 13603-13613. <https://doi.org/10.1523/JNEUROSCI.3985-07.2007>
- Lee, S., Park, D., Lim, C., Kim, J. I., & Min, K. T. (2022). mtIF3 is locally translated in axons and regulates mitochondrial translation for axonal growth. *BMC Biol*, 20(1), 12. <https://doi.org/10.1186/s12915-021-01215-w>
- Lee, S., Sato, Y., & Nixon, R. A. (2011). Lysosomal proteolysis inhibition selectively disrupts axonal transport of degradative organelles and causes an Alzheimer's-like axonal dystrophy. *J Neurosci*, 31(21), 7817-7830. <https://doi.org/10.1523/JNEUROSCI.6412-10.2011>
- Lees, R. M., Johnson, J. D., & Ashby, M. C. (2019). Presynaptic Boutons That Contain Mitochondria Are More Stable. *Front Synaptic Neurosci*, 11, 37. <https://doi.org/10.3389/fnsyn.2019.00037>
- Lewis, M. R., & Lewis, W. H. (1914). Mitochondria in Tissue Culture. *Science*, 39(1000), 330-333. <https://doi.org/10.1126/science.39.1000.330>
- Lewis, T. L., Jr., Kwon, S. K., Lee, A., Shaw, R., & Polleux, F. (2018). MFF-dependent mitochondrial fission regulates presynaptic release and axon branching by limiting axonal mitochondria size. *Nat Commun*, 9(1), 5008. <https://doi.org/10.1038/s41467-018-07416-2>
- Lewis, T. L., Jr., Turi, G. F., Kwon, S. K., Losonczy, A., & Polleux, F. (2016). Progressive Decrease of Mitochondrial Motility during Maturation of Cortical Axons In Vitro and In Vivo. *Curr Biol*, 26(19), 2602-2608. <https://doi.org/10.1016/j.cub.2016.07.064>
- Li, H., & Chen, G. (2016). In Vivo Reprogramming for CNS Repair: Regenerating Neurons from Endogenous Glial Cells. *Neuron*, 91(4), 728-738. <https://doi.org/10.1016/j.neuron.2016.08.004>
- Li, S., Xiong, G. J., Huang, N., & Sheng, Z. H. (2020). The cross-talk of energy sensing and mitochondrial anchoring sustains synaptic efficacy by maintaining presynaptic metabolism. *Nat Metab*, 2(10), 1077-1095. <https://doi.org/10.1038/s42255-020-00289-0>
- Li, Z., Jo, J., Jia, J. M., Lo, S. C., Whitcomb, D. J., Jiao, S., Cho, K., & Sheng, M. (2010). Caspase-3 activation via mitochondria is required for long-term depression and AMPA receptor internalization. *Cell*, 141(5), 859-871. <https://doi.org/10.1016/j.cell.2010.03.053>
- Licht-Mayer, S., Campbell, G. R., Mehta, A. R., McGill, K., Symonds, A., Al-Azki, S., Pryce, G., Zandee, S., Zhao, C., Kipp, M., Smith, K. J., Baker, D., Altmann, D., Anderton, S. M., Kap, Y. S., Laman, J. D., t'Hart, B. A., Rodriguez, M., Franklin, R. J. M., . . . Mahad, D. J. (2022). Axonal response of mitochondria to demyelination and complex IV activity within demyelinated axons in experimental models of multiple sclerosis. *Neuropathol Appl Neurobiol*, e12851. <https://doi.org/10.1111/nan.12851>
- Lie, P. P. Y., Yang, D. S., Stavrides, P., Goulbourne, C. N., Zheng, P., Mohan, P. S., Cataldo, A. M., & Nixon, R. A. (2021). Post-Golgi carriers, not lysosomes, confer lysosomal properties to pre-degradative organelles in normal and dystrophic axons. *Cell Rep*, 35(4), 109034. <https://doi.org/10.1016/j.celrep.2021.109034>

- Liesa, M., & Shirihai, O. S. (2013). Mitochondrial dynamics in the regulation of nutrient utilization and energy expenditure. *Cell Metab*, 17(4), 491-506. <https://doi.org/10.1016/j.cmet.2013.03.002>
- Lill, R. (2009). Function and biogenesis of iron-sulphur proteins. *Nature*, 460(7257), 831-838. <https://doi.org/10.1038/nature08301>
- Lin, A. L., Fox, P. T., Hardies, J., Duong, T. Q., & Gao, J. H. (2010). Nonlinear coupling between cerebral blood flow, oxygen consumption, and ATP production in human visual cortex. *Proc Natl Acad Sci U S A*, 107(18), 8446-8451. <https://doi.org/10.1073/pnas.0909711107>
- Lin, J., Wu, P. H., Tarr, P. T., Lindenberg, K. S., St-Pierre, J., Zhang, C. Y., Mootha, V. K., Jager, S., Vianna, C. R., Reznick, R. M., Cui, L., Manieri, M., Donovan, M. X., Wu, Z., Cooper, M. P., Fan, M. C., Rohas, L. M., Zavacki, A. M., Cinti, S., . . . Spiegelman, B. M. (2004). Defects in adaptive energy metabolism with CNS-linked hyperactivity in PGC-1alpha null mice. *Cell*, 119(1), 121-135. <https://doi.org/10.1016/j.cell.2004.09.013>
- Lin, M. Y., Cheng, X. T., Tamminen, P., Xie, Y., Zhou, B., Cai, Q., & Sheng, Z. H. (2017). Releasing Syntaphilin Removes Stressed Mitochondria from Axons Independent of Mitophagy under Pathophysiological Conditions. *Neuron*, 94(3), 595-610 e596. <https://doi.org/10.1016/j.neuron.2017.04.004>
- Lin, Y., Li, L. L., Nie, W., Liu, X., Adler, A., Xiao, C., Lu, F., Wang, L., Han, H., Wang, X., Gan, W. B., & Cheng, H. (2019). Brain activity regulates loose coupling between mitochondrial and cytosolic Ca(2+) transients. *Nat Commun*, 10(1), 5277. <https://doi.org/10.1038/s41467-019-13142-0>
- Lipinski, M. M., Zheng, B., Lu, T., Yan, Z., Py, B. F., Ng, A., Xavier, R. J., Li, C., Yankner, B. A., Scherzer, C. R., & Yuan, J. (2010). Genome-wide analysis reveals mechanisms modulating autophagy in normal brain aging and in Alzheimer's disease. *Proc Natl Acad Sci U S A*, 107(32), 14164-14169. <https://doi.org/10.1073/pnas.1009485107>
- Lippincott-Schwartz, J., & Patterson, G. H. (2003). Development and use of fluorescent protein markers in living cells. *Science*, 300(5616), 87-91. <https://doi.org/10.1126/science.1082520>
- Liu, H. Y., Gale, J. R., Reynolds, I. J., Weiss, J. H., & Aizenman, E. (2021). The Multifaceted Roles of Zinc in Neuronal Mitochondrial Dysfunction. *Biomedicines*, 9(5). <https://doi.org/10.3390/biomedicines9050489>
- Liu, X., Weaver, D., Shirihai, O., & Hajnoczky, G. (2009). Mitochondrial 'kiss-and-run': interplay between mitochondrial motility and fusion-fission dynamics. *EMBO J*, 28(20), 3074-3089. <https://doi.org/10.1038/emboj.2009.255>
- Long, Q., Zhao, D., Fan, W., Yang, L., Zhou, Y., Qi, J., Wang, X., & Liu, X. (2015). Modeling of Mitochondrial Donut Formation. *Biophys J*, 109(5), 892-899. <https://doi.org/10.1016/j.bpj.2015.07.039>
- Lopez-Domenech, G., Covill-Cooke, C., Ivankovic, D., Halff, E. F., Sheehan, D. F., Norkett, R., Birsa, N., & Kittler, J. T. (2018). Miro proteins coordinate microtubule- and actin-dependent mitochondrial transport and distribution. *EMBO J*, 37(3), 321-336. <https://doi.org/10.15252/emboj.201696380>
- Lopez-Domenech, G., & Kittler, J. T. (2023). Mitochondrial regulation of local supply of energy in neurons. *Curr Opin Neurobiol*, 81, 102747. <https://doi.org/10.1016/j.conb.2023.102747>
- Lopez-Lluch, G., Irusta, P. M., Navas, P., & de Cabo, R. (2008). Mitochondrial biogenesis and healthy aging. *Exp Gerontol*, 43(9), 813-819. <https://doi.org/10.1016/j.exger.2008.06.014>
- Lopez-Otin, C., Blasco, M. A., Partridge, L., Serrano, M., & Kroemer, G. (2023). Hallmarks of aging: An expanding universe. *Cell*, 186(2), 243-278. <https://doi.org/10.1016/j.cell.2022.11.001>

- Loson, O. C., Song, Z., Chen, H., & Chan, D. C. (2013). Fis1, Mff, MiD49, and MiD51 mediate Drp1 recruitment in mitochondrial fission. *Mol Biol Cell*, 24(5), 659-667. <https://doi.org/10.1091/mbc.E12-10-0721>
- Lu, T., & Trussell, L. O. (2007). Development and elimination of endbulb synapses in the chick cochlear nucleus. *J Neurosci*, 27(4), 808-817. <https://doi.org/10.1523/JNEUROSCI.4871-06.2007>
- Luo, L. (2021). Architectures of neuronal circuits. *Science*, 373(6559), eabg7285. <https://doi.org/10.1126/science.abg7285>
- Lutz, A. K., Exner, N., Fett, M. E., Schlehe, J. S., Kloos, K., Lammermann, K., Brunner, B., Kurz-Drexler, A., Vogel, F., Reichert, A. S., Bouman, L., Vogt-Weisenhorn, D., Wurst, W., Tatzelt, J., Haass, C., & Winklhofer, K. F. (2009). Loss of parkin or PINK1 function increases Drp1-dependent mitochondrial fragmentation. *J Biol Chem*, 284(34), 22938-22951. <https://doi.org/10.1074/jbc.M109.035774>
- MacAskill, A. F., & Kittler, J. T. (2010). Control of mitochondrial transport and localization in neurons. *Trends Cell Biol*, 20(2), 102-112. <https://doi.org/10.1016/j.tcb.2009.11.002>
- Macaskill, A. F., Rinholm, J. E., Twelvetrees, A. E., Arancibia-Carcamo, I. L., Muir, J., Fransson, A., Aspenstrom, P., Attwell, D., & Kittler, J. T. (2009). Miro1 is a calcium sensor for glutamate receptor-dependent localization of mitochondria at synapses. *Neuron*, 61(4), 541-555. <https://doi.org/10.1016/j.neuron.2009.01.030>
- Macdonald, P. J., Stepanyants, N., Mehrotra, N., Mears, J. A., Qi, X., Sesaki, H., & Ramachandran, R. (2014). A dimeric equilibrium intermediate nucleates Drp1 reassembly on mitochondrial membranes for fission. *Mol Biol Cell*, 25(12), 1905-1915. <https://doi.org/10.1091/mbc.E14-02-0728>
- Maday, S. (2016). Mechanisms of neuronal homeostasis: Autophagy in the axon. *Brain Res*, 1649(Pt B), 143-150. <https://doi.org/10.1016/j.brainres.2016.03.047>
- Maday, S., & Holzbaur, E. L. (2014). Autophagosome biogenesis in primary neurons follows an ordered and spatially regulated pathway. *Dev Cell*, 30(1), 71-85. <https://doi.org/10.1016/j.devcel.2014.06.001>
- Maday, S., & Holzbaur, E. L. (2016). Compartment-Specific Regulation of Autophagy in Primary Neurons. *J Neurosci*, 36(22), 5933-5945. <https://doi.org/10.1523/JNEUROSCI.4401-15.2016>
- Maday, S., Twelvetrees, A. E., Moughamian, A. J., & Holzbaur, E. L. (2014). Axonal transport: cargo-specific mechanisms of motility and regulation. *Neuron*, 84(2), 292-309. <https://doi.org/10.1016/j.neuron.2014.10.019>
- Maday, S., Wallace, K. E., & Holzbaur, E. L. (2012). Autophagosomes initiate distally and mature during transport toward the cell soma in primary neurons. *J Cell Biol*, 196(4), 407-417. <https://doi.org/10.1083/jcb.201106120>
- Magrane, J., Cortez, C., Gan, W. B., & Manfredi, G. (2014). Abnormal mitochondrial transport and morphology are common pathological denominators in SOD1 and TDP43 ALS mouse models. *Hum Mol Genet*, 23(6), 1413-1424. <https://doi.org/10.1093/hmg/ddt528>
- Magrane, J., Sahawneh, M. A., Przedborski, S., Estevez, A. G., & Manfredi, G. (2012). Mitochondrial dynamics and bioenergetic dysfunction is associated with synaptic alterations in mutant SOD1 motor neurons. *J Neurosci*, 32(1), 229-242. <https://doi.org/10.1523/JNEUROSCI.1233-11.2012>
- Mahar, M., & Cavalli, V. (2018). Intrinsic mechanisms of neuronal axon regeneration. *Nat Rev Neurosci*, 19(6), 323-337. <https://doi.org/10.1038/s41583-018-0001-8>
- Mandal, A., Wong, H. C., Pinter, K., Mosqueda, N., Beirl, A., Lomash, R. M., Won, S., Kindt, K. S., & Drerup, C. M. (2021). Retrograde Mitochondrial Transport Is Essential for Organelle Distribution and

- Health in Zebrafish Neurons. *J Neurosci*, 41(7), 1371-1392. <https://doi.org/10.1523/JNEUROSCI.1316-20.2020>
- Mannella, C. A. (2006). The relevance of mitochondrial membrane topology to mitochondrial function. *Biochim Biophys Acta*, 1762(2), 140-147. <https://doi.org/10.1016/j.bbadis.2005.07.001>
- Mannella, C. A., Lederer, W. J., & Jafri, M. S. (2013). The connection between inner membrane topology and mitochondrial function. *J Mol Cell Cardiol*, 62, 51-57. <https://doi.org/10.1016/j.yjmcc.2013.05.001>
- Mao, K., Wang, K., Liu, X., & Klionsky, D. J. (2013). The scaffold protein Atg11 recruits fission machinery to drive selective mitochondria degradation by autophagy. *Dev Cell*, 26(1), 9-18. <https://doi.org/10.1016/j.devcel.2013.05.024>
- Mariano, V., Dominguez-Iturza, N., Neukomm, L. J., & Bagni, C. (2018). Maintenance mechanisms of circuit-integrated axons. *Curr Opin Neurobiol*, 53, 162-173. <https://doi.org/10.1016/j.conb.2018.08.007>
- Marinkovic, P., Godinho, L., & Misgeld, T. (2015a). Generation and Screening of Transgenic Mice with Neuronal Labeling Controlled by Thy1 Regulatory Elements. *Cold Spring Harb Protoc*, 2015(10), 875-882. <https://doi.org/10.1101/pdb.top087668>
- Marinkovic, P., Godinho, L., & Misgeld, T. (2015b). Generation of Thy1 Constructs for Pronuclear Injection. *Cold Spring Harb Protoc*, 2015(10), 937-940. <https://doi.org/10.1101/pdb.prot087676>
- Marinkovic, P., Godinho, L., & Misgeld, T. (2015c). Generation of Tissue Sections for Screening Thy1 Mouse Lines. *Cold Spring Harb Protoc*, 2015(9), pdb prot087684. <https://doi.org/10.1101/pdb.prot087684>
- Marinkovic, P., Reuter, M. S., Brill, M. S., Godinho, L., Kerschensteiner, M., & Misgeld, T. (2012). Axonal transport deficits and degeneration can evolve independently in mouse models of amyotrophic lateral sclerosis. *Proc Natl Acad Sci U S A*, 109(11), 4296-4301. <https://doi.org/10.1073/pnas.1200658109>
- Markovinovic, A., Cimbro, R., Ljutic, T., Kriz, J., Rogelj, B., & Munitic, I. (2017). Optineurin in amyotrophic lateral sclerosis: Multifunctional adaptor protein at the crossroads of different neuroprotective mechanisms. *Prog Neurobiol*, 154, 1-20. <https://doi.org/10.1016/j.pneurobio.2017.04.005>
- Markovinovic, A., Ljutic, T., Beland, L. C., & Munitic, I. (2018). Optineurin Insufficiency Disbalances Proinflammatory and Anti-inflammatory Factors by Reducing Microglial IFN-beta Responses. *Neuroscience*, 388, 139-151. <https://doi.org/10.1016/j.neuroscience.2018.07.007>
- Martijn, J., Vosseberg, J., Guy, L., Offre, P., & Ettema, T. J. G. (2018). Deep mitochondrial origin outside the sampled alphaproteobacteria. *Nature*, 557(7703), 101-105. <https://doi.org/10.1038/s41586-018-0059-5>
- Martin, J., Mahlke, K., & Pfanner, N. (1991). Role of an energized inner membrane in mitochondrial protein import. Delta psi drives the movement of presequences. *J Biol Chem*, 266(27), 18051-18057. <https://www.ncbi.nlm.nih.gov/pubmed/1833391>
- Maruyama, H., Morino, H., Ito, H., Izumi, Y., Kato, H., Watanabe, Y., Kinoshita, Y., Kamada, M., Nodera, H., Suzuki, H., Komure, O., Matsuura, S., Kobatake, K., Morimoto, N., Abe, K., Suzuki, N., Aoki, M., Kawata, A., Hirai, T., . . . Kawakami, H. (2010). Mutations of optineurin in amyotrophic lateral sclerosis. *Nature*, 465(7295), 223-226. <https://doi.org/10.1038/nature08971>
- Matsuda, N., Sato, S., Shiba, K., Okatsu, K., Saisho, K., Gautier, C. A., Sou, Y. S., Saiki, S., Kawajiri, S., Sato, F., Kimura, M., Komatsu, M., Hattori, N., & Tanaka, K. (2010). PINK1 stabilized by

- mitochondrial depolarization recruits Parkin to damaged mitochondria and activates latent Parkin for mitophagy. *J Cell Biol*, 189(2), 211-221. <https://doi.org/10.1083/jcb.200910140>
- Matsuda, W., Furuta, T., Nakamura, K. C., Hioki, H., Fujiyama, F., Arai, R., & Kaneko, T. (2009). Single nigrostriatal dopaminergic neurons form widely spread and highly dense axonal arborizations in the neostriatum. *J Neurosci*, 29(2), 444-453. <https://doi.org/10.1523/JNEUROSCI.4029-08.2009>
- McKenzie, M., Lazarou, M., & Ryan, M. T. (2009). Chapter 18 Analysis of respiratory chain complex assembly with radiolabeled nuclear- and mitochondrial-encoded subunits. *Methods Enzymol*, 456, 321-339. [https://doi.org/10.1016/S0076-6879\(08\)04418-2](https://doi.org/10.1016/S0076-6879(08)04418-2)
- McWilliams, T. G., Prescott, A. R., Montava-Garriga, L., Ball, G., Singh, F., Barini, E., Muqit, M. M. K., Brooks, S. P., & Ganley, I. G. (2018). Basal Mitophagy Occurs Independently of PINK1 in Mouse Tissues of High Metabolic Demand. *Cell Metab*, 27(2), 439-449 e435. <https://doi.org/10.1016/j.cmet.2017.12.008>
- Mead, R. J., Shan, N., Reiser, H. J., Marshall, F., & Shaw, P. J. (2023). Amyotrophic lateral sclerosis: a neurodegenerative disorder poised for successful therapeutic translation. *Nat Rev Drug Discov*, 22(3), 185-212. <https://doi.org/10.1038/s41573-022-00612-2>
- Mears, J. A., Lackner, L. L., Fang, S., Ingerman, E., Nunnari, J., & Hinshaw, J. E. (2011). Conformational changes in Dnm1 support a contractile mechanism for mitochondrial fission. *Nat Struct Mol Biol*, 18(1), 20-26. <https://doi.org/10.1038/nsmb.1949>
- Medeiros, D. M. (2008). Assessing mitochondria biogenesis. *Methods*, 46(4), 288-294. <https://doi.org/10.1016/j.ymeth.2008.09.026>
- Meeusen, S., McCaffery, J. M., & Nunnari, J. (2004). Mitochondrial fusion intermediates revealed in vitro. *Science*, 305(5691), 1747-1752. <https://doi.org/10.1126/science.1100612>
- Meftah, S., & Gan, J. (2023). Alzheimer's disease as a synaptopathy: Evidence for dysfunction of synapses during disease progression. *Front Synaptic Neurosci*, 15, 1129036. <https://doi.org/10.3389/fnsyn.2023.1129036>
- Meirovitch, Y., Kang, K., Draft, R. W., Pavarino, E. C., Echeverri, M. F. H., Yang, F., Turney, S. G., Berger, D. R., Peleg, A., Montero-Crespo, M., Schalek, R. L., Lu, J., Livet, J., Tapia, J.-C., & Lichtman, J. W. (2023). Neuromuscular connectomes across development reveal synaptic ordering rules. *bioRxiv*, 2021.2009.2020.460480. <https://doi.org/10.1101/2021.09.20.460480>
- Menzies, R. A., & Gold, P. H. (1971). The turnover of mitochondria in a variety of tissues of young adult and aged rats. *J Biol Chem*, 246(8), 2425-2429. <https://www.ncbi.nlm.nih.gov/pubmed/5553400>
- Menzies, R. A., & Gold, P. H. (1972). The apparent turnover of mitochondria, ribosomes and sRNA of the brain in young adult and aged rats. *J Neurochem*, 19(7), 1671-1683. <https://doi.org/10.1111/j.1471-4159.1972.tb06212.x>
- Miller, B. F., & Hamilton, K. L. (2012). A perspective on the determination of mitochondrial biogenesis. *Am J Physiol Endocrinol Metab*, 302(5), E496-499. <https://doi.org/10.1152/ajpendo.00578.2011>
- Miller, K. E., & Sheetz, M. P. (2004). Axonal mitochondrial transport and potential are correlated. *J Cell Sci*, 117(Pt 13), 2791-2804. <https://doi.org/10.1242/jcs.01130>
- Milton, V. J., & Sweeney, S. T. (2012). Oxidative stress in synapse development and function. *Dev Neurobiol*, 72(1), 100-110. <https://doi.org/10.1002/dneu.20957>
- Minakaki, G., Krainc, D., & Burbulla, L. F. (2020). The Convergence of Alpha-Synuclein, Mitochondrial, and Lysosomal Pathways in Vulnerability of Midbrain Dopaminergic Neurons in Parkinson's Disease. *Front Cell Dev Biol*, 8, 580634. <https://doi.org/10.3389/fcell.2020.580634>

- Mink, J. W., Blumenshine, R. J., & Adams, D. B. (1981). Ratio of central nervous system to body metabolism in vertebrates: its constancy and functional basis. *Am J Physiol*, 241(3), R203-212. <https://doi.org/10.1152/ajpregu.1981.241.3.R203>
- Misgeld, T., Kerschensteiner, M., Bareyre, F. M., Burgess, R. W., & Lichtman, J. W. (2007). Imaging axonal transport of mitochondria in vivo. *Nat Methods*, 4(7), 559-561. <https://doi.org/10.1038/nmeth1055>
- Misgeld, T., & Schwarz, T. L. (2017). Mitostasis in Neurons: Maintaining Mitochondria in an Extended Cellular Architecture. *Neuron*, 96(3), 651-666. <https://doi.org/10.1016/j.neuron.2017.09.055>
- Mishra, P., Carelli, V., Manfredi, G., & Chan, D. C. (2014). Proteolytic cleavage of Opa1 stimulates mitochondrial inner membrane fusion and couples fusion to oxidative phosphorylation. *Cell Metab*, 19(4), 630-641. <https://doi.org/10.1016/j.cmet.2014.03.011>
- Misko, A., Jiang, S., Wegorzewska, I., Milbrandt, J., & Baloh, R. H. (2010). Mitofusin 2 is necessary for transport of axonal mitochondria and interacts with the Miro/Milton complex. *J Neurosci*, 30(12), 4232-4240. <https://doi.org/10.1523/JNEUROSCI.6248-09.2010>
- Misko, A. L., Sasaki, Y., Tuck, E., Milbrandt, J., & Baloh, R. H. (2012). Mitofusin2 mutations disrupt axonal mitochondrial positioning and promote axon degeneration. *J Neurosci*, 32(12), 4145-4155. <https://doi.org/10.1523/JNEUROSCI.6338-11.2012>
- Miterko, L. N., Lackey, E. P., Heck, D. H., & Sillitoe, R. V. (2018). Shaping Diversity Into the Brain's Form and Function. *Front Neural Circuits*, 12, 83. <https://doi.org/10.3389/fncir.2018.00083>
- Miwa, S., Lawless, C., & von Zglinicki, T. (2010). Correction of radiolabel pulse-chase data by a mathematical model: application to mitochondrial turnover studies. *Biochem Soc Trans*, 38(5), 1322-1328. <https://doi.org/10.1042/BST0381322>
- Mizushima, N., Yamamoto, A., Matsui, M., Yoshimori, T., & Ohsumi, Y. (2004). In vivo analysis of autophagy in response to nutrient starvation using transgenic mice expressing a fluorescent autophagosome marker. *Mol Biol Cell*, 15(3), 1101-1111. <https://doi.org/10.1091/mbc.E03-09-0704>
- Monzel, A. S., Enriquez, J. A., & Picard, M. (2023). Multifaceted mitochondria: moving mitochondrial science beyond function and dysfunction. *Nat Metab*, 5(4), 546-562. <https://doi.org/10.1038/s42255-023-00783-1>
- Morris, R. L., & Hollenbeck, P. J. (1995). Axonal transport of mitochondria along microtubules and F-actin in living vertebrate neurons. *J Cell Biol*, 131(5), 1315-1326. <https://doi.org/10.1083/jcb.131.5.1315>
- Muller-Deku, A., Meiring, J. C. M., Loy, K., Kraus, Y., Heise, C., Bingham, R., Jansen, K. I., Qu, X., Bartolini, F., Kapitein, L. C., Akhmanova, A., Ahlfeld, J., Trauner, D., & Thorn-Seshold, O. (2020). Photoswitchable paclitaxel-based microtubule stabilisers allow optical control over the microtubule cytoskeleton. *Nat Commun*, 11(1), 4640. <https://doi.org/10.1038/s41467-020-18389-6>
- Munitic, I., Giardino Torchia, M. L., Meena, N. P., Zhu, G., Li, C. C., & Ashwell, J. D. (2013). Optineurin insufficiency impairs IRF3 but not NF-kappaB activation in immune cells. *J Immunol*, 191(12), 6231-6240. <https://doi.org/10.4049/jimmunol.1301696>
- Munn, E. A. (1974). *The structure of mitochondria*. Academic Press.
- Nakada, C., Ritchie, K., Oba, Y., Nakamura, M., Hotta, Y., Iino, R., Kasai, R. S., Yamaguchi, K., Fujiwara, T., & Kusumi, A. (2003). Accumulation of anchored proteins forms membrane diffusion barriers during neuronal polarization. *Nat Cell Biol*, 5(7), 626-632. <https://doi.org/10.1038/ncb1009>
- Nakagawa, T., Tanaka, Y., Matsuoka, E., Kondo, S., Okada, Y., Noda, Y., Kanai, Y., & Hirokawa, N. (1997). Identification and classification of 16 new kinesin superfamily (KIF) proteins in mouse

- genome. *Proc Natl Acad Sci U S A*, 94(18), 9654-9659. <https://www.ncbi.nlm.nih.gov/pubmed/9275178>
- Nakazawa, S., Oikawa, D., Ishii, R., Ayaki, T., Takahashi, H., Takeda, H., Ishitani, R., Kamei, K., Takeyoshi, I., Kawakami, H., Iwai, K., Hatada, I., Sawasaki, T., Ito, H., Nureki, O., & Tokunaga, F. (2016). Linear ubiquitination is involved in the pathogenesis of optineurin-associated amyotrophic lateral sclerosis. *Nat Commun*, 7, 12547. <https://doi.org/10.1038/ncomms12547>
- Nangaku, M., Sato-Yoshitake, R., Okada, Y., Noda, Y., Takemura, R., Yamazaki, H., & Hirokawa, N. (1994). KIF1B, a novel microtubule plus end-directed monomeric motor protein for transport of mitochondria. *Cell*, 79(7), 1209-1220. <https://www.ncbi.nlm.nih.gov/pubmed/7528108>
- Narendra, D., Tanaka, A., Suen, D. F., & Youle, R. J. (2008). Parkin is recruited selectively to impaired mitochondria and promotes their autophagy. *J Cell Biol*, 183(5), 795-803. <https://doi.org/10.1083/jcb.200809125>
- Narendra, D. P., Jin, S. M., Tanaka, A., Suen, D. F., Gautier, C. A., Shen, J., Cookson, M. R., & Youle, R. J. (2010). PINK1 is selectively stabilized on impaired mitochondria to activate Parkin. *PLoS Biol*, 8(1), e1000298. <https://doi.org/10.1371/journal.pbio.1000298>
- Nave, K. A. (2010). Myelination and support of axonal integrity by glia. *Nature*, 468(7321), 244-252. <https://doi.org/10.1038/nature09614>
- Neisch, A. L., Neufeld, T. P., & Hays, T. S. (2017). A STRIPAK complex mediates axonal transport of autophagosomes and dense core vesicles through PP2A regulation. *J Cell Biol*, 216(2), 441-461. <https://doi.org/10.1083/jcb.201606082>
- Neupert, W. (2012). SnapShot: Mitochondrial architecture. *Cell*, 149(3), 722-722 e721. <https://doi.org/10.1016/j.cell.2012.04.010>
- Neupert, W., & Herrmann, J. M. (2007). Translocation of proteins into mitochondria. *Annu Rev Biochem*, 76, 723-749. <https://doi.org/10.1146/annurev.biochem.76.052705.163409>
- Nicholls, D. G. (2004). Mitochondrial membrane potential and aging. *Aging Cell*, 3(1), 35-40. <https://doi.org/10.1111/j.1474-9728.2003.00079.x>
- Nicholls, D. G., & Ferguson, S. J. (2013). *Bioenergetics* (Fourth edition / ed.). Academic Press, Elsevier.
- Nikic, I., Merkler, D., Sorbara, C., Brinkoetter, M., Kreutzfeldt, M., Bareyre, F. M., Bruck, W., Bishop, D., Misgeld, T., & Kerschensteiner, M. (2011). A reversible form of axon damage in experimental autoimmune encephalomyelitis and multiple sclerosis. *Nat Med*, 17(4), 495-499. <https://doi.org/10.1038/nm.2324>
- Nikoletopoulou, V., & Tavernarakis, N. (2018). Regulation and Roles of Autophagy at Synapses. *Trends Cell Biol*, 28(8), 646-661. <https://doi.org/10.1016/j.tcb.2018.03.006>
- Nunnari, J., Marshall, W. F., Straight, A., Murray, A., Sedat, J. W., & Walter, P. (1997). Mitochondrial transmission during mating in *Saccharomyces cerevisiae* is determined by mitochondrial fusion and fission and the intramitochondrial segregation of mitochondrial DNA. *Mol Biol Cell*, 8(7), 1233-1242. <https://doi.org/10.1091/mbc.8.7.1233>
- Nunnari, J., & Suomalainen, A. (2012). Mitochondria: in sickness and in health. *Cell*, 148(6), 1145-1159. <https://doi.org/10.1016/j.cell.2012.02.035>
- O'Brien, K. D., & Tian, R. (2021). Boosting mitochondrial metabolism with dietary supplements in heart failure. *Nat Rev Cardiol*, 18(10), 685-686. <https://doi.org/10.1038/s41569-021-00610-8>
- O'Rourke, B. (2010). From bioblasts to mitochondria: ever expanding roles of mitochondria in cell physiology. *Front Physiol*, 1, 7. <https://doi.org/10.3389/fphys.2010.00007>

- Oeding, S. J., Majstrowicz, K., Hu, X. P., Schwarz, V., Freitag, A., Honnert, U., Nikolaus, P., & Bahler, M. (2018). Identification of Miro1 and Miro2 as mitochondrial receptors for myosin XIX. *J Cell Sci*, 131(17). <https://doi.org/10.1242/jcs.219469>
- Ohno, N., Kidd, G. J., Mahad, D., Kiryu-Seo, S., Avishai, A., Komuro, H., & Trapp, B. D. (2011). Myelination and axonal electrical activity modulate the distribution and motility of mitochondria at CNS nodes of Ranvier. *J Neurosci*, 31(20), 7249-7258. <https://doi.org/10.1523/JNEUROSCI.0095-11.2011>
- Ohsumi, Y. (1999). Molecular mechanism of autophagy in yeast, *Saccharomyces cerevisiae*. *Philos Trans R Soc Lond B Biol Sci*, 354(1389), 1577-1580; discussion 1580-1571. <https://doi.org/10.1098/rstb.1999.0501>
- Ohsumi, Y. (2014). Historical landmarks of autophagy research. *Cell Res*, 24(1), 9-23. <https://doi.org/10.1038/cr.2013.169>
- Orr, B. O., Hauswirth, A. G., Celona, B., Fetter, R. D., Zunino, G., Kvon, E. Z., Zhu, Y., Pennacchio, L. A., Black, B. L., & Davis, G. W. (2020). Presynaptic Homeostasis Opposes Disease Progression in Mouse Models of ALS-Like Degeneration: Evidence for Homeostatic Neuroprotection. *Neuron*, 107(1), 95-111 e116. <https://doi.org/10.1016/j.neuron.2020.04.009>
- Otera, H., Wang, C., Cleland, M. M., Setoguchi, K., Yokota, S., Youle, R. J., & Mihara, K. (2010). Mff is an essential factor for mitochondrial recruitment of Drp1 during mitochondrial fission in mammalian cells. *J Cell Biol*, 191(6), 1141-1158. <https://doi.org/10.1083/jcb.201007152>
- Overly, C. C., Rieff, H. I., & Hollenbeck, P. J. (1996). Organelle motility and metabolism in axons vs dendrites of cultured hippocampal neurons. *J Cell Sci*, 109 (Pt 5), 971-980. <https://doi.org/10.1242/jcs.109.5.971>
- Pacelli, C., Giguere, N., Bourque, M. J., Levesque, M., Slack, R. S., & Trudeau, L. E. (2015). Elevated Mitochondrial Bioenergetics and Axonal Arborization Size Are Key Contributors to the Vulnerability of Dopamine Neurons. *Curr Biol*, 25(18), 2349-2360. <https://doi.org/10.1016/j.cub.2015.07.050>
- Pagliarini, D. J., Calvo, S. E., Chang, B., Sheth, S. A., Vafai, S. B., Ong, S. E., Walford, G. A., Sugiana, C., Boneh, A., Chen, W. K., Hill, D. E., Vidal, M., Evans, J. G., Thorburn, D. R., Carr, S. A., & Mootha, V. K. (2008). A mitochondrial protein compendium elucidates complex I disease biology. *Cell*, 134(1), 112-123. <https://doi.org/10.1016/j.cell.2008.06.016>
- Palade, G. E. (1952). The fine structure of mitochondria. *Anat Rec*, 114(3), 427-451. <https://doi.org/10.1002/ar.1091140304>
- Palikaras, K., Lionaki, E., & Tavernarakis, N. (2018). Mechanisms of mitophagy in cellular homeostasis, physiology and pathology. *Nat Cell Biol*, 20(9), 1013-1022. <https://doi.org/10.1038/s41556-018-0176-2>
- Palmer, C. S., Osellame, L. D., Laine, D., Koutsopoulos, O. S., Frazier, A. E., & Ryan, M. T. (2011). MiD49 and MiD51, new components of the mitochondrial fission machinery. *EMBO Rep*, 12(6), 565-573. <https://doi.org/10.1038/embor.2011.54>
- Paquet, D., Plucinska, G., & Misgeld, T. (2014). In vivo imaging of mitochondria in intact zebrafish larvae. *Methods Enzymol*, 547, 151-164. <https://doi.org/10.1016/B978-0-12-801415-8.00009-6>
- Parone, P. A., Da Cruz, S., Tondera, D., Mattenberger, Y., James, D. I., Maechler, P., Barja, F., & Martinou, J. C. (2008). Preventing mitochondrial fission impairs mitochondrial function and leads to loss of mitochondrial DNA. *PLoS One*, 3(9), e3257. <https://doi.org/10.1371/journal.pone.0003257>
- Parton, R. G., & Dotti, C. G. (1993). Cell biology of neuronal endocytosis. *J Neurosci Res*, 36(1), 1-9. <https://doi.org/10.1002/jnr.490360102>

- Parton, R. G., Simons, K., & Dotti, C. G. (1992). Axonal and dendritic endocytic pathways in cultured neurons. *J Cell Biol*, 119(1), 123-137. <https://doi.org/10.1083/jcb.119.1.123>
- Pasquini, J. M., Krawiec, L., & Soto, E. F. (1973). Turnover of phosphatidylcholine in cell membranes of adult rat brain. *J Neurochem*, 21(3), 647-653. <https://doi.org/10.1111/j.1471-4159.1973.tb06009.x>
- Patterson, G. H., & Lippincott-Schwartz, J. (2002). A photoactivatable GFP for selective photolabeling of proteins and cells. *Science*, 297(5588), 1873-1877. <https://doi.org/10.1126/science.1074952>
- Pekkurnaz, G., Trinidad, J. C., Wang, X., Kong, D., & Schwarz, T. L. (2014). Glucose regulates mitochondrial motility via Milton modification by O-GlcNAc transferase. *Cell*, 158(1), 54-68. <https://doi.org/10.1016/j.cell.2014.06.007>
- Pekkurnaz, G., & Wang, X. (2022). Mitochondrial heterogeneity and homeostasis through the lens of a neuron. *Nat Metab*. <https://doi.org/10.1038/s42255-022-00594-w>
- Pfanner, N., Warscheid, B., & Wiedemann, N. (2019). Mitochondrial proteins: from biogenesis to functional networks. *Nat Rev Mol Cell Biol*, 20(5), 267-284. <https://doi.org/10.1038/s41580-018-0092-0>
- Pham, A. H., McCaffery, J. M., & Chan, D. C. (2012). Mouse lines with photo-activatable mitochondria to study mitochondrial dynamics. *Genesis*, 50(11), 833-843. <https://doi.org/10.1002/dvg.22050>
- Phinney, D. G., Di Giuseppe, M., Njah, J., Sala, E., Shiva, S., St Croix, C. M., Stolz, D. B., Watkins, S. C., Di, Y. P., Leikauf, G. D., Kolls, J., Riches, D. W., Deiuliis, G., Kaminski, N., Boregowda, S. V., McKenna, D. H., & Ortiz, L. A. (2015). Mesenchymal stem cells use extracellular vesicles to outsource mitophagy and shuttle microRNAs. *Nat Commun*, 6, 8472. <https://doi.org/10.1038/ncomms9472>
- Picard, M., & McEwen, B. S. (2014). Mitochondria impact brain function and cognition. *Proc Natl Acad Sci U S A*, 111(1), 7-8. <https://doi.org/10.1073/pnas.1321881111>
- Picard, M., Shiriha, O. S., Gentil, B. J., & Burelle, Y. (2013). Mitochondrial morphology transitions and functions: implications for retrograde signaling? *Am J Physiol Regul Integr Comp Physiol*, 304(6), R393-406. <https://doi.org/10.1152/ajpregu.00584.2012>
- Piccoli, G., Verpelli, C., Tonna, N., Romorini, S., Alessio, M., Nairn, A. C., Bachi, A., & Sala, C. (2007). Proteomic analysis of activity-dependent synaptic plasticity in hippocampal neurons. *J Proteome Res*, 6(8), 3203-3215. <https://doi.org/10.1021/pr0701308>
- Pickrell, A. M., & Youle, R. J. (2015). The roles of PINK1, parkin, and mitochondrial fidelity in Parkinson's disease. *Neuron*, 85(2), 257-273. <https://doi.org/10.1016/j.neuron.2014.12.007>
- Pilli, M., Arko-Mensah, J., Ponpuak, M., Roberts, E., Master, S., Mandell, M. A., Dupont, N., Ornatowski, W., Jiang, S., Bradfute, S. B., Bruun, J. A., Hansen, T. E., Johansen, T., & Deretic, V. (2012). TBK-1 promotes autophagy-mediated antimicrobial defense by controlling autophagosome maturation. *Immunity*, 37(2), 223-234. <https://doi.org/10.1016/j.immuni.2012.04.015>
- Pilling, A. D., Horiuchi, D., Lively, C. M., & Saxton, W. M. (2006). Kinesin-1 and Dynein are the primary motors for fast transport of mitochondria in Drosophila motor axons. *Mol Biol Cell*, 17(4), 2057-2068. <https://doi.org/10.1091/mbc.e05-06-0526>
- Ploumi, C., Daskalaki, I., & Tavernarakis, N. (2017). Mitochondrial biogenesis and clearance: a balancing act. *FEBS J*, 284(2), 183-195. <https://doi.org/10.1111/febs.13820>
- Plucinska, G., & Misgeld, T. (2016). Imaging of neuronal mitochondria in situ. *Curr Opin Neurobiol*, 39, 152-163. <https://doi.org/10.1016/j.conb.2016.06.006>

- Plucinska, G., Paquet, D., Hruscha, A., Godinho, L., Haass, C., Schmid, B., & Misgeld, T. (2012). In vivo imaging of disease-related mitochondrial dynamics in a vertebrate model system. *J Neurosci*, 32(46), 16203-16212. <https://doi.org/10.1523/JNEUROSCI.1327-12.2012>
- Poliak, S., & Peles, E. (2003). The local differentiation of myelinated axons at nodes of Ranvier. *Nat Rev Neurosci*, 4(12), 968-980. <https://doi.org/10.1038/nrn1253>
- Popov, L. D. (2020). Mitochondrial biogenesis: An update. *J Cell Mol Med*, 24(9), 4892-4899. <https://doi.org/10.1111/jcmm.15194>
- Popov, V., Medvedev, N. I., Davies, H. A., & Stewart, M. G. (2005). Mitochondria form a filamentous reticular network in hippocampal dendrites but are present as discrete bodies in axons: a three-dimensional ultrastructural study. *J Comp Neurol*, 492(1), 50-65. <https://doi.org/10.1002/cne.20682>
- Pourcelot, M., Zemirli, N., Silva Da Costa, L., Loyant, R., Garcin, D., Vitour, D., Munitic, I., Vazquez, A., & Arnoult, D. (2016). The Golgi apparatus acts as a platform for TBK1 activation after viral RNA sensing. *BMC Biol*, 14, 69. <https://doi.org/10.1186/s12915-016-0292-z>
- Praefcke, G. J., & McMahon, H. T. (2004). The dynamin superfamily: universal membrane tubulation and fission molecules? *Nat Rev Mol Cell Biol*, 5(2), 133-147. <https://doi.org/10.1038/nrm1313>
- Protasoni, M., & Zeviani, M. (2021). Mitochondrial Structure and Bioenergetics in Normal and Disease Conditions. *Int J Mol Sci*, 22(2). <https://doi.org/10.3390/ijms22020586>
- Qi, Y., Yan, L., Yu, C., Guo, X., Zhou, X., Hu, X., Huang, X., Rao, Z., Lou, Z., & Hu, J. (2016). Structures of human mitofusin 1 provide insight into mitochondrial tethering. *J Cell Biol*, 215(5), 621-629. <https://doi.org/10.1083/jcb.201609019>
- Quintana-Cabrera, R., & Scorrano, L. (2023). Determinants and outcomes of mitochondrial dynamics. *Mol Cell*, 83(6), 857-876. <https://doi.org/10.1016/j.molcel.2023.02.012>
- Quintero, O. A., DiVito, M. M., Adikes, R. C., Kortan, M. B., Case, L. B., Lier, A. J., Panaretos, N. S., Slater, S. Q., Rengarajan, M., Feliu, M., & Cheney, R. E. (2009). Human Myo19 is a novel myosin that associates with mitochondria. *Curr Biol*, 19(23), 2008-2013. <https://doi.org/10.1016/j.cub.2009.10.026>
- Rai, A., Pathak, D., Thakur, S., Singh, S., Dubey, A. K., & Mallik, R. (2016). Dynein Clusters into Lipid Microdomains on Phagosomes to Drive Rapid Transport toward Lysosomes. *Cell*, 164(4), 722-734. <https://doi.org/10.1016/j.cell.2015.12.054>
- Rai, A. K., Rai, A., Ramaiya, A. J., Jha, R., & Mallik, R. (2013). Molecular adaptations allow dynein to generate large collective forces inside cells. *Cell*, 152(1-2), 172-182. <https://doi.org/10.1016/j.cell.2012.11.044>
- Ramon y Cajal, S. (1928). *Degeneration and regeneration of the nervous system*. Clarendon Press.
- Rangaraju, V., Calloway, N., & Ryan, T. A. (2014). Activity-driven local ATP synthesis is required for synaptic function. *Cell*, 156(4), 825-835. <https://doi.org/10.1016/j.cell.2013.12.042>
- Rangaraju, V., Lauterbach, M., & Schuman, E. M. (2019). Spatially Stable Mitochondrial Compartments Fuel Local Translation during Plasticity. *Cell*, 176(1-2), 73-84 e15. <https://doi.org/10.1016/j.cell.2018.12.013>
- Rangaraju, V., Tom Dieck, S., & Schuman, E. M. (2017). Local translation in neuronal compartments: how local is local? *EMBO Rep*, 18(5), 693-711. <https://doi.org/10.15252/embr.201744045>
- Rath, S., Sharma, R., Gupta, R., Ast, T., Chan, C., Durham, T. J., Goodman, R. P., Grabarek, Z., Haas, M. E., Hung, W. H. W., Joshi, P. R., Jourdain, A. A., Kim, S. H., Kotrys, A. V., Lam, S. S., McCoy, J. G., Meisel, J. D., Miranda, M., Panda, A., . . . Mootha, V. K. (2021). MitoCarta3.0: an updated mitochondrial proteome now with sub-organelle localization and pathway annotations. *Nucleic Acids Res*, 49(D1), D1541-D1547. <https://doi.org/10.1093/nar/gkaa1011>

- Richards, S. E. V., & Van Hooser, S. D. (2018). Neural architecture: from cells to circuits. *J Neurophysiol*, 120(2), 854-866. <https://doi.org/10.1152/jn.00044.2018>
- Richter, B., Sliter, D. A., Herhaus, L., Stolz, A., Wang, C., Beli, P., Zaffagnini, G., Wild, P., Martens, S., Wagner, S. A., Youle, R. J., & Dikic, I. (2016). Phosphorylation of OPTN by TBK1 enhances its binding to Ub chains and promotes selective autophagy of damaged mitochondria. *Proc Natl Acad Sci U S A*, 113(15), 4039-4044. <https://doi.org/10.1073/pnas.1523926113>
- Rishal, I., & Fainzilber, M. (2014). Axon-soma communication in neuronal injury. *Nat Rev Neurosci*, 15(1), 32-42. <https://doi.org/10.1038/nrn3609>
- Rizzuto, R., & Pozzan, T. (2006). Microdomains of intracellular Ca²⁺: molecular determinants and functional consequences. *Physiol Rev*, 86(1), 369-408. <https://doi.org/10.1152/physrev.00004.2005>
- Roberts, A. J., Kon, T., Knight, P. J., Sutoh, K., & Burgess, S. A. (2013). Functions and mechanics of dynein motor proteins. *Nat Rev Mol Cell Biol*, 14(11), 713-726. <https://doi.org/10.1038/nrm3667>
- Rocha, A. G., Franco, A., Krezel, A. M., Rumsey, J. M., Alberti, J. M., Knight, W. C., Biris, N., Zacharioudakis, E., Janetka, J. W., Baloh, R. H., Kitsis, R. N., Mochly-Rosen, D., Townsend, R. R., Gavathiotis, E., & Dorn, G. W., 2nd. (2018). MFN2 agonists reverse mitochondrial defects in preclinical models of Charcot-Marie-Tooth disease type 2A. *Science*, 360(6386), 336-341. <https://doi.org/10.1126/science.aao1785>
- Roger, A. J., Munoz-Gomez, S. A., & Kamikawa, R. (2017). The Origin and Diversification of Mitochondria. *Curr Biol*, 27(21), R1177-R1192. <https://doi.org/10.1016/j.cub.2017.09.015>
- Rogers, R. S., Tungtur, S., Tanaka, T., Nadeau, L. L., Badawi, Y., Wang, H., Ni, H. M., Ding, W. X., & Nishimune, H. (2017). Impaired Mitophagy Plays a Role in Denervation of Neuromuscular Junctions in ALS Mice. *Front Neurosci*, 11, 473. <https://doi.org/10.3389/fnins.2017.00473>
- Rojansky, R., Cha, M. Y., & Chan, D. C. (2016). Elimination of paternal mitochondria in mouse embryos occurs through autophagic degradation dependent on PARKIN and MUL1. *Elife*, 5. <https://doi.org/10.7554/eLife.17896>
- Rojo, M., Legros, F., Chateau, D., & Lombes, A. (2002). Membrane topology and mitochondrial targeting of mitofusins, ubiquitous mammalian homologs of the transmembrane GTPase Fzo. *J Cell Sci*, 115(Pt 8), 1663-1674. <https://doi.org/10.1242/jcs.115.8.1663>
- Rolfe, D. F., & Brown, G. C. (1997). Cellular energy utilization and molecular origin of standard metabolic rate in mammals. *Physiol Rev*, 77(3), 731-758. <https://doi.org/10.1152/physrev.1997.77.3.731>
- Rosenberg, A. M., Saggari, M., Monzel, A. S., Devine, J., Rogu, P., Limoges, A., Junker, A., Sandi, C., Mosharov, E. V., Dumitriu, D., Anacker, C., & Picard, M. (2023). Brain mitochondrial diversity and network organization predict anxiety-like behavior in male mice. *Nat Commun*, 14(1), 4726. <https://doi.org/10.1038/s41467-023-39941-0>
- Rossi, J., Balthasar, N., Olson, D., Scott, M., Berglund, E., Lee, C. E., Choi, M. J., Lauzon, D., Lowell, B. B., & Elmquist, J. K. (2011). Melanocortin-4 receptors expressed by cholinergic neurons regulate energy balance and glucose homeostasis. *Cell Metab*, 13(2), 195-204. <https://doi.org/10.1016/j.cmet.2011.01.010>
- Rowland, K. C., Irby, N. K., & Spirou, G. A. (2000). Specialized synapse-associated structures within the calyx of Held. *J Neurosci*, 20(24), 9135-9144. <https://doi.org/10.1523/JNEUROSCI.20-24-09135.2000>
- Roy, S. (2020). Finding order in slow axonal transport. *Curr Opin Neurobiol*, 63, 87-94. <https://doi.org/10.1016/j.conb.2020.03.015>

- Roy, S., Yang, G., Tang, Y., & Scott, D. A. (2011). A simple photoactivation and image analysis module for visualizing and analyzing axonal transport with high temporal resolution. *Nat Protoc*, 7(1), 62-68. <https://doi.org/10.1038/nprot.2011.428>
- Rubenstein, J. L. R., & Rakic, P. (2013). *Comprehensive developmental neuroscience : patterning and cell type specification in the developing CNS and PNS* (First edition. ed.). Elsevier/Academic Press.
- Rugarli, E. I., & Langer, T. (2012). Mitochondrial quality control: a matter of life and death for neurons. *EMBO J*, 31(6), 1336-1349. <https://doi.org/10.1038/emboj.2012.38>
- Ryan, M. T., & Hoogenraad, N. J. (2007). Mitochondrial-nuclear communications. *Annu Rev Biochem*, 76, 701-722. <https://doi.org/10.1146/annurev.biochem.76.052305.091720>
- Ryan, T. A., & Tumbarello, D. A. (2018). Optineurin: A Coordinator of Membrane-Associated Cargo Trafficking and Autophagy. *Front Immunol*, 9, 1024. <https://doi.org/10.3389/fimmu.2018.01024>
- Sagan, L. (1967). On the origin of mitosing cells. *J Theor Biol*, 14(3), 255-274. [https://doi.org/10.1016/0022-5193\(67\)90079-3](https://doi.org/10.1016/0022-5193(67)90079-3)
- Sajic, M., Mastrolia, V., Lee, C. Y., Trigo, D., Sadeghian, M., Mosley, A. J., Gregson, N. A., Duchen, M. R., & Smith, K. J. (2013). Impulse conduction increases mitochondrial transport in adult mammalian peripheral nerves in vivo. *PLoS Biol*, 11(12), e1001754. <https://doi.org/10.1371/journal.pbio.1001754>
- Salvadores, N., Sanhueza, M., Manque, P., & Court, F. A. (2017). Axonal Degeneration during Aging and Its Functional Role in Neurodegenerative Disorders. *Front Neurosci*, 11, 451. <https://doi.org/10.3389/fnins.2017.00451>
- Sanes, J. R., & Lichtman, J. W. (1999). Development of the vertebrate neuromuscular junction. *Annu Rev Neurosci*, 22, 389-442. <https://doi.org/10.1146/annurev.neuro.22.1.389>
- Sanes, J. R., & Lichtman, J. W. (2001). Induction, assembly, maturation and maintenance of a postsynaptic apparatus. *Nat Rev Neurosci*, 2(11), 791-805. <https://doi.org/10.1038/35097557>
- Santel, A., & Fuller, M. T. (2001). Control of mitochondrial morphology by a human mitofusin. *J Cell Sci*, 114(Pt 5), 867-874. <https://doi.org/10.1242/jcs.114.5.867>
- Santuy, A., Turegano-Lopez, M., Rodriguez, J. R., Alonso-Nanclares, L., DeFelipe, J., & Merchan-Perez, A. (2018). A Quantitative Study on the Distribution of Mitochondria in the Neuropil of the Juvenile Rat Somatosensory Cortex. *Cereb Cortex*, 28(10), 3673-3684. <https://doi.org/10.1093/cercor/bhy159>
- Saotome, M., Safiulina, D., Szabadkai, G., Das, S., Fransson, A., Aspenstrom, P., Rizzuto, R., & Hajnoczky, G. (2008). Bidirectional Ca²⁺-dependent control of mitochondrial dynamics by the Miro GTPase. *Proc Natl Acad Sci U S A*, 105(52), 20728-20733. <https://doi.org/10.1073/pnas.0808953105>
- Sato, O., Sakai, T., Choo, Y. Y., Ikebe, R., Watanabe, T. M., & Ikebe, M. (2022). Mitochondria-associated myosin 19 processively transports mitochondria on actin tracks in living cells. *J Biol Chem*, 298(5), 101883. <https://doi.org/10.1016/j.jbc.2022.101883>
- Saxena, S., & Caroni, P. (2011). Selective neuronal vulnerability in neurodegenerative diseases: from stressor thresholds to degeneration. *Neuron*, 71(1), 35-48. <https://doi.org/10.1016/j.neuron.2011.06.031>
- Schalek, R., Wilson, A., Lichtman, J., Josh, M., Kasthuri, N., Berger, D., Seung, S., Anger, P., Hayworth, K., & Aderhold, D. (2012). ATUM-based SEM for High-Speed Large-Volume Biological Reconstructions. *Microscopy and Microanalysis*, 18(S2), 572-573. <https://doi.org/10.1017/s1431927612004710>

- Schindelin, J., Arganda-Carreras, I., Frise, E., Kaynig, V., Longair, M., Pietzsch, T., Preibisch, S., Rueden, C., Saalfeld, S., Schmid, B., Tinevez, J. Y., White, D. J., Hartenstein, V., Eliceiri, K., Tomancak, P., & Cardona, A. (2012). Fiji: an open-source platform for biological-image analysis. *Nat Methods*, 9(7), 676-682. <https://doi.org/10.1038/nmeth.2019>
- Schliebs, R., & Arendt, T. (2011). The cholinergic system in aging and neuronal degeneration. *Behav Brain Res*, 221(2), 555-563. <https://doi.org/10.1016/j.bbr.2010.11.058>
- Schludi, M. H., Becker, L., Garrett, L., Gendron, T. F., Zhou, Q., Schreiber, F., Popper, B., Dimou, L., Strom, T. M., Winkelmann, J., von Thaden, A., Rentzsch, K., May, S., Michaelson, M., Schwenk, B. M., Tan, J., Schoser, B., Dieterich, M., Petrucelli, L., . . . Edbauer, D. (2017). Spinal poly-GA inclusions in a C9orf72 mouse model trigger motor deficits and inflammation without neuron loss. *Acta Neuropathol*, 134(2), 241-254. <https://doi.org/10.1007/s00401-017-1711-0>
- Schnapp, B. J., Vale, R. D., Sheetz, M. P., & Reese, T. S. (1985). Single microtubules from squid axoplasm support bidirectional movement of organelles. *Cell*, 40(2), 455-462. <https://www.ncbi.nlm.nih.gov/pubmed/2578325>
- Schroer, T. A. (2004). Dynactin. *Annu Rev Cell Dev Biol*, 20, 759-779. <https://doi.org/10.1146/annurev.cellbio.20.012103.094623>
- Schroer, T. A., Steuer, E. R., & Sheetz, M. P. (1989). Cytoplasmic dynein is a minus end-directed motor for membranous organelles. *Cell*, 56(6), 937-946. <https://www.ncbi.nlm.nih.gov/pubmed/2522353>
- Shen, K., Pender, C. L., Bar-Ziv, R., Zhang, H., Wickham, K., Willey, E., Durieux, J., Ahmad, Q., & Dillin, A. (2022). Mitochondria as Cellular and Organismal Signaling Hubs. *Annu Rev Cell Dev Biol*, 38, 179-218. <https://doi.org/10.1146/annurev-cellbio-120420-015303>
- Shen, Q., Yamano, K., Head, B. P., Kawajiri, S., Cheung, J. T., Wang, C., Cho, J. H., Hattori, N., Youle, R. J., & van der Blik, A. M. (2014). Mutations in Fis1 disrupt orderly disposal of defective mitochondria. *Mol Biol Cell*, 25(1), 145-159. <https://doi.org/10.1091/mbc.E13-09-0525>
- Sheng, Z. H. (2014). Mitochondrial trafficking and anchoring in neurons: New insight and implications. *J Cell Biol*, 204(7), 1087-1098. <https://doi.org/10.1083/jcb.201312123>
- Sheng, Z. H., & Cai, Q. (2012). Mitochondrial transport in neurons: impact on synaptic homeostasis and neurodegeneration. *Nat Rev Neurosci*, 13(2), 77-93. <https://doi.org/10.1038/nrn3156>
- Shepherd, G. M., & Harris, K. M. (1998). Three-dimensional structure and composition of CA3-->CA1 axons in rat hippocampal slices: implications for presynaptic connectivity and compartmentalization. *J Neurosci*, 18(20), 8300-8310. <https://www.ncbi.nlm.nih.gov/pubmed/9763474>
<http://www.jneurosci.org/content/jneuro/18/20/8300.full.pdf>
- Shigeoka, T., Jung, H., Jung, J., Turner-Bridger, B., Ohk, J., Lin, J. Q., Amieux, P. S., & Holt, C. E. (2016). Dynamic Axonal Translation in Developing and Mature Visual Circuits. *Cell*, 166(1), 181-192. <https://doi.org/10.1016/j.cell.2016.05.029>
- Shimura, H., Hattori, N., Kubo, S., Mizuno, Y., Asakawa, S., Minoshima, S., Shimizu, N., Iwai, K., Chiba, T., Tanaka, K., & Suzuki, T. (2000). Familial Parkinson disease gene product, parkin, is a ubiquitin-protein ligase. *Nat Genet*, 25(3), 302-305. <https://doi.org/10.1038/77060>
- Shin, J. H., Ko, H. S., Kang, H., Lee, Y., Lee, Y. I., Pletinkova, O., Troconso, J. C., Dawson, V. L., & Dawson, T. M. (2011). PARIS (ZNF746) repression of PGC-1alpha contributes to neurodegeneration in Parkinson's disease. *Cell*, 144(5), 689-702. <https://doi.org/10.1016/j.cell.2011.02.010>
- Shirendeb, U. P., Calkins, M. J., Manczak, M., Anekonda, V., Dufour, B., McBride, J. L., Mao, P., & Reddy, P. H. (2012). Mutant huntingtin's interaction with mitochondrial protein Drp1 impairs mitochondrial biogenesis and causes defective axonal transport and synaptic degeneration

- in Huntington's disease. *Hum Mol Genet*, 21(2), 406-420. <https://doi.org/10.1093/hmg/ddr475>
- Sjostrand, F. S. (1953). Electron microscopy of mitochondria and cytoplasmic double membranes. *Nature*, 171(4340), 30-32. <https://doi.org/10.1038/171030a0>
- Skulachev, V. P. (2001). Mitochondrial filaments and clusters as intracellular power-transmitting cables. *Trends Biochem Sci*, 26(1), 23-29. [https://doi.org/10.1016/s0968-0004\(00\)01735-7](https://doi.org/10.1016/s0968-0004(00)01735-7)
- Smirnova, E., Griparic, L., Shurland, D. L., & van der Bliek, A. M. (2001). Dynamin-related protein Drp1 is required for mitochondrial division in mammalian cells. *Mol Biol Cell*, 12(8), 2245-2256. <https://doi.org/10.1091/mbc.12.8.2245>
- Smit-Rigter, L., Rajendran, R., Silva, C. A., Spierenburg, L., Groeneweg, F., Ruimschotel, E. M., van Versendaal, D., van der Togt, C., Eysel, U. T., Heimel, J. A., Lohmann, C., & Levelt, C. N. (2016). Mitochondrial Dynamics in Visual Cortex Are Limited In Vivo and Not Affected by Axonal Structural Plasticity. *Curr Biol*, 26(19), 2609-2616. <https://doi.org/10.1016/j.cub.2016.07.033>
- Smith, H. L., Bourne, J. N., Cao, G., Chirillo, M. A., Ostroff, L. E., Watson, D. J., & Harris, K. M. (2016). Mitochondrial support of persistent presynaptic vesicle mobilization with age-dependent synaptic growth after LTP. *Elife*, 5. <https://doi.org/10.7554/eLife.15275>
- Sokoloff, L. (1960). The metabolism of the central nervous system in vivo. In J. Field, H. W. Magoun, & V. E. Hall (Eds.), *Handbook of physiology, section 1, neurophysiology* (Vol. 3, pp. 1843–1864). American Physiological Society.
- Song, J. W., Misgeld, T., Kang, H., Knecht, S., Lu, J., Cao, Y., Cotman, S. L., Bishop, D. L., & Lichtman, J. W. (2008). Lysosomal activity associated with developmental axon pruning. *J Neurosci*, 28(36), 8993-9001. <https://doi.org/10.1523/JNEUROSCI.0720-08.2008>
- Song, W., Chen, J., Petrilli, A., Liot, G., Klinglmayr, E., Zhou, Y., Poquiz, P., Tjong, J., Pouladi, M. A., Hayden, M. R., Masliah, E., Ellisman, M., Rouiller, I., Schwarzenbacher, R., Bossy, B., Perkins, G., & Bossy-Wetzler, E. (2011). Mutant huntingtin binds the mitochondrial fission GTPase dynamin-related protein-1 and increases its enzymatic activity. *Nat Med*, 17(3), 377-382. <https://doi.org/10.1038/nm.2313>
- Song, Z., Chen, H., Fiket, M., Alexander, C., & Chan, D. C. (2007). OPA1 processing controls mitochondrial fusion and is regulated by mRNA splicing, membrane potential, and Yme1L. *J Cell Biol*, 178(5), 749-755. <https://doi.org/10.1083/jcb.200704110>
- Song, Z., Ghochani, M., McCaffery, J. M., Frey, T. G., & Chan, D. C. (2009). Mitofusins and OPA1 mediate sequential steps in mitochondrial membrane fusion. *Mol Biol Cell*, 20(15), 3525-3532. <https://doi.org/10.1091/mbc.e09-03-0252>
- Sorbara, C. D., Wagner, N. E., Ladwig, A., Nikic, I., Merkler, D., Kleele, T., Marinkovic, P., Naumann, R., Godinho, L., Bareyre, F. M., Bishop, D., Misgeld, T., & Kerschensteiner, M. (2014). Pervasive axonal transport deficits in multiple sclerosis models. *Neuron*, 84(6), 1183-1190. <https://doi.org/10.1016/j.neuron.2014.11.006>
- Soubannier, V., McLelland, G. L., Zunino, R., Braschi, E., Rippstein, P., Fon, E. A., & McBride, H. M. (2012). A vesicular transport pathway shuttles cargo from mitochondria to lysosomes. *Curr Biol*, 22(2), 135-141. <https://doi.org/10.1016/j.cub.2011.11.057>
- Spillane, M., Ketschek, A., Merianda, T. T., Twiss, J. L., & Gallo, G. (2013). Mitochondria coordinate sites of axon branching through localized intra-axonal protein synthesis. *Cell Rep*, 5(6), 1564-1575. <https://doi.org/10.1016/j.celrep.2013.11.022>
- Stauch, K. L., Purnell, P. R., & Fox, H. S. (2014). Quantitative proteomics of synaptic and nonsynaptic mitochondria: insights for synaptic mitochondrial vulnerability. *J Proteome Res*, 13(5), 2620-2636. <https://doi.org/10.1021/pr500295n>

- Stavoe, A. K. H., & Holzbaur, E. L. F. (2019). Autophagy in Neurons. *Annu Rev Cell Dev Biol*, 35, 477-500. <https://doi.org/10.1146/annurev-cellbio-100818-125242>
- Stevens, D. A., Lee, Y., Kang, H. C., Lee, B. D., Lee, Y. I., Bower, A., Jiang, H., Kang, S. U., Andrabi, S. A., Dawson, V. L., Shin, J. H., & Dawson, T. M. (2015). Parkin loss leads to PARIS-dependent declines in mitochondrial mass and respiration. *Proc Natl Acad Sci U S A*, 112(37), 11696-11701. <https://doi.org/10.1073/pnas.1500624112>
- Stowers, R. S., Megeath, L. J., Gorska-Andrzejak, J., Meinertzhagen, I. A., & Schwarz, T. L. (2002). Axonal transport of mitochondria to synapses depends on milton, a novel Drosophila protein. *Neuron*, 36(6), 1063-1077. <https://www.ncbi.nlm.nih.gov/pubmed/12495622>
- Strohm, L., & Behrends, C. (2020). Glia-specific autophagy dysfunction in ALS. *Semin Cell Dev Biol*, 99, 172-182. <https://doi.org/10.1016/j.semcdb.2019.05.024>
- Su, B., Ji, Y. S., Sun, X. L., Liu, X. H., & Chen, Z. Y. (2014). Brain-derived neurotrophic factor (BDNF)-induced mitochondrial motility arrest and presynaptic docking contribute to BDNF-enhanced synaptic transmission. *J Biol Chem*, 289(3), 1213-1226. <https://doi.org/10.1074/jbc.M113.526129>
- Sun, L., Zhao, M., Yu, X. J., Wang, H., He, X., Liu, J. K., & Zang, W. J. (2013). Cardioprotection by acetylcholine: a novel mechanism via mitochondrial biogenesis and function involving the PGC-1alpha pathway. *J Cell Physiol*, 228(6), 1238-1248. <https://doi.org/10.1002/jcp.24277>
- Sun, T., Qiao, H., Pan, P. Y., Chen, Y., & Sheng, Z. H. (2013). Motile axonal mitochondria contribute to the variability of presynaptic strength. *Cell Rep*, 4(3), 413-419. <https://doi.org/10.1016/j.celrep.2013.06.040>
- Sung, H., Tandarich, L. C., Nguyen, K., & Hollenbeck, P. J. (2016). Compartmentalized Regulation of Parkin-Mediated Mitochondrial Quality Control in the Drosophila Nervous System In Vivo. *J Neurosci*, 36(28), 7375-7391. <https://doi.org/10.1523/JNEUROSCI.0633-16.2016>
- Sung, J. Y., Engmann, O., Teylan, M. A., Nairn, A. C., Greengard, P., & Kim, Y. (2008). WAVE1 controls neuronal activity-induced mitochondrial distribution in dendritic spines. *Proc Natl Acad Sci U S A*, 105(8), 3112-3116. <https://doi.org/10.1073/pnas.0712180105>
- Suomalainen, A. (1997). Mitochondrial DNA and disease. *Ann Med*, 29(3), 235-246. <https://doi.org/10.3109/07853899708999341>
- Surmeier, D. J., Obeso, J. A., & Halliday, G. M. (2017). Selective neuronal vulnerability in Parkinson disease. *Nat Rev Neurosci*, 18(2), 101-113. <https://doi.org/10.1038/nrn.2016.178>
- Takano, T., Xu, C., Funahashi, Y., Namba, T., & Kaibuchi, K. (2015). Neuronal polarization. *Development*, 142(12), 2088-2093. <https://doi.org/10.1242/dev.114454>
- Tamada, H. (2023). Three-dimensional ultrastructure analysis of organelles in injured motor neuron. *Anat Sci Int*, 98(3), 360-369. <https://doi.org/10.1007/s12565-023-00720-y>
- Tanaka, Y., Kanai, Y., Okada, Y., Nonaka, S., Takeda, S., Harada, A., & Hirokawa, N. (1998). Targeted disruption of mouse conventional kinesin heavy chain, kif5B, results in abnormal perinuclear clustering of mitochondria. *Cell*, 93(7), 1147-1158. <https://www.ncbi.nlm.nih.gov/pubmed/9657148>
- Tang, Y., & Zucker, R. S. (1997). Mitochondrial involvement in post-tetanic potentiation of synaptic transmission. *Neuron*, 18(3), 483-491. <https://www.ncbi.nlm.nih.gov/pubmed/9115741>
- Tanida, I. (2011). Autophagy basics. *Microbiol Immunol*, 55(1), 1-11. <https://doi.org/10.1111/j.1348-0421.2010.00271.x>
- Tansey, E. M. (2006). Henry Dale and the discovery of acetylcholine. *C R Biol*, 329(5-6), 419-425. <https://doi.org/10.1016/j.crv.2006.03.012>

- Terman, A., Gustafsson, B., & Brunk, U. T. (2006). The lysosomal-mitochondrial axis theory of postmitotic aging and cell death. *Chem Biol Interact*, 163(1-2), 29-37. <https://doi.org/10.1016/j.cbi.2006.04.013>
- Terman, A., Kurz, T., Navratil, M., Arriaga, E. A., & Brunk, U. T. (2010). Mitochondrial turnover and aging of long-lived postmitotic cells: the mitochondrial-lysosomal axis theory of aging. *Antioxid Redox Signal*, 12(4), 503-535. <https://doi.org/10.1089/ars.2009.2598>
- Thomsen, K., Yokota, T., Hasan-Olive, M. M., Sherazi, N., Fakouri, N. B., Desler, C., Regnell, C. E., Larsen, S., Rasmussen, L. J., Dela, F., Bergersen, L. H., & Lauritzen, M. (2018). Initial brain aging: heterogeneity of mitochondrial size is associated with decline in complex I-linked respiration in cortex and hippocampus. *Neurobiol Aging*, 61, 215-224. <https://doi.org/10.1016/j.neurobiolaging.2017.08.004>
- Toyama, E. Q., Herzig, S., Courchet, J., Lewis, T. L., Jr., Loson, O. C., Hellberg, K., Young, N. P., Chen, H., Polleux, F., Chan, D. C., & Shaw, R. J. (2016). Metabolism. AMP-activated protein kinase mediates mitochondrial fission in response to energy stress. *Science*, 351(6270), 275-281. <https://doi.org/10.1126/science.aab4138>
- Trudeau, K. M., Gottlieb, R. A., & Shirihai, O. S. (2014). Measurement of mitochondrial turnover and life cycle using MitoTimer. *Methods Enzymol*, 547, 21-38. <https://doi.org/10.1016/B978-0-12-801415-8.00002-3>
- Tseng, Q., Wang, I., Duchemin-Pelletier, E., Azioune, A., Carpi, N., Gao, J., Filhol, O., Piel, M., Theyry, M., & Balland, M. (2011). A new micropatterning method of soft substrates reveals that different tumorigenic signals can promote or reduce cell contraction levels. *Lab Chip*, 11(13), 2231-2240. <https://doi.org/10.1039/c0lc00641f>
- Tsien, R. Y. (1998). The green fluorescent protein. *Annu Rev Biochem*, 67, 509-544. <https://doi.org/10.1146/annurev.biochem.67.1.509>
- Tumbarello, D. A., Waxse, B. J., Arden, S. D., Bright, N. A., Kendrick-Jones, J., & Buss, F. (2012). Autophagy receptors link myosin VI to autophagosomes to mediate Tom1-dependent autophagosome maturation and fusion with the lysosome. *Nat Cell Biol*, 14(10), 1024-1035. <https://doi.org/10.1038/ncb2589>
- Tuppen, H. A., Blakely, E. L., Turnbull, D. M., & Taylor, R. W. (2010). Mitochondrial DNA mutations and human disease. *Biochim Biophys Acta*, 1797(2), 113-128. <https://doi.org/10.1016/j.bbabi.2009.09.005>
- Turner, N. L., Macrina, T., Bae, J. A., Yang, R., Wilson, A. M., Schneider-Mizell, C., Lee, K., Lu, R., Wu, J., Bodor, A. L., Bleckert, A. A., Brittain, D., Froudarakis, E., Dorkenwald, S., Collman, F., Kemnitz, N., Ih, D., Silversmith, W. M., Zung, J., . . . Seung, H. S. (2022). Reconstruction of neocortex: Organelles, compartments, cells, circuits, and activity. *Cell*, 185(6), 1082-1100 e1024. <https://doi.org/10.1016/j.cell.2022.01.023>
- Turney, S. G., Walsh, M. K., & Lichtman, J. W. (2012). In vivo imaging of the developing neuromuscular junction in neonatal mice. *Cold Spring Harb Protoc*, 2012(11), 1166-1176. <https://doi.org/10.1101/pdb.prot072082>
- Twig, G., Elorza, A., Molina, A. J., Mohamed, H., Wikstrom, J. D., Walzer, G., Stiles, L., Haigh, S. E., Katz, S., Las, G., Alroy, J., Wu, M., Py, B. F., Yuan, J., Deeney, J. T., Corkey, B. E., & Shirihai, O. S. (2008). Fission and selective fusion govern mitochondrial segregation and elimination by autophagy. *EMBO J*, 27(2), 433-446. <https://doi.org/10.1038/sj.emboj.7601963>
- Twig, G., Graf, S. A., Wikstrom, J. D., Mohamed, H., Haigh, S. E., Elorza, A., Deutsch, M., Zurgil, N., Reynolds, N., & Shirihai, O. S. (2006). Tagging and tracking individual networks within a complex mitochondrial web with photoactivatable GFP. *Am J Physiol Cell Physiol*, 291(1), C176-184. <https://doi.org/10.1152/ajpcell.00348.2005>

- Tymanskyj, S. R., Curran, B. M., & Ma, L. (2022). Selective axonal transport through branch junctions is directed by growth cone signaling and mediated by KIF1/kinesin-3 motors. *Cell Rep*, 39(4), 110748. <https://doi.org/10.1016/j.celrep.2022.110748>
- Tymanskyj, S. R., & Ma, L. (2019). MAP7 Prevents Axonal Branch Retraction by Creating a Stable Microtubule Boundary to Rescue Polymerization. *J Neurosci*, 39(36), 7118-7131. <https://doi.org/10.1523/JNEUROSCI.0775-19.2019>
- Tymanskyj, S. R., Yang, B., Fahnkar, A., Lepore, A. C., & Ma, L. (2017). MAP7 Regulates Axon Collateral Branch Development in Dorsal Root Ganglion Neurons. *J Neurosci*, 37(6), 1648-1661. <https://doi.org/10.1523/JNEUROSCI.3260-16.2017>
- Tymanskyj, S. R., Yang, B. H., Verhey, K. J., & Ma, L. (2018). MAP7 regulates axon morphogenesis by recruiting kinesin-1 to microtubules and modulating organelle transport. *Elife*, 7. <https://doi.org/10.7554/eLife.36374>
- Uittenbogaard, M., & Chiaramello, A. (2014). Mitochondrial biogenesis: a therapeutic target for neurodevelopmental disorders and neurodegenerative diseases. *Curr Pharm Des*, 20(35), 5574-5593. <https://doi.org/10.2174/1381612820666140305224906>
- Vafai, S. B., & Mootha, V. K. (2012). Mitochondrial disorders as windows into an ancient organelle. *Nature*, 491(7424), 374-383. <https://doi.org/10.1038/nature11707>
- Vale, R. D., Reese, T. S., & Sheetz, M. P. (1985). Identification of a novel force-generating protein, kinesin, involved in microtubule-based motility. *Cell*, 42(1), 39-50. <https://www.ncbi.nlm.nih.gov/pubmed/3926325>
- Vale, R. D., Schnapp, B. J., Mitchison, T., Steuer, E., Reese, T. S., & Sheetz, M. P. (1985). Different axoplasmic proteins generate movement in opposite directions along microtubules in vitro. *Cell*, 43(3 Pt 2), 623-632. <https://www.ncbi.nlm.nih.gov/pubmed/2416467>
- Valente, E. M., Abou-Sleiman, P. M., Caputo, V., Muqit, M. M., Harvey, K., Gispert, S., Ali, Z., Del Turco, D., Bentivoglio, A. R., Healy, D. G., Albanese, A., Nussbaum, R., Gonzalez-Maldonado, R., Deller, T., Salvi, S., Cortelli, P., Gilks, W. P., Latchman, D. S., Harvey, R. J., . . . Wood, N. W. (2004). Hereditary early-onset Parkinson's disease caused by mutations in PINK1. *Science*, 304(5674), 1158-1160. <https://doi.org/10.1126/science.1096284>
- Van Laar, V. S., Arnold, B., Howlett, E. H., Calderon, M. J., St Croix, C. M., Greenamyre, J. T., Sanders, L. H., & Berman, S. B. (2018). Evidence for Compartmentalized Axonal Mitochondrial Biogenesis: Mitochondrial DNA Replication Increases in Distal Axons As an Early Response to Parkinson's Disease-Relevant Stress. *J Neurosci*, 38(34), 7505-7515. <https://doi.org/10.1523/JNEUROSCI.0541-18.2018>
- van Oostrum, M., Blok, T. M., Giandomenico, S. L., Tom Dieck, S., Tushev, G., Furst, N., Langer, J. D., & Schuman, E. M. (2023). The proteomic landscape of synaptic diversity across brain regions and cell types. *Cell*, 186(24), 5411-5427 e5423. <https://doi.org/10.1016/j.cell.2023.09.028>
- Vasquez-Vivar, J., Shi, Z., & Tan, S. (2022). Tetrahydrobiopterin in Cell Function and Death Mechanisms. *Antioxid Redox Signal*, 37(1-3), 171-183. <https://doi.org/10.1089/ars.2021.0136>
- Venkatesh, K., Mathew, A., & Koushika, S. P. (2020). Role of actin in organelle trafficking in neurons. *Cytoskeleton (Hoboken)*, 77(3-4), 97-109. <https://doi.org/10.1002/cm.21580>
- Ventura-Clapier, R., Garnier, A., & Veksler, V. (2008). Transcriptional control of mitochondrial biogenesis: the central role of PGC-1alpha. *Cardiovasc Res*, 79(2), 208-217. <https://doi.org/10.1093/cvr/cvn098>
- Verburg, J., & Hollenbeck, P. J. (2008). Mitochondrial membrane potential in axons increases with local nerve growth factor or semaphorin signaling. *J Neurosci*, 28(33), 8306-8315. <https://doi.org/10.1523/JNEUROSCI.2614-08.2008>

- Verma, M., Lizama, B. N., & Chu, C. T. (2022). Excitotoxicity, calcium and mitochondria: a triad in synaptic neurodegeneration. *Transl Neurodegener*, 11(1), 3. <https://doi.org/10.1186/s40035-021-00278-7>
- Verstreken, P., Ly, C. V., Venken, K. J., Koh, T. W., Zhou, Y., & Bellen, H. J. (2005). Synaptic mitochondria are critical for mobilization of reserve pool vesicles at Drosophila neuromuscular junctions. *Neuron*, 47(3), 365-378. <https://doi.org/10.1016/j.neuron.2005.06.018>
- Vives-Bauza, C., Zhou, C., Huang, Y., Cui, M., de Vries, R. L., Kim, J., May, J., Tocilescu, M. A., Liu, W., Ko, H. S., Magrane, J., Moore, D. J., Dawson, V. L., Grailhe, R., Dawson, T. M., Li, C., Tieu, K., & Przedborski, S. (2010). PINK1-dependent recruitment of Parkin to mitochondria in mitophagy. *Proc Natl Acad Sci U S A*, 107(1), 378-383. <https://doi.org/10.1073/pnas.0911187107>
- Volgyi, K., Gulyassy, P., Haden, K., Kis, V., Badics, K., Kekesi, K. A., Simor, A., Gyorffy, B., Toth, E. A., Lubec, G., Juhasz, G., & Dobolyi, A. (2015). Synaptic mitochondria: a brain mitochondria cluster with a specific proteome. *J Proteomics*, 120, 142-157. <https://doi.org/10.1016/j.jprot.2015.03.005>
- Von Hungen, K., Mahler, H. R., & Moore, W. J. (1968). Turnover of protein and ribonucleic acid in synaptic subcellular fractions from rat brain. *J Biol Chem*, 243(7), 1415-1423. <https://www.ncbi.nlm.nih.gov/pubmed/5647262>
- Waagepetersen, H. S., Sonnewald, U., & Schousboe, A. (2003). Compartmentation of glutamine, glutamate, and GABA metabolism in neurons and astrocytes: functional implications. *Neuroscientist*, 9(5), 398-403. <https://doi.org/10.1177/1073858403254006>
- Wang, J. T., Medress, Z. A., & Barres, B. A. (2012). Axon degeneration: molecular mechanisms of a self-destruction pathway. *J Cell Biol*, 196(1), 7-18. <https://doi.org/10.1083/jcb.201108111>
- Wang, M., Kleele, T., Xiao, Y., Plucinska, G., Avramopoulos, P., Engelhardt, S., Schwab, M. H., Kneussel, M., Czopka, T., Sherman, D. L., Brophy, P. J., Misgeld, T., & Brill, M. S. (2021). Completion of neuronal remodeling prompts myelination along developing motor axon branches. *J Cell Biol*, 220(4). <https://doi.org/10.1083/jcb.201911114>
- Wang, X., Su, B., Lee, H. G., Li, X., Perry, G., Smith, M. A., & Zhu, X. (2009). Impaired balance of mitochondrial fission and fusion in Alzheimer's disease. *J Neurosci*, 29(28), 9090-9103. <https://doi.org/10.1523/JNEUROSCI.1357-09.2009>
- Wang, X., Winter, D., Ashrafi, G., Schlehe, J., Wong, Y. L., Selkoe, D., Rice, S., Steen, J., LaVoie, M. J., & Schwarz, T. L. (2011). PINK1 and Parkin target Miro for phosphorylation and degradation to arrest mitochondrial motility. *Cell*, 147(4), 893-906. <https://doi.org/10.1016/j.cell.2011.10.018>
- Wareski, P., Vaarmann, A., Choubey, V., Safiulina, D., Liiv, J., Kuum, M., & Kaasik, A. (2009). PGC-1alpha and PGC-1beta regulate mitochondrial density in neurons. *J Biol Chem*, 284(32), 21379-21385. <https://doi.org/10.1074/jbc.M109.018911>
- Waterham, H. R., Koster, J., van Roermund, C. W., Mooyer, P. A., Wanders, R. J., & Leonard, J. V. (2007). A lethal defect of mitochondrial and peroxisomal fission. *N Engl J Med*, 356(17), 1736-1741. <https://doi.org/10.1056/NEJMoa064436>
- Wehnekamp, F., Plucinska, G., Thong, R., Misgeld, T., & Lamb, D. C. (2019). Nanoresolution real-time 3D orbital tracking for studying mitochondrial trafficking in vertebrate axons in vivo. *Elife*, 8. <https://doi.org/10.7554/eLife.46059>
- Westermann, B. (2002). Merging mitochondria matters: cellular role and molecular machinery of mitochondrial fusion. *EMBO Rep*, 3(6), 527-531. <https://doi.org/10.1093/embo-reports/kvf113>
- Wild, P., Farhan, H., McEwan, D. G., Wagner, S., Rogov, V. V., Brady, N. R., Richter, B., Korac, J., Waidmann, O., Choudhary, C., Dotsch, V., Bumann, D., & Dikic, I. (2011). Phosphorylation of

- the autophagy receptor optineurin restricts Salmonella growth. *Science*, 333(6039), 228-233. <https://doi.org/10.1126/science.1205405>
- Wilson, D. M., 3rd, Cookson, M. R., Van Den Bosch, L., Zetterberg, H., Holtzman, D. M., & Dewachter, I. (2023). Hallmarks of neurodegenerative diseases. *Cell*, 186(4), 693-714. <https://doi.org/10.1016/j.cell.2022.12.032>
- Winckler, B., Forscher, P., & Mellman, I. (1999). A diffusion barrier maintains distribution of membrane proteins in polarized neurons. *Nature*, 397(6721), 698-701. <https://doi.org/10.1038/17806>
- Wolf, D. M., Segawa, M., Kondadi, A. K., Anand, R., Bailey, S. T., Reichert, A. S., van der Bliek, A. M., Shackelford, D. B., Liesa, M., & Shirihai, O. S. (2019). Individual cristae within the same mitochondrion display different membrane potentials and are functionally independent. *EMBO J*, 38(22), e101056. <https://doi.org/10.15252/embj.2018101056>
- Wong-Riley, M., & Carroll, E. W. (1984). Effect of impulse blockage on cytochrome oxidase activity in monkey visual system. *Nature*, 307(5948), 262-264. <https://www.ncbi.nlm.nih.gov/pubmed/6319997>
<https://www.nature.com/articles/307262a0>
- Wong-Riley, M. T. (1989). Cytochrome oxidase: an endogenous metabolic marker for neuronal activity. *Trends Neurosci*, 12(3), 94-101. <https://www.ncbi.nlm.nih.gov/pubmed/2469224>
<https://www.sciencedirect.com/science/article/abs/pii/0166223689901653?via%3Dihub>
- Wong-Riley, M. T., & Welt, C. (1980). Histochemical changes in cytochrome oxidase of cortical barrels after vibrissal removal in neonatal and adult mice. *Proc Natl Acad Sci U S A*, 77(4), 2333-2337. <https://doi.org/10.1073/pnas.77.4.2333>
- Wong, M. Y., Zhou, C., Shakiryanova, D., Lloyd, T. E., Deitcher, D. L., & Levitan, E. S. (2012). Neuropeptide delivery to synapses by long-range vesicle circulation and sporadic capture. *Cell*, 148(5), 1029-1038. <https://doi.org/10.1016/j.cell.2011.12.036>
- Wong, Y. C., & Holzbaur, E. L. (2014). Optineurin is an autophagy receptor for damaged mitochondria in parkin-mediated mitophagy that is disrupted by an ALS-linked mutation. *Proc Natl Acad Sci U S A*, 111(42), E4439-4448. <https://doi.org/10.1073/pnas.1405752111>
- Wong, Y. C., Luk, K., Purtell, K., Burke Nanni, S., Stoessl, A. J., Trudeau, L. E., Yue, Z., Krainc, D., Oertel, W., Obeso, J. A., & Volpicelli-Daley, L. A. (2019). Neuronal vulnerability in Parkinson disease: Should the focus be on axons and synaptic terminals? *Mov Disord*. <https://doi.org/10.1002/mds.27823>
- Wood, S. J., & Slater, C. R. (2001). Safety factor at the neuromuscular junction. *Prog Neurobiol*, 64(4), 393-429. [https://doi.org/10.1016/s0301-0082\(00\)00055-1](https://doi.org/10.1016/s0301-0082(00)00055-1)
- World Health Organization. (2020). *Global Health Estimates 2020: Deaths by Cause, Age, Sex, by Country and by Region, 2000-2019* <https://www.who.int/data/gho/data/themes/mortality-and-global-health-estimates/ghe-leading-causes-of-death>
- Xiao, C., Chen, X., Li, W., Li, L., Wang, L., Xie, Q., & Han, H. (2018). Automatic Mitochondria Segmentation for EM Data Using a 3D Supervised Convolutional Network. *Front Neuroanat*, 12, 92. <https://doi.org/10.3389/fnana.2018.00092>
- Xie, Y., Zhou, B., Lin, M. Y., Wang, S., Foust, K. D., & Sheng, Z. H. (2015). Endolysosomal Deficits Augment Mitochondria Pathology in Spinal Motor Neurons of Asymptomatic fALS Mice. *Neuron*, 87(2), 355-370. <https://doi.org/10.1016/j.neuron.2015.06.026>
- Xu, Y., Chen, M., Hu, B., Huang, R., & Hu, B. (2017). In vivo Imaging of Mitochondrial Transport in Single-Axon Regeneration of Zebrafish Mauthner Cells. *Front Cell Neurosci*, 11, 4. <https://doi.org/10.3389/fncel.2017.00004>

- Yamano, K., Fogel, A. I., Wang, C., van der Blik, A. M., & Youle, R. J. (2014). Mitochondrial Rab GAPs govern autophagosome biogenesis during mitophagy. *Elife*, 3, e01612. <https://doi.org/10.7554/eLife.01612>
- Ye, X., Sun, X., Starovoytov, V., & Cai, Q. (2015). Parkin-mediated mitophagy in mutant hAPP neurons and Alzheimer's disease patient brains. *Hum Mol Genet*, 24(10), 2938-2951. <https://doi.org/10.1093/hmg/ddv056>
- Yogev, S., Cooper, R., Fetter, R., Horowitz, M., & Shen, K. (2016). Microtubule Organization Determines Axonal Transport Dynamics. *Neuron*, 92(2), 449-460. <https://doi.org/10.1016/j.neuron.2016.09.036>
- Yonashiro, R., Ishido, S., Kyo, S., Fukuda, T., Goto, E., Matsuki, Y., Ohmura-Hoshino, M., Sada, K., Hotta, H., Yamamura, H., Inatome, R., & Yanagi, S. (2006). A novel mitochondrial ubiquitin ligase plays a critical role in mitochondrial dynamics. *EMBO J*, 25(15), 3618-3626. <https://doi.org/10.1038/sj.emboj.7601249>
- Yoon, B. C., Jung, H., Dwivedy, A., O'Hare, C. M., Zivraj, K. H., & Holt, C. E. (2012). Local translation of extranuclear lamin B promotes axon maintenance. *Cell*, 148(4), 752-764. <https://doi.org/10.1016/j.cell.2011.11.064>
- Yoon, Y. (2004). Sharpening the scissors: mitochondrial fission with aid. *Cell Biochem Biophys*, 41(2), 193-206. <https://doi.org/10.1385/CBB:41:2:193>
- Yoshii, S. R., Kuma, A., Akashi, T., Hara, T., Yamamoto, A., Kurikawa, Y., Itakura, E., Tsukamoto, S., Shitara, H., Eishi, Y., & Mizushima, N. (2016). Systemic Analysis of Atg5-Null Mice Rescued from Neonatal Lethality by Transgenic ATG5 Expression in Neurons. *Dev Cell*, 39(1), 116-130. <https://doi.org/10.1016/j.devcel.2016.09.001>
- Yousefi, R., Fornasiero, E. F., Cyganek, L., Montoya, J., Jakobs, S., Rizzoli, S. O., Rehling, P., & Pacheu-Grau, D. (2021). Monitoring mitochondrial translation in living cells. *EMBO Rep*, 22(4), e51635. <https://doi.org/10.15252/embr.202051635>
- Yuan, Y., Cruzat, V. F., Newsholme, P., Cheng, J., Chen, Y., & Lu, Y. (2016). Regulation of SIRT1 in aging: Roles in mitochondrial function and biogenesis. *Mech Ageing Dev*, 155, 10-21. <https://doi.org/10.1016/j.mad.2016.02.003>
- Yuste, R. (2015). From the neuron doctrine to neural networks. *Nat Rev Neurosci*, 16(8), 487-497. <https://doi.org/10.1038/nrn3962>
- Zhang, C. L., Ho, P. L., Kintner, D. B., Sun, D., & Chiu, S. Y. (2010). Activity-dependent regulation of mitochondrial motility by calcium and Na/K-ATPase at nodes of Ranvier of myelinated nerves. *J Neurosci*, 30(10), 3555-3566. <https://doi.org/10.1523/JNEUROSCI.4551-09.2010>
- Zhang, Z., Kageyama, Y., & Sesaki, H. (2012). Mitochondrial division prevents neurodegeneration. *Autophagy*, 8(10), 1531-1533. <https://doi.org/10.4161/auto.21213>
- Zhao, J., Liu, T., Jin, S., Wang, X., Qu, M., Uhlen, P., Tomilin, N., Shupliakov, O., Lendahl, U., & Nister, M. (2011). Human MIEF1 recruits Drp1 to mitochondrial outer membranes and promotes mitochondrial fusion rather than fission. *EMBO J*, 30(14), 2762-2778. <https://doi.org/10.1038/emboj.2011.198>
- Zheng, Y. R., Zhang, X. N., & Chen, Z. (2019). Mitochondrial transport serves as a mitochondrial quality control strategy in axons: Implications for central nervous system disorders. *CNS Neurosci Ther*, 25(7), 876-886. <https://doi.org/10.1111/cns.13122>
- Zhou, X. X., & Lin, M. Z. (2013). Photoswitchable fluorescent proteins: ten years of colorful chemistry and exciting applications. *Curr Opin Chem Biol*, 17(4), 682-690. <https://doi.org/10.1016/j.cbpa.2013.05.031>
- Zhu, J., Wang, K. Z., & Chu, C. T. (2013). After the banquet: mitochondrial biogenesis, mitophagy, and cell survival. *Autophagy*, 9(11), 1663-1676. <https://doi.org/10.4161/auto.24135>

- Zick, M., Rabl, R., & Reichert, A. S. (2009). Cristae formation-linking ultrastructure and function of mitochondria. *Biochim Biophys Acta*, 1793(1), 5-19. <https://doi.org/10.1016/j.bbamcr.2008.06.013>
- Zivraj, K. H., Tung, Y. C., Piper, M., Gumy, L., Fawcett, J. W., Yeo, G. S., & Holt, C. E. (2010). Subcellular profiling reveals distinct and developmentally regulated repertoire of growth cone mRNAs. *J Neurosci*, 30(46), 15464-15478. <https://doi.org/10.1523/JNEUROSCI.1800-10.2010>
- Zorkau, M., Albus, C. A., Berlinguer-Palmini, R., Chrzanowska-Lightowlers, Z. M. A., & Lightowlers, R. N. (2021). High-resolution imaging reveals compartmentalization of mitochondrial protein synthesis in cultured human cells. *Proc Natl Acad Sci U S A*, 118(6). <https://doi.org/10.1073/pnas.2008778118>
- Zott, B., Busche, M. A., Sperling, R. A., & Konnerth, A. (2018). What Happens with the Circuit in Alzheimer's Disease in Mice and Humans? *Annu Rev Neurosci*, 41, 277-297. <https://doi.org/10.1146/annurev-neuro-080317-061725>